STRUCTURE-PROPERTY RELATIONSHIPS OF BISMALEIMIDES

A Dissertation

Presented to

The Graduate Faculty of The University of Akron

In Partial Fulfillment

Of the Requirements for the Degree

Doctor of Philosophy in Polymer Science

Anita D. Tenteris-Noebe

December, 1997

Anita Tenteris-Noebe

2510 1/2 Medina Road
Medina, OH 44256
(330) 725-0363
E-Mail: Noebe@Bright.Net

The University of Akron
Polymer Science Dept.
Akron, OH 44325-3909
(330) 972-6674

BACKGROUND SUMMARY

- Diverse training and experience in polymers, biomaterials, and metals. Highly analytical with mature technical and communication skills. Self-sufficient, industrious, reliable, adaptable, works well with others. Seeking a research or product development position in a polymer-related company.

EDUCATION

Present Ph.D. (Polymer Science), December, 1997, The University of Akron, Polymer Science Dept., Akron, OH 44352. Dissertation topic: *Structure-Property Relationships in Bismaleimides*. Advisor: Prof. Frank N. Kelley. Recipient of B. F. Goodrich Fellowship - 1 year. Mentored Upward Bound student and 2 summer interns.

1986 MS (Biomedical Engineering), Case Western Reserve University, Cleveland, OH 44106. Thesis: *Tissue Response Around a Stimulated Electrode*. Thesis Advisor: Prof. P.H. Peckham.

1983 BS (Biomedical Engineering, Materials Discipline - with Honors), Case Western Reserve University, Cleveland, OH 44106. Ohio Board of Reagents Scholarship - 4 years. Case Western Reserve University Matching Scholarship - 4 years.

PROFESSIONAL EXPERIENCE

6/91 - 9/91 Polymer Scientist for Acro Med Corp, Cleveland, OH 44115. Synthesized and compounded rubber used in the fabrication of a prototype artificial spinal disk. Responsibilities included writing and revising protocol procedures, physical testing and characterization of the synthesized rubber. Temporary summer position. Dr. Carl McMillin - Supervisor.

8/88 - 3/91 General Manager for Reynolds Corner Recreation Bowling Center, Toledo, OH 43615. Weekend responsibilities in the family business included: customer service, inventory, general maintenance, snack bar concessions, bartending, and waitressing. Sandra Tenteris - Supervisor.

6/88 - 9/89 Student Assistant for Applied Research, Akron, OH 44352. Performed GC/FTIR analyses on unknown samples.

1/86 - 1/87 Research Assistant at University of Michigan Transportation Research Institute, Ann Arbor, MI 48109. Principal Investigator: Investigation of Intravenous and Intramuscular Needle Penetrations. Performed needle testing, prepared reports with statistical data analysis, and monthly financial statements. Developed protocol for

the evaluation of bone biopsy needles, including statistical analysis and SEM of biopsy core samples. Dr. L. W. Schneider - Supervisor.

6/84 - 10/85 Graduate student in the Department of Biomedical Engineering at Case Western Reserve University. Performed animal surgeries, set up and operated histology laboratory, and prepared tissue samples for histological evaluation. Taught an introductory materials laboratory to undergraduates.

PROFESSIONAL AFFLIATIONS AND COMMUNITY-BASED ACTIVITIES

- Member: Society of Plastics Engineering, Society for the Advancement of Materials Processing and Engineering, American Chemical Society - Rubber Division.
- Active member of Student Chapter of SAMPE. Previously held offices - President, 1989-1992; Vice-President, 1987-1989. Principle student organizer of a one day seminar - "Advancing Composites into the 90's" held February, 1990.
- Assistant coach for U14 boys soccer (Highland Hornets) in Medina, OH.
- Actively participates in several organized leagues of women's and co-ed softball and women's soccer.
- Participated in the Volunteer Reading Program at Medina County Library, in Medina, OH.

PUBLICATIONS AND PRESENTATIONS

A. Tenteris-Noebe and L.W. Schneider: "Comparative Evaluation of Disposable Bone Marrow Biopsy Needles", Technical Report for The University of Michigan Transportation Research Institute, UMTRI-87-14, February, 1987.

A. Tenteris-Noebe: Chemtracts Macromolecular Chemistry Condensation of the article: "Rheological Studies on Solutions of Poly-p-phenylene Terephthalamide in H_2SO_4" by Y. Xu and R. Qian,, *Intern. Polymer Proc.*, **4**, 1990, 250.

A. Tenteris-Noebe: Chemtracts Macromolecular Chemistry Condensation of the article "Knit Line Fractures in Injection Molded Liquid Crystalline Polymers" by K. Engberg, A. Knutsson, P. E. Werner, and U. W. Gedde, *Polymer Eng. Sci.*, 30(24), 1990, 1620.

A. Tenteris-Noebe: Chemtracts Macromolecular Chemistry Condensation of the article "Rheology and Morphology of Polymer Bends Containing Liquid-Crystalline Component in Melt and Solid State" by V. G. Kulichikhin, O. V. Vasil'eva, I. A. Litvinov, E. M. Antipov, I. L. Parsanyan, and N. A. Plate, *J. Appl. Polymer Sci.*, 42, 1991, 363.

A. Tenteris-Noebe: Chemtracts Macromolecular Chemistry Condensation of the article "Fatigue Behavior of Oriented Ultra-High Molecular Weight Polyethylene Prepared by Gel Drawing" by N. Kaiya, A. Takahara, and T. Kajiyama, *Polymer J.*, 22, 1990, 859.

A. Tenteris-Noebe: Review of the book **Introduction to Plastics and Composites Mechanical Properties and Engineering Applications**, by Edward Miller, for *Materials and Manufacturing Processes*, 11, 1996, pp. 891-892.

A. Tenteris-Noebe and Dr. Frank N. Kelley, "Structure-Property Relationships in Bismaleimides", presented at The College of Polymer Science and Polymer Engineering, Sponsor's Day Symposium, October 24, 1996.

ACKNOWLEDGMENTS

There are many people that I have to acknowledge and thank for all of their help and support during this research effort. I sincerely acknowledge and am indebted to Dr. Frank Kelley for his help, support, and guidance throughout this project. He accepted my need for independence and was extremely patient with me throughout this investigation.

The second person who richly deserves my sincere gratitude is Dr. Gary Roberts for his help at NASA Lewis Research Center and his guidance on polyimides. The financial assistance for this research was supplied to us in a grant from NASA Lewis Research Center.

Several companies furnished the necessary material for this research: Shell Chemical Co, of Texas supplied BMI and Ciba Geigy Polymers, New York supplied DABA.

At NASA Lewis Research Center, a plethora of personal contributed to this research effort. My sincere thanks extend to: H. Eakin, D. Schiemann, L. McCorkle,

P. Dickerson, J. Kamvouris, V. Klans, T. Leonhardt, M. Miller, A. Garg, and M. Meador.

Dr. Kelley and I would like to gratefully acknowledge Wright Patterson Air Force Base and specifically, Dr. Allan Crasto, K. Lindsay, and W. Price for their help while I was at WPAFB. The use of their laboratories greatly aided in the completion of this work.

I want to thank Dr. Galiatsatos for his contributions to this work. In the dielectric work, Xiaofeng Xu greatly aided in the experimentation while Jeff Sherman helped with the modelling.

I would like to thank the supporting cast of RoseMary Kolton, Paul Easterling, Linda Seib, Brian Gudhe, Jeremy Jones, Justin Spradley and Jeff Deisz Sr for their help and assistance.

I would like to thank the Tenteris and Noebe families for all their support, encouragement, and love. I would also like to thank Helen Witkowski for her wisdom and guidance.

Last but not in the least, I would like to acknowledge and thank Ron. His help, guidance, patience and knowledge in putting this dissertation together were invaluable. I could not have finished this research without him.

DEDICATION

This is dedicated to the four men in my life. The first man has cared for me all my life, faults and all. When I was in the darkest, deepest, black hole, the second man lifted me on his shoulders and carried me around until I could almost see daylight. The third man gave me his hand, pulled me up out of the hole, and pointed me in the direction of the mountain. The fourth person put his arm around my shoulders and led me to the top of this mountain. These four men were and always will be my mentors, my heroes, and most of all, my friends. Thank you.

ABSTRACT

The purpose of this research was to control and systematically vary the network topology of bismaleimides through cure temperature and chemistry (addition of various coreactants) and subsequently attempt to determine structure-mechanical property relationships. Characterization of the bismaleimide structures by dielectric, rheological, and thermal analyses, and density measurements was subsequently correlated with mechanical properties such as modulus, yield strength, fracture energy, and stress relaxation.

The model material used in this investigation was 4,4'-bismaleimidodiphenyl methane (BMI). BMI was coreacted with either 4,4'-methylene dianiline (MDA), o,o'-diallyl bisphenol A (DABA) from Ciba Geigy, or diamino diphenyl sulfone (DDS). Three cure paths were employed: a low-temperature cure of 140 °C where chain extension should predominate, a high-temperature cure of 220 °C where both chain extension and crosslinking should occur

simultaneously, and a low-temperature (140 °C) cure followed immediately by a high-temperature (220 °C) cure where the chain extension reaction or amine addition precedes BMI homopolymerization or crosslinking. Samples of cured and postcured PMR-15 were also tested to determine the effects of postcuring on the mechanical properties.

The low-temperature cure condition of BMI/MDA exhibited the highest modulus values for a given mole fraction of BMI with the modulus decreasing with decreasing concentration of BMI. The higher elastic modulus is the result of steric hindrance by unreacted BMI molecules in the glassy state. The moduli values for the high- and low/high-temperature cure conditions of BMI/MDA decreased as the amount of diamine increased. All the moduli values mimic the yield strength and density trends.

For the high-temperature cure condition, the room-temperature modulus remained constant with decreasing mole fraction of BMI for the BMI/DABA and BMI/DDS systems. Postcuring PMR-15 increases the modulus over that of the cured material even though density values of cured and postcured PMR were essentially the same.

Preliminary results of a continuous and intermittent stress relaxation experiment for BMI:MDA in a 2:1 molar

ratio indicate that crosslinking is occurring when the sample is in the undeformed state.

Computer simulation of properties such as density, glass transition temperature, and modulus for the low-temperature cure conditions of BMI/MDA and BMI/DABA were completed. The computer modeling was used to help further understand and confirm the structure characterization results. The simulations correctly predicted the trends of these properties versus mole fraction BMI and were extended to other BMI/diamine systems.

TABLE OF CONTENTS

CHAPTER Page

LIST OF TABLES

LIST OF FIGURES

CHAPTER I

INTRODUCTION

One of the oldest and most useful types of polymers in modern technology is the crosslinked polymer network or thermoset. Thermosets are polymeric materials, which, when heated, form permanent network structures via the formation of intermolecular crosslinks between chains. Due to their network structure, thermosets exhibit good dimensional stability, resist viscous flow at elevated temperatures, and are considered water and solvent resistant. Therefore, thermosets fill many common engineering needs for structural applications, usually at elevated temperatures.

Epoxies have been the most widely used and extensively studied class of thermosets. They are easy to handle and process. However, there are several problems associated with epoxies. For one, their upper use temperature is approximately 180 °C, which limits applications to non-thermally critical structural parts. Another detrimental feature is their low resistance to brittle fracture.

Many researchers have tried to determine the mechanisms responsible for this low fracture resistance in an effort to correct this deficiency. But because of the intractable nature of epoxies, direct structural characterization is extremely difficult. Therefore, the structure-property relationships of epoxies and glassy thermosets in general are not so well understood. The increasing use of crosslinked polymers for critical and demanding engineering applications requires better fundamental knowledge of the molecular network and the relationships between processing and mechanical properties.

LeMay[1] and Swetlin[2] investigated the effects of crosslink density on fracture and the fracture processes of highly crosslinked epoxy networks. Mudrich[3] studied the crack tip plastic zone in epoxies with plane strain constraints, while Ajbani[4] incorporated alumina and rubber particles in fiber reinforced epoxy composites and determined the crack speed during fracture. One interesting discovery in the epoxy work was made by LeMay[1], who found a 1/2 power dependence when he plotted the arrest values of fracture energy versus M_c, the number average molecular weight between crosslinks. He concluded that the fracture energy of epoxies is related to the plastic zone size, which is determined by crosslink density.

There has been an increased effort in the development of high temperature, high performance resin systems. Uses include advanced composite matrices for commercial and military aircraft structures. Seemingly every day a new and improved polyimide is discovered to meet the challenges of advanced composites. One relatively new class of addition polymers is the bismaleimides, (BMI). BMI's were developed for applications requiring higher temperatures than the thermal capabilities of epoxy matrix systems. Bismaleimides display excellent processability and excellent thermal and mechanical properties. Sometimes BMI's have been added to epoxies to improve T_g and thermal stability. BMI's by themselves are inherently brittle; they are usually reacted with a chain extender in order to increase the molecular weight between crosslinks. However, BMI's have been bypassed as a potential candidate for advanced composites due to their brittle behavior, weight loss at elevated temperatures, and observed microcracking.

At the start this research, a model thermosetting system was sought, for which the structure-property relationships could potentially be investigated in the same manner as epoxies have been historically examined. Two papers by Donnellan and Roylance[5,6] were recently published on the properties of BMI and methylene dianiline (MDA). The fracture data was replotted against the estimated molecular

weight between crosslinks and a ½ power dependence was found. This was a promising sign in the search for a model resin system to study.

The BMI/MDA system is cure path dependent. By varying the reactant ratios or by changing the cure path, the structure of the network formed will be affected, which in turn, will influence the thermal and mechanical properties of the resin. A schematic of the cure schedules and expected structures is shown in Figure 1.1. If the BMI/MDA is cured at low temperatures, chain extension would be the predominate reaction and result in linear chains of BMI/MDA with few or no crosslinks. When BMI/MDA is cured at high temperatures only, there would be simultaneous chain extension and crosslinking occurring. The resultant network would have short chains with network defects. Finally, if the BMI/MDA system were cured at low temperature to promote chain extension and then cured at high temperature to crosslink the linear chains of BMI/MDA, a cross-linked network would form with long chains and minimal chain defects. Even though BMI has been investigated before, the quantitative dependence of the physical properties on the network topology is undetermined, mainly due to the lack of adequate characterization techniques for densely crosslinked materials.

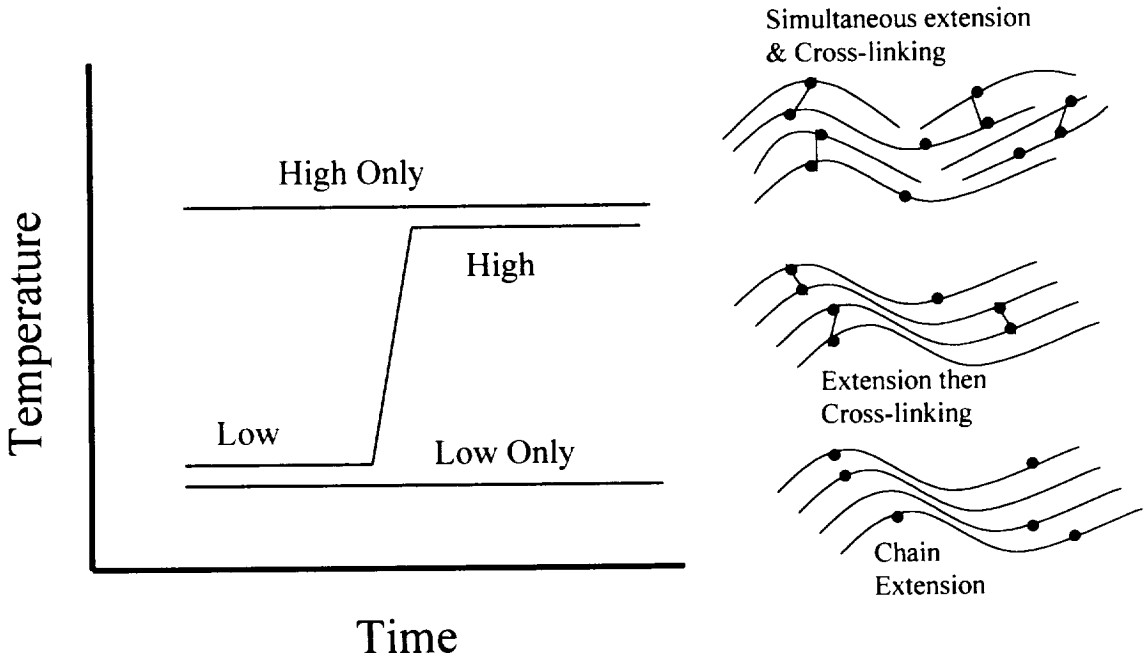

Figure 1.1. Schematic representation of the cure schedules and expected network structures under investigation.

The purpose of this research was to determine the structure-property relationships of BMI by changing the cure histories, the reactants, and the reactant ratios and examining these effects on thermal and mechanical properties. Two diamines and a chain extender were used in conjunction with BMI in varying mole ratios. The specific objectives of this research were: to monitor the curing reactions of the bismaleimide and the crosslinking agent, to apply the same type of experimental techniques used previously in epoxy research to bismaleimides, and to test the predictive capacities of the Synthia module of Biosym Technologies.[7]

The methodology used is shown in Figure 1.2. Curing reactions were monitored with dielectric analysis, differential scanning calorimetry, and TGA/FTIR. The effects of each curing condition on T_g, density, and the mechanical properties were determined. Samples of cured and postcured PMR, supplied by NASA Lewis Research Center were also tested in the same manner. PMR is the acronym for polymerization of monomer reactants and is considered one of the leading commercial polyimides in the aerospace industry.[8]

Relevant epoxy research and previous work on BMI's are reviewed in Chapter 2. The experimental procedures and conditions under which each technique was employed are

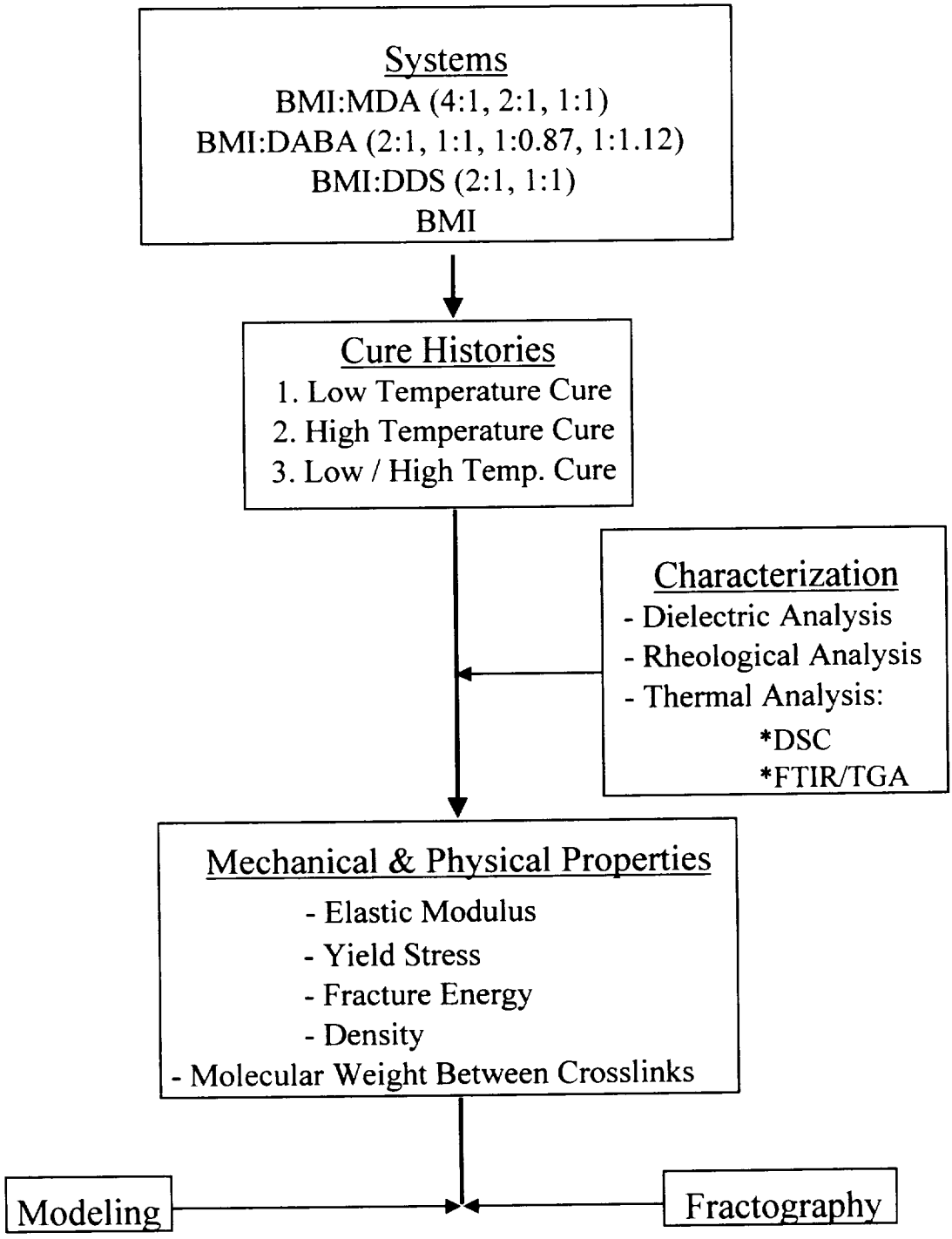

Figure 1.2. Outline of the methodology used in this research.

discussed in Chapter 3. The results and discussion are described in Chapter 4. Finally, in Chapter 5, a summary of this work plus recommendations for future work is presented.

CHAPTER II

HISTORICAL REVIEW

2.1. Introduction

Thermosetting polymers are being used in adhesive as well as structural applications. Therefore, a complete understanding of the mechanical behavior and especially fracture properties of thermosetting polymers is very important. There are several major variables that affect the fracture properties of thermosets: type of resin and curing agent used, amount of curing agent, and the cure schedule (times and temperatures). All affect the crosslink density of the material and ultimately its mechanical behavior. The purpose of this dissertation is to add to the understanding of structure-property relationships in thermosets by studying a model polyimide system.

2.2. Epoxies

Of all the thermoset systems, epoxies have been much more widely studied, especially in terms of structure-property relationships. However, it is difficult to

correlate the fracture property results from a variety of studies that used different epoxy resins, cured under dissimilar conditions. Vakil and Martin[9] studied the yield strength and the fracture energies of a series of crosslinked epoxy resins. They found that the most densely crosslinked network had the highest yield strength and that the yield stress decreased as the molecular weight between crosslinks increased. Also, the initiation and arrest values of the fracture energy both increased as the molecular weight between crosslinks increased.

Epoxies can be polymerized with many different crosslinking agents. The type of crosslinking agent and the amount used can influence the physical properties of epoxies. Phillips et al.[10] found that the amine type influenced the fracture behavior of DGEBA (diglycidyl ether of Bisphenol A) epoxies. They investigated stoichiometric amounts of DGEBA cured with two different series of aliphatic amines. The first was a difunctional primary diamine and the second diamine studied was a polyfunctional diamine. They found that the fracture initiation energy of the DGEBA/primary diamine series increased as the molecular weight of the curing agent increased. The fracture initiation values for the mixed amine series was independent of molecular weight. They determined that the crosslink density of the mixed amine series did not change because the

molecular distance between the amines remained constant even though the amine molecular weight increased.

The effect of crosslink density on the properties of epoxies has been studied primarily by varying the epoxy/curing agent ratio. The ratio of crosslinking agent to epoxy resin is usually reported as A/E where 'A' is the number of moles of amine hydrogen atoms in the curing agent and 'E' is the number of moles of epoxide endgroups in the epoxy. Many researchers have investigated the effect of reactant ratio on the physical properties and fracture behavior of epoxy systems. Meyers et al.[11] varied the A/E ratio for DGEBA and DDS and determined that for A/E = 1, T_g and crosslink density was highest. The epoxy-rich system exhibited the highest room-temperature flexural modulus and flexural stress. Gupta et al.[12] varied the A/E ratio for DGEBA and meta-phenylene diamine and found similar results for the modulus and the tensile stress.

On the other hand, Kim et al.[13] studied a series of Epon epoxies coreacted with MDA and found that the ultimate tensile properties were "relatively" insensitive to stoichiometry over a wide range of A/E ratios. The tensile stress did show a slight minima at A/E = 1. Many of the investigators used A/E ratio as an effective way to vary crosslink density. However, the results, all pooled together, prove that using A/E ratio for epoxies is not

always an appropriate way to change the crosslink density and to determine the structure-property relationships of epoxies.

The final way to vary the structure of the network is by controlling the curing times and/or temperatures. By altering the curing temperature, the reaction kinetics of the developing network are affected. Chang et al.[14] tried to vary the crosslink density over a wide range to determine the effect of crosslinking on the physical properties. They used a fixed stoichiometric amount of DGEBA and DDS. In effect, they regulated the extent of cure by controlling the curing conditions. As the postcuring time increased, the extent of cure, density, and modulus increased. However, it is difficult to use cure schedules to control structure. While the structure may change appreciably with different temperatures and cure times, the network structure can not be realistically qualified or quantified. Consequently, while a great deal of work has been done to characterize the fracture of epoxies, most studies listed above, have been performed by varying the curing agents, curing conditions, or reactant ratios without fully understanding the resultant changes in structure.

Swetlin[2] and LeMay[1] examined the effects of crosslink density in DGEBA epoxy resins, crosslinked with MDA or DDS, on various physical properties. They systematically varied

M_c by curing with stoichiometric and nonstoichiometric amounts of epoxy and crosslinking agents. This was significant because they created a series of homologous epoxy networks, whose networks varied by endlinking chemistry rather than nonstoichiometric reactions.[15] Network M_c's were determined by measuring the near-equilibrium rubbery modulus in tension at temperatures above the T_g.

They determined that stoichiometric amounts of epoxy and crosslinking agent had the tightest network and that M_c was nearly equal to M_n for Epon 828/MDA.[1,2] For nonstoichiometric concentrations of epoxy and curing agent, M_c increased as the epoxy/curing agent ratio moved farther from 1:1 or stoichiometry.

The effective molecular weight between crosslinks, M_c, can be calculated from equilibrium rubbery modulus measurements when they are performed well above T_g. The experimental concept and calculation of M_c are based on the theory of rubbery elasticity where:

$$M_c = \frac{\Phi \rho R T}{G_e} \qquad (2.1)$$

Φ is the front factor, assumed to be unity, which is the ratio of the mean square end to end distance of a matrix chain between crosslinks to an equivalent random coiled chain. ρ is the sample's density, R is the gas constant, T

is the test temperature in Kelvin, and G_e is the rubbery shear modulus. The theory predicts that M_c or the level of crosslinking is inversely proportional to G_e. When the tests are performed in tension and the sample is considered in a rubbery state, G_e is estimated as $E_e/3$ because deformation at constant volume is assumed.

However, some researchers have assumed that G_e is equivalent to the equilibrium elastic shear modulus, when the value is determined from dynamic shear measurements. They assumed that Equation 2.1 is valid even though the tests were performed dynamically. It is not absolutely valid to assume this approach, especially for polyimides, which are notorious for G' minimas not plateau values.[6,16]

Another interesting discovery by LeMay[1] was a 1/2 - power dependence in the arrest fracture energies and M_c. This implied that the ultimate fracture properties of the epoxy system he was studying were proportional to the plastic zone size. This indicated that the chains in front of a crack tip undergo yielding and dissipate energy during extension.

2.3. Polyimides

Another class of thermosets with significant technological applications is the high-temperature polyimides. Polyimides are derived from monomers containing

the maleimide functionality.[17] The synthesis route of the monomer to fully cured polyimide dictates the type of polyimide: condensation or addition.

2.3.1. Condensation Polyimides

Condensation polymerization involves the reaction of a soluble polyamic acid precursor and a final cyclization step for the end product. Maintaining high purity for the solvent and reactants is required to obtain high molecular weight polymers. The ratio of the reactants is also a critical variable in condensation polymerization. Volatiles generated during the cyclization reaction can cause the formation of voids during processing. Condensation polyimides are known for their high-temperature stability, but are, at times, difficult to process into useable shapes.

2.3.2. Addition Polyimides

The second type of polyimide is addition polyimides that are formed by the polymerization of low molecular weight polyimide resins. Contrary to condensation polymerization of polyimides, addition polymerization does not evolve byproducts. (Though, during composite processing, solvent is usually used to reduce the viscosity of the resin during prepregging.) Stenzenberger[18] outlines three types or classes of addition polyimides: acetylene-terminated oligomers, PMR-polyimides, and Bismaleimides.

2.3.2.1. Acetylene-Terminated Oligomers

Hughes Aircraft Company developed the acetylene-terminated polyimides in the 1970's.[8] These resins are produced by a two-step reaction process. In the first stage, the acetylene-terminating group is the reaction site. Since it is sterically unhindered, these reactive groups will react very quickly by free radical polymerization. In a very short period of time, a linear structure is formed. When high temperature is reached, the reaction forms a crosslinked network. Small processing windows are the result of fast reaction rates, which usually produce a matrix filled with voids.

2.3.2.2. PMR Polyimides

PMR (polymerization of monomeric reactants) polyimides are considered one of the leading commercial polyimides in the aerospace industry. PMR was developed in the 1970's at NASA Lewis Research Center.[8] PMR consists of three components: 5-norbornene-2, 3-dicarboxylic acid monomethyl ester (NE), dimethyl ester of 3,3', 4,4'-benzophenone-tetracarboxylic acid (BTDE), and 4,4'-methylene dianiline (MDA). The chemical structures of NE, BTDE, and MDA are shown in Figure 2.1. The polymerization of PMR is considered a two-step process. Short chains of imide oligomers with norbornene endcaps are formed in the first step when NE, BTDE, and MDA are combined in molar ratios of

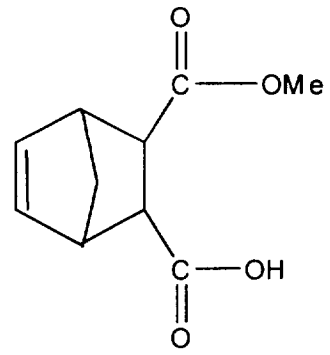

a.) Monomethyl ester of 5-norbornene-2, 3-dicarboxylic acid
(NE)

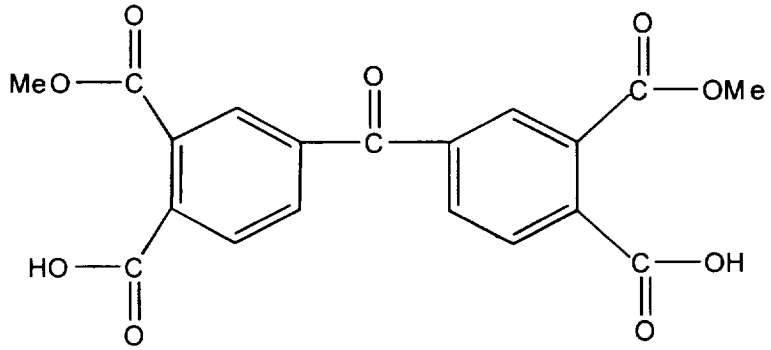

b.) Dimethyl ester of 3,3', 4,4'-benzophenone-tetracarboxylic acid
(BTDE)

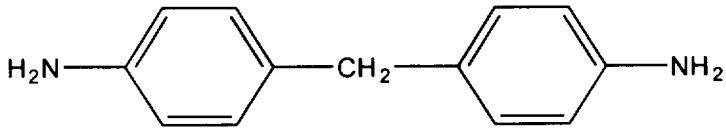

c.) 4,4'-Methylenedianiline
(MDA)

Figure 2.1. The chemical structures of a.) NE, b.) BTDE, and c.) MDA.

2/2.087/3.087. (The formulated molecular weight, FMWT, is calculated to be 1500. Hence, the designation of PMR is PMR-15.) In the second reaction step the norbornene endcaps are reacted to form a crosslinked network.

For composite processing, the three monomers are usually dissolved in a low-boiling point alkyl alcohol.[8] This solution is impregnated within the reinforcing fibers and allowed to polymerize *in-situ*. Since a low-boiling point solvent is used with the low molecular weight monomers, little to no evolution of volatile materials occurs during the final cure step. PMR-15 is easily processed, has good mechanical properties, even at elevated temperatures, and is known for its excellent thermo-oxidative stability.

For neat resin plates of PMR-15, commercially available imidized PMR-15 powder is used. In this investigation, four neat PMR-15 plates were received from NASA Lewis Research Center. These were molded from imidized PMR-15 powder at the appropriate cure schedules. Two of the four plates were given a postcuring treatment.

2.3.2.3. Bismaleimides

Bismaleimides, BMI, are the third type of addition polyimides.[18] BMI's are like epoxies in that they can be processed at fairly low temperatures with little pressure. BMI's can be processed by a variety of techniques such as

autoclave or resin transfer molding (RTM) for composite applications.

Bismaleimide monomer is prepared from the reaction of maleic anhydride and a diamine.[18] The general structure of BMI is shown in Figure 2.2 where R' can be an aromatic or an aliphatic molecule, depending upon the diamine used to synthesize BMI. 4,4' Bismaleimidodiphenyl methane from the diamine MDA is the most common and is commercially available.

The aromatic nature of the BMI imparts thermal stability to the resultant polymer while the imide moiety adds rigidity. However, a major drawback of cured neat BMI is its inherent brittleness due to a high crosslink density and therefore, it is not used in structural applications by itself. Bismaleimides are, therefore, reacted with aromatic diamines to increase the molecular weight between crosslinks, but at the expense of thermal stability. The type of diamine used as a chain extender can vary depending upon the properties required in a specific application.

The reactivity of the double bond in the maleimide group is a consequence of the electron withdrawing nature of the two adjacent carbonyl groups, which create an electron deficient double bond.[19] Therefore, bismaleimides are very susceptible to homopolymerization and co-polymerization.

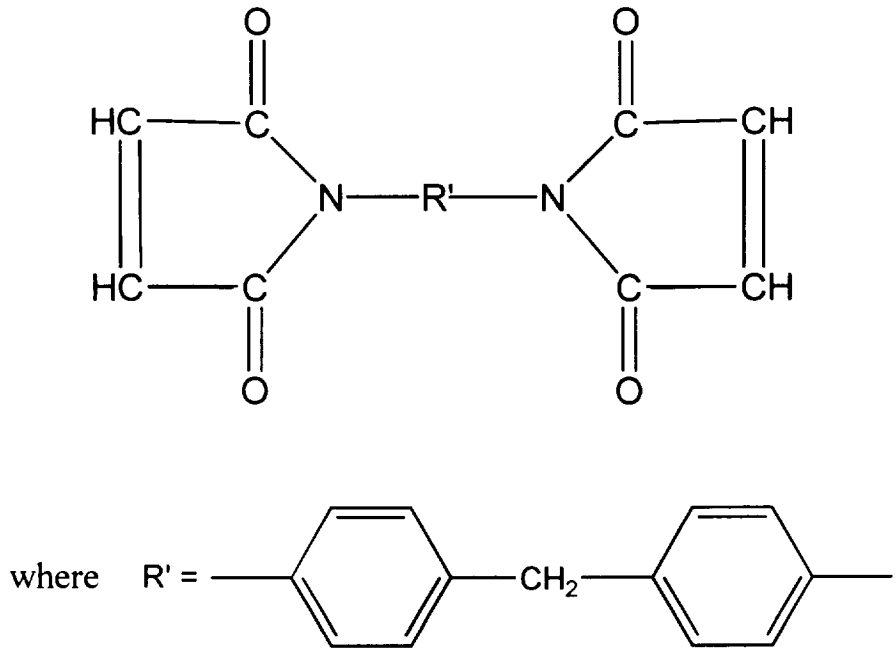

Figure 2.2. The general structure of BMI.

Generally, most BMI resins do not fully cure until they reach temperatures of 205 to 260 °C.

2.3.2.3.1. Chemistry of BMI/Diamine

There are two chemical reactions that occur during the polymerization of a bismaleimide with an amine: amine addition and bismaleimide homopolymerization.[19] The amine addition to the maleimide double bond, or the chain extension reaction, occurs by a second order mechanism and results in extension of the network chains.[20] Figure 2.3a illustrates the chain extension reaction between BMI and a diamine.

The second reaction, which occurs in the bismaleimide polymerization, is the homopolymerization reaction of the maleimide double bonds. It is a thermally initiated, multistep radical mechanism that leads to crosslinking.[20] Again, the maleimide double bonds of the bismaleimide are weakened by the electron withdrawing nature of the adjacent carbonyl groups and they readily react in the molten state by free radical polymerization.[21] The homopolymerization reaction of BMI is shown in Figure 2.3b.

The chain propagation of BMI is slower than the initiation or termination steps and is therefore, considered the rate-controlling step.[20] Since the amine addition is a one-step reaction and occurs more rapidly than the chain propagation of the bismaleimide homopolymerization, at low

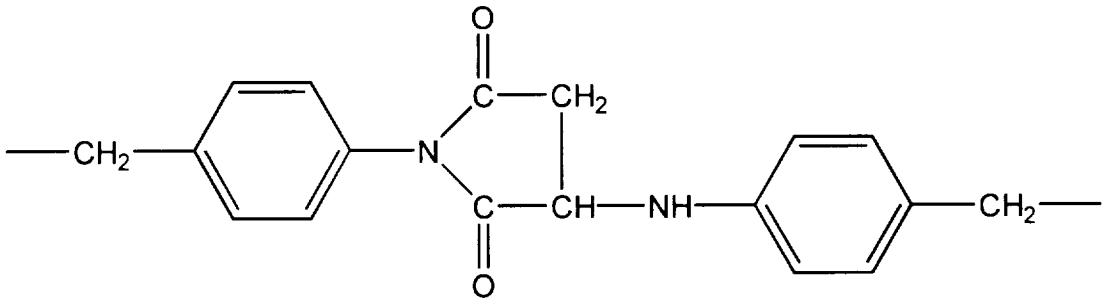

a.) Chain extension due to Amine addition

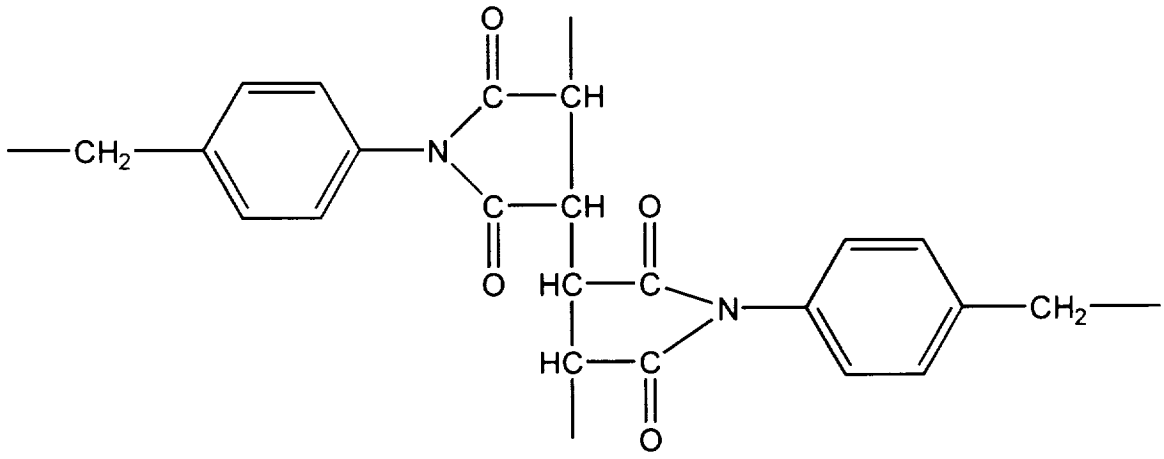

b.) Crosslinking due to homopolymerization

Figure 2.3 Chemical reactions that occur during the polymerization of a bismaleimide with an amine: a.) amine addition and b.) bismaleimide homopolymerization.

temperatures, the chain extension reaction is favored over the homopolymerization reaction. However, the propagation reaction becomes competitive with the amine addition reaction at high temperatures.

The rates of amine addition and homopolymerization reactions determine the network topology during the early stages of cure. The amine addition is an order of magnitude faster than the BMI homopolymerization reaction and occurs until most of the amine is consumed, which reduces the crosslink density of the final network.[20,22]

2.3.2.3.1.1. temperature effects

The two reactions have different effects on the topology of the network formed. The nucleophillic addition of the amine to the maleimide double bond occurs readily at low temperatures. Tungare and Martin[20] found that the amine addition occurs at 125 °C and that above 150 °C, the crosslinking reaction competes with the chain extension reaction. Donnellan and Roylance,[5] determined from FTIR analysis that only the chain extension reaction occurs readily up to 145 °C. In the temperature range of approximately 130-180 °C, chain extension is favored over the homopolymerization or crosslinking reaction. This does not mean that some initial crosslinking does not occur, however.

During a high-temperature cure, at greater than 180 °C, both reactions occur simultaneously, but with different rate constants. This leads to the formation of a fully connected network at the gel point. The reactions continue to occur but become diffusion controlled rather than chemically controlled.[23]

Cure to completion in bismaleimides is often not possible because conversion of liquefied monomer to a highly crosslinked glassy matrix is limited by the restricted translational movement of unsaturated imide groups.[24] The cure reaction ceases at a certain degree even though there are many active functional groups still present. The bulk viscosity increases with the increase in chain branching, and finally crosslinking, which restricts the mobility of the functional groups.

With two different reactions, one may use different temperature regions for cure. In the low-temperature regime, the amine addition reaction will predominate. In the high-temperature region, both the amine and homopolymerization reactions can occur, possibly resulting in a tight, inflexible network. Finally, with a two-step cure, the amine addition reaction can occur at low temperatures followed by the homopolymerization reaction at high temperatures.

2.3.2.3.1.2. transition temperature

The temperature of cure plays a very important role in forming the network. As the cure proceeds at a given temperature, a network develops and its T_g increases. However, when the T_g of the network reaches the cure temperature, the rate of further cure or crosslinking is drastically reduced because of the slowing of reactant diffusion. If the specimen is then heated to above its original cure temperature, additional curing may occur. Therefore, the cure temperature should be higher than the maximum use temperature if a stable network is desired during testing.[25]

The glass transition temperature is a property that can be used to estimate network development and is dependent on the curing chemistry of the resin. When a resin system cures by only one reaction, the T_g is a function of the extent of reaction or cure and is independent of curing conditions. The curing of BMI resins involve two reactions, amine addition and BMI homopolymerization. Therefore, the glass transition temperature is dependent on two types of reaction, which in turn, are dependent on resin composition and curing conditions.

For a particular cure temperature, T_g initially rises as a function of cure time, but eventually reaches a limiting value. The magnitude of this value depends on the

cure temperature: the higher the cure temperature, the higher the final T_g.

With additional heat, such as that applied during postcuring, the T_g of a material prepared by a low-temperature cure can attain and surpass that of a corresponding intermediate-temperature cured material. When postcured, the unreacted BMI molecules undergo homopolymerization and network rearrangement. Therefore, a large, rapid increase in T_g is observable.

Tungare[22] showed by experimentation and computer modeling that a significant increase in T_g is observed from the cured state to the postcured state. The large difference in T_g occurs due to the curing conditions or cure-path dependence of the network. During a short-time, low-temperature cure, most of the amine is depleted with BMI. However, some BMI remains unreacted in the resin. The unreacted BMI in the polymer reacts with the previously extended chains during the postcuring reaction and the T_g increases dramatically. During a long-time, low-temperature cure more BMI is consumed. Therefore, there is less opportunity for crosslinking during postcure and the T_g does not increase as much as in the previous case.

Several researchers have used thermal and mechanical properties to characterize the state of cure of BMI to determine the cure path dependence of the properties. Leung

et al.[26] found that the T_g, tensile stress, and fracture energy increased as the cure temperature increased from 130 °C to 180 °C, even though the extents of reaction, as determined by DSC, were the same. Therefore, they concluded that different network structures formed at different curing temperatures.

2.3.2.3.1.3. reactant ratios

Resin composition governs the rate of amine addition and BMI homopolymerization reactions. Stoichiometric reaction of BMI and a diamine leads to the formation of linear chains with few crosslinks.[27] With BMI in excess, the coreaction of BMI with a diamine results in a crosslinkable resin.

Leung et al.[28] determined the effects of resin composition on T_g. As the concentration of BMI increases from 1:1 to a 2:1 mole ratio, the T_g increases. Tung[29] measured the fracture energy of various BMI/MDA copolymers at two different cure temperatures. The fracture energy decreased as the concentration of BMI increased. Fracture energy increased with the two-step cure temperature over just high-temperature cure alone.

2.3.2.3.2. Chemistry of BMI/Alkenylphenols

Because BMI is inherently brittle when reacted with itself, diamines have been used to increase the molecular weight between crosslinks. In recent years, chain extenders

other than diamines have also been developed and reacted with BMI in order to lengthen the chains between crosslinks. A new system was introduced by Ciba-Geigy in the 1980's, which consists of a two-component bismaleimide resin: 4,4'-bismaleimidodiphenyl methane (BMI) and o,o'-diallylbisphenol A (DABA). The structure of DABA is shown in Figure 2.4. This figure shows the common bisphenol A with two allyl functions attached to it. This system is attractive because DABA is a liquid at room temperature and will facilitate the melting of BMI when heated to the appropriate temperatures.

Morgan et al.[30] report that the reaction scheme for BMI/DABA consists of an addition reaction occurring between the allyl groups that are attached to an aromatic ring and the double bond of the maleimide. These will undergo an 'ene' type linear chain reaction. The resulting "substituted styrene" undergoes a Diels-Alder reaction with another maleimide group. The reaction of a diene with a dienophile, resulting in a ring-containing compound is the Diels-Alder reaction. Once the two components have reacted, the BMI/DABA 'ene' adduct prepolymer is considered pentafunctional: three double bonds, capable of chain extension and crosslinking and two hydroxyl groups, capable of etherification by hydroxyl dehydration. A schematic of this pentafunctional prepolymer is shown in Figure 2.5.

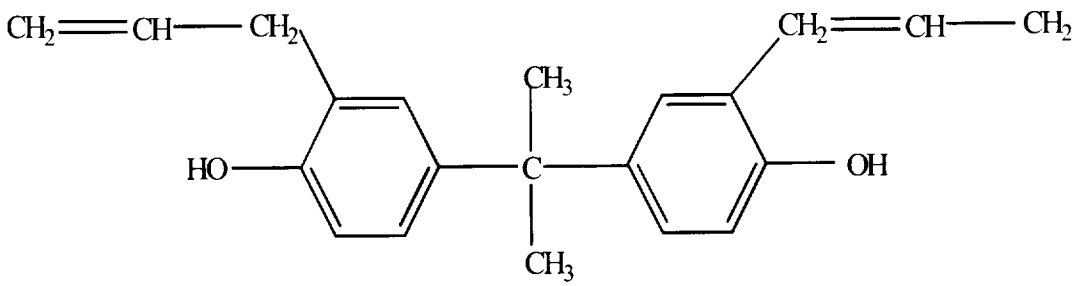

o,o'-Diallyl bisphenol A
(DABA)

Figure 2.4. The chemical structure of DABA.

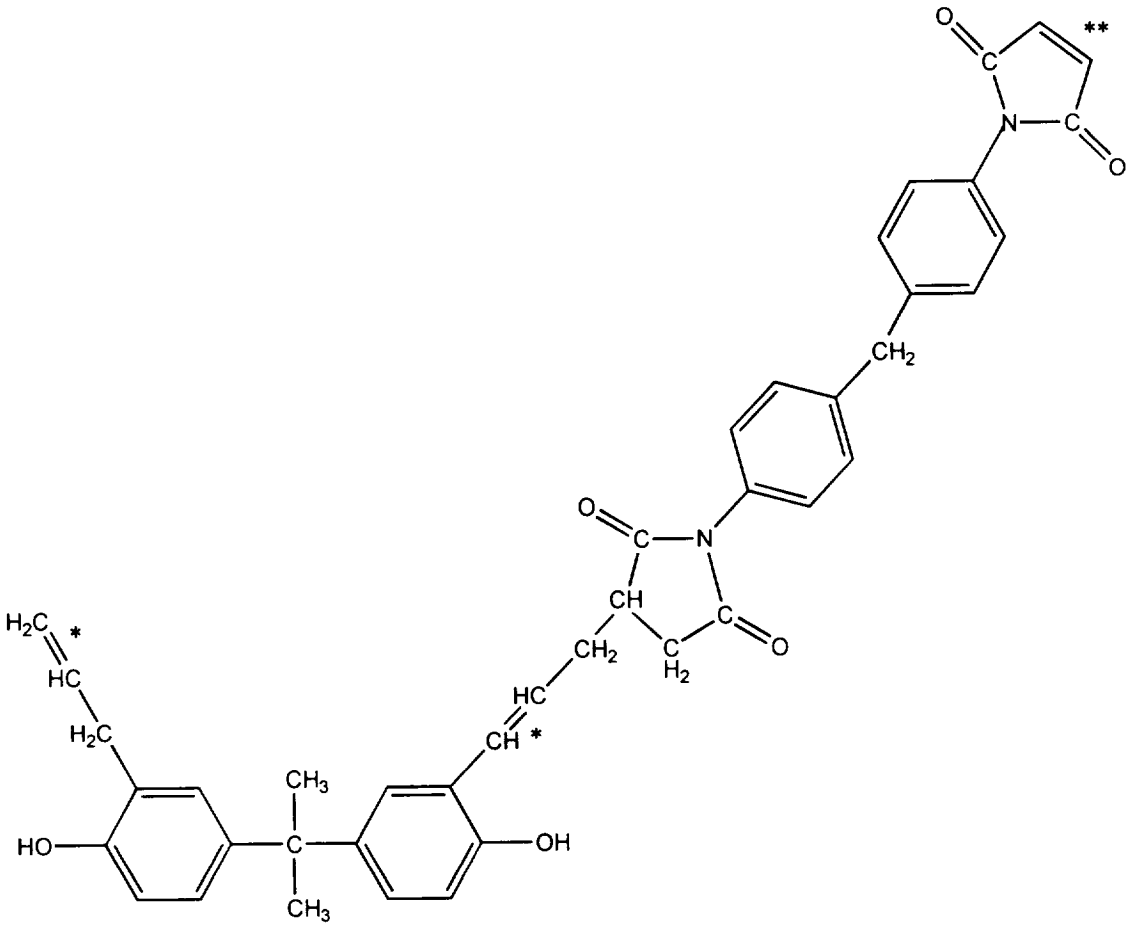

* "ENE" double bond polymerization

** BMI double bond polymerization

Figure 2.5. Schematic illustration of the pentafunctional prepolymer of BMI/DABA.

2.3.2.3.2.1. temperature effects

There are three temperature ranges associated with the cure reactions in the BMI/DABA system, as determined by FTIR spectroscopy and DSC:[30] 1.) 100-200 °C, 2.) 200-300 °C, and 3.) 300-350 °C. In the 100-200 °C range, the 'ene' reaction occurs between the allyl groups and the double bond of the maleimide. There are three active double bond sites capable of polymerization, as well as two hydroxyl groups, making the prepolymer a pentafunctional chain.

In the 200-300 °C range several reactions occur in the following sequence: 1.) 'ene' reaction at a significant rate, 2.) BMI homopolymerization, which occurs at approximately 210 °C, 3.) 'ene' homopolymerization and the Diels-Alder reaction, at approximately 255 °C, and 4.) Above 240 °C, dehydration of the hydroxyl groups that form ether crosslinks.

In the 300-350 °C range, further cure occurs as the test temperature approaches the glass transition temperature of the material. Therefore, by manipulating the curing temperatures, the network topologies may be controlled for the BMI/Alkenylphenol system.

Recently there has been some debate over the reaction of BMI with DABA. The reaction mechanism is not necessarily in question, but the temperature ranges over which these

reactions occur are in doubt. Mijovic and Andjelic[31] determined with FTIR spectroscopy that the principle reaction in the temperature range of 140 to 200 °C was the copolymerization between the maleimide and the allyl double bonds, a chain extension 'ene' reaction. They determined that the 'ene' reaction was the only one that involved double bonds below 200 °C until all of the double bonds were consumed. At about 180 °C, the etherification reaction involving two -OH groups occurs, which controls the crosslink density of the system. Finally, at temperatures above 200 °C, the homopolymerization reaction of BMI occurs. Yet regardless of the number of specific chemical reactions occurring, BMI/DABA is basically considered a two-step reaction: chain extension by an 'ene' reaction and BMI homopolymerization.

2.3.2.3.3. Mechanical Properties of Bismaleimides

Because of the need to fulfill aerospace needs, many of the polyimides synthesized have been mechanically tested at room temperature and at the upper use temperature. Strain rates and test temperatures have not been extensively varied to determine the viscoelastic properties. As with epoxies, investigators have studied BMI with different chain extenders by varying the resin composition, cure schedule,

and cure history to determine the room temperature mechanical properties.

Tung et al.[29] found that the fracture energies for samples that were cured by a two-step process were higher than the fracture energies for samples cured only at high temperatures. They attributed the difference in fracture energies for a given mole ratio to network topology differences.

Donnellan and Roylance[6] also investigated the effects of changing the resin composition and cure schedule on BMI and MDA. They found that by increasing the amount of BMI in the composition the density, yield stress, and modulus increase while the free volume and fracture toughness decrease. The ability to yield is the controlling factor in fracture toughness. Yielding induces crack tip blunting which increases the energy needed for a crack to grow.

Compact tension fracture toughness data from Donnellan and Roylance[6] was replotted in this investigation as fracture energy versus the molecular weight between crosslinks, derived from rheological data, and a ½ -power dependence was obtained, Figure 2.6. This is the same result observed by LeMay[1] for epoxies even though LeMay plotted the log of the arrest values of fracture energies versus the log of the molecular weight between crosslinks, calculated from measurements of rubbery modulus. This

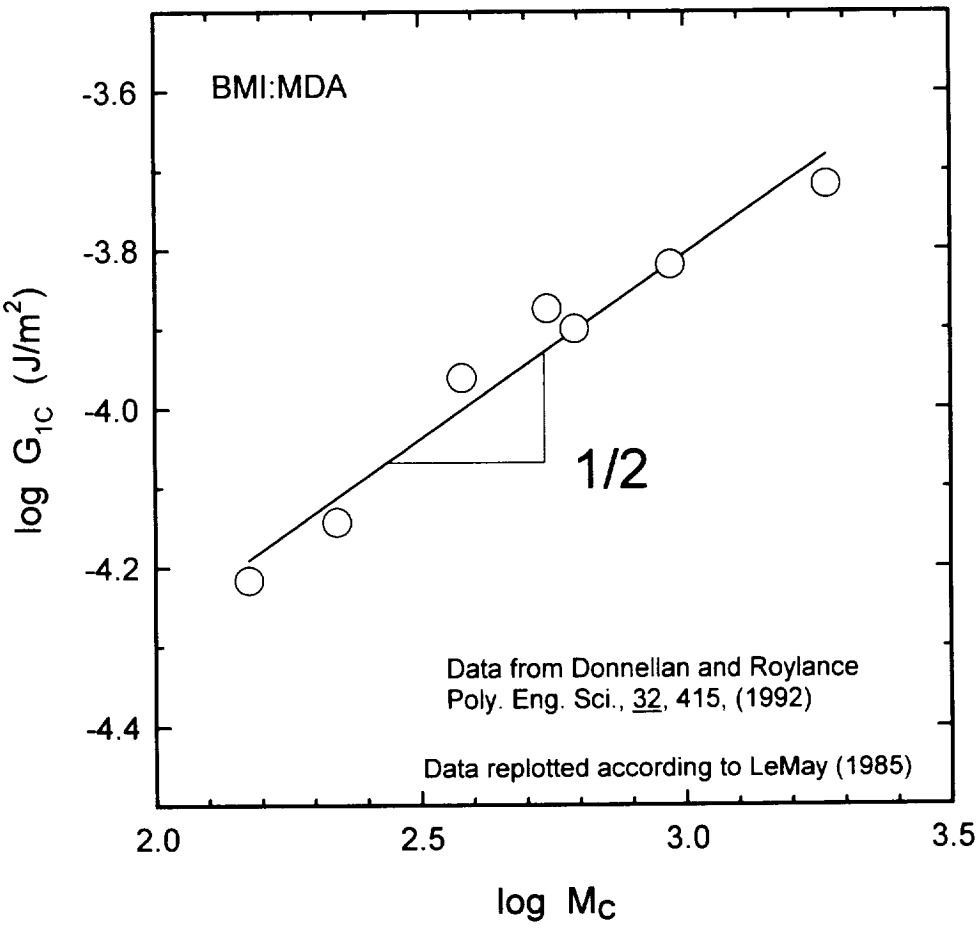

Figure 2.6. Compact tension fracture energies data from Donnellan and Roylance's investigation versus the molecular weight between crosslinks, derived from rheological data, resulting in a ½ -power dependence.

implies that the ductile yielding occurring at the crack tip controls the ultimate fracture properties of the BMI/MDA system.

The mechanical properties of DABA from various investigators have been hard to correlate with each other. The curing conditions all vary from study to study. Some investigators have even reported mechanical properties as a function of DABA without specifying cure conditions.[32] Ciba Geigy has recommended specific molar ratios and curing conditions when using their products. Generally, the room temperature mechanical properties for each formulation are similar. System II, (1:0.87 BMI:DABA) usually exhibits the highest fracture toughness and strength over the other formulations investigated.[33] Overall, according to Stenzenberger[32] the fracture energy increases with increasing amounts of DABA up to approximately 40% DABA while the modulus in flexure remains constant with increasing amounts of DABA.

2.4. Advanced Polymer Characterization Techniques

2.4.1. Continuous and Intermittent Stress Relaxation

When a polymer is tested above its T_g at several strain levels, in the rubbery state, the stress will decrease with time to asymptotic values. The plateau stress can be plotted against the strain values to obtain a near-

equilibrium stress-strain curve. The slope of this stress-strain plot is inversely proportional to M_c.

Stress relaxation experiments are also used to evaluate separately the effects of chain scission and crosslinking of polymers as they are related to changes in stress.[34] Stress will diminish with time during stress relaxation. In a continuous stress relaxation experiment, a constant deformation is applied to the specimen while the retractive force and changes in the retractive force with time are recorded. The force usually decreases with time. Initially, the decline is large due to conformational changes and alignment of polymer chains.[35]

Crosslinking reactions make no contribution to the retractive force measured by continuous stress relaxation.[35] For example, when a sample is "aged" at constant elongation, chain scission will result because a number of the chains will not be able to support the applied stress. If crosslinks do form in the stretched state, they will not contribute to support the stress.

Continuous and intermittent stress relaxation experiments are performed as complementary tests. In an intermittent stress relaxation experiment, the specimen is maintained in a relaxed, undeformed condition at the appropriate test temperature.[35] At widely spaced time intervals, a predetermined fixed deformation is applied to

the specimen and the instantaneous stress is measured. The specimen is unloaded until the next "time" at the appropriate test temperature. If the material is "aged" in the unstretched state and then stretched, the stress will reflect both chain scission and crosslinking. The peak value of stress at the different time intervals are recorded and plotted against the continuous stress relaxation experiment at the same fixed deformation.

In general, during an intermittent stress relaxation experiment, the sum of bond scission and crosslinking reactions is determined. When these reactions are equal, the peak values of stress are constant as a function of time and reversible network degradation is observed. If the peak values of stress diminish with time the bond scission reactions are predominant. Only irreversible network degradation occurs - no rearrangement reactions and no crosslinking reactions of any consequence are occurring. In this case, the continuous and intermittent stress relaxation curves have the same stress values with time. The peak values of stress increase with time when crosslinking reactions are predominant.[35] Crosslinking reactions are detected by intermittent stress relaxation with an increase in retractive forces because the network density increases while the continuous stress relaxation experiment is unaffected.

2.4.2. Frequency-Dependent Impedance Sensing Techniques

FDIMS techniques are useful characterization methods, which monitor the cure process of both thermoplastics and thermosets.[36] Dielectric analysis is one of the few methods available for studying the molecular properties of both solid and liquid states by using frequency dependence in the Hz to MHz range to separate the ionic and dipolar mobility.[37] This method of characterization is able to continuously monitor the curing process from a monomeric liquid to a crosslinked, insoluble high-temperature solid *in-situ* and relate the electric measurements to chemical changes in the polymeric structure.[38]

In structure-property relationship investigations, the mechanical and rheological properties of a material can be associated with macroscopic scale processes. Spectroscopic analysis such as FTIR focuses on the molecular or microscopic level. Dielectric analysis measures both the macroscopic and microscopic levels of polymeric behavior. Microscopically, dipoles orient during an alternating field. Macroscopically, the viscosity of the system and the tightness of the network as chains form affect the dipole orientation.[39] Dielectric analysis, however, has its weak points. There are insufficient models available to aid in the interpretation of data and a lack of correlation between

the data and other material characterization methods such as mechanical measurements.[40]

2.4.2.1. Electric Dipole Moments and Polarization

Dipole moments are called permanent electric dipole moments.[41] Dipole moments form in nonconducting molecules as a result of asymmetry of charges in the bonding electrons when atoms of different electon-negativities join, unequal sizes of the two orbitals being joined, or as the result of the hybrid character of the orbitals.

In an electric field, the nonconducting molecules' electrons will shift in the positive direction of the field. No continuous flow of electrons will occur since the electrons are centered about the nuclei. If the electric field is alternating, the electron cloud will "sway" back and forth, pivoting about its nucleus to keep up with the changing field. The nucleus will move in the negative direction, opposite to the direction of the electron cloud.

As a result of movements of the positive nucleus and the negative electrons, a polar atom is produced.[42] A molecule with positive and negative charged ends is called a dipole. In a very strong field, electrons can become displaced from the atom to produce ions.

Nonpolar molecules have symmetry of the distribution of charges and no permanent moment exists. Nonpolar molecules can acquire a dipole moment in the presence of an

alternating electric field. A distortion of the electron cloud, coupled with the relative displacement of the atomic nuclei produces electron and atomic polarizability.

2.4.2.2. Experimental Theory

A sample is placed between two conducting plates and a time-varying voltage of 1-2 volts is applied between the electrodes, whose spacing is less than the electrode area, creating an electric field in the sample.[43] If the electric field is on the order of 10^6 V/cm, a dielectric breakdown will occur. The time-varying current is measured as the response. The sample becomes polarized and can also conduct net charge from electrode to electrode.

An impedance bridge is used to measure the difficulty a material experiences in following an alternating current. Since the source function is current and the response is voltage, the system function is called impedance, designated as Z. The impedance at a frequency can be represented by an equivalent parallel capacitance, C, and conductance, G, circuit where:[38]

$$Z^{-1} = G + i\omega C \qquad (\omega=2\pi f) \qquad (2.2)$$

Since the electrical conductance of polymer resins is low and the capacitive properties are high, the geometry-dependent electrical measurements of G and C for polymers are expressed in terms of the complex permittivity ε^*, where

$\varepsilon^* = \varepsilon' - i\varepsilon''$. The complex permittivity is defined as the vector sum of the in-phase and out-of phase permittivity, analogous to G′ and G″ in dynamic mechanical testing. When a time-varying electric field is applied to a material, the dielectric constant, ε, can then be regarded as a complex number. ε' is the dielectric permittivity or the storage component and ε'' is the dielectric loss factor or the loss component. Furthermore, ε' and ε'' can be expressed as:

$$\varepsilon'(\omega) = \frac{C(\omega)\,material}{C_o} \qquad (2.3a)$$

$$\varepsilon''(\omega) = \frac{G(\omega)\,material}{C_o\,2\pi f} \qquad (2.3b)$$

where C_o is the air-filled capacitance and f is the measured frequency.

Two types of molecular processes contribute to the impedance of a resin:[38] ionic and dipolar. The impedance of a resin is determined as a function of frequency in terms of the molecular processes. Both the real and the imaginary parts of ε^* have a dipolar and an ionic component.

$$\varepsilon'(\omega) = \varepsilon'(\omega)_d + \varepsilon'(\omega)_i \qquad (2.4a)$$

$$\varepsilon''(\omega) = \varepsilon''(\omega)_d + \varepsilon''(\omega)_i \qquad (2.4b)$$

The dipolar component contributes to the impedance signal at high frequencies and in viscous mediums. The

dipolar component is due to rotational diffusion of dipolar moments and bound charges. The dipoles of a curing resin that are contained in a viscous medium, are hindered by being attached to a growing network and therefore, can't keep up with the alternating electric field. The time measured for rotational mobility of the dipoles is the dipole relaxation time, τ_d. Early in the cure, τ_d is short. When dipolar molecules can align with the electric field perfectly to the maximum extent possible, usually at low frequencies, the permittivity is considered the relaxed permittivity and is denoted as ε_r. As the cure proceeds, chains become longer , the resin vitrifies, and τ_d is long. The high frequency permittivity value is considered the unrelaxed permittivity and is denoted as ε_u. Because the growing chains cannot keep up with the alternating electric field, there is a hindrance mechanism or an energy loss.[38]

The ionic component dominates at low frequencies, low viscosities, and/or high temperatures.[38] The ionic component is governed by ion charge diffusion, the hindered translation of mobile ions, and the interaction of these ions with other charged species. The conductivity, σ, is an experimentally determined parameter that measures translational mobility of ions.

The frequency dependent dipolar components and the contribution due to conductivity for a single relaxation time may be expressed as:

$$\varepsilon'_d = \frac{\varepsilon_r - \varepsilon_u}{(1 + i\,\omega\,\tau_d)} + \varepsilon_u \qquad (2.5a)$$

$$\varepsilon''_d = \frac{\sigma}{\omega\,\varepsilon_o} + \frac{(\varepsilon_r - \varepsilon_u)\omega\,\tau_d}{1 + (\omega\,\tau_d)^2} \qquad (2.5b)$$

where ε_r and ε_u are the limiting low and high frequency values of ε^*, σ is the ionic conductivity in $(\text{ohm cm})^{-1}$, ω is the angular frequency, and τ_d is the single relaxation time. This is an ideal representation of the dipolar contributions to permittivity and loss factor. In most systems, a distribution of relaxation times is observed due to the presence of more than one polar species, the asymmetric shape of the polar groups, and intra- and intermolecular forces.[38]

By plotting ε' versus ε'', the frequency dependence of ε' and ε'' is determined. This is called a Cole-Cole plot.[39] When conductivity or ion mobility does not contribute to the loss factor and a single relaxation time is observed, a perfect semi-circle will result with ε_u and ε_r as the endpoints and the maximum value of ε'' is less than ε_u-$\varepsilon_r/2$. As the conductivity contribution to the loss factor increases the semi-circle of the Cole-Cole plot becomes less

circular. The Cole-Cole plot also reveals details about the distribution of relaxation times. If the semi-circle plot is skewed at the high permittivity end of the plot, a distribution of times may be responsible. Finally, if the semi-circle passes through the origin, no blocking layer occurs on the electrode.[43]

2.4.2.3. Dielectric Measurement Techniques

Permittivity, ε', is a measure of the degree of alignment of dipoles and is a function of the strength, amount and mobility of dipoles in a resin.[44] Permittivity values usually begin at a high level during cure because initially, the liquid resin contains a high concentration of highly mobile dipoles. As the material hardens, the permittivity values decrease because the dipole motion is restricted by network formation.

The dielectric loss factor, analogous to the loss modulus, G", can be considered the change in dissipated energy when an alternating electric field is applied between capacitor plates that hold the material during the cure cycle. The loss factor, ε'', is a measure of the energy required to align dipoles and move ions. The loss factor is the sum of both dipole motion and ionic conduction:[45]

$$\varepsilon'' = \sigma/\omega\varepsilon_o + \text{dipole terms} \qquad (2.6)$$

where ε" is the loss factor, ε_o is the permittivity of free space (8.854 picoFarads/m), ω is $2\pi f$, where f is the frequency of measurement, and σ is the bulk ionic conductivity. At low frequencies, the dipole terms become negligible. The ionic conductivity, σ, arises from movement of ionic impurities in the material, is frequency independent, and is very sensitive to network changes. At the beginning of cure, the ion mobility is high and therefore, ionic conductivity is high. Before gelation, σ is inversely proportional to the viscosity. As the cure proceeds, the ionic conductivity decreases because the mobility of ions decreases due to a highly crosslinked network. Ionic conductivity can be used to follow the "tightening of the crosslinked matrix until the very end of the reaction."[40]

2.4.2.3.1. Parallel Plate Electrodes

The simplest way to measure the dielectric properties of a resin is with a parallel plate electrode configuration.[43] A sample is placed between two closely spaced conducting plates. The advantage of this type of electrode is the simple analysis of the phase angle and amplitude. The disadvantage of this type of electrode is the need to control the plate spacing and electrode area in order to measure ε′ and ε″. During cure, materials will

undergo shrinkage. It is then hard to maintain calibration of the space between the plates. Therefore, this type of electrode is not useful in monitoring thermosets *in-situ*.

2.4.2.3.2. Comb Electrodes

By using an interdigitated or comb design for an electrode circumvents the problem associated with the parallel plate electrodes.[43] Electrodes are fabricated on an insulating substrate such as ceramic to prevent the variable geometry changes due to curing or applied pressure. The major advantage with this type of electrode is its reproducibility or calibration, miniaturized integrated circuit, and ease of use in composite manufacture. Calibration is insensitive to applied pressure or temperature changes. The disadvantage of this electrode is that it is less sensitive than the parallel plate design.

2.4.2.3.3. Microdielectrometry

Microdielectrometry was developed by Senturia and became commercially available in 1983.[43] Geometry-independent electrodes allows for the measurement of impedance instead of admittance. Since impedance is measured, measurements can be made at low frequencies.

The electrode used in microdielectrometry is an improvement over the comb electrode. The electrode combines a pair of field-effect transistors on the same plane of the silicon integrated microcircuit electrode. The sample is

placed over the electrode surface. The electric properties measured generate an excitation signal at a given frequency. The change in gain and phase is the response and that is converted into ε' and ε'' by a calibration contour plot. Amplification of the signal is required because the electrode geometry is less efficient than the parallel plate configuration. A thermal diode is also located on the electrode to measure changes in temperature during the experimentation. Sensitivities of measurement are comparable to the parallel plate electrodes without worrying about the spacing between electrode plates. This was the technique utilized in the present investigation.

2.4.2.4. Dielectric Analysis of Polymeric Networks During Cure

Dielectric analysis is a means of characterizing cure processes by non-destructive methods. Many researchers have used dielectric analysis to determine processing windows, curing parameters, and to gain insight into ionic mobility with temperature.[38,43] The common thread of cure monitoring for any thermosetting resin is that when chemical reaction starts, the loss factor increases gradually until a maximum is reached. Onset of crosslinking is indicated by a rapid decrease in loss factor due to a decrease in ionic mobility. Finally, when the slope of the loss factor is zero, cure is complete.[40]

2.4.3. Polymer Modeling

2.4.3.1. QSPR

The purpose of modeling or computer simulation is to provide estimates of polymer properties by empirical methods.[46] Biosym Technologies, Inc. produces computer simulation software with Insight II user interface. The software contains two modules to estimate properties of polymers: QSPR and Synthia. QSPR is the acronym for Quantitative Structure Property Relationships, which is a method based on group additivity. Selected molecular groups contribute to the polymer property of interest, independent of the environment. A physical/chemical property of a polymer system is assumed to be the scalar sum of the property for each group of the entire polymer. The more groups recognized within the polymer, the more accurate the estimated properties. Therefore, QSPR requires a 'group property' database. The estimation of properties is based on additive molar functions. Some of the properties that can be estimated are molar mass, cohesive energy, and T_g. Again, the estimation of properties depends on how many groups of the polymer system are recognized by the computer software program. QSPR, however, does not provide an insight into atomistic calculations nor can the program account for special interactions.[46]

Within the QSPR module, are two complementary techniques: Dow and van Krevelan. Using empirical and semi-empirical relationships to predict the properties of amorphous polymers, the Dow technique depends on the contribution of six groups.[46] The van Krevelan methodology is based on the calculations of various molar properties of the average repeat unit.

2.4.3.1.1. Dow

The Dow methodology tries to limit the database of group contributions by relating the amorphous polymer properties of the repeat units to molecular properties such as cohesive energy, molecular size, and chain mobility. For example, the mechanical properties of a polymer can be determined from the interaction energy between the repeat units of the polymer. All properties calculated by the Dow methodology are based on cohesive energy, which is the net attractive force of interaction and the van der Waal volume that is proportional to interaction distances of the atoms.

2.4.3.1.2. van Krevelan

The van Krevelan approach is based on molar properties of the average repeat units, which are then used to calculate the macroscopic properties. The molar properties, such as cohesive energy, mass, or number of backbone atoms, are summed over the entire polymer, group by group, and then that sum is divided by the total number of repeat units.

The van Krevelan approach can calculate more properties for amorphous and semi-crystalline polymers, but requires a much larger database of group contributions. Properties that can be estimated are: thermophysical, mechanical, ultimate mechanical, transport, electrical, optical, magnetic, and thermal stability. The van Krevelan methodology however, cannot be used for new types of polymers that are not in the 'group property' database nor can it improvise and predict new properties.

The two methodologies described above are fast and easy to use, especially if all the groups within the polymer are contained in the database of 'group contributions'. If the polymer contains a group that is not recognized by the database, then the properties of that polymer can not be determined. For example, neither approach recognizes the -NH group nor the maleimide group attached to a benzene ring, both of which are present in the bismaleimide system. A program named Synthia was developed, based on connectivity indices to predict and estimate thermodynamic, mechanical and transport properties of bulk amorphous polymers.

2.4.3.2. Synthia

Synthia, developed by Dr. Jozef Bicernano of Dow Chemical Company, utilizes topological information about the polymer instead of group contributions to predict properties of the polymer.[46] Properties of polymers containing any of

the nine following elements can be estimated: C, H, O, Si, S, Fl, Cl, and Br.

Connectivity indices based on graph theory are used to estimate properties of amorphous polymers. The repeat unit is represented as a hydrogen-suppressed graph. Zeroth (0th) and the first (1st) order connectivity indices are the basic structural descriptors of the model. The 0th order atom indices can be described in terms of two atomic indices (δ and δ^V). δ describes the number of non-hydrogen atoms bonded to the specific atom while δ^V describes the numerical characterization of the electronic configuration of the atom. δ^V is given by the following equation:

$$\delta^V = \left(\frac{Z^V - N_H}{Z - Z^V - 1} \right) \tag{2.7}$$

where Z^V is the number of valence electrons, N_H is the number of hydrogen atoms attached, and Z is the atomic number of the atom.

Once the atomic indices have been determined for an atom then the 1st order bond indices have to be defined in terms of the atomic indices:

$$\beta_{ij} = \delta_i \delta_j \tag{2.8}$$

and

$$\beta_{ij}^v = \delta_i^v \delta_j^v \tag{2.9}$$

After the atomic and bond indices are defined for the repeat unit, the connectivity indices for the polymer chain may be characterized and then later correlated to the polymer properties. The zeroth-order (atomic) indices are given as the summation of δ and δ^V:

$$0_\chi = \sum \frac{1}{\sqrt{\delta}} \tag{2.10}$$

$$0_\chi^V = \sum \frac{1}{\sqrt{\delta^V}} \tag{2.11}$$

The first order (bond) connectivity indices for the polymer molecule is described in terms of:

$$1_\chi = \sum \frac{1}{\sqrt{\beta}} \tag{2.12}$$

$$1_\chi^V = \sum \frac{1}{\sqrt{\beta^V}} \tag{2.13}$$

These connectivity indices are augmented by other descriptors such as the number of different types of groups or the number of different atoms and repeat unit lengths. The connectivity indices are then correlated to extensive and intensive properties.[46] Extensive properties of a polymer are properties that depend upon the size of the system and the amount of material present. These properties include the molar mass and cohesive energy. Intensive properties are properties that are independent of the amount

of polymer present. The two general forms of properties are:

$$\text{(Extensive Property)} = \sum a\chi + \text{(extensive structural parameters, and atomic correction terms)}$$

and

$$\text{(Intensive Property)} = \sum b\xi + \text{(intensive structural parameters, and atomic correction terms) + constant}$$

The structural parameters are combinations of connectivity indices and geometrical parameters that are used in the correlations of certain properties. The atomic group terms are dependent upon the number of certain atoms that are present.

Synthia may be used for isotropic, unoriented amorphous atactic polymers and alternating, random copolymers as long as the repeat unit is correctly represented. This approach allows the input of known measurements such as Tg or density to produce more accurate results or predictions of the polymer and no dependence of molecular weight on properties. There are certain types of polymers that are beyond the scope of Synthia. These are polymers that contain additives or impurities, are crosslinked, or display some type of tacticity, orientation or ordering.

CHAPTER III

EXPERIMENTAL DETAILS

3.1. Introduction

3.1.1. Experimental Materials

3.1.1.1. Bismaleimides

The bismaleimide used in this study was Compimide Resin MDAB or N,N'-bismaleimido-4,4'-diphenylmethane (BMI) and was commercially obtained from Shell Chemical Co. The molecular weight of BMI is 358.36 g/mole with a melting point of approximately 155 °C. The BMI consisted of a fine, yellow powder at room temperature with a purity of greater than 90 %wt and contained no free methylene dianiline. The chemical structure is shown in Figure 3.1. The aromatic content of the BMI adds to the high-temperature stability while the imide moiety imparts rigidity to the resin.

Bismaleimides, when cured alone, are very brittle due to the high crosslink density. To increase the flexibility, BMI is reacted in excess with an aromatic diamine to reduce the crosslink density and to ensure a final product susceptible to crosslinking.

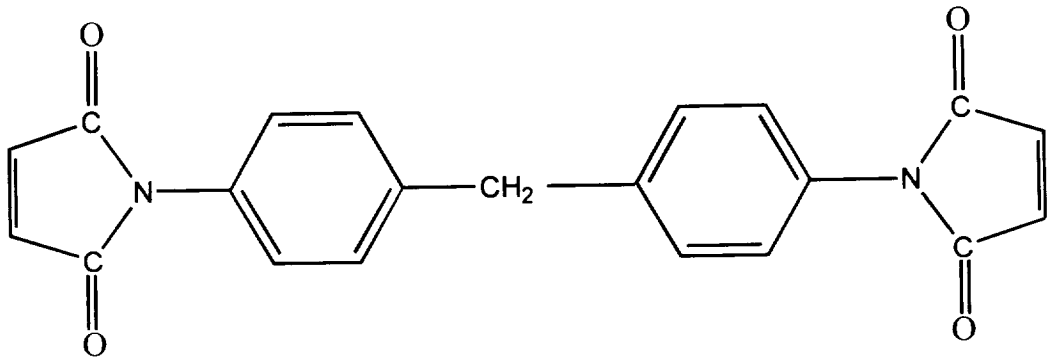

Figure 3.1. Chemical structure of N,N' bismaleimido 4,4' diphenyl methane (BMI).

3.1.1.2. Crosslinking Agents

Three different crosslinking agents were used in this study: 4,4' - methylene dianiline (MDA), 4,4'- diaminodiphenyl sulfone (DDS), and o,o'- diallyl bisphenol A (DABA). The structures of the three crosslinking agents are shown in Figure 3.2.

MDA is an aromatic primary diamine with a molecular weight of 198.29 g/mole and a melting point of 89 °C. The MDA was purchased from Lancaster Synthesis of Windham, New Hampshire and existed as yellow flakes.

The DDS is a tetrafunctional aromatic amine crosslinker with a molecular weight of 248.30 g/mole and has a melting point range of 175-178 °C. DDS, a white powder at room temperature, was purchased from Aldrich Chemical Company and has a purity of 98-99%, and required no further purification.

The third crosslinking agent was o,o'-diallyl bisphenol A (DABA), commercially available under the trademark Matrimid 5292 from Ciba-Geigy. The DABA is an amber, high viscosity liquid at 25 °C.

3.1.1.3. Chemistry - BMI/MDA and BMI/DDS

The chemical reactions between BMI and MDA are temperature dependent and have different effects on the topology of the network formed. The amine addition to the maleimide double bonds is a chain extension reaction and

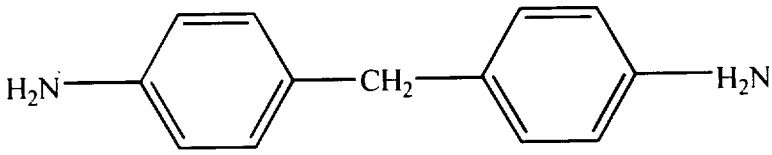

a.) 4,4'-Diaminodiphenyl methane
(MDA)

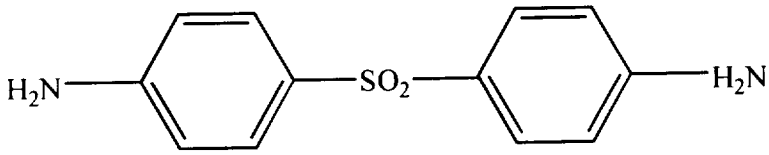

b.) 4,4'-Diaminodiphenyl sulfone
(DDS)

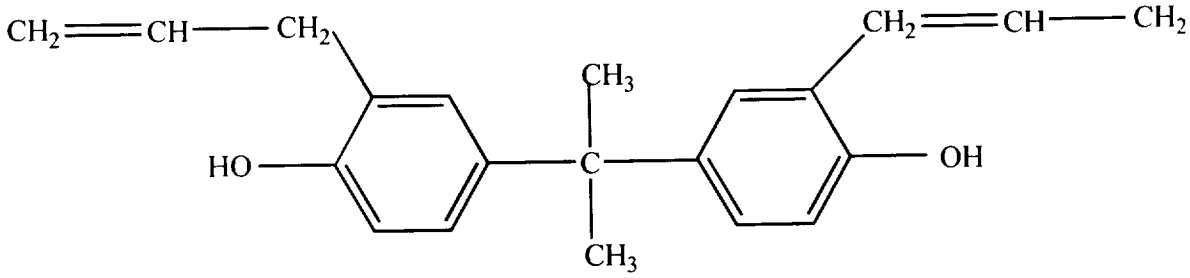

c.) o,o'-Diallyl bisphenol A
(DABA)

Figure 3.2. Chemical structures of the crosslinking agents used in this study: a.) 4,4'-diaminodiphenyl methane (MDA), b.) 4,4'-diaminodiphenyl sulfone (DDS), c.) o,o'-diallyl bisphenol A (DABA).

occurs by a second order reaction mechanism. "Thermal" or BMI homopolymerization, occurs with the opening of the double bond above 180 °C. The two reactions are shown in simplified form in Figure 3.3. These two reactions would also occur for the BMI/DDS system.

By processing these systems in three different temperature ranges, three distinct types of network structures are assumed to form: i.) low-temperature cure so that only chain extension occurs, ii.) high-temperature cure so that both chain extension and crosslinking occur simultaneously, and iii.) low-temperature cure and then a high-temperature postcure so that chain extension occurs to completion, followed by crosslinking.

3.1.1.3.1. Reactant Ratios - BMI/MDA

Homogeneous formulations of three different stoichiometric mole ratios of BMI to MDA were prepared and investigated, 1:1, 2:1, and 4:1. BMI alone was also prepared and cured as a control material.

3.1.1.3.2. Reactant Ratios - BMI/DDS

Homogeneous formulations of two different stoichiometric mole ratios of BMI to MDA, 2:1 and 1:1, were prepared and investigated.

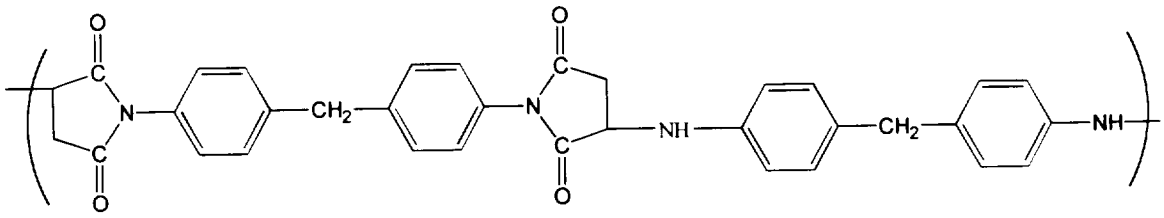

a.) Chain Extension Reaction

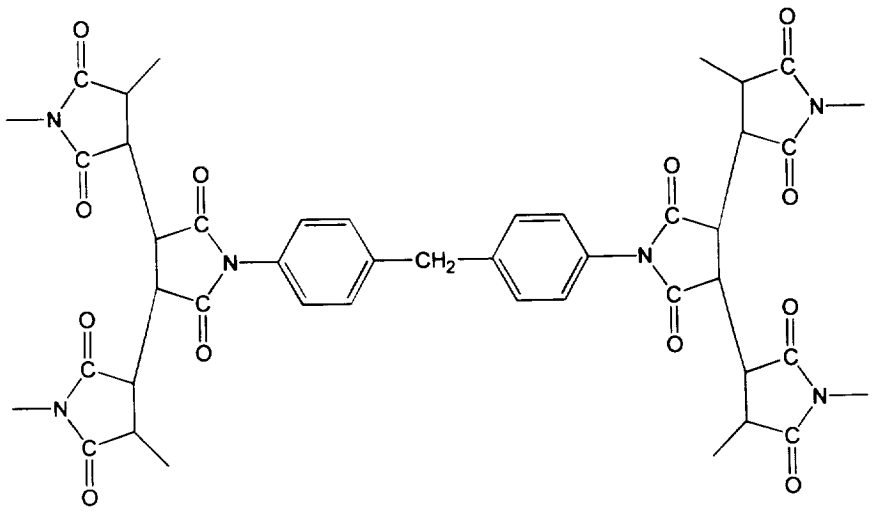

b.) BMI Homopolymerization

Figure 3.3. Steps in the BMI/MDA reaction. a.) Chain extension due to amine addition. b.) BMI homopolymerization.

3.1.1.4. Chemistry - BMI/DABA

The reaction scheme for BMI/DABA is complex.[47] An addition reaction occurs between the allyl groups that are attached to an aromatic ring with the double bond of the maleimide and will undergo an 'ene' type linear chain reaction. This is shown in Figure 3.4. The resulting "substituted styrene" then undergoes a Diels-Alder reaction with another maleimide group. The reaction of a diene with a dienophile, resulting in a ring-containing compound is called a Diels-Alder reaction. Bismaleimides are highly active bis(dienophiles). Once the two components have reacted, the BMI/DABA 'ene' adduct prepolymer is considered pentafunctional:[48] three double bonds capable of chain extension and crosslinking, and two hydroxyl groups, capable of etherification by hydroxyl dehydration. With an increase in temperature, the double bonds can react with other prepolymers or with BMI through a BMI homopolymerization reaction.

3.1.1.4.1. Reactant Ratios - BMI/DABA

Homogeneous formulations of four different stoichiometric mole ratios of BMI to DABA were prepared and investigated: 2:1, 1:1, 1:1.12, and 1:0.87. The latter three formulations are the supplier recommended molar ratios for BMI/DABA.[49]

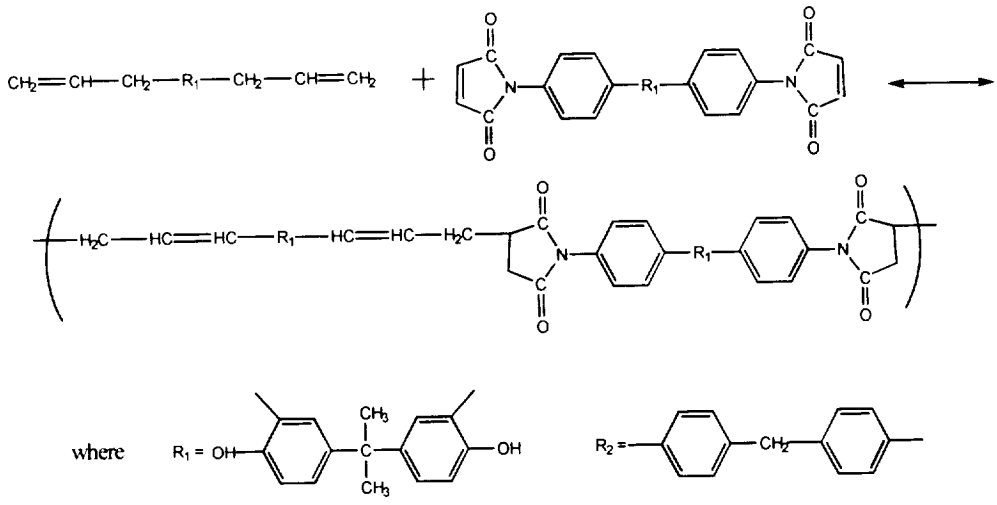

a.) 'Ene' Reaction

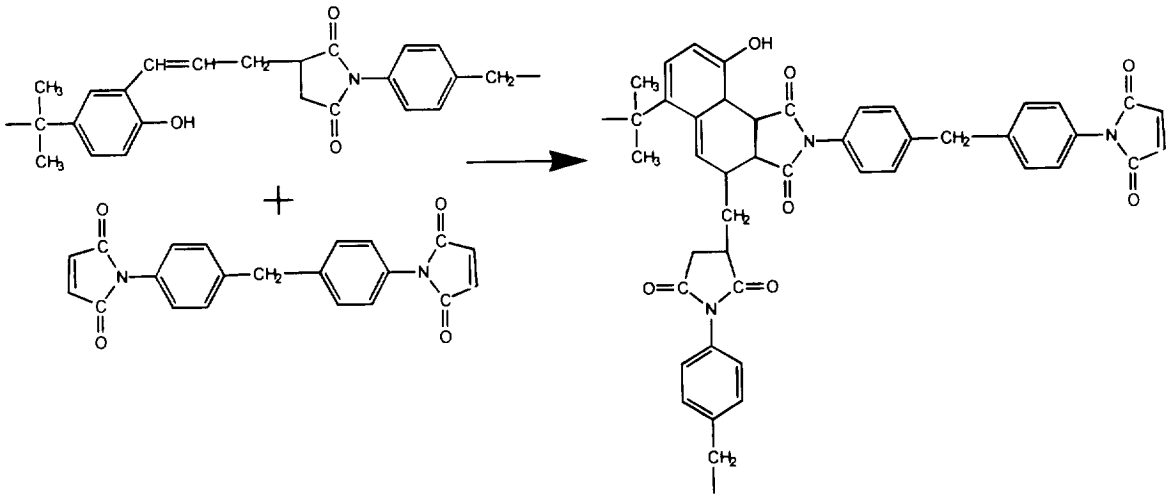

b.) Diels-Alder Reaction

Figure 3.4. Potential reactions in the BMI/DABA system. a.) 'ene' reaction. b.) Diels-Alder reaction. c.) BMI homopolymerization. d.) Idealized pentafunctional prepolymer.

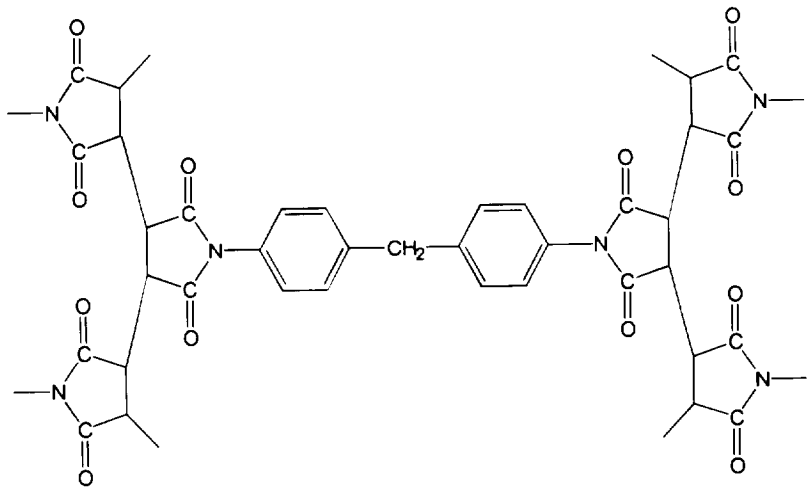

c.) BMI Homopolymerization

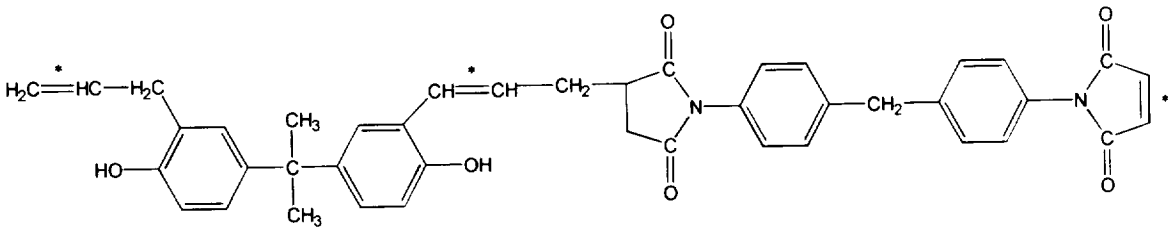

* Double bonds capable of further reaction.

d.) Idealized Pentafunctional Prepolymer

Figure 3.4 cont. Potential reactions in the BMI/DABA system. a.) 'ene' reaction. b.) Diels-Alder reaction. c.) BMI homopolymerization. d.) Idealized pentafunctional prepolymer.

3.1.1.5. PMR-15

Three 6 inch x 6 inch plates of PMR-15, produced at NASA Lewis Research Center, were also investigated in order to compare the results to the bismaleimide data. PMR polyimides are addition curing thermoset polymers, based on the monomers 5-norbornene-2, 3-dicarboxylic acid monomethyl ester (NE), dimethyl ester of 3,3', 4,4'-benzophenonetetracarboxylic acid (BTDE) and 4,4' methylene dianiline (MDA).[50] The NE, BTDE, and MDA are combined in a 2.0/2.087/3.087 molar ratio to obtain norbornene endcapped imide oligomers with a formulated number average molecular weight of 1500.[51] The norbornene endcaps react with further heat to form a crosslinked network.

3.2 Raw Material Characterization

3.2.1. Dynamic Thermogravimetric Analysis/Fourier Transform Infrared Spectrophotometer

A Fourier transform infrared spectrophotometer (FTIR) interfaced with thermogravimetric analysis (TGA) instrumentation allows the simultaneous quantification and identification of evolved decomposition products.[52] TGA/FTIR was performed at NASA Lewis Research Center on BMI, MDA, DDS, and DABA. This simultaneous analysis was performed by coupling an Omnitherm TGA 1000 with a BioRad FTS-45 3200 Data Station. Samples were heated at a rate of

10 °C/min between room temperature and 700 °C in a flowing nitrogen atmosphere.

3.2.2. Differential Calorimetry Spectroscopy

Differential scanning calorimetry (DSC) was performed at NASA Lewis Research Center on BMI, MDA, DDS, and DABA to determine the melting behavior of the resin and the crosslinking agents. All measurements were made on a DuPont Model 910 DSC instrument. Indium metal, whose melting point is 156.6 °C, was used to calibrate the temperature control. Samples weighing approximately 40 mg were placed in open aluminum DSC pans and were heated at a rate of 10 °C/min in a nitrogen atmosphere.

3.3. Network Preparation

3.3.1. Powder Technology - BMI/MDA and BMI/DDS

The procedure for preparing the polymers was based on an English patent by Bargain,[53] but with several processing modifications. In this patent, a homogeneous mixture of virgin powders was prepared and was spread on a plane surface. The mixture was placed in a 200 °C oven for 7 minutes and then removed and allowed to cool. The product was ground to a fine powder with a mean particle diameter of 80 μm. The powder was then placed in a mold and pressed at 200 °C with a pressure of 50 kg/cm^2 for 1 hour. The mold was released at elevated temperatures to reduce the chances

of material shrinkage and possible breakage of the molded material. The authors then suggest that the material should be heated to 220 °C for 24 hours and then 240 °C for an additional 24 hours. However, at these temperatures the material experiences cure conditions that would promote the BMI homopolymerization reaction.

In this investigation, virgin powders of BMI and MDA in the appropriate mole ratio were initially mixed and placed in a preheated glass beaker in a vacuum oven set at 95 °C, just above the melting temperature of MDA. The MDA melted and "wetted" the BMI, producing a discontinuous phase (BMI) within a continuous matrix (MDA). At the appropriate consistency, the material was removed from the beaker and placed on a preheated Teflon coated plate and placed in a 120 °C oven for approximately 7-10 minutes or until the BMI melted. The plate with material was then removed from the oven and allowed to cool to room temperature. Once cooled, the gelled material was removed from the plate and broken into small pieces. A mortar and pestle were used to crush the pieces into fine powder, whose particle size was less than 250 μm in diameter.

The criterion for powder sieving in this research was that all the fine powder must pass through a 250 μm mesh sieve into the three remaining levels: 212 μm sieve, 160 μm sieve, bottom pan. The sieves were stacked in descending

order of mesh size. The ground powder was placed in the first sieve along with a number of Grade 25 stainless steel ball bearings to aid in the powder flow. A lid was placed on the top sieve and the entire stack of sieve layers was sealed with electrical tape at the joints and placed in a sieve shaker for approximately 20 minutes. After that time powder remaining in the top sieve was removed and reground. The process is repeated until all the powder has been forced through the sieve with a mesh opening of 250 μm. The weight of powder at each sieve level was determined before and after screening to determine how much material is "caught" by the procedure.

The process of manipulating the virgin powders in an intermediate step is called "B-Staging" in industrial circles. The B-staged powders were placed in appropriately marked vials and stored in desiccators until needed for molding or dielectric cure monitoring analyses.

3.3.1.1. Powder Characterization

3.3.1.1.1. Gel Point Determination

During the melting of a polymer, the viscosity decreases. An increase in the viscosity with further time indicates that the resin has begun to solidify. This is considered the gel point. In fabricating the compression-molded material, it is necessary to determine the time required for material to reach its gel point. One method

for determining the gel point is based on the measurement of the steady state viscosity of the liquid phase, ASTM D2471. This method determines the time between initial mixing of the reactants of a resin and the time when solidification begins.[54]

Approximately 4.2 grams of each powder were placed in a 5-dram vial for gel point determination. Three vials of each powder were used to determine the average time and standard deviation of the gel point. Each vial was partially submerged in either a 140 °C or 220 °C oil bath, depending upon the curing condition and the time required for gelation was measured. Every 15 seconds the centers of the vials were probed with an applicator stick. When the material no longer adhered to the end of a clean stick, the gel time was recorded.

3.3.1.1.2. TGA/FTIR

As with the original components, the B-staged powders were characterized by TGA/FTIR at NASA Lewis Research Center. The BMI/MDA and BMI/DDS powders were heated at a rate of 10 °C/min between room temperature and 700 °C in a flowing nitrogen atmosphere.

3.3.1.1.3. Differential Scanning Calorimetry

Differential scanning calorimetry (DSC) was performed at NASA Lewis Research Center on appropriate mole ratios of BMI/MDA and BMI/DDS powders prior to curing to determine the

melting behavior of the B-staged powders. Samples weighing approximately 40 mg were placed in open aluminum DSC pans and were heated at a rate of 10 °C/min in a nitrogen atmosphere.

3.3.2. Processing of BMI/MDA and BMI/DDS

3.3.2.1. General

An important processing variable that needs to be kept constant in any investigation is the cure schedule.[2] The cure schedule is considered the period of heating, which affects the polymerization rate of the material. Cure schedules are typically chosen such that further thermal treatment will not cause changes in the network structures or properties. The glass transition temperature, number average molecular weight between crosslinks, and sol fraction are a few characterization properties that can be used to determine state of cure of thermosetting resins.

When a resin system cures by only one reaction, the T_g is a function of the extent of reaction or cure and is independent of cure schedules. The curing of BMI resins involves at least two reactions, amine addition and BMI homopolymerization. The glass transition temperature is dependent on two extents of reaction, which are dependent on resin composition and cure schedules. For example, Leung et al.[26] found that the T_g and fracture energy of BMI/MDA in a 2.5:1 mole ratio increased as the cure temperature increased

from 130 °C to 180 °C, even though the DSC extents of reaction were the same. They concluded that different network structures formed during the different cure schedules.

The rates of the amine addition and homopolymerization reactions determine the network topology during the early stages of cure. The amine addition is an order of magnitude faster than the BMI homopolymerization reaction and continues until most of the amine is consumed.[22] For a particular cure temperature, T_g rises initially as a function of cure time but eventually reaches a limiting value. The magnitude of this value depends on the cure temperature: the higher the cure temperature, the higher the final T_g.

During postcuring, the T_g of the low-temperature cured material can attain and surpass that of material cured at intermediate temperature.[22] At low temperature, the curing reaction is mainly chain extension with few crosslinks. When postcured, the unreacted BMI undergoes homopolymerization and network rearrangement. Therefore, a large, rapid increase in T_g occurs.

During a short time, low-temperature cure, most of the amine is depleted with the BMI. However, some BMI remains unreacted in the resin. The unreacted BMI in the polymer crosslinks the previously extended chains during the

postcuring reaction and the T_g increases dramatically over the T_g of the "cured only" reaction. During a long time, low-temperature cure more BMI is consumed. Therefore, there is less crosslinking that can occur during the postcure and the T_g does not increase as much as in the previous case. Therefore, the cure schedule strongly affects the BMI network and ultimately the T_g.

3.3.2.1.1. Differential Scanning Calorimetry

In order to get the appropriate time of cure at a given temperature, B-staged powder samples of BMI/MDA and BMI/DDS in the appropriate mole ratios were cured for varying increments of time. These samples were used to determine the percent conversion at 140 °C and 220 °C versus cure time by DSC, which was performed at NASA Lewis Research Center. Samples weighing approximately 20 mg were placed in open aluminum DSC pans and were heated at a rate of 10 °C/min in a nitrogen atmosphere.

The approximate states of cure for BMI/MDA and BMI/DDS as a function of time and temperature were determined by measuring the residual heat of polymerization of the samples. This was accomplished by determining the percent conversion versus time and temperature. The % conversion, *R*, is given by:

$$R = \frac{\Delta H_T - \Delta H}{\Delta H_T} \times 100\% \qquad (3.1)$$

where ΔH_T is the total heat of reaction and ΔH is the residual heat of polymerization.

This method is considered a rough estimate for the extent of reaction because DSC analysis for bismaleimides is not very reproducible, sometimes not discernible, and many times not practical.[55] For some polyimides, DSC shows only weak exotherms that are sometimes mistaken for noise.

3.3.2.2. Molds

The powders were consolidated in a 6" x 6" tool steel mold at NASA Lewis Research Center. Figure 3.5 is a schematic diagram of the mold. The mold consists of a U-shaped bottom with two removable sides. The bottom of the mold has four equidistant 1/2-inch diameter holes that are used to punch out the cured material. Two flat metal plates are the support platforms for the curing material. The top of the mold has lipped edges so that the top will rest on the sides of the mold. A small hole, 1/16-inch diameter, 1 inch deep has been drilled into the side of the mold to accommodate a thermocouple sensor to monitor the mold temperature.

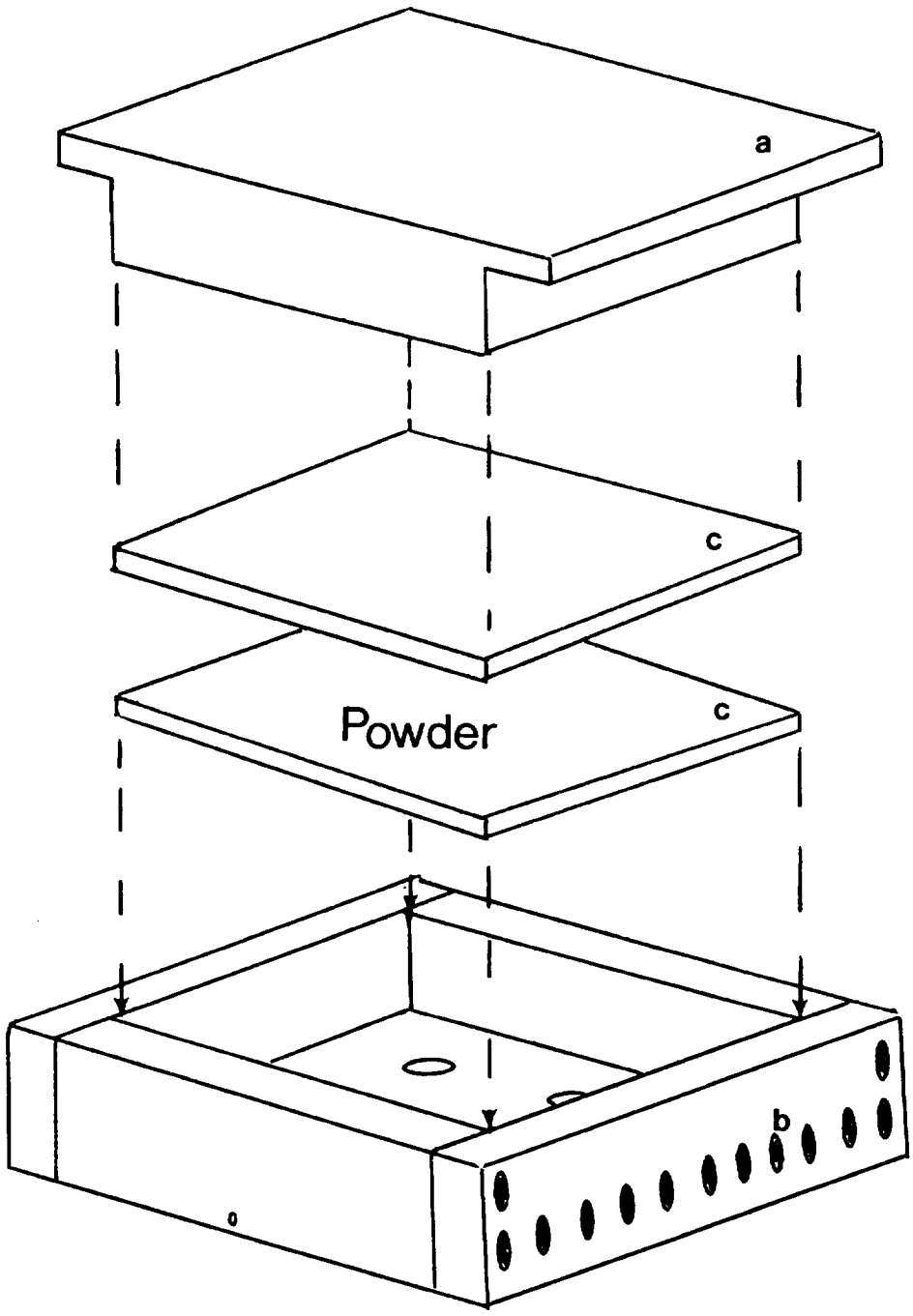

Figure 3.5. Schematic diagram of the 6" x 6" tempered steel mold, used to consolidate BMI/MDA and BMI/DDS powders. The labels denote the following: a = mold lid, b = 'U-shaped' bottom mold with detachable sides, c = platform plates for containing the powders.

3.3.2.3. Thermal Histories - BMI/MDA and BMI/DDS

Each BMI/MDA formulation was prepared using three different cure cycles: 16 hr at a low temperature of 140 °C, 6 hr at a high temperature of 220 °C, or 16 hr at a low temperature of 140 °C followed immediately by 6 hr at a high temperature of 220 °C. Each BMI/DDS formulation was prepared using only the high-temperature cure cycle of 6 hr at 220 °C.

The thermal histories for the BMI/MDA and BMI/DDS are listed in Table 3.1. The temperatures in the table refer to the mold temperature and consequently, the material temperature. The times listed are the periods of time that the materials experience at that particular temperature.

A typical thermal history with pressure versus time is shown in Figure 3.6. Cooling was not controlled because the cured material was removed quickly from the mold to prevent the cured material from cracking. Any constraint on the cured material as it is cooling will cause stress cracks throughout the material. Finally, any heat treatment below the curing temperature such as heating the material at 105 °C in a vacuum oven for the elimination of residual water was not deemed part of the thermal history.

Table 3.1. Cure and Postcure Schedules for the BMI/MDA and BMI/DDS Systems.

BMI:MDA mole ratios	Time at the Indicated Temperatures		
	140 °C	220 °C	140 °C/220 °C
4:1	16 hr	6 hr	16 hr/6 hr
2:1	16 hr	6 hr	16 hr/6 hr
1:1	16 hr	6 hr	16 hr/6 hr
1:0	--	6 hr	--
BMI:DDS			
1:1	--	6 hr	--
2:1	--	6 hr	--

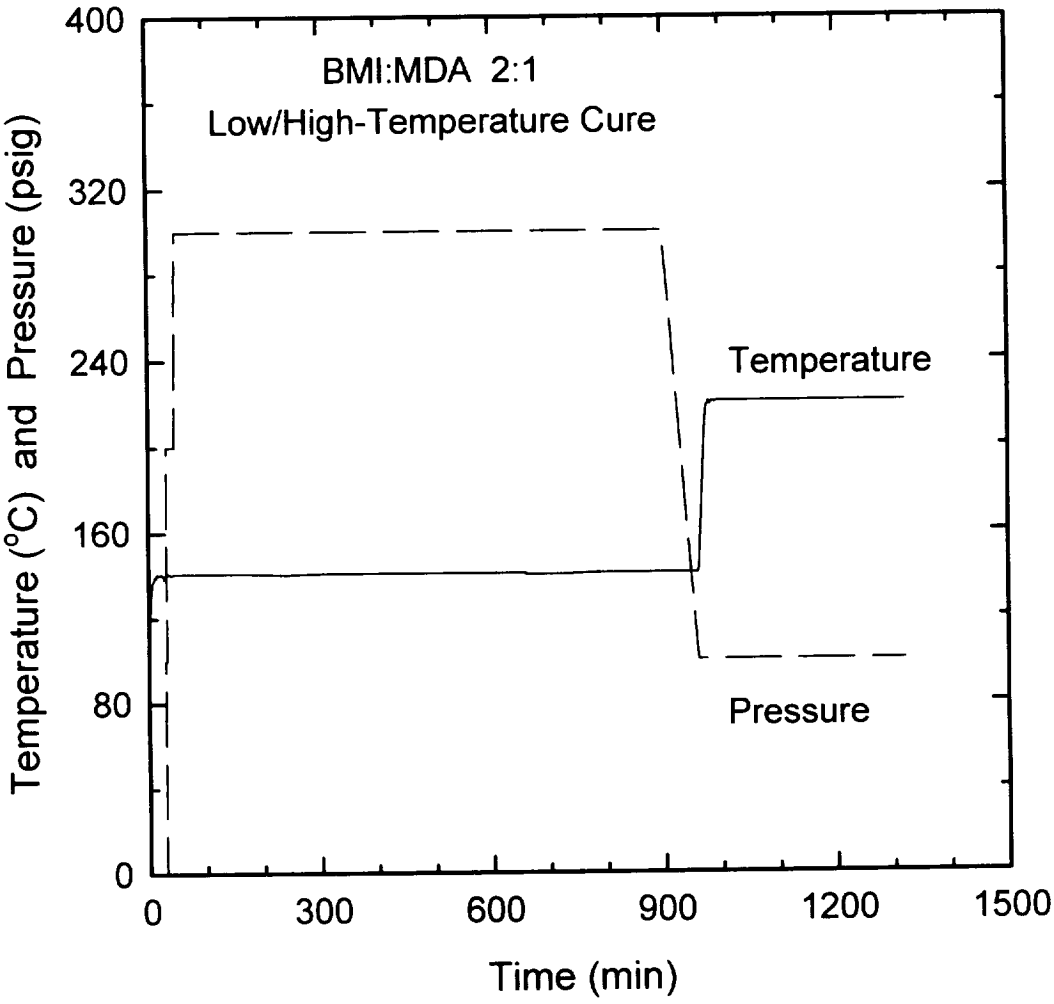

Figure 3.6. Typical thermal history and pressure profile for BMI/MDA in a 2:1 mole ratio, cured for 16 hr at low temperature and then postcured for 6 hr at high temperature.

3.3.2.3.1. Curing Procedure - BMI/MDA, BMI/DDS

The individual pieces of the mold were coated liberally with MonoCoat E63FF 7A Chem Trend MultiRelease agent. When dried, the sides of the mold were bolted to the bottom U-shaped piece. Approximately 80 g of ground powder was placed between the two platform plates. After the top lid was placed onto the mold, the entire mold was inserted into a preheated Wabash 12 ton press with a ram diameter of 4". A thermocouple placed into the side of the mold was used to monitor the mold temperature. Five minutes after the gel point of the material was reached, slight pressure (100 psig) from the platens was added and released several times to squeeze out any trapped air in the material. The pressure was then increased to 600 psi or 1800 psig for the remainder of the cure schedule.

When the cure time was complete, the pressure was released and the two sides were quickly removed. Flash that flowed over the two platform plates was scored with a razor blade prior to removing the mold from the press. The entire mold was removed from the press and turned upside down. The upside down mold was returned to the press and positioned onto two 2" x 1" x 8" aluminum bars, six inches apart. Four 1.5" dia. stainless steel rods were placed into the holes on the bottom of the mold. A flat 1/4" thick aluminum plate was placed over the rods and the top platen of the

press was slowly lowered to push the plate and subsequently the rods into the bottom of the mold, thereby forcing the cured material, sandwiched between the platform plates out of the mold. The two platform plates were removed, leaving the cured material of BMI/MDA, BMI/DDS, or BMI. The cured plate of material was stored in a desiccator until needed.

3.3.2.3.2. Postcuring Procedure - BMI/MDA

One of the thermal histories for BMI/MDA was 16 hr at low temperature followed immediately by 6 hr at high temperature. The material was not removed from the press during the postcure. Pressure was slightly decreased (1500 psig) in case of material expansion during heating. The cured material was removed at the end of the cure schedule and then cut into testpieces.

3.3.3. Synthesis - BMI/DABA

According to the supplier's recommended procedure,[49] the appropriate amount of DABA was placed in a 1000 ml reaction kettle, equipped with a heating mantle, thermometer, stirring rod, and a vacuum line, as shown in Figure 3.7.[3] When the DABA was the consistency of water, the appropriate quantity of BMI was added. Under constant stirring with a Teflon paddle in a N_2 atmosphere, the two components were heated to 125 °C until a clear homogeneous solution was obtained. The mixture was degassed for 20 minutes without stirring before it was poured into a

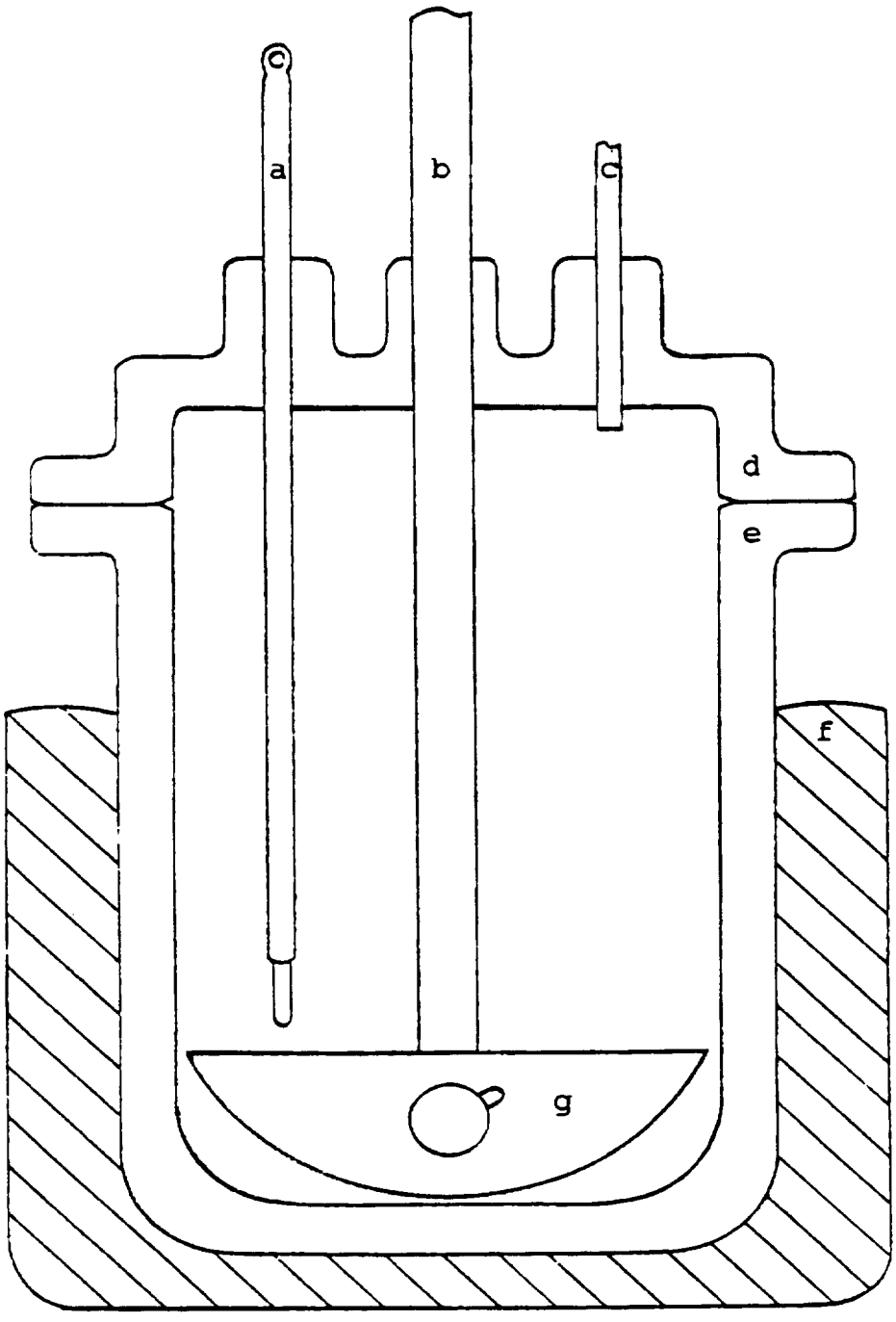

Figure 3.7. Reaction kettle setup used in preparing BMI/DABA networks. (Figure obtained from S. Mudrich[3]) Labels denote the following: a) thermometer, b) glass stirring rod, c) vacuum hose, d) reaction kettle lid, e) 1000 ml reaction kettle, f) heating mantle, g) Teflon stirring blade.

preheated upright mold, shown in Figure 3.8. The material was placed in a 155 °C vacuum oven. After two hours, the oven temperature was raised to 177 °C for 16 hours. The material remaining in the reaction kettle was scraped out and placed in marked vials and stored in a desiccator for use in dielectric analysis.

3.3.3.1. Molds - BMI/DABA

An upright Teflon coated aluminum 8" x 8" mold, shown in Figure 3.8,[3] was used for the BMI/DABA material. The aluminum molds were machined from cast aluminum sheet stock, polished, and then coated with a Teflon film by Falholt, Inc. Akron, OH. One half of the mold consists of the material cavity, (8" x 8" x .157"), surrounded by a venting channel that allows trapped air to escape from the bottom of the mold up through the sides of the mold. The other half of the mold is a rectangular aluminum plate. The mold was held together by four 6" C clamps.

3.3.3.2. Thermal Histories - BMI/DABA

Each BMI/DABA formulation was prepared using three different cure cycles, recommended by Ciba Geigy: 16 hr at a low temperature of 177 °C, 16 hr at a high temperature of 250 °C, or 16 hr at a low temperature of 177 °C followed by 16 hr at a high temperature of 250 °C.

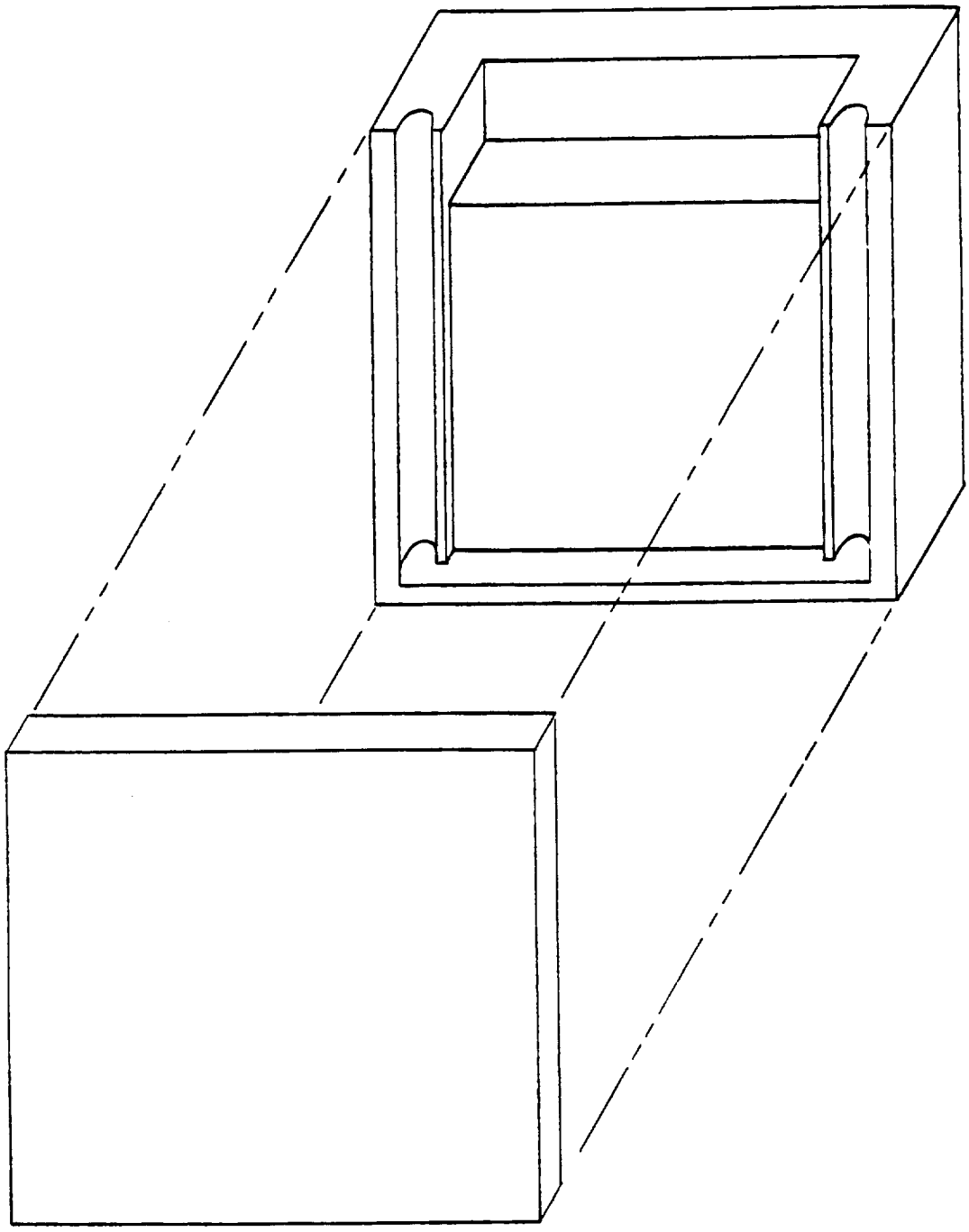

Figure 3.8. Schematic diagram of the Teflon coated aluminum mold used to cure BMI/DABA sheets. (Figure obtained from S. Mudrich.[3])

The thermal histories for BMI/DABA are detailed in Table 3.2. The temperatures listed refer to the mold temperatures, and consequently the material or cure temperatures. The times represent the times the materials are held at the cure temperature.

A typical thermal history versus time for BMI/DABA is shown in Figure 3.9. The cooling rate is not monitored since the material is removed from the mold as soon as the cure schedule is complete.

3.3.3.2.1. Curing Procedures - BMI/DABA

After pouring the clear, homogeneous material into the preheated upright mold, the mold was placed in a vacuum oven for 2 hours at 155 °C until the gel point was reached. The temperature of the oven was then increased to 177 °C for the remaining 16 hours. After the cure time was reached, the mold was removed from the oven. The C-clamps were quickly removed and the mold was disassembled. The material was removed from the mold while still hot so that the material would not crack during cooling. Once removed, the material was allowed to cool to room temperature and then stored in a desiccator.

3.3.3.2.2. Postcuring Procedures - BMI/DABA

One of the cure schedules for BMI/DABA was 16 hr at 177 °C followed by 16 hr at 250 °C. After the 177 °C cure, the cured plate was cut into testpieces and then heated to

Table 3.2.
Cure and Postcure Schedules for BMI/DABA.

BMI:DABA mole ratios	Time at the Cure Temperatures		
	177 °C ♦	250 °C ♦	177 °C/250 °C♦
2:1	16 hr	16 hr	*
1:1	16 hr	16 hr	*
1:0.87	16 hr	16 hr	*
1:1.2	16 hr	16 hr	16 hr/16 hr

♦Each sample experienced 2 hr at 155 °C prior to curing, according to manufacturer's recommendations.[49]

* Only the rheological dynamic shear and density samples were given the step cure.

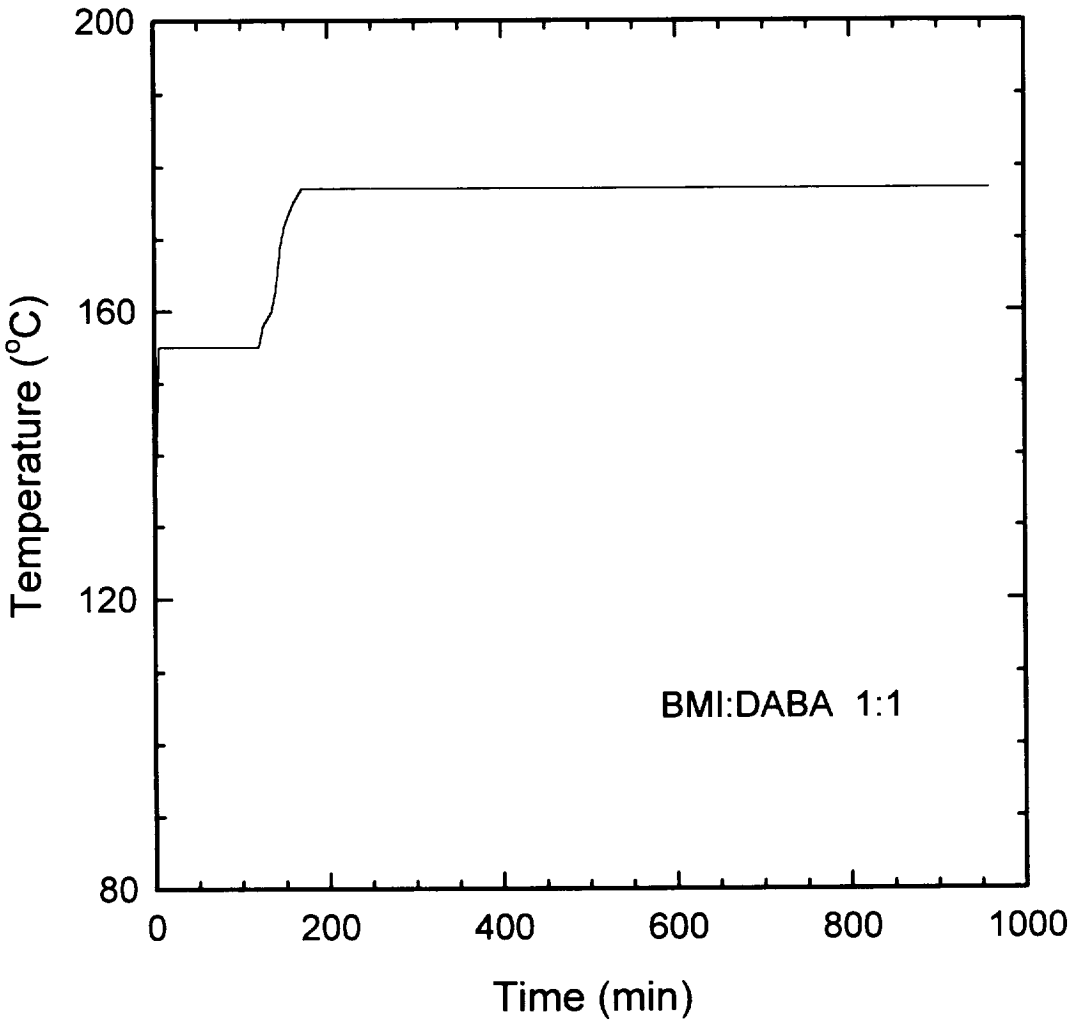

Figure 3.9. Typical processing history for BMI:DABA in a 1:1 mole ratio.

105 °C in a vacuum oven for 24 hr to remove any residual moisture. The testpieces were weighed and measured before being inserted into a preheated 250 °C vacuum oven backfilled with a N_2 atmosphere for 18 hr. Postcuring the testpieces in a N_2 atmosphere minimized oxidative degradation. The postcured testpieces were weighed and measured and then stored in a desiccator until use.

3.3.4. Thermal History - PMR-15

Samples from one of the three cured PMR sheets obtained from NASA Lewis Research Center, were postcured after being cut by the diamond saw. The testpieces were heated to 105 °C for 24 hr in a vacuum oven to remove water. The testpieces were weighed and measured before inserting them into a preheated 316 °C oven for 16 hr. The samples were again weighed, measured, and stored in a desiccator until use.

3.4. Testpiece Preparation

3.4.1. General

All mold flash and extraneous material were removed from the cured plates with a file. Various test samples were cut from the plates using a diamond impregnated cutting wheel on a water-cooled Micro-Matic Precision table, manufactured by Micromech MFG, Corp. Figure 3.10 illustrates the cutting patterns for the 6" x 6" and the

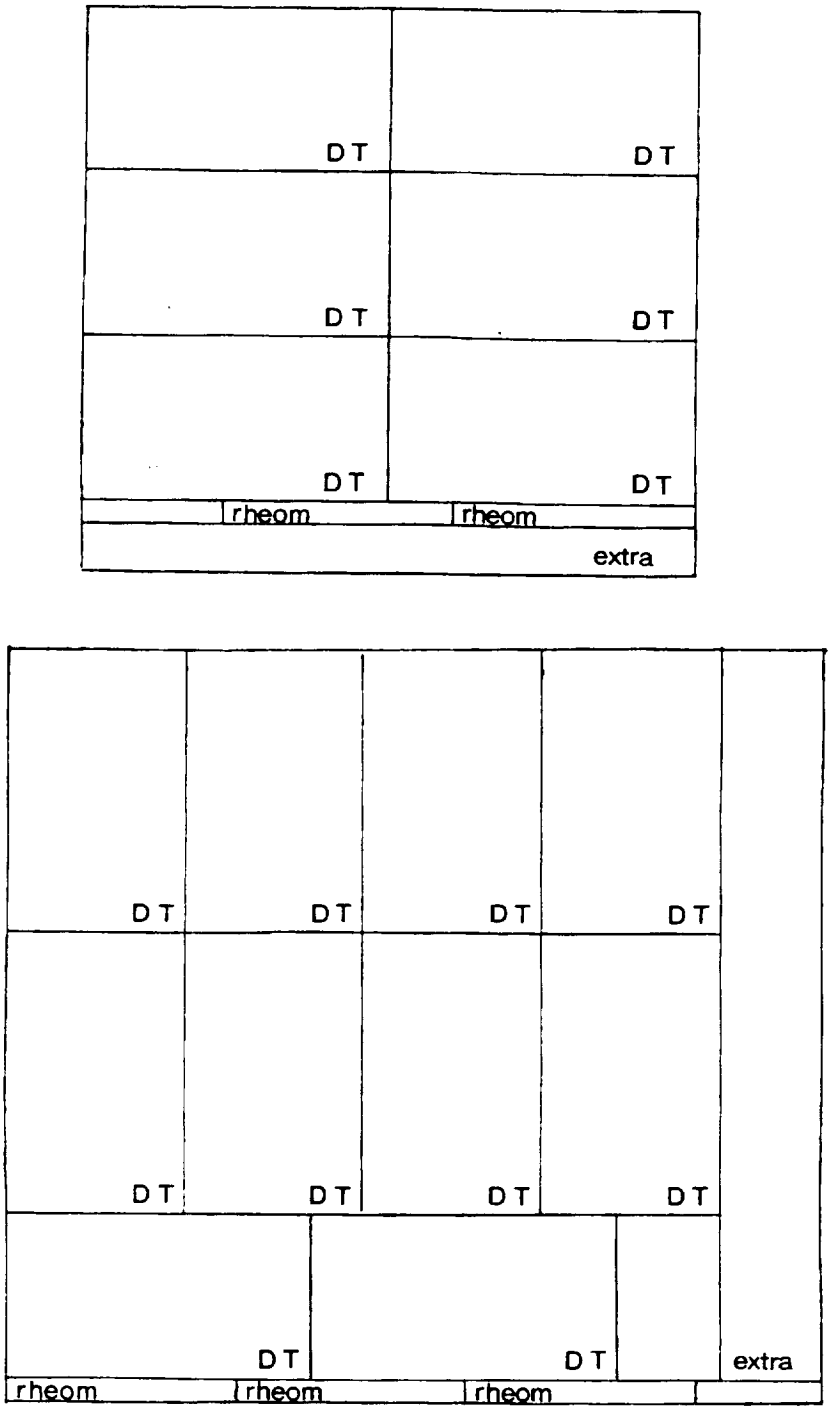

Figure 3.10. Patterns for cutting the various test-piece configurations from the 6" x 6" (top) and 8" x 8" (bottom) cured plates. Labels denote the following: 'DT' = double-torsion sample, 'rheom' = rheological test sample, 'extra' = extra material, not used for mechanical testing.

8" x 8" material plates. Two or more plates were made for each cure condition and material combination.

After the plates were cut by a diamond saw into testpieces, the samples were measured and weighed, heated to 105 °C for 24 hours to remove any residual water from cutting, and then measured and weighed again. The cut testpieces were labeled and stored in desiccators until needed.

Throughout the investigation, rigorous effort was made to track all weight measurements from after cure to after post cure and before testing. Polyimides,[55] in general, can absorb as much as 2% moisture. Therefore, drying at 105 °C is necessary for the elimination of moisture. Elimination of moisture has been successfully achieved by placing the material in an oven at 105 °C for 16-24 hours. Weight gains may be due to absorbed moisture and swelling. All materials were stored in a desiccator from the start to end of this investigation.

3.4.2. Rheological Testpieces

Several rheological testpieces (2" x 1/4") were cut from each cured plate on a water lubricated diamond saw. Samples were then heated to 105 °C in a vacuum oven to remove any residual moisture. The samples were weighed, measured and stored in a desiccator until use.

3.4.3. Double-Torsion Samples

Rectangular samples (2.95" x 1.77") were cut from the cured plates with a water lubricated diamond saw. Six double torsion specimens were cut from each plate of BMI/MDA, BMI/DDS, BMI, and PMR. Ten double torsion specimens were cut from each BMI/DABA plate. After the sides of the testpieces were squared on a Bridgeport mill to uniform dimensions, a V-notch was centrally milled the entire length of the testpiece with a carbon-coated circular slotting cutter, ground to a 30° included angle. The depth of the V-notch was roughly one half the thickness of the sample. The V-groove on each sample was scored with a dental pick to ensure that a crack would propagate along the V-groove. Before a crack could be initiated along the V-groove with a razor blade, a notch, 1/4" in length, was sawed perpendicular along the V-groove with a jeweler saw. Just prior to testing, a razor blade was forced into the notch with a rubber mallet to induce a sharp precrack. A new razor blade was used for each sample. A mark with a metallic marker was placed 2 mm from the edge of the sample along the V-groove over the precrack to aid in the tup placement during testing.

3.4.4. Sonic Modulus Samples

Once the double-torsion tests were performed, one half of the testpiece was used for sonic modulus measurements.

Eight to twelve specimens of each BMI/MDA and BMI/DDS ratio, BMI, and PMR-15 were used during the sonic modulus measurements. Twelve to fifteen samples for each ratio of BMI/DABA were utilized during the sonic modulus measurements. The fractured V-groove surfaces were ground off using a circular, water lubricated grinding wheel with 400 grit silicon carbide paper. Only the fractured surface was in contact with the water.

3.4.5. Plane Strain Compression Testpieces

The plane-strain compression yield samples (1.77" x 0.87") were cut from the sonic modulus testpieces using a water lubricated diamond saw. After cutting, the samples were heated to 105 °C for 24 hr to remove any residual water. The samples were measured, weighed, and stored in a desiccator until tested. Eight to twelve samples were tested for each cure condition and composition.

3.4.6. Density Testpieces

Density samples (0.87" x 0.99") were cut from the sonic modulus testpieces. The samples were heated to 105 °C in a vacuum oven to remove any residual water. The samples were weighed, measured, and stored in a desiccator until use. Three samples were cut from one sonic modulus testpiece; twenty-four to thirty-six samples were tested for each cure condition and composition and only the average and standard

deviation values are reported in the Results and Discussion section.

3.4.7. Equilibrium Rubbery Modulus Testpieces

The second half of each double-torsion sample was cut lengthwise with a diamond saw into two equal pieces for the equilibrium rubbery modulus tests and the intermittent stress relaxation experiments. Dumbbell samples were not possible due to the inherently brittle nature of the BMI-based material. The samples were heated to 105 °C to remove residual moisture, measured, weighed, and stored in a desiccator until use. Three samples each of the high- and low/high-temperature cure conditions for each ratio of BMI/MDA were tested. The low-temperature cure condition of BMI/MDA and the high-temperature cure condition of BMI/DDS and BMI were too brittle to be tested in this manner.

3.5. Network Characterization

3.5.1. Dynamic Shear Measurements

A Rheometrics mechanical spectrometer at Wright Patterson Air Force Base was used to determine the rheological properties of the BMI/MDA, BMI/DDS, BMI/DABA, BMI and PMR samples. The dynamic shear moduli were measured by deforming the test specimens in torsion at a frequency of 1 Hz with a maximum strain of 0.2%. The heating rate was 5 °C/min from room temperature to 450 °C.

The glass transition temperatures were determined by a line intercept method. Lines are drawn through the glassy region and the transition region. The point at which these lines intersect is considered the glass transition temperature, Figure 3.11. Even though figures and tables in this dissertation contain the symbol "T_g", it is recognized that the glass transition temperature is an apparent measure, not done at near-equilibrium but in a dynamic mechanical test. From these rheological curves, the temperature range of the rubbery plateau regions or the minimum value of G′ was determined for future equilibrium rubbery moduli measurements.

Some dynamic mechanical spectroscopy was also performed at NASA Lewis Research Center under the conditions listed above. Researchers at NASA Lewis Research Center have found rheological analysis to be a useful and reproducible technique, capable of discerning moisture in the material, which can be identified by a lower T_g and a drop in G′ at about 100 °C. Finally, rheological analysis can determine the general state of cure.[55] Undercured material exhibits a broad secondary transition after the rubbery plateau. A slight increase in G′ after the minimum is also indicative of undercuring in the material. Since tan δ is the ratio of G′ to G″, any transition in G′ or G″, such as undercuring,

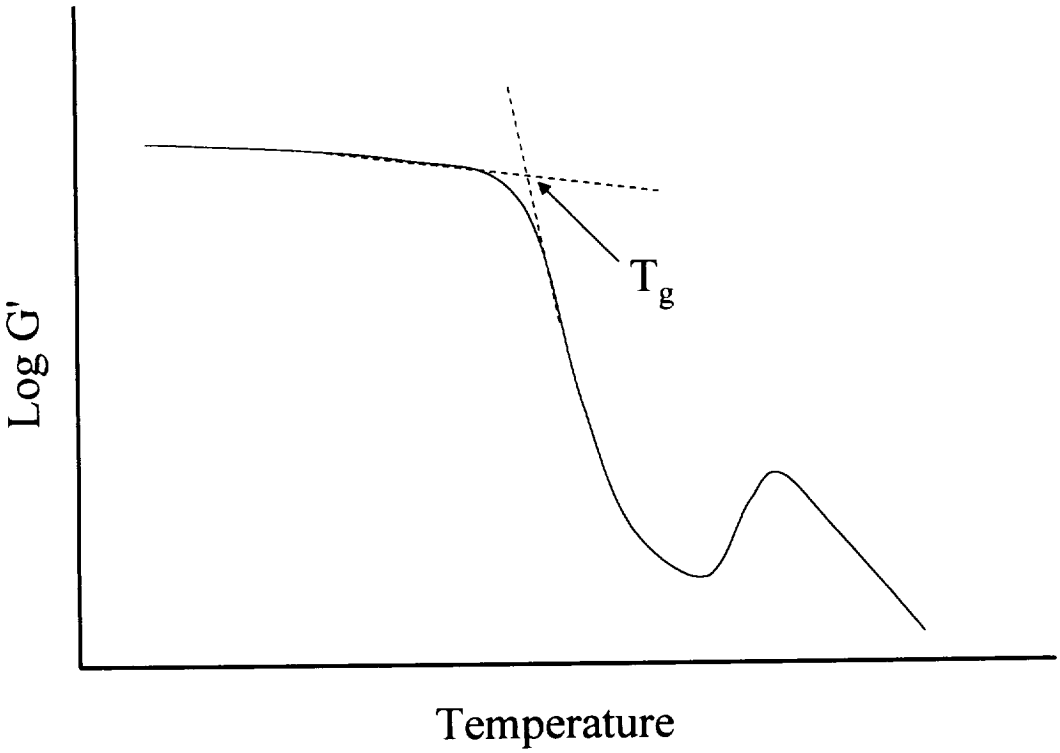

Figure 3.11. Schematic illustration of the relationship between storage modulus (G') and temperature for a typical BMI network. The glass transition temperature, T_g was determined by an intercept method, indicated by the dashed lines.

will be reflected in tan δ. Therefore, the midpoint between the glassy region and the rubbery plateau should not be used as an indication of the glass transition temperature.

Dynamic shear measurements were also performed in order to determine if network changes occurred during an isothermal hold above the network's glass transition temperature. Initially, the temperature was ramped to a set temperature and held for one hour while G' was measured. The sample was returned to room temperature and was then retested. This time the experiment proceeded as normal to verify if the isothermal hold resulted in an increase in the network's glass transition temperature.

3.5.2. Density by the Method of Hydrostatic Weighing

Density measurements provide a measure of molecular packing within a network. Therefore, hydrostatic weighing was used to determine the densities of the samples produced, according to ASTM 792-86.[56] Samples, approximately ½ inch long were cut from the ends of the sonic modulus specimens. The samples were weighed in air and then submerged in distilled water and weighed on a coiled wire platform of known weight in water. From these weights and the density of water, the densities of the BMI-based materials could be determined from the following equation:

$$\rho = \left(\frac{0.9975 \times a}{a + w - b} \right) \tag{3.2}$$

where a is the weight of the sample in air, b is the weight of the sample in water, and w is the weight of the coiled wire platform in water.

3.5.3. Molecular Weight between Crosslinks, M_c

Near equilibrium stress-strain measurements were performed on BMI/MDA samples at least 20 °C above the network T_g. A rubbery tensile modulus, E_e, was calculated from these measurements and then related to the number average molecular weight of effective network chains between crosslinks, M_c, through the kinetic theory of rubber elasticity.[57] E_e is given as:

$$E_e = 3\Phi\rho RT / M_c \tag{3.3}$$

where Φ is the front factor assumed to be unity in this investigation, ρ is the density at the test temperature, R is the universal gas constant, and T is the absolute temperature.

These experiments are performed 20 to 60 °C above the T_g of the network. Due to the presence of unreacted BMI in the cured material, an increase in G′ after the minimum with further heating has been reported. This implies that as the near-equilibrium stress-strain experiment proceeds to a

temperature greater than T_g the unreacted BMI could conceivably react to form new crosslinks. A continuously changing network would then further confound the determination of M_c. However, the values obtained in a period of minutes are relative rankings of M_c.

3.5.4. Materialography

Several methods were utilized to ascertain whether intimate mixing of the powders occurred without use of a solvent during processing and if the consolidation of the powders resulted in a uniform network structure. Standard materialographic methods were used to prepare the specimens for viewing. Samples were cut to fit in 1-inch diameter rubber molds. Epoxy was poured into the mold and cured to provide support for the sample. The embedded sample was ground on a water-lubricated grinding wheel with sandpapers ranging from 120 to 600 grit. Water flows over the sandpaper to cool the sample and to remove the debris away from the grinding surface. The sample was then polished using graded alumina suspensions down to 0.5 μm on a rotating cloth covered wheel followed by ultrasonic cleaning to remove the polishing media.

3.5.4.1. Optical Microscopy

Optical microscopy provides details of the structure such as length, shape, and arrangement of visible features.[58] A Leica Reichert MeF3 inverted metallograph,

equipped with a Polaroid camera was used to view the resin samples. The resolution is on the order of 0.5 μm with a magnification of approximately 1500x.

A second optical microscope used was the Olympus SZH, equipped with a Sony Color Video Camera (Model 38-386) and a Sony Color Video Printer Mavigraph. This camera offers low power microscopy with instantaneous documentation of results.

3.5.4.2. Solvent Etch

The process of etching is used to assess differences in the microstructure that may not be readily observable directly. After the grinding and polishing procedures, an etching solution of sodium boric acid was used to etch the newly exposed surface to reveal if any powder particles existed after curing.

3.5.4.3. Nomarski Differential Interference Contrast

Nomarski differential interference contrast (DIC) microscopy is used to view the surface topography. Flow patterns, greatly enhanced from polishing, are obvious with DIC. The DIC uses oblique lighting that shadows the sample. A cross-polarizer is employed to align two beams of light; one beam of light is focused onto the plane of the specimen and the other beam of light is reflected off of a reference mirror. The beams of light are rejoined back into the lens to give contrast by interference.[58] The Reichert-Jung MeF3

microscope was used for differential interference contrast observations.

3.5.4.4. O_2 Plasma Etch

An oxygen plasma etch is the bombardment of charged particles onto a polished surface to etch away the top layer of surface atoms. Etching was done in two stages, for 7 minutes under vacuum and for 9 minutes under 1 mbar of O_2. Great care is needed with O_2 plasma etching because textures can be introduced on the surface, which appear as artifacts and not microstructure.

3.5.4.5. Scanning Electron Microscopy (SEM)

Examination of a fractured surface allows one to investigate localized plastic deformation and any departures from ideal brittle fracture. Samples of BMI/MDA were submerged in liquid N_2 for two minutes. When the samples were pulled out of the liquid N_2, they were immediately fractured to induce a brittle failure. The fractured surfaces would also reveal the presence of unreacted powder within the cured material, if any.

The cryogenically fractured surfaces were coated in carbon for 20 minutes, mounted on an appropriate specimen holder, and viewed in a JEOL 6100 scanning electron microscope at NASA Lewis Research Center. A Polaroid camera was used to take photomicrographs.

3.5.5. Gel Permeation Chromatography (GPC)

Gel Permeation Chromatography (GPC) was performed at NASA Lewis Research Center on low-temperature cured samples of BMI/MDA. For GPC analysis, a Waters 6000 pump, equipped with a Valco injector and three phenogel columns, from Phenomex Co., were employed. The three columns had pore sizes of 1000, 500, and 100 Angstroms. Low-temperature cured samples of BMI/MDA were dissolved in NMP and filtered with a syringe, equipped with a disposable filter cartridge Leur tip.

A sample size of 100 μL was injected into the columns, heated to 90 °C with NMP flowing at a rate of 0.5 cc/min. A Waters Refractive Index Detector was used to monitor the difference in refractive index between the pure solvent and the dilute polymer solution. The Waters Maxima GPC software was employed to calculate the molecular weight distribution from the amount of solute versus retention volume curves.

3.6. Mechanical Properties

3.6.1. Plane Strain Compression

The compressive yield stress behavior in plane strain was obtained for the cured and postcured materials. Ford and Williams[59] were the first to test plastics in plane strain compression. In compression yield testing, a flat

sample with parallel faces is placed between two level, highly polished rectangular steel dies. A schematic diagram of the test specimen and dies is shown in Figure 3.12. The die fixture was loaded on an Instron, Model 1125 screw driven load frame. The upper die was attached to the crosshead and the lower die rested on the platform of a compression load cell. The Instron is loaded in compression at a crosshead speed of 0.5 mm/min until yield or fracture. To eliminate friction between the sample and the steel dies, Dow Corning's MolyKote G-N lubricating paste was used.

The compressive yield stress is given as:

$$\sigma_y = \sqrt{3}\,P \Big/ \left(2\,W_o\,b\right) \tag{3.4}$$

where P is the load at yield, W_o is the undeformed width of sample, and b is the width of the steel die in contact with the sample. The following guidelines were observed when performing the plane strain compression yield test: 1.) $b < h$, 2.) $8h < W_o < 16h$ and 3.) $L > 3b$. The test is considered "plane strain" because deformation is restricted in the 2,3 plane of loading. Since the area of specimen in contact with the die remains constant during deformation the strain values obtained in these experiments correspond to the true strain values. The mean value and standard deviation reported in the Results and Discussion section

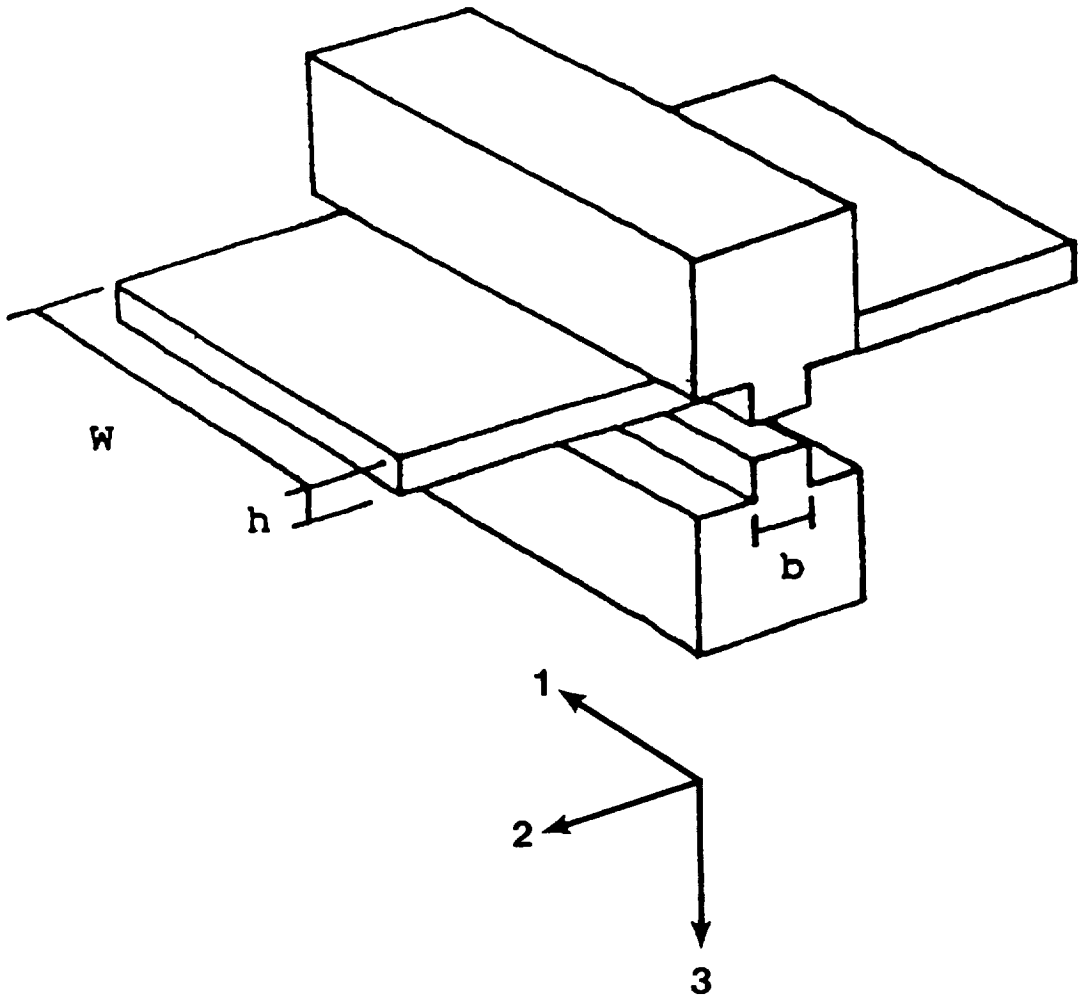

Figure 3.12. Schematic representation of the plane strain compression yield test fixture.

represent eight to twelve BMI/MDA, BMI/DDS, BMI, and PMR-15 samples for each condition.

3.7. Double-Torsion Fracture Energy Measurements

3.7.1. Experimental

The double torsion test was initially proposed by Outwater[60] but was developed more fully by Kies and Clark.[61] The double torsion test is a simple method for analyzing the slow crack growth of brittle materials.[62] An important feature of this test method is the crack length independence of the stress intensity factor.[62] The specimen is a simple rectangular plate that is supported on two parallel rollers. A "V" groove is machined along the lower face of the plate to ensure that the crack propagates along the specimen's long axis. A precrack is carefully introduced into one end of the sample, with a length as long as ½ of the specimen's width. A load via a tup is applied to the end with the precrack. The crack then propagates along the length of the specimen.

A schematic diagram of the double-torsion testpiece is shown in Figure 3.13. The specimen itself can be considered as two elastic torsion bars.[63] The displacement of these bars under a load is related to torsional deflections. Neither bending nor shearing contribute to the specimen

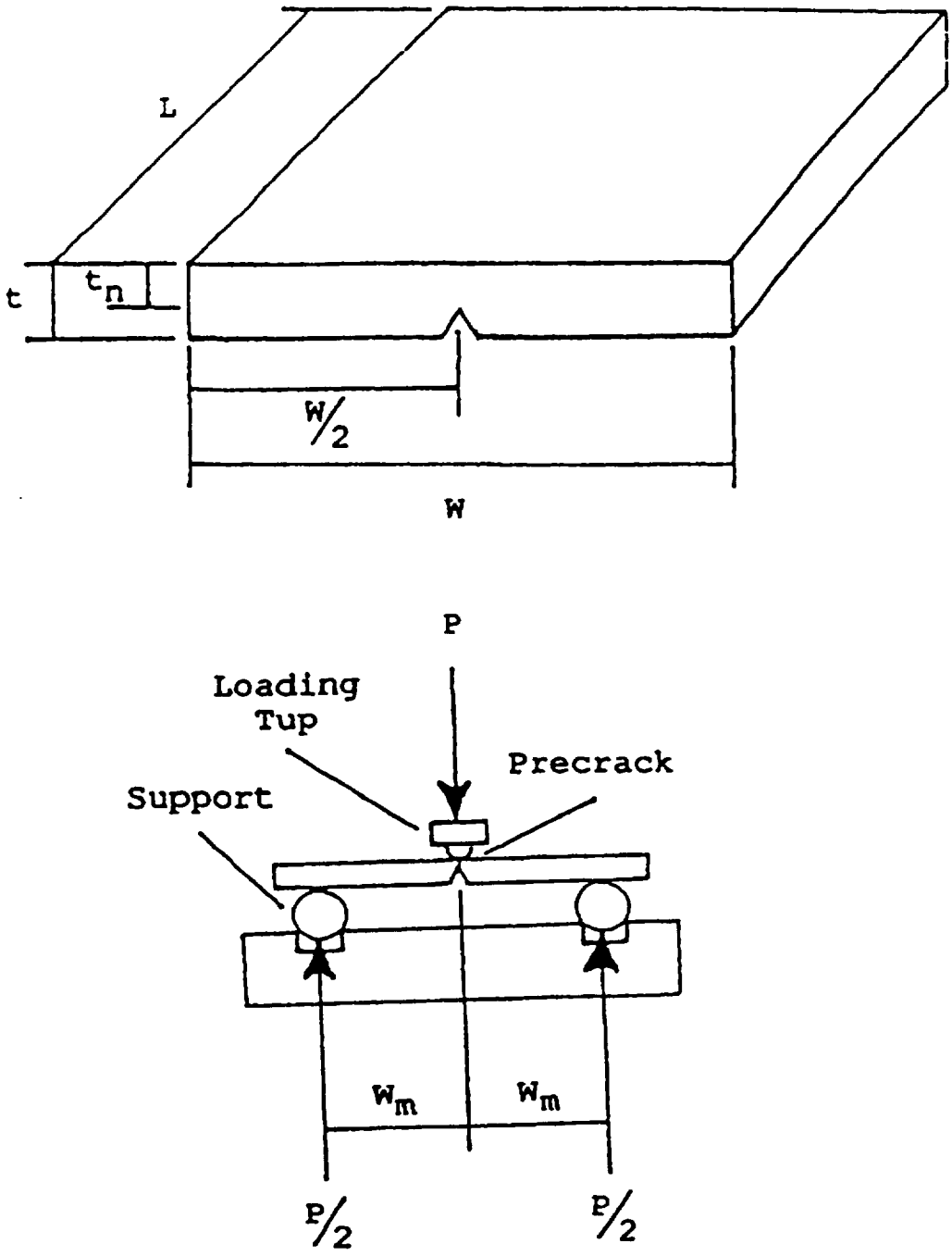

Figure 3.13. Schematic representation of the double-torsion sample and loading configuration.

deflection. All deflections can be attributed to elastic, torsional motions of the two arms. There is no need to measure sample deflections, crack lengths, or compliance relationships with this test method.

Under a compressive load, crack extension will occur in the direction that yields plane strain conditions. In general, a crack will move in an orthogonal direction to the crack front. The test method can be performed in three different modes: fixed displacement, which is the most effective mode to obtain continuous crack growth, constant displacement, and constant load.

The glassy fracture energies of cured and postcured networks were performed using double-torsion samples. All testing was done on an Instron, Model TM universal test machine in compression with a crosshead rate of 0.05 cm/min (0.02 in/min) at room temperature. The test setup is shown in Figure 3.14.[3] An aluminum platform (1/4" x 3" x 5") with six 1/8" wide by 1/8" deep alignment grooves was used to support two 1/4" diameter aluminum rods. The double-torsion testpiece, V-notch down, was placed on the two rods, held 1.5" apart. The precrack was positioned halfway between the two rods and aligned directly over the crosshead ram. On the mark, 2 mm away from the edge of the sample, two ball bearings (1/4" dia.) partially embedded into an aluminum disk (1/4" x 1" x 1") were situated on either side of the

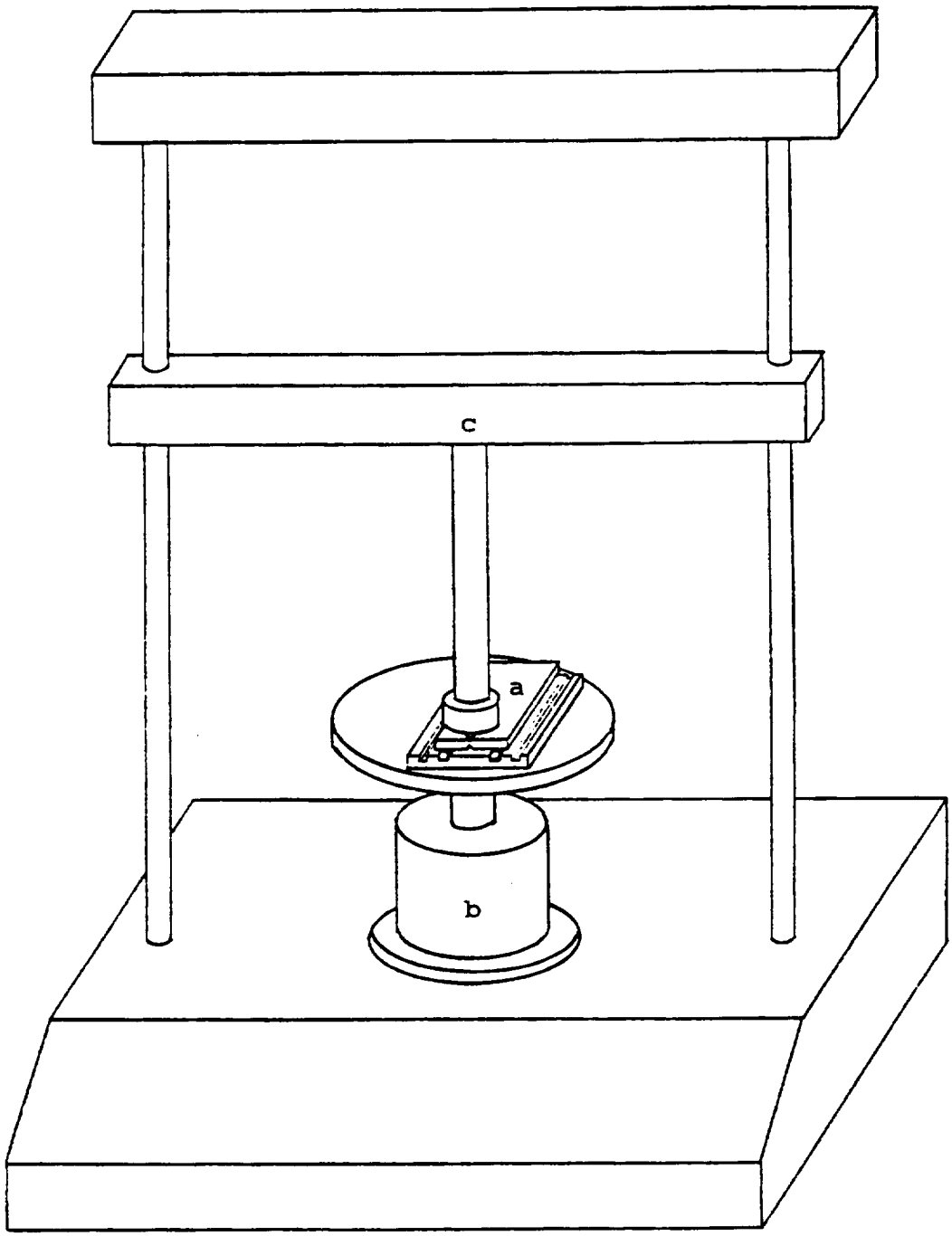

Figure 3.14. Schematic diagram of the Instron, Model TM universal test machine with double-torsion setup. (Figure from S. Mudrich.[3]) Labels denote the following: a) double-torsion sample, b) compression load cell, and c) Instron crosshead.

precrack, directly beneath the center of the crosshead ram. The load was applied when the crosshead ram, via constant crosshead displacement made contact with the ball bearing plate. The test continued until the sample failed into two pieces along the V-groove. After failure, the thicknesses of the fracture surfaces, t_n, were measured with a cathetometer and recorded.

The load versus time trace was registered on a strip chart recorder. The distance along the strip chart was converted to sample deflection by:

$$\text{Deflection (d)} = \frac{\text{(Crosshead speed)}}{\text{(Chart speed)}} \text{ X Chart distance} \qquad (3.5)$$

In this investigation, the chart speed was 6 cm/min.

3.7.2. Calculations

Both types of crack growth, unstable and stable, were observed for the cured and postcured materials. Stable crack growth occurs at a constant load where the rate of crack propagation is proportional to the rate of crosshead speed. A typical load-displacement curve for the double torsion test is shown in Figure 3.15a. Usually, this type of behavior occurs with fast strain rates or low test temperatures.

Unstable crack growth exhibits a stick-slip or saw-tooth behavior. A typical load-displacement curve for

unstable crack growth is shown in Figure 3.15b. This type of crack growth occurs at low strain rates or high test temperatures. Besides varying the strain rates or test temperatures, other factors that influence the type of crack growth are curing agents and cure schedules.[64]

For unstable crack growth, the first crack initiation load was not used. The subsequent critical loads, P_c, or the maximum values from the strip chart recorder were used to obtain the critical crack initiation loads, P^i. The minimum values from the strip chart recorder were considered the critical crack arrest loads, P^a. All load values were determined from the strip chart with an HP Digitizing Tablet.

The fracture energies of the cured and postcured BMI networks were determined from the following relationship:

$$G_{Ic} = \left[\frac{3 P_C^2 \quad W_m^2}{E(1-\nu) W t^3 t_n}\right]\left(\frac{C_{LD}}{C_{FT}}\right) \qquad (3.6)$$

where G_{IC} is the plane strain fracture energy, P_c is the critical load, W_m is the moment arm from the support rod to the ball bearing, E is Young's modulus, ν is Poisson's ratio, assumed to be 0.35, W is the width of the sample, t is the sample thickness, t_n is the fracture path thickness, C_{LD} is the displacement correction factor for the torsional bars undergoing loading, and C_{FT} is the finite thickness correction factor. The correction factors, C_{LD} and C_{FT}, are

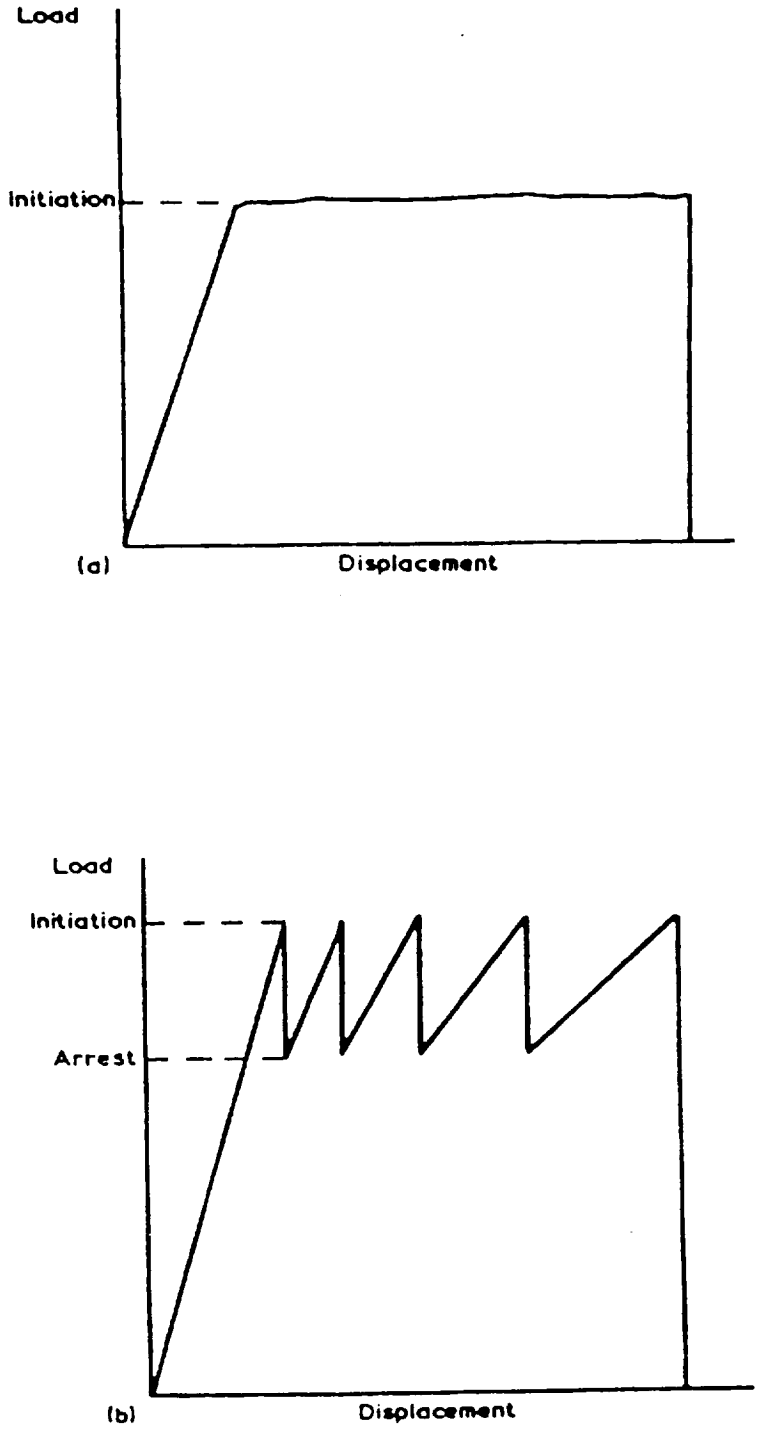

Figure 3.15. Typical load-displacement curves for a.) stable, continuous crack propagation and b.) unstable, stick-slip crack propagation.

described precisely in Geisler's dissertation[15] and will not be discussed here. The plane strain condition was used since t_n met the plane strain requirement for all BMI networks:

$$t_n \geq 2.5\left(G_{IC} E / \sigma_Y\right)^2 \qquad (3.7)$$

where σ_y is the yield stress determined at the same crosshead rate and temperature as G_{IC}. In order to minimize the number of samples tested in plane strain conditions, the general guidelines for fracture specimen dimensions of metallic materials were also employed: $L \geq 2.5\ (K_{IC}/\sigma_Y)^2$ and $L \geq 50 r_p$, where r_p is the plastic zone size radius. The modulus values, E, were determined sonically by an impulse excitation technique. The mean value and the standard deviation represent eight to twelve samples of BMI/MDA, BMI/DDS, BMI, and PMR-15 and ten to fifteen samples of BMI/DABA at each mole ratio.

3.7.3. Plastic Zone Size Calculations

There is a simple relationship that exists between fracture energy, G, and the stress intensity factor, K, using linear elastic fracture mechanics (LEFM). Under plane strain conditions, the fracture energy of a crack in a homogeneous material for Mode I deformation can be described as:

$$G_c = \left(\frac{K_{Ic}^2}{E}\right)\left(1-\nu^2\right) \qquad (3.8)$$

where ν is the material's Poisson ratio. LEFM also predicts that infinite stresses occur at the crack tip but in real materials this is not the case. A yield zone does form at the crack tip and the Irwin model can estimate the size of this plastic zone.[65] Irwin assumed that the plastic zone had a circular cross section. Employing plane strain conditions where yielding is suppressed by the triaxial stress state, the plastic zone size is given as:

$$r_p = \left(\frac{1}{6\pi}\right)\left(\frac{K_I}{\sigma_{Yt}}\right)^2 \qquad (3.9)$$

where r_p is the radius of the estimated plastic zone and σ_{Yt} is the yield stress in tension. Wronski[66] found that for epoxies, the yield stress in compression was approximately 0.75 that of the yield stress in tension. This relationship has been used in this investigation. Equation 3.9 then becomes:

$$r_p = \left(\frac{1}{6\pi}\right)\left(\frac{K_I}{0.75\,\sigma_{Yc}}\right)^2 \qquad (3.10)$$

where σ_{Yc} is the yield stress, measured in plane strain compression.

3.8. Rubbery Modulus Measurements

3.8.1. Above T_g - Near-Equilibrium Stress-Strain Testing

3.8.1.1. Experimental

The molecular weight between crosslinks, M_c, of the networks was determined based on the kinetic theory of rubber elasticity[57] from rubbery tensile moduli measurements. The rubbery tensile moduli were determined from stress-strain tests performed on an Instron Model 4505 universal testing machine equipped with an environmental chamber, capable of reaching 400 °C.

Due to the inherent brittleness of the networks, samples were not dumbbell-shaped. Benchmarks were placed in the middle of the rectangular samples with white correction fluid. The sample dimensions and weight of each sample were recorded prior to testing.

The chamber temperature was set to approximately 20 °C above the glass transition temperature of the sample to be tested. Each testpiece was loaded into the upper clamp and allowed to equilibrate to the test temperature. A thermocouple loosely encircled the sample in the benchmark area to provide accurate control of the test temperature. Once the test temperature was reached, the sample was mounted into the lower clamp and allowed to equilibrate to the test temperature.

The load cell was balanced and the crosshead was incremented at a very slow rate (0.05 cm/min) until the total crosshead travel was 0.38 mm, which does not translate to sample displacement. Instead the elongation was determined by measuring the distance between the benchmarks on the testpiece with a cathetometer after the retractive force was permitted to diminish to an apparent equilibrium value. The load was recorded manually. After reaching a nearly constant value of load, the crosshead displacement was increased by 0.38 mm and the procedure was repeated.

The BMI based networks were not able to approach strains of >10% due to their brittleness. In addition, the low-temperature cure condition and the BMI samples were too brittle to test at 20 °C above their T_g. Moreover, the low-temperature cured samples would further cure with the addition of heat.

3.8.1.2. Calculations

The initial unstrained benchmark length, l_o, may be calculated by plotting the length versus equilibrium load and extrapolating back to zero load. The nominal strain, ε, was calculated as:

$$\varepsilon = \left(\frac{l - l_o}{l_o}\right) \qquad (3.11)$$

where l is the length between the benchmarks during loading.

The engineering stress, σ_e, was calculated as:

$$\sigma_e = f / A_o \qquad (3.12)$$

where A_o is the initial cross-sectional area of the sample and f is the retractive force applied to the specimen. The engineering stress versus time for the various strain levels was plotted for each sample to illustrate stress relaxation.

True stress, σ_t, calculated from the equilibrium load value was further manipulated to give $\sigma_t/3\rho RT$. The linear plots of $\sigma_t/3\rho RT$ versus strain gave slopes equal to the rubbery tensile moduli for the samples. Three samples from the high- and low/high-temperature cure condition of BMI/MDA were tested and averaged.

3.8.2. Intermittent Stress Relaxation

3.8.2.1. Experimental

An Instron Model 4505, screw driven load frame, equipped with an environmental chamber was used for the intermittent stress relaxation experiments. The sample consisted of a rectangular shaped specimen with benchmarks. Only the low/high-temperature and high-temperature cured BMI:MDA materials in a 2:1 mole ratio were tested.

In an intermittent stress relaxation experiment, the specimen was maintained in an undeformed condition in the upper grip at the test temperature. At widely spaced time intervals, the sample was tightened into the bottom grip. A

fixed deformation was applied to the specimen and the initial retractive force was measured. Before the specimen was unloaded, the benchmarks were measured with a cathetometer. The sample was removed from the lower grip until the next time interval when the process was repeated. The length of the sample was checked after returning to zero strain and zero stress to make sure no elongation of the sample is observed between test measurements.

3.8.2.2. Calculations

After the nominal strain was determined by Equation 3.11, the engineering stress was calculated using the initial retractive force and employing Equation 3.12. The engineering stress versus time was plotted against the stress relaxation plots described earlier.

3.8.3. Below T_g - Sonic Modulus

3.8.3.1. Experimental

A non-destructive test that measures the resonant frequency of a sample and can be used to calculate the modulus, which is a function of the measured frequency, dimensions, and weight of the sample, is an attractive alternative to mechanical tests which rely on difficult cathetometer measurements on a deformed sample. The impulse excitation technique utilizes a sensitive microphone and electronics to analyze sound waves emitted from the vibrating sample.[67]

To determine the appropriateness of this technique, a sample of BMI/DABA in a 1:0.87 mole ratio was used in the correlation of the modulus determined by three-point bending with strain measured by cathetometer, the sonic test technique, and four-point bending with strain measured by a series of strain gages. These values were also compared to previously determined values reported by the manufacturer of Matrimid 5292 (BMI:DABA).

The recommended setup for the operation of the impulse excitation technique is shown in Figure 3.16. A sample was placed on two pieces of Styrofoam so that the ends of the sample hung over the Styrofoam support rods by approximately 0.224L, where L is the length of the sample. A small mallet with a ball bearing head was used to strike the surface of the sample, causing the specimen to vibrate. A microphone detected the vibrating wave and a GrindoSonic Instrument, manufactured by Lemmens-Elektroniks, Belgium measured the frequency of the resonant wave.

3.8.3.2. Calculations

The frequency values were tabulated and inserted into a computer program specifically designed by the makers of the GrindoSonic, which calculated Young's modulus through the following equation:

$$E = 0.94642\ \rho\ L^4\ f^2\ T/\ t^2 \qquad (3.13)$$

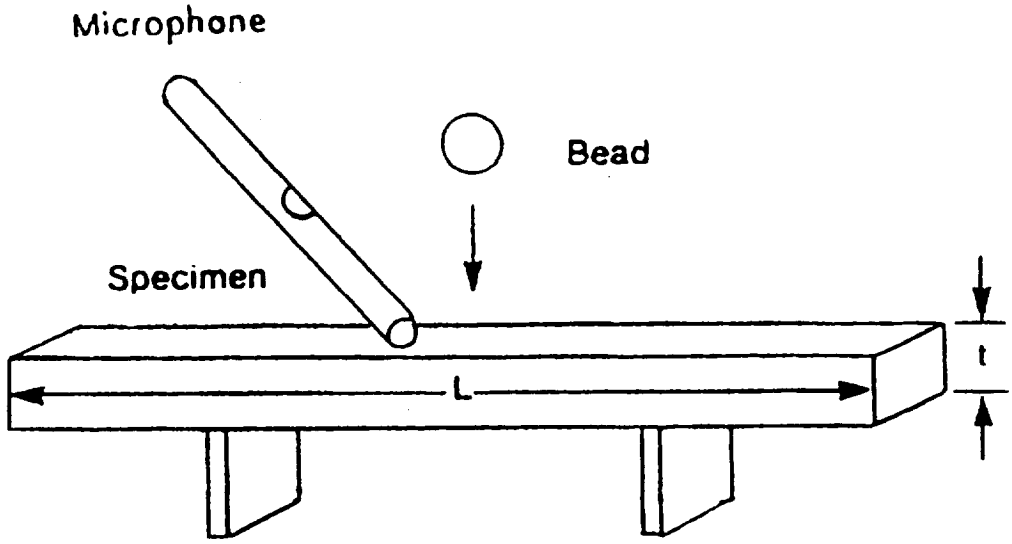

Figure 3.16. Schematic diagram for setup of the impulse excitation technique, or sonic modulus experiment.[67]

where ρ is the density of the sample, L is the sample length, f is the frequency of the wave measured, T is the shape factor dependent on Poisson's ratio, and t is the specimen thickness. The mean value and standard deviation of eight to twelve samples of each cure condition and composition of BMI/MDA, BMI/DDS, BMI, and PMR and ten to fifteen samples of each cure condition of BMI/DABA are plotted verses mole fraction BMI.

3.9. Dielectric Measurements

3.9.1. Instrumentation

Cure measurements were conducted on a Eumetric System III Microdielectrometer, manufactured by Micromet Instruments. The small microsensor (0.2" x 0.1" x 0.01") employed by the instrument contained a microthermal diode which could monitor the temperature as well as measure the phase and amplitude of the output current at each frequency tested. A schematic diagram of the experimental setup is shown in Figure 3.17.[7]

3.9.2. Dielectric Measurements - BMI/MDA and BMI/DDS

Dielectric cure monitoring was used to characterize the powders previously discussed. After a sensor was placed on a Teflon coated aluminum mold specifically designed to hold

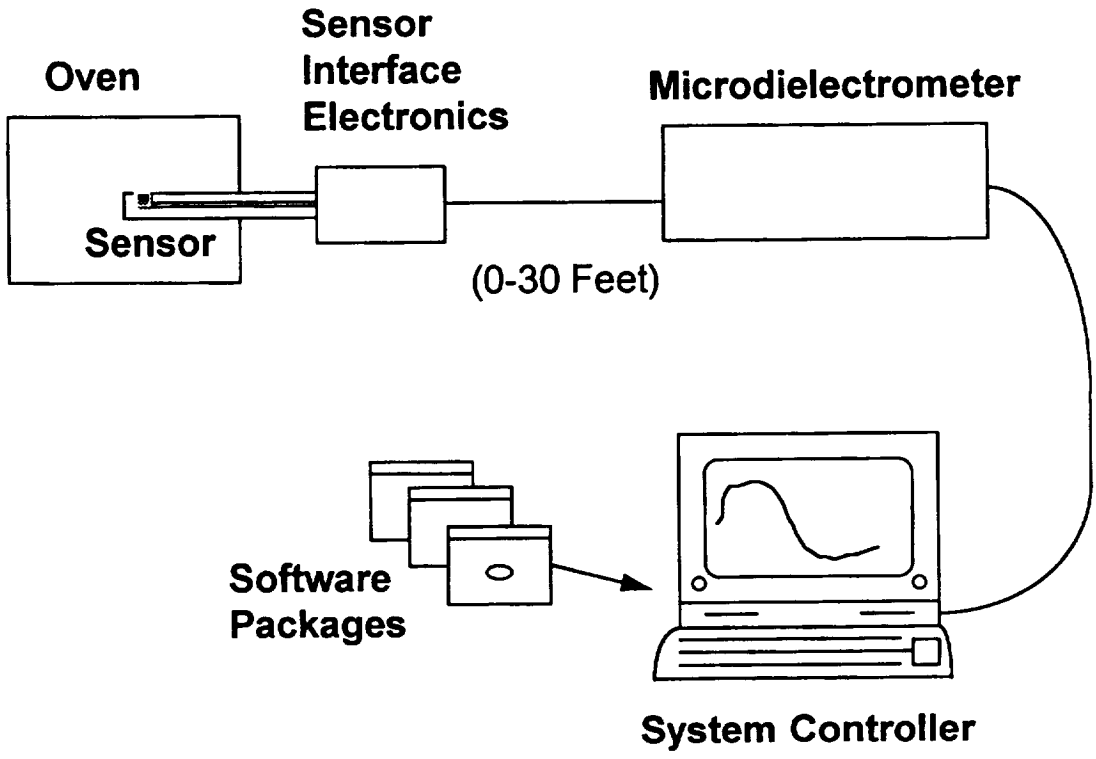

Figure 3.17. Schematic diagram of the microdielectric measurement system.

the sensor in place, a small amount of powder (approximately 2 grams) was placed over the sensor pad. The entire fixture was inserted into a preheated oven for 4 to 8 hours to monitor the chain extension reaction. During the experiment, the temperature of the material slowly increased while the BMI/MDA or BMI/DDS powder melted and intimately covered the sensor pad. The frequency was cycled from 0.1 Hz to 100,000 Hz while the gain, phase, and temperature were monitored as a function of time.

3.9.3. Dielectric Measurements - BMI/DABA

Dielectric analysis was used to characterize the gelled material of BMI/DABA, which was produced in a reaction kettle and stored in a desiccator. After a dielectric sensor was placed on a Teflon coated aluminum mold specifically designed to hold the sensor in place, approximately 2 grams, of the BMI/DABA was positioned over the sensor pad. The entire fixture was placed in a preheated oven for 8.5 hours to monitor the dielectric response. During the experiment, the material temperature slowly increased to the set temperature. The frequency was cycled from 0.1 to 100,000 Hz while the gain, phase, and temperature were monitored as a function of time.

3.10. Polymer Modeling

Biosym software, with Insight *II* user interface and the Synthia module, by Biosym Technologies, Inc. was employed to model chain stiffness and entanglement properties.[68] A Silicon Graphics workstation equipped with the software was used. Room-temperature properties such as density and Young's modulus were calculated as well as the glass transition temperature for the low-temperature cure conditions of the BMI/MDA and BMI/DABA. Only the low-temperature cure condition for each system was modelled since the Synthia module cannot take into account network crosslinks.

The mole ratios of the BMI/MDA system that were modelled were 4:1, 2:1, 1:1, and 1:2. The mole ratios of the BMI/DABA system were varied from 4:1, 2:1, 1:1, 1:0.87, and 1:1.2.

In modeling with the Synthia module, the mole ratios should be expressed in decimal notation, less than 1. For example, a 4:1 mole ratio would be represented as 0.8:0.2.

In addition to the systems listed above, three other diamines were modelled in a 2:1 and 1:1 mole ratio with BMI. These are p-phenylene diamine (PPD), p-xylenediamine (PXD), and 4,4'-diaminobiphenyl (DBP). The structures of the three diamine monomers are shown in Figure 3.18.

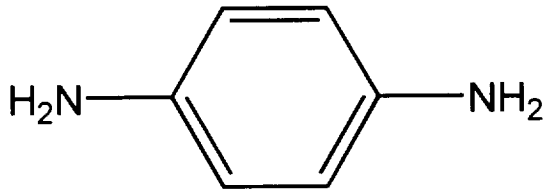

a.) p-phenylene diamine (PPD)

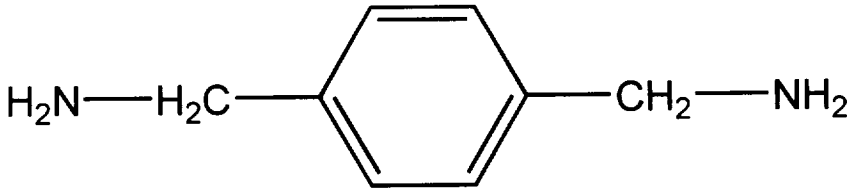

b.) p-xylenediamine (PXD)

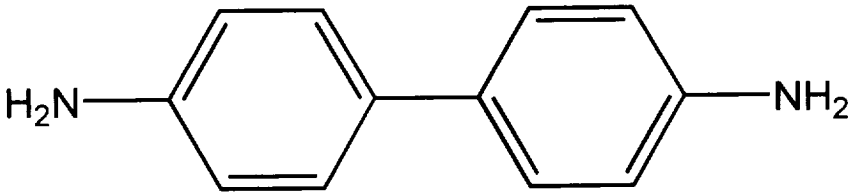

c.) 4,4'-diaminobiphenyl (DBP)

Figure 3.18. The chemical structure of a.) p-phenylene diamine (PPD), b.) p-xylenediamine (PXD), and c.) 4,4'-diaminobiphenyl (DBP).

CHAPTER IV

RESULTS AND DISCUSSION

4.1. Introduction

In processing the BMI/MDA and BMI/DDS copolymers, a powder melt technique was utilized to prepare the constituents prior to molding. Dielectric analysis was used to determine the cure conditions for the BMI-MDA system. The powders and molded materials were characterized by various methods to determine cure times, molecular weights, thermal stability, rheological properties, and mechanical properties as a function of mole fraction BMI. Modelling of the mechanical properties of these systems was performed to verify the validity of current molecular simulation techniques and to try to gain additional insight into the behavior of these materials.

The hypothesis or premise of this research was to determine whether curing along different thermal paths produce networks with differing topologies and hence, differing physical and mechanical properties.

4.2. Network Preparation and Characterization

4.2.1. BMI/MDA and BMI/DDS Processing

Much effort was expended in determining an appropriate method for preparation of cured BMI/MDA and BMI/DDS materials. The most common practice for producing BMI-based copolymers found in the literature,[19,20,27] was based on solvent-powder processing methods. With this technique the two starting materials are dissolved and combined in an appropriate solvent, the solvent is extracted, and the resultant powder material is molded. The disadvantages[69] of this procedure are incorporation of solvent into the polymer structure leading to the formation of voids by volatilization of the solvent, a plasticization effect due to excess solvent, and reduced thermal stability due to occluded solvent.

The first attempts at producing material for this study were modeled after these solvent-powder processing methods[19,20,27] using Methylene Chloride (MeCl) to intimately mix the BMI and MDA powder together. After the BMI and MDA were dissolved in MeCl, the solvent was evaporated off in a vacuum oven. The remaining material was ground to a fine powder and compression molded. The result of the compression-molded powder is shown in Figure 4.1.

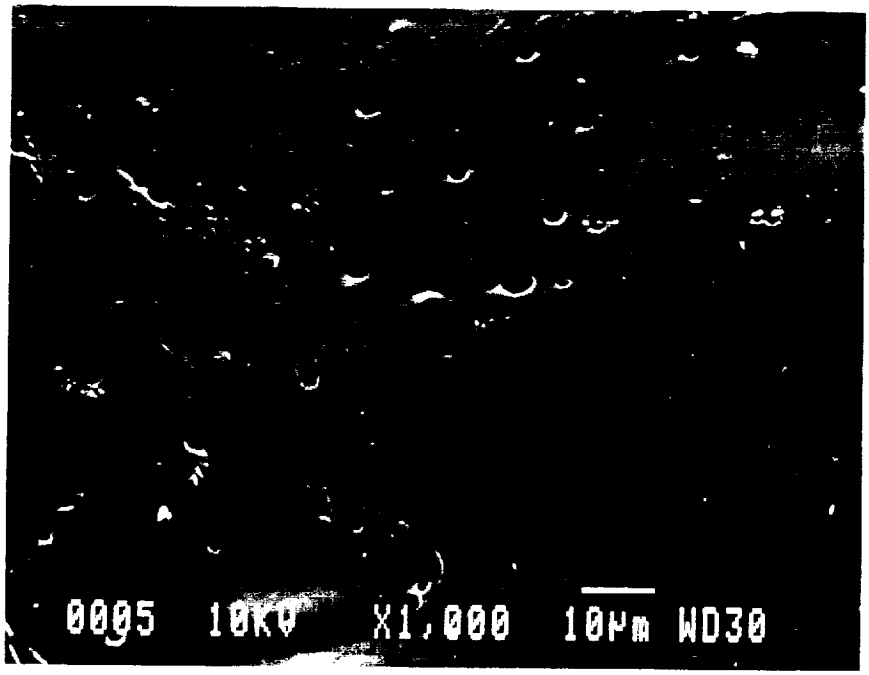

Figure 4.1. Photomicrograph of BMI/MDA produced by the solvent-powder processing method.

Impressions of tiny bubbles on the order of 2-5 μm are clearly visible in Figure 4.1, which are indicative of solvent retention after drying and its volatilization during curing. Over 70 different attempts were made using the solvent-powder processing route, varying the solvent and other processing parameters. All these attempts using solvent-powder processes were equally unsuccessful with evidence for solvent retention observed in all cases.

Therefore, an alternative technique found in the patent literature[53] and recommended by Donnellan[70] was instituted. This alternative technique was based on a melt-processing method. During this process the two constituents are mixed together and heated until the lower melting point constituent melts and wets the second, resulting in a heterogeneous mixture. This mixture is then cooled and ground into a fine powder and subsequently reacted during molding.

For example, in preparing BMI:MDA copolymers both individual constituents initially consist of fine powder. These are mixed together in a beaker at the appropriate mole ratio and heated to 80 °C in vacuum at which point the MDA melts and wets (but does not react with) the BMI powder. Once the two constituents are thoroughly mixed

together the mixture is allowed to cool. After the mixture cools and solidifies it has the consistency of peanut brittle. Grinding is used to reduce the particle size of this gelled substance and for further mixing and blending of the two constituent materials. After grinding, the resulting powder is screened - a mechanical method of separating the powder in terms of particle size. The screen surfaces act as a "go/no-go" criterion. The smaller particles are allowed to pass through the surface opening while retaining the larger particles. The net effect is a physical separation of the powder based on particle size, resulting in a particle size distribution.[71] Screening was also used to make sure that all the powder used for molding was no larger than 250 μm. All the gelled material was ground repeatedly until it passed through at least this first sieve.

Particle size distributions were recorded for all the systems (as shown in Figure 4.2). For all the systems, approximately 42-46 weight percent of the total amount of the melt-processed powder consisted of particle sizes of 107 to 211 μm. All the powder used for molding was less than 250 μm in diameter.

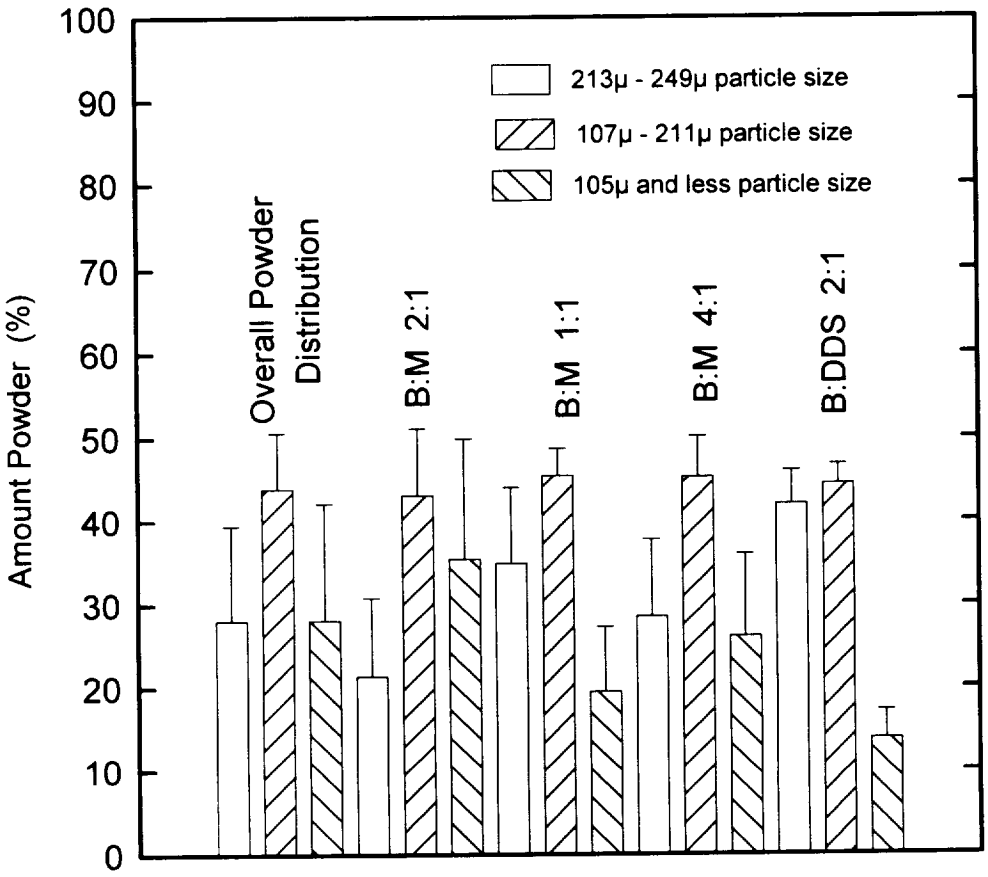

Figure 4.2. Powder size distributions for the material molded for this investigation.

The ground powder is then placed in a mold and compacted under light pressure. It was found that a wide particle size distribution was actually beneficial for molding compared to using a narrow size range. In the case of a wide powder size range, particles of a smaller size fit into the interstices between the larger particles. This ensures a higher packing density than with a single large particle size alone. It was found that using a too narrow range of powder size resulted in not all the powder melting and properly mixing during heating. After the initial compaction process, the material is heated or cured under various conditions during molding to control the final structure of the co-polymer.

4.2.2. Materialographic Examination of Cured Plates

To ensure that intimate mixing of the powders occurred during curing, various materialographic techniques[58] were used to characterize cured plates. While analysis of various materials was conducted, the bulk of the materialography was performed on samples of BMI:MDA in a 2:1 mole ratio, cured at 140 °C for 16 hours and the descriptions provided below are for this material unless the cure condition is otherwise stated. Materialography was also performed on the as-screened powder.

After blending of the constituents, the question that still remained was whether any individual powder particles were present in the molded material. Bright field optical microscopy, where the 'direct unscattered beam is allowed to reach the image plane'[58] is used to distinguish macro- to microstructural features within the material, ranging from 1 cm to 0.2μm. At a magnification of 100x, individual powder particles were not apparent as demonstrated in Figure 4.3. The dark random spots are contaminants within the powder from the grinding process. In contrast, Figure 4.4 is a bright field micrograph of the as-ground powders embedded in an epoxy matrix. This figure indicates how powders or the presence of powders would tend to appear under bright field techniques. Such features were never observed in the consolidated co-polymer plates.

With the solvent etch/acid etch method, the microstructure is revealed by preferentially etching amorphous regions. Since BMI is a crystalline powder, this technique would etch the matrix material around unreacted BMI revealing its presence. If the entire sample is amorphous, it will etch the bulk material more or less evenly. Figure 4.5 is an optical micrograph of a sample that was solvent/acid etched. The micrograph does not

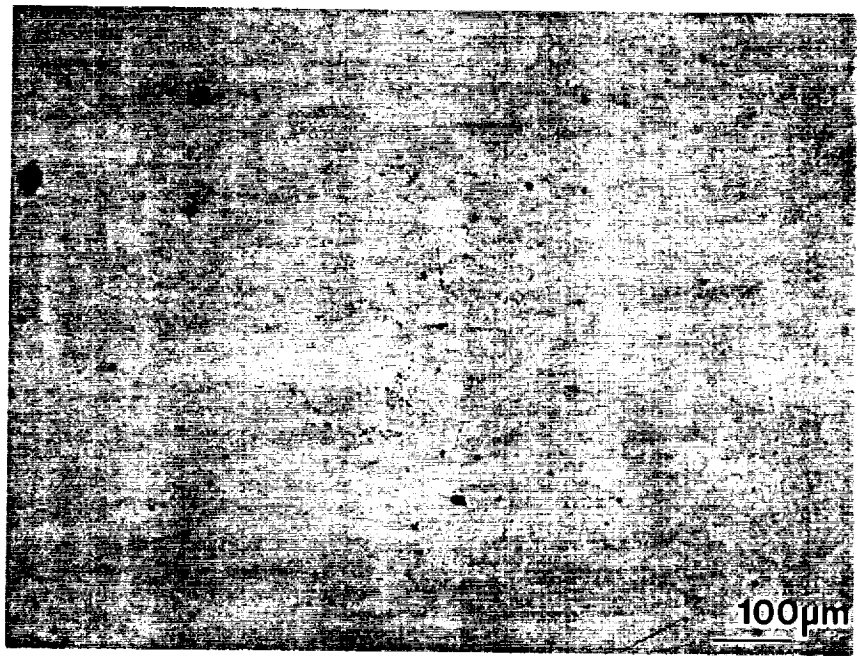

Figure 4.3. Bright-field optical photomicrograph of BMI:MDA in a 2:1 mole ratio, cured at 140 °C for 16 hours.

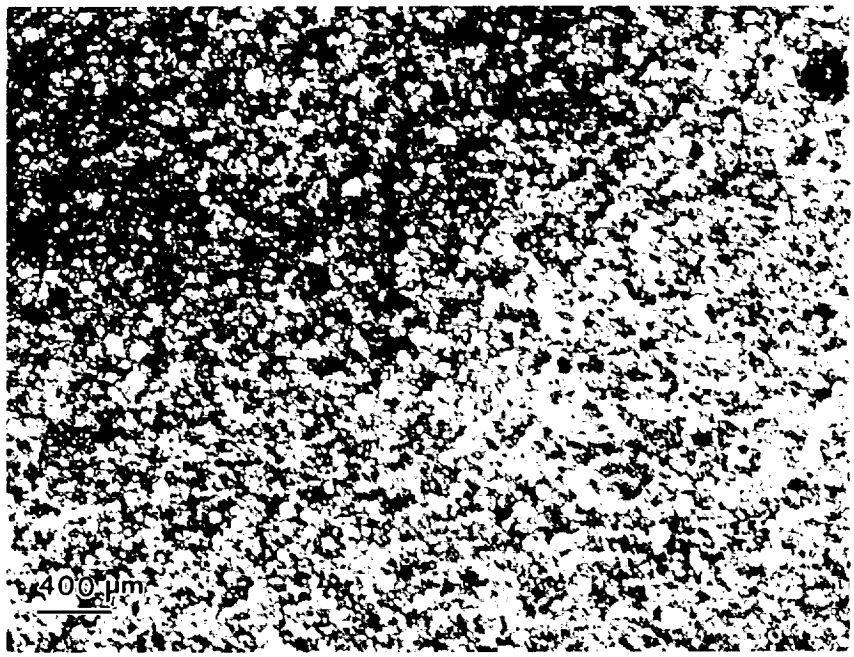

Figure 4.4. Bright-field optical photomicrograph of the as-ground powders.

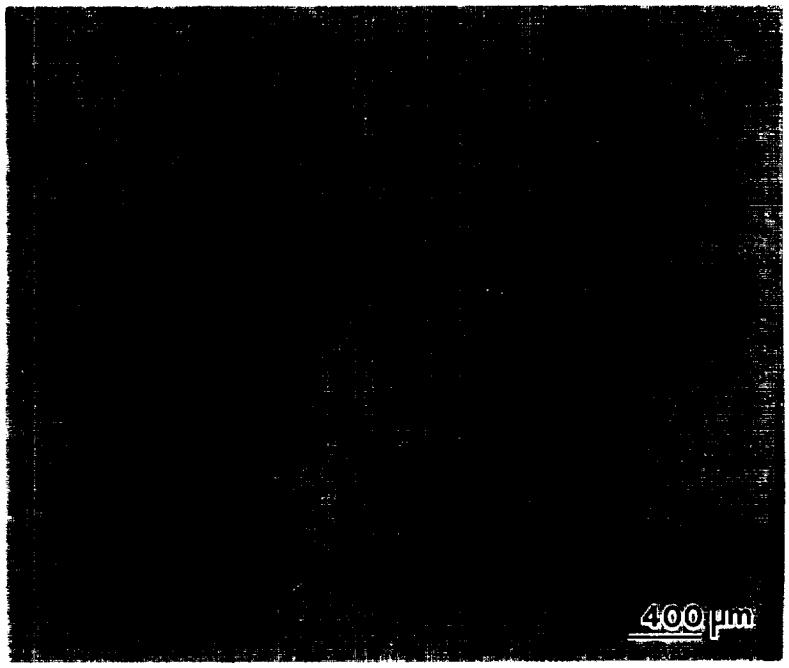

Figure 4.5. Bright-field optical photomicrograph of BMI:MDA in a 2:1 mole ratio, cured at 140 °C for 16 hours after solvent etch/acid etch.

reveal any pronounced microstructural features or the presence of BMI-rich powder particles.

Samples were also plasma-etched for 7 minutes and then again for 9 minutes. Plasma etching is the bombardment of a surface with ions, in this case, oxygen ions. One of the problems associated with plasma etching is that textures can be introduced which are artifacts. Figure 4.6 is a bright-field micrograph of a plasma-etched surface. In spite of the rough surface appearance, individual powder particles are not apparent after preferentially etching the surface by plasma techniques.

Figure 4.7 is the differential interference contrast (DIC) micrograph of a polished surface of BMI:MDA in a 2:1 mole ratio. DIC microscopy illuminates the surface topography and produces a pseudo- 3-D image of the surface.[58] One disadvantage associated with DIC is that flow patterns are usually observed. These are artifacts from either processing or polishing the sample. In Figure 4.7, only the polishing patterns are observed; evidence of powder particles was not observed.

The final characterization technique used to determine if powder particles were left in the consolidated material was viewing of the cryogenic fracture surfaces by scanning

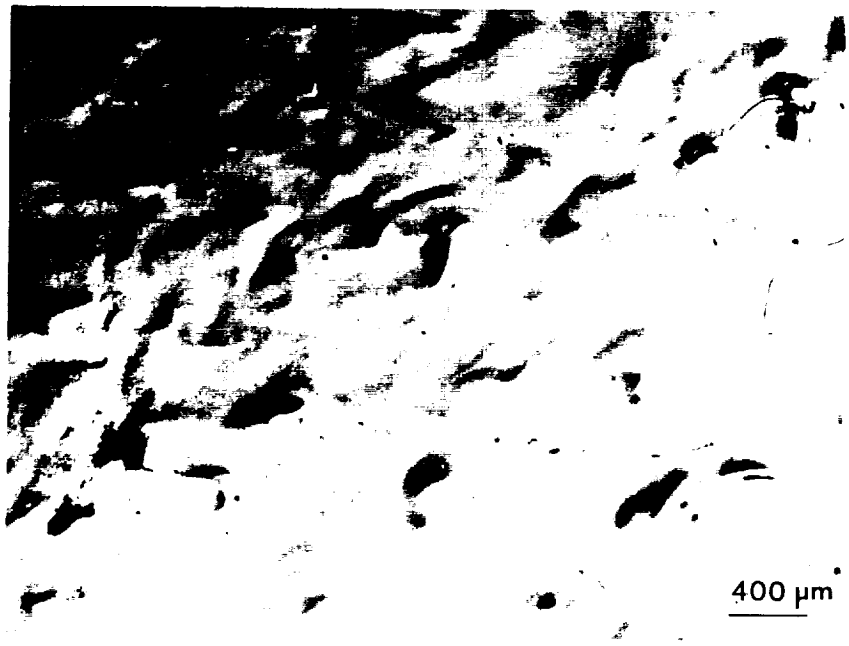

Figure 4.6. Bright-field optical photomicrograph of BMI:MDA in a 2:1 mole ratio, cured at 140 °C for 16 hours after plasma etching.

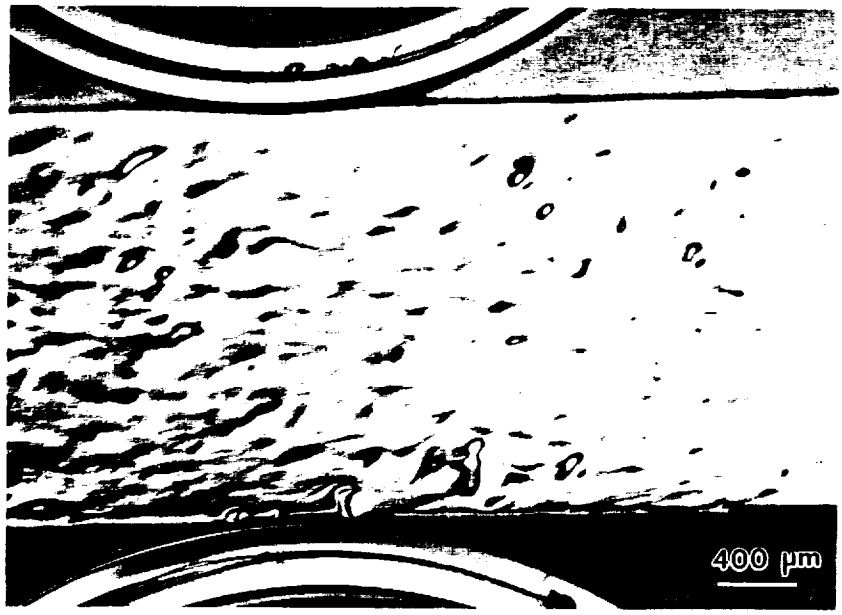

Figure 4.7. Dark-field optical photomicrograph of BMI:MDA in a 2:1 mole ratio, cured at 140 °C for 16 hours.

electron microscopy (SEM). After immersing the samples in liquid nitrogen for 10 minutes, brittle fracture was induced to determine the existence of any dispersed phase. Figure 4.8 is a SEM micrograph of the BMI:MDA in a 2:1 mole ratio, cured for 16 hours at 140 °C. There is evidence of cleavage brittle fracture but no sign of fracture along powder particles. Incidentally, there is also no indication of solvent bubbles as shown in Figure 4.1.

Consequently, a number of materialographic techniques were used to characterize the as-processed plates of BMI:MDA and all the techniques revealed that the material was uniform and homogeneous, without significant porosity or unreacted powder particles, thus justifying use of the melt-processing method for production of polymer plates.

The first indication that there were at least two distinct network topologies produced by the various cure cycles was during the cryogenic fracturing of BMI:MDA in a 2:1 mole ratio, cured at 140 °C for 16 hours versus cured at 220 °C for 6 hours. The sample cured at low-temperature shattered into many pieces during the immersion into liquid nitrogen (Figure 4.9). The sample cured at high temperature did not shatter and was difficult to break on impact, as evident in Figure 4.10.

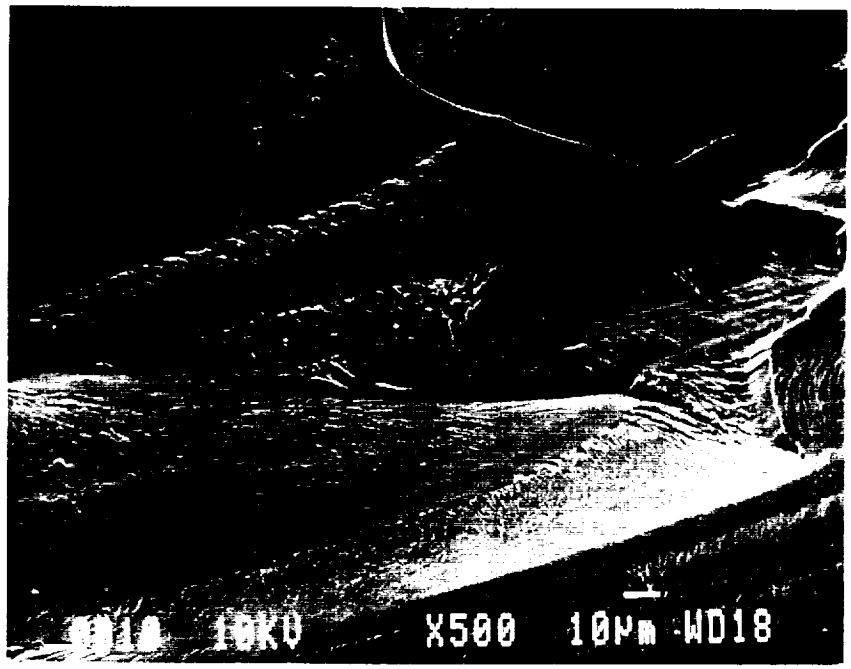

Figure 4.8. Scanning electron micrograph of BMI:MDA in a 2:1 mole ratio, cured at 140 °C for 16 hours after fracturing at cryogenic temperatures.

Figure 4.9. Optical photomicrograph of BMI:MDA in a 2:1 mole ratio, cured at 140 °C for 16 hours after fracturing at cryogenic temperatures.

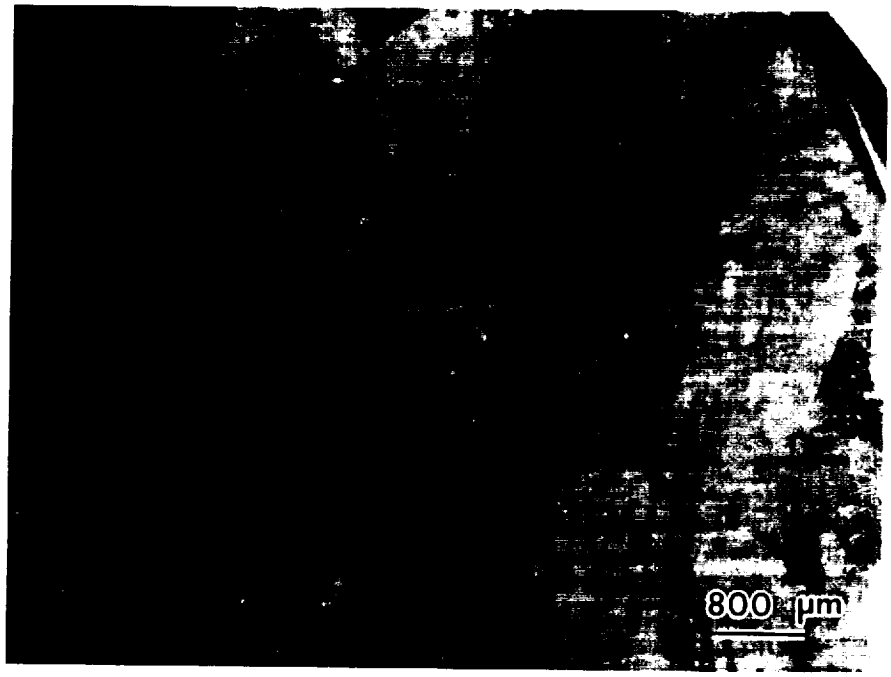

Figure 4.10. Optical photomicrograph of BMI:MDA in a 2:1 mole ratio, cured at 220 °C for 6 hours after fracturing at cryogenic temperatures.

4.3. Dielectric Measurements of Thermosets

Processing variables such as viscosity and the times for the beginning and end of the reaction must be determined and controlled during the curing of a resin. *In-situ* cure monitoring using frequency-dependent electromagnetic impedance measurements is useful in evaluating these processing variables by correlating the chemical reactions and rheology of the system to the electrical properties of the polymer.[72] By monitoring the temperature, time, and the frequency dependence of the impedance, chemical and rheological changes and consequently key processing variables may be determined. The dielectric properties measured are characteristic of the number and magnitude of the dipole moments of the molecular segments, ionic transport, and molecular chain diffusion. The amount of dipoles in the material is dependent upon the chemical nature of the reactants.

The dielectric properties of an uncured thermosetting resin change as a result of three effects:[73] 1.) A decrease in the concentration and mobility of protons which are produced by dissociation of amine groups, 2.) A decrease in the dipole moment per unit chain segment as the length of the chain and the crosslink density increase, and 3.) A

rapid increase in the dielectric relaxation time as the diffusion of the chain or network segments carrying the dipoles become progressively slower with the growth of the chains and networks (steric hindrance). All of these effects lead to a slowdown of dipole movement and ion mobility. As chain propagation or crosslinking increases the molecular weight of the network, the viscosity increases and the permittivity value decreases.

Permittivity, ε', is a measure of the degree of alignment of dipoles and is a function of the strength, amount, and mobility of the dipoles in a resin.[44] Permittivity values usually begin at a high level during cure because initially, the liquid resin contains a high concentration of highly mobile dipoles. As the material hardens, the permittivity values decrease because the dipole motion is restricted by network formation. In the case of the BMI:MDA system, the starting material is powder; hence, there is a transition from powder (solid) to liquid to solid and the permittivity does not begin at a high level due to the immobile dipoles of the powder state. Thus for this system, permittivity would be expected to start low, increase dramatically, and then drop off again.

The loss factor, ε'', is a measure of the energy required to align dipoles and move ions. The loss factor is the sum of both the dipole motion and ionic conduction:[44]

$$\varepsilon'' = \sigma / \varepsilon_o\omega + \text{dipole terms} \qquad (4.1)$$

where ε'' is the loss factor, ε_o is the permittivity of free space (8.854×10^{-14}), ω, the angular frequency, is $2\pi f$, where f is the applied frequency, and σ is the bulk ionic conductivity. At low frequencies, the dipole terms become negligible. The ionic conductivity is a molecular parameter that arises from movement of ionic impurities in the material, is frequency dependent and is very sensitive to network changes. At the beginning of the cure, the ion mobility is high, and therefore, ionic conductivity is high. Before gelation, σ is inversely proportional to the viscosity. As the cure proceeds, the ionic conductivity decreases because the mobility of the ions decreases due to the formation of a highly crosslinked network.

The use of different frequencies within an experiment demonstrates the extent of restriction of orientational mobility of polar groups within the resin as the temperature increases.[74]

Figure 4.11 illustrates the dielectric properties of permittivitity and loss factor as a function of time and

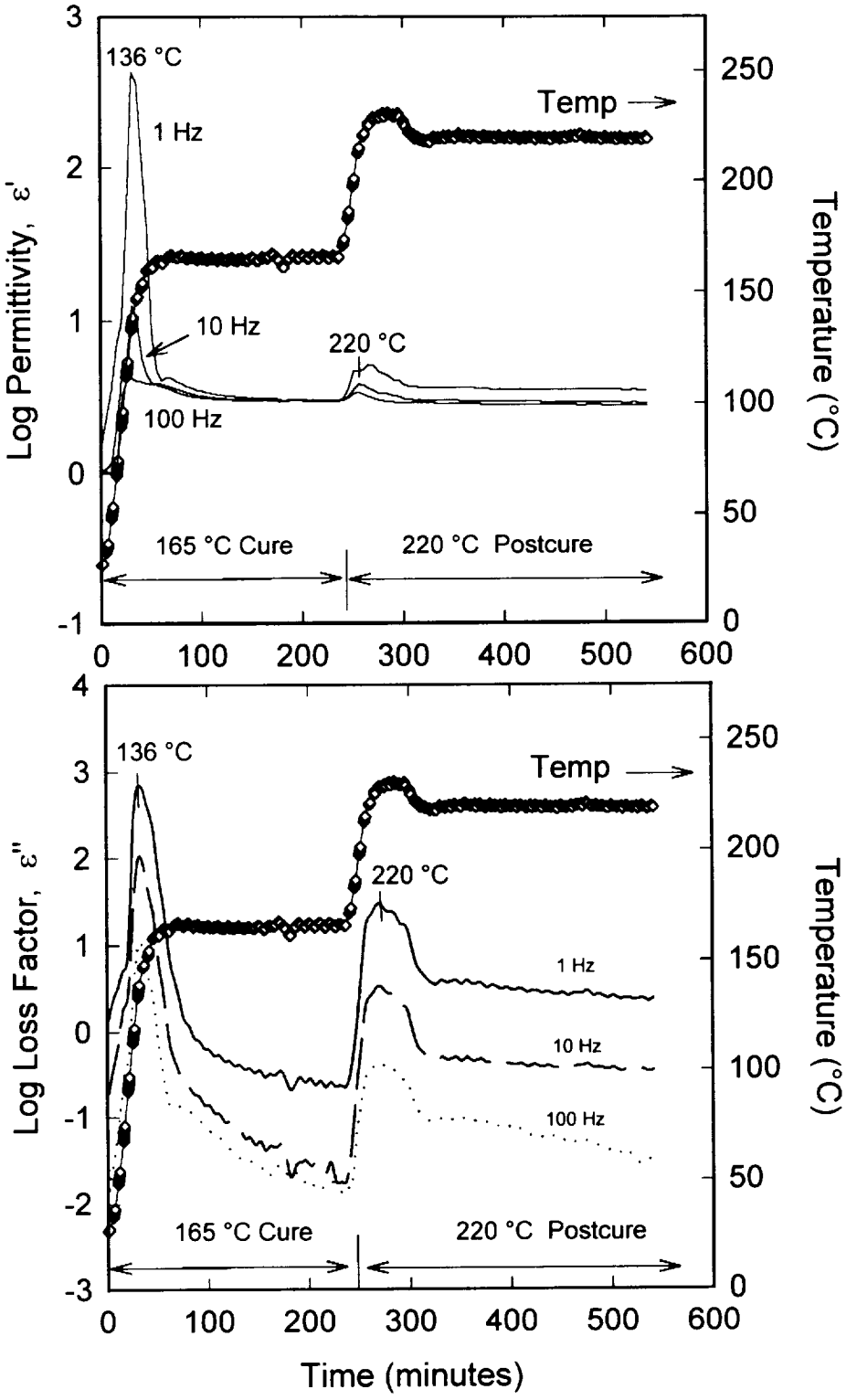

Figure 4.11. Permittivitity and loss factor as a function of time and temperature for BMI:MDA in a 2:1 mole ratio during a 165 °C cure and a 220 °C postcure processing cycle.

temperature for BMI:MDA in a 2:1 mole ratio during a 165 °C cure and a 220 °C postcure processing cycle. Low frequencies exhibit greater sensitivity to an absolute change in magnitude of permittivity. At low frequencies during the low-temperature cure, a large single peak occurs. A single peak at all frequencies indicates a frequency independent phenomenon. Here, a single peak indicates that dipole rotation and bulk conduction are occurring.

Initially, permittivity increases due to the low molecular weight chains. The chains can adjust to an alternating field. At a given time, as frequency increases, the permittivity falls because of the inability of the chains to track the alternating electric field. With increasing temperature the molecular weight of the resin increases, driving the viscosity up and the permittivity down. The permittivity reaches an asymptotic value or steady state value after reaching 165 °C during the curing procedure, typical of gelation. There is no dielectric event such as a peak, which accompanies gelation.[75]

When the temperature is increased to approximately 220 °C, the low frequency permittivity values follow the slope

and change in temperature even though the material has gelled with infinite viscosity.[76] Local viscosity, which is related to the diffusion of individual molecules that are able to move despite formation of a network, pushes the glass transition of the network toward the postcure temperature. The curing of a thermoset becomes diffusion controlled at high viscosity or longer times.

The permittivity reaches an asymptotic value after the cure temperature reaches 220 °C. This is indicative of vitrification, the point where dipolar reorientation ceases. Again, no dielectric event characterizes the vitrification process.[77]

The loss factor in Figure 4.11b initially rises with increasing temperature. The loss factor measures the energy dissipated while dipoles try to track the alternating field. The peak in the loss factor reflects the maximum mobility of trace ions in the resin and corresponds to increased fluidity of the resin. A single maximum in the loss factor indicates that ionic effects dominate the region of high fluidity. Here diffusion controlled translation of ions is occurring.[78] As the network builds, the segmental mobility diminishes. Chemical reaction onset is marked by a sudden drop in dε"/dt

which reflects the reduced mobility of ions with molecular weight buildup.[72] As the chemical reactions continue, the loss factor decreases due to deficient ionic conduction. When the loss reaches an asymptotic value, the cure reaction is considered complete. No further changes in mobility can be detected. The cure completion time is approximately 75 minutes.

As the temperature is raised for the postcuring reaction, the loss factor follows the temperature profile for all frequencies tested. Due to the larger thermal energy imparted to the system, greater mobility of the ions and dipoles with the electric field is observed for at least 50 minutes. After that time, the loss factor is invariant with temperature and time, indicating vitrification.

The permittivity and loss factor verses time and temperature are shown in Figure 4.12 for the BMI:MDA in a 2:1 mole ratio. The material was heated to 220 °C to simulate high-temperature cure. During the high-temperature cure, the permittivity and loss factor initially increase and then fall with time. After the temperature reaches 220 °C, the permittivity and loss factor both experience another minor rise in value.

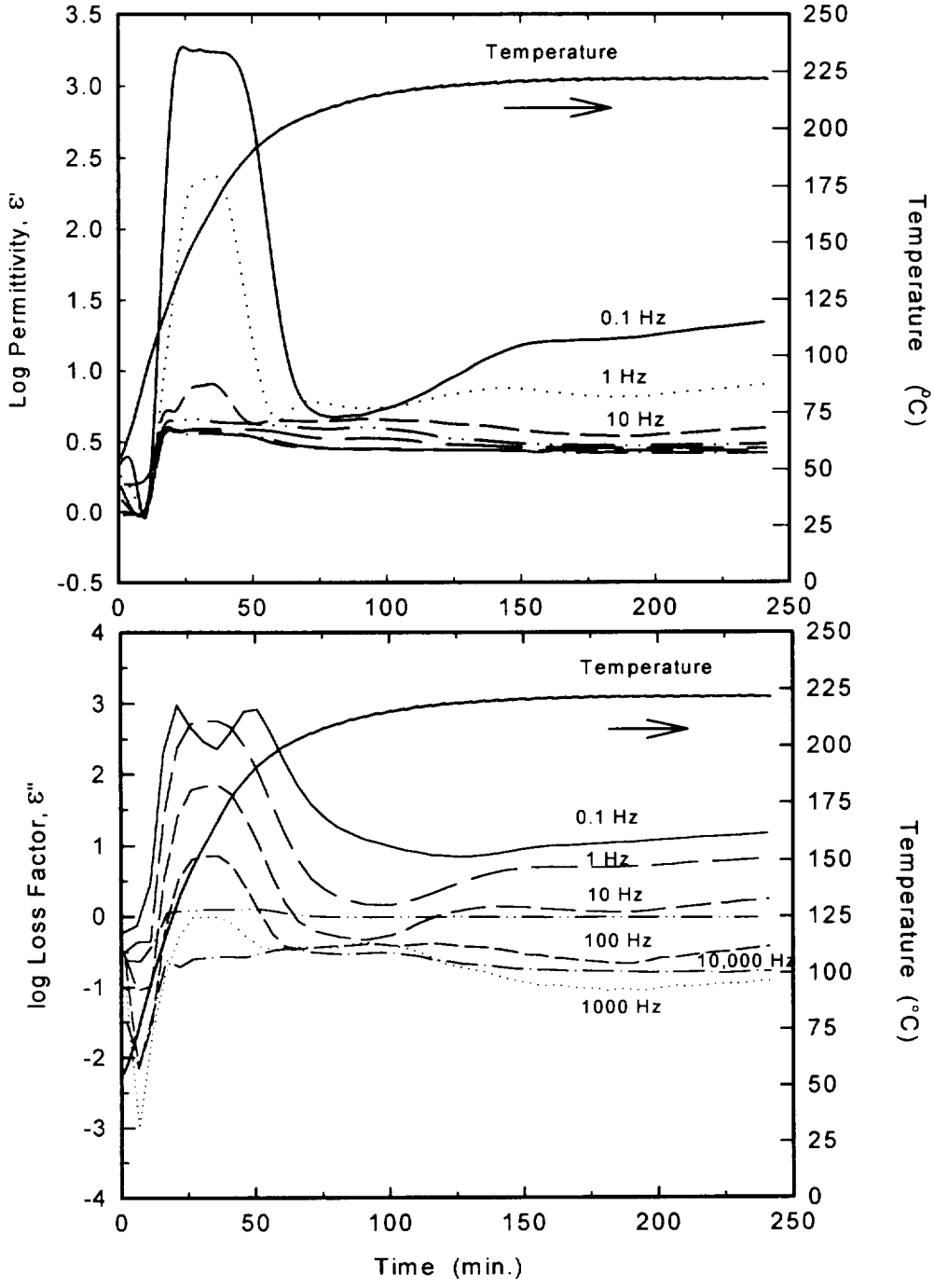

Figure 4.12. Permittivity and loss factor versus time and temperature for 2:1 BMI:MDA heated to 220 °C.

At the higher frequencies, the permittivity does not change greatly with time. For the lower frequencies, the permittivity initially increases as the cure temperature approaches 156 °C. Then the permittivity falls. The broad width of the first peak, compared to the peak widths in Figure 4.11, could be the result of both chain extension and crosslinking reactions occurring almost simultaneously. After the amine is depleted, the BMI crosslinking reaction occurs as the temperature approaches 220 °C, as indicated by another rise in the permittivity.

The loss factor maxima occur at a temperature lower than the final cure temperature. The chemical reaction onset is marked by a sudden drop in dε"/dt at 36 minutes and 167 °C. Again, this reflects the decreasing mobility of ions with molecular weight buildup.

As the temperature further increases to 220 °C, segmental mobility of the "gelled" material increases as evident by a slight increase in the loss factor. This is due to ionic conduction, which is predominantly diffusion controlled. The further increase in temperature facilitates the chemical reactions between the remaining unreacted molecules.[76]

According to Kranbuehl,[72] another way to view data from Figure 4.11 in order to differentiate the dipolar and ionic contributions to the loss term is with a plot of log ($\varepsilon'' * \omega$), versus time, where $\omega = 2\pi f$ and f is the measurement frequency. Plots of the product of angular frequency (ω) and the imaginary component of the complex permittivity $\varepsilon''(\omega)$, ($\varepsilon'' * \omega$), allow the visual determination of frequency dependent molecular mobility. When the ($\varepsilon'' * \omega$) curves differ at each frequency, the dominant molecular process is due to rotational diffusion of dipoles. When the ($\varepsilon'' * \omega$) curves overlap, the dominate molecular process is translational diffusion of charged species. The ionic component usually dominates the loss factor at low frequencies, at low viscosities, and/or high temperature.

The ionic properties are determined by charge diffusion, the hindered translational mobility of the ions within the material, and the interaction with other charged species in the network.[38] The dipolar component dominates the loss factor at high frequencies and high viscosities.

Figure 4.13 shows the ($\varepsilon'' * \omega$) plots versus time and temperature for the 165 °C/220 °C cure of BMI:MDA in a 2:1 mole ratio. Initially, at low frequencies (less than 1,000

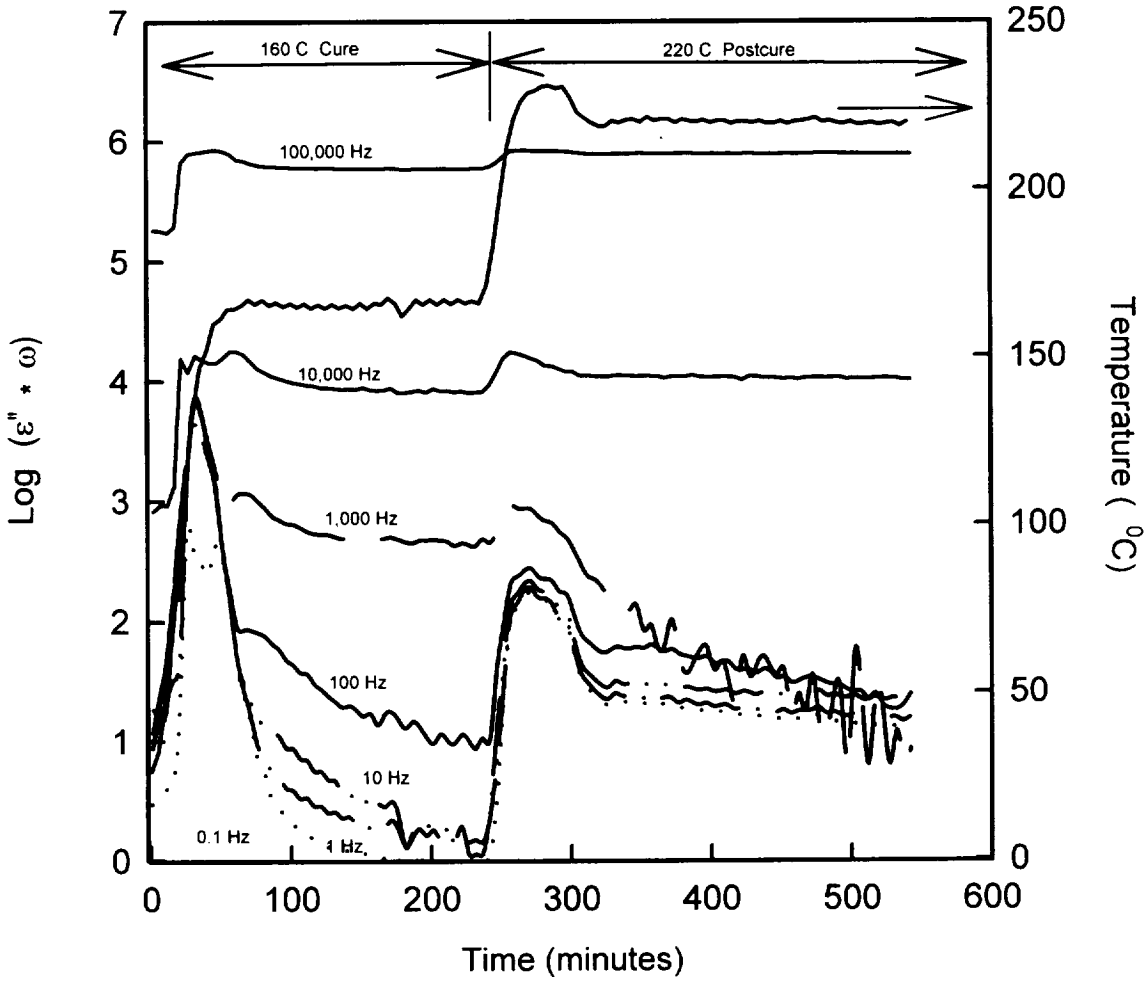

Figure 4.13. ($\varepsilon'' * \omega$) plots versus time and temperature for the 165 °C/220 °C cure of BMI:MDA in a 2:1 mole ratio.

Hz), the loss factor plots overlap, indicating an ionic translational contribution. The rise in the ($\varepsilon'' * \omega$) curves represents a decrease in viscosity due to the pending exotherm. The time at which the low frequency ($\varepsilon'' * \omega$) curves reach a peak is when ionic mobility and resin fluidity are maximum. The time at which a peak occurs also typifies the time occurrence of the mean dipolar relaxation time, $\tau = 1/(2\pi f)$.

The mean dipolar relaxation time is the "characteristic time" needed for the majority of dipoles to respond completely to the alternating electric field and to overcome the viscous drag of the surrounding molecules.[74] The mean relaxation time is a first order response and is used to characterize the magnitude of the rate of a material's time-dependent elastic response. Strictly speaking, the mean relaxation time is the time required for the material to reach (1 - (1/e)) or 63.2% of the ultimate retarded elastic response to a step change.

In most systems, a distribution of relaxation times will be observed. A distribution of relaxation times is due to a combination of molecular phenomena such as the presence of more than one polar species, the asymmetrical shape of the polar groups, and the strength of the intra-

and intermolecular forces.[38] Dipolar relaxation times usually become shorter at successively higher frequencies. This results because the viscosity decreases while the temperature increases. However, as the cure proceeds, larger and more complex molecules are produced. The large chains interfere with the movements of the dipoles and cause an increase in the relaxation times.

At the first sign of the ($\varepsilon'' * \omega$) peak, the exotherm reaction begins. As the temperature increases, the ($\varepsilon'' * \omega$) curves do not overlap, indicative of rotational diffusion of dipoles. At high frequencies (greater than 10,000 Hz), the curves do not overlap at all, indicating that at high frequencies more energy is required to align and move the dipoles than what is available. When the temperature is increased to 220 °C, thermal energy supplied to the system results in the ionic translation of the ions at frequencies less than 1,000 Hz.

It is not possible to compare qualitatively the permittivity and loss factors of each cure condition due to inconsistent temperature ramping of the oven. Therefore, ($\varepsilon'' * \omega$) curves were constructed for each cure condition. The combination of the ionic and dipolar mobility is useful in cure monitoring for the determination of the point of

maximum fluidity, onset of reaction, and the approach of the reaction completion. Cure variables such as time until the exotherm, time until dipolar relaxation, end reaction time, and the glass transition temperature were determined from each ($\varepsilon'' * \omega$) plot in order to compare the system to system cure conditions. Tables 4.1 - 4.3 consist of times and temperatures of exotherms, relaxation peaks, and the occurrence of the end of the reactions for BMI:MDA, BMI:DDS, and BMI:DABA. The time and temperature of the end of the crossover point of the ($\varepsilon'' * \omega$) curves were also listed for each cure history. For the high-temperature conditions, the times reflect when the temperature was raised for the "high-temperature cure" condition.

4.3.1. Low/High Step Cure Condition: BMI/MDA

4.3.1.1. Low-Temperature Cure

For the low-temperature conditions of 2:1, 4:1, and 1:1 mole ratios of BMI:MDA, the times and temperatures of the exotherms or maximum fluidity and ionic mobility all occur at approximately the same time and temperature, 21 minutes and 140 °C, as shown in Table 4.1. This temperature was then used as the low-temperature cure condition for the rest of this investigation. No process window was observed

Table 4.1
Dielectric Properties of BMI/MDA in Various Mole Ratios.

BMI:MDA Sample		Exotherm		Relaxation f = 100 Hz		Cure Temp. (°C)	Process Window Y/N	End of Reaction f = 100 Hz		Tg (°C)	Crossover	
		Time (min)	Temp. (°C)	Time (min)	Temp. (°C)			Time (min)	Temp. (°C)		Time (min)	Temp. (°C)
2:1	Lo	21	136	16	129	150	N	96	152	150	50	150
	Hi	31	228	26	228	220	N	71	228	218	*	185
4:1	Lo	21	141	16	134	160	N	116	161	161	80	161
	Hi	26	215	21	207	220	N	130	217	218	*	173
1:1	Lo	21	140	16.5	134	155	N	91	155	155	41	155
	Hi	36	220	31	218	220	N	60	218	218	10	180
1:2	Lo	36	152	31	146	155	N	151	164	165	25	135

* No Crossover or overlaps in ($\varepsilon'' * \omega$) plots observed.

Table 4.2
Dielectric Properties of BMI/MDA in a 2:1 Mole Ratio (High-Temperature Cure) and BMI.

BMI:MDA Sample		Exotherm					Relaxation					End of Rxn		Crossover	
		Amine Rxn		BMI Homo. Rxn			Amine Rxn		BMI Homo. Rxn			f = 100 Hz			
		Time (min)	Temp (°C)	Freq (Hz)	Time (min)	Temp (°C)	Time (min)	Temp (°C)	Freq (Hz)	Time (min)	Temp (°C)	Time (min)	Temp (°C)	Time (min)	Temp (°C)
2:1	Hi	36	167	1	146	220	31	167	1	146	220	--	--	--	--
				10	146	220	--	--	10	141	220	--	--	--	--
				100	96.3	214	--	--	100	91.3	213	200	200	81	182
				1000	96.5	214	--	--	1000	91.5	213	--	--	--	--
BMI	Hi	--	--	100	156	162	--	--	100	150	162	340	215	100	152

Table 4.3
Dielectric Properties of BMI/DABA and BMI/DDS in Various Mole Ratios.

Sample BMI:DABA		Exotherm		Relaxation f = 100 Hz		Cure Temp. (°C)	Process Window Y/N	End of Reaction f = 100 Hz		Tg (°C)	Crossover	
		Time (min)	Temp. (°C)	Time (min)	Temp. (°C)			Time (min)	Temp. (°C)		Time (min)	Temp. (°C)
1:1	Lo	52	178	46	176	180	N	192	185	186	110	190
	Hi	36	248	31	247	250	N	100	250	250	--	--
2:1	Lo	46.5	170	41	166	180	N	100	153	170	162	170
	Hi	16.5	233	11.5	217	250	N	36	250	248	11	217
1:.87	Lo	47	176	41	172	180	N	146	181	180	125	180
	Hi	26	247	21	247	250	N	41	247	245	--	--
BMI:DDS												
1:1	Lo	46	161	42	160	165	N	100	165	--	--	--
	Hi	17	202	12	195	220	N	--	--	220	212	220

for any of the cure conditions; the peaks all had one maximum at the same time and temperature.

The relaxation times for the 3 mole ratios were again, similar, 16 minutes at 133 °C, at f = 100 Hz. The peaks coincide at the same time and temperature in the loss factor, indicating that dipolar rotational diffusion processes control all the mole ratios for the low-temperature condition.

An Arrhenius plot of log conductivity versus 1/temperature should yield a straight line if there is a single relaxation time.[79] The slope of this line is the "apparent" activation energy. In the frequency range of 0.1 to 100 Hz, a single line with a slope of 12.76 can be drawn through the data from room temperature to 155 °C, Figure 4.14. Therefore, the single line in this case represents a single relaxation time. At the higher frequencies, greater than 1000 Hz, a distribution of relaxation times exists.

With increased molecular size and more molecular interactions, a wider distribution of relaxation times results. The more rigid the network environment, the wider the distribution of relaxation times due to the segmental chains inability to follow the alternating fields.[80] The

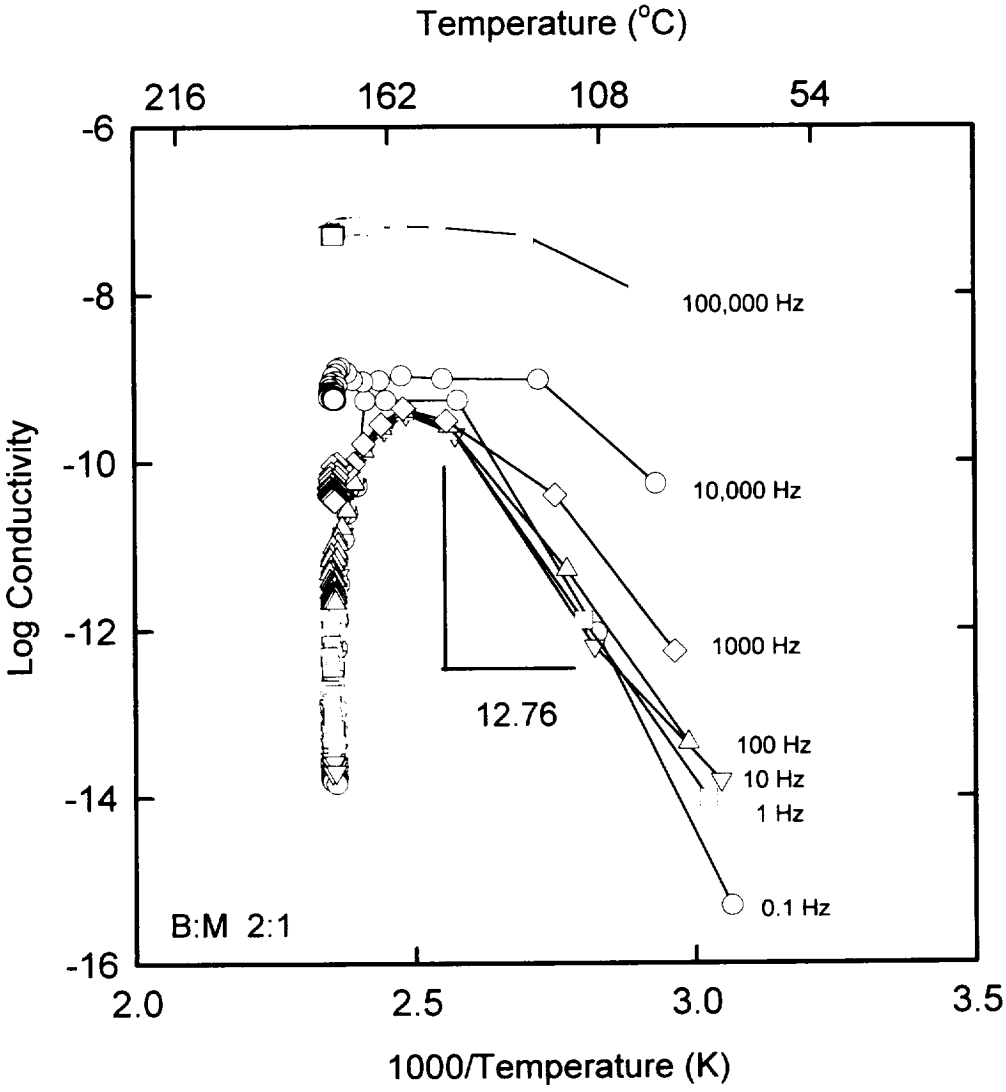

Figure 4.14. Arrhenius plot of log conductivity versus 1/temperature for BMI:MDA in a 2:1 mole ratio for the low-temperature cure condition.

establishment of a distribution of relaxation times, however, has not been correlated to the molecular structure of the sample.

The most direct evidence for a distribution of relaxation times is the departure of the Cole-Cole plot from a semi-circle.[43] The Cole-Cole plot forms a symmetrical arc whose intercepts are ε_u, the unrelaxed permittivity and ε_r, the relaxed permittivity. The arc's maximum observes the following relationship:

$$\varepsilon_{max} < (\varepsilon_r - \varepsilon_u)/2. \qquad (4.2)$$

Figure 4.15 is a representative Cole-Cole plot for a 2:1 BMI:MDA cured at 165 °C and postcured at 220 °C. When the Cole-Cole plot is skewed at the low permittivity end of the plot, conductivity contributions dominate. When the Cole-Cole plot is skewed at the high permittivity end of the plot, a distribution of relaxation times is responsible. The arc in Figure 4.15 does not continue to be circular at the high permittivity end of the plot, indicative of a distribution of relaxation times and an increase in ionic conductivity. The beginning of the arc passes through the origin, which means that there is no blocking layer ion build up at the electrodes at very low frequencies.

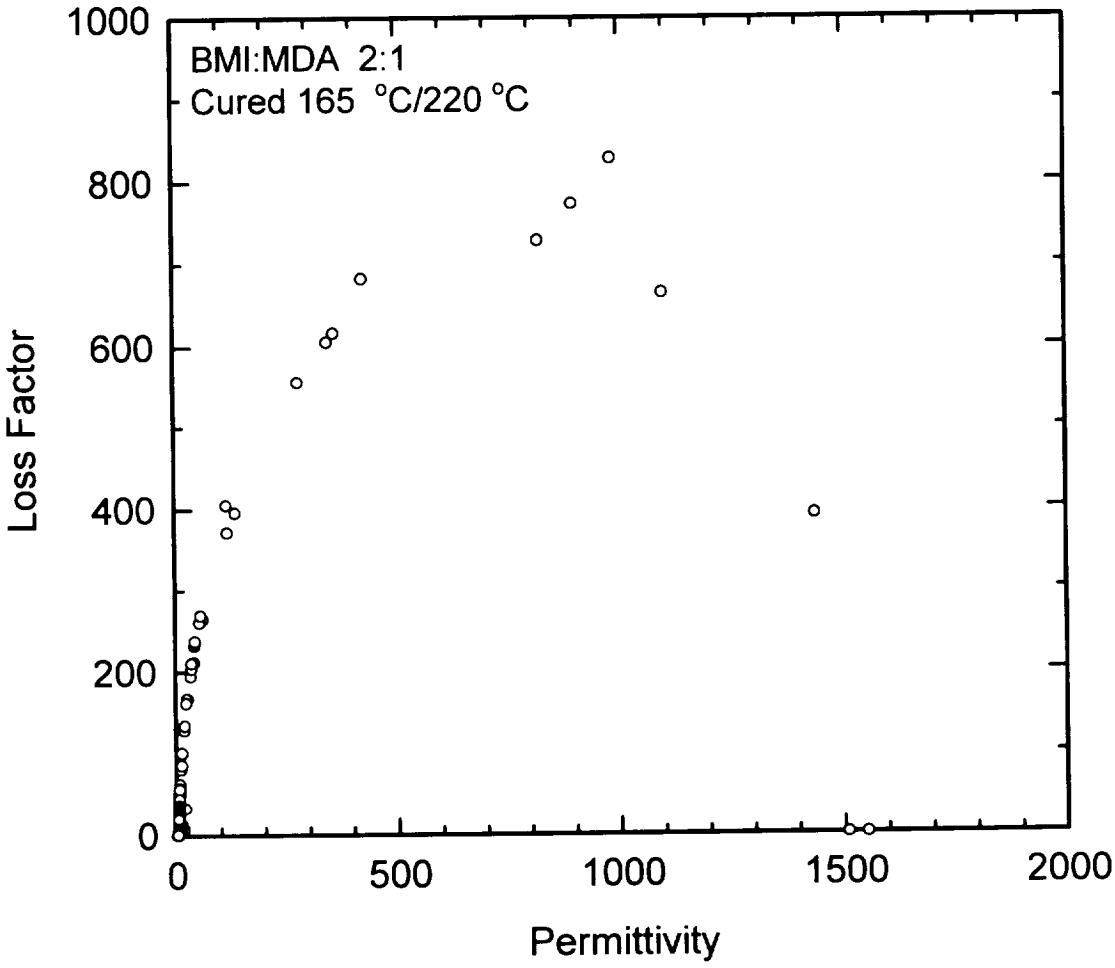

Figure 4.15. Cole-Cole plot for 2:1 BMI:MDA cured at 165 °C and postcured at 220 °C.

The crossover or overlaps in ($\varepsilon'' * \omega$) for differing frequencies, indications of when and at what time ionic translation diffusion dominates physical processes, are tabulated in Table 4.1. The overlaps occur up to 41 minutes for 1:1, up to 50 minutes for 2:1, and up to 80 minutes for the 4:1 mole ratios of BMI:MDA.

At cure temperatures below 180 °C, the amine addition reaction occurs at least two orders of magnitude faster than the homopolymerization reaction.[22] The stoichiometric amounts of BMI and MDA theoretically result in long, linear chains of relatively high molecular weight. The 2:1 and the 4:1 mole ratios of BMI:MDA are amine deficient and during the low-temperature cure, excess BMI remains unreacted. The higher the BMI concentration, the more diffusion-controlled reactions occur.

For the 1:2 mole ratio of BMI:MDA, the time to exotherm, or maximum fluidity and ionic mobility was slightly longer (36 minutes) at a higher temperature of 152 °C than the other low cure conditions, Table 4.1. The 1:2 mole ratio of BMI:MDA contains excess of MDA; during curing the chain ends become endcapped with MDA. The BMI is therefore consumed early and very little BMI remains for crosslinking. The end of the reaction for the 1:2 mole

ratio case was 151 minutes at a temperature of 164 °C while the crossover or overlap in ($\varepsilon'' * \omega$) extended for 25 minutes up to 135 °C. For the first 25 minutes, the curing reaction of 1:2 mole ratio of BMI:MDA is controlled by ionic translational diffusion. Then the short, MDA endcapped chains no longer translate but rotate about the center axes of the chains.

Glass transition occurs when the conductivity approaches zero. In this investigation, the T_g was always the final cure temperature. The glass transition temperatures, determined from the dielectric analyses do not take into account physical entanglements.

4.3.1.2. High-Temperature Cure

Figure 4.16 is Figure 4.12, replotted as ($\varepsilon'' * \omega$) plots versus time and temperature for the high-temperature cure of BMI:MDA in a 2:1 mole ratio. The double peak for the 0.1 Hz is probably due to charge polarization effects of the electrode for the low frequency and indicates a highly fluid system.[81] There are two major peaks observed in the high-temperature cure of BMI:MDA. The first major peak for a given frequency is due to the initiation and propagation of the BMI:MDA oligomers. For low frequencies (less than 1000 Hz), the ($\varepsilon'' * \omega$) plots for differing frequencies

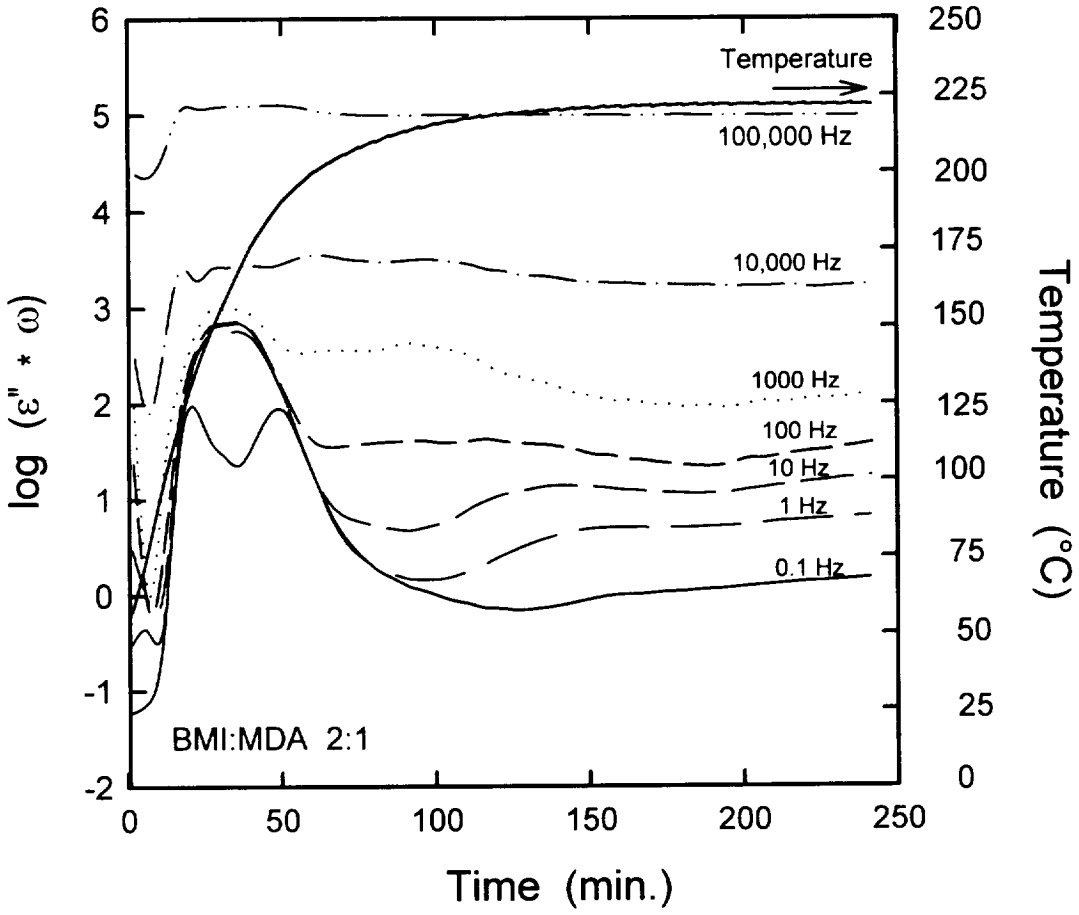

Figure 4.16. Data from Fig. 4.12, replotted as ($\varepsilon'' * \omega$) plots versus time and temperature for the high-temperature cure of BMI:MDA in a 2:1 mole ratio.

exhibit a coincidental peak. The curve beyond the peak falls gradually due to the increasing viscosity with increasing molecular weight. The first peak exhibits a broader width due to the occurrence of both amine addition and BMI homopolymerization reactions.

The first peak's time and temperature, or the relaxation time and temperature are 31 minutes and 156 °C, (as shown in Table 4.2). This is slightly longer than exhibited for the low-temperature cure condition in Table 4.1. However, the broader width of the peak indicates a wide distribution of chain lengths.

The relaxation times differ for each frequency when the temperature approaches 220 °C, Table 4.2. Different peak times imply a frequency dependent process. The characteristic times increase from 91 minutes to 146 minutes as the frequency decreases from 1000 Hz to 1 Hz. Hence, the dipole relaxation occurs sooner at higher frequencies. Also, the relaxation times decrease as the temperature increases due to an increase in dipolar mobility. This is due to a buildup of resin viscosity. The end of the reaction occurs after 220 minutes at f = 100 Hz. Up to 81 minutes of the cure, the reaction is controlled by translational diffusion of the charged

species. After that time, the translational movement of unsaturated imide groups is restricted.

For the high-temperature cure of BMI alone, only the homopolymerization reaction occurs. The time of the exotherm is 156 minutes for all frequencies. This implies that the polymerization is a frequency independent process. The relaxation time at f = 100 Hz was 150 minutes. The times of the exotherm and relaxation for BMI are longer than the times of the exotherm and relaxation at f = 100 Hz for all mole ratios of the BMI/MDA system. Pure BMI forms a network of short chains. With the addition of MDA, at high temperature, BMI can react with MDA or with another BMI. Since the BMI/MDA rate of reaction is faster than BMI homopolymerization rate of reaction, the addition of MDA at high temperatures produces a frequency dependent process with shorter exotherms, relaxation times, and end of reaction times than BMI alone.

4.3.2. Low/High Step Cure Condition: BMI/DABA

4.3.2.1. Low-Temperature Cure

For the low-temperature conditions of 1:1, 2:1, and 1:0.87 mole ratios of BMI:DABA, the times and temperatures of the exotherms or maximum fluidity and ionic mobility all occur at approximately the same time and temperature, 50

minutes and 170 °C, Table 4.3. This is within the supplier's[49] recommended cure history of 177 °C for 18 hours. No process window was observed for any of the cure conditions; the peaks all had one maximum at the same time and temperature. In the temperature range of 140-250 °C, the copolymerization reaction of BMI and DABA occurs through the double bonds, otherwise known as the 'ene' reaction.

The relaxation times at f = 100 Hz for the 3 mole ratios were again, similar, roughly 41 minutes at 170 °C, Table 4.3. This means that the peaks coincide at the same time and temperature for the ($\varepsilon'' * \omega$) plots, indicating that dipolar rotational diffusion processes control all the mole ratios for the low-temperature condition.

The crossover or overlaps in ($\varepsilon'' * \omega$) for differing frequencies, indicate when ionic translation diffusion dominates physical processes. The overlap times, listed in Table 4.3, occur up to 110 minutes for 1:1, up to 162 minutes for 2:1 and up to 120 minutes for the 1:0.87 mole ratio case. After these times, the translational movements of the unsaturated imide groups are restricted.

The end of reaction times at f = 100 Hz for the three mole ratios occurred at roughly 180 °C for the 1:1 and

1:0.87 mole ratios and at 153 °C for the 2:1 mole ratio of BMI:DABA, Table 4.3. The times for the 1:1, 2:1, and 1:0.87 mole ratios of BMI:DABA were 192, 100, and 146 minutes, respectively.

Glass transition occurs when the first derivative of conductivity ($d\sigma/dt$) approaches zero. However, in the dielectric analyses, the T_g was always the final cure temperature.

The Cole-Cole plot of BMI:DABA in a 2:1 mole ratio cured at 155 °C is shown in Figure 4.17. Since the plot is semi-circular and follows Equation 4.2, a single relaxation time may be assumed.[43] Because the arc passes through the origin, no blocking layer buildup occurs on the electrode.

4.3.2.2. High-Temperature Cure

For low frequencies (less than 1000 Hz), the ($\varepsilon'' * \omega$) plots for differing frequencies exhibit a coincidental peak, Table 4.3. The first major peak for a given frequency, is due to the formation of the BMI:DABA oligimers occurring during the 'ene' type chain extension reaction. The peak falls gradually due to the increasing viscosity with increasing molecular weight.

The peak times and temperatures, or the relaxation times and temperatures at 100 Hz are 31 minutes and 247 °C

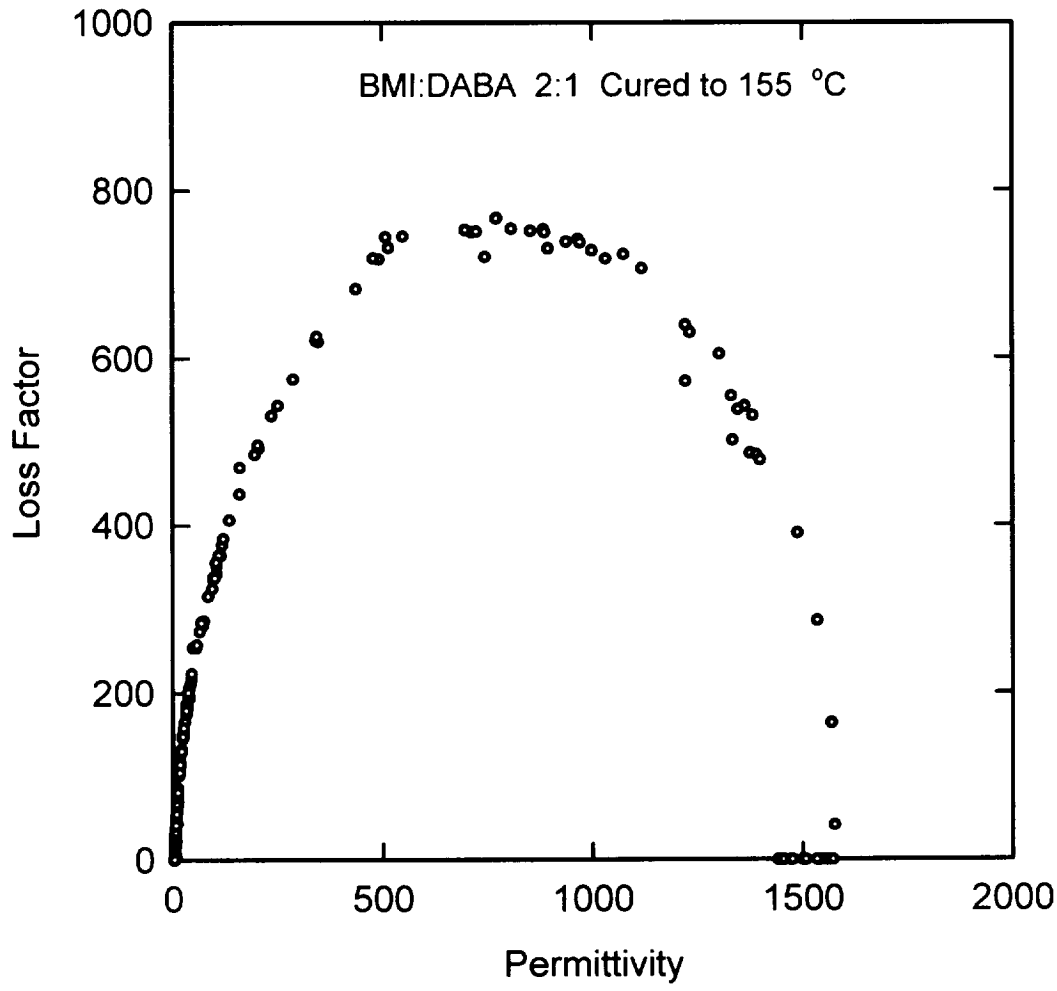

Figure 4.17. Cole-Cole plot of BMI:DABA in a 2:1 mole ratio cured at 155 °C.

for the 1:1 case, 11.5 minutes and 217 °C for the 2:1 case, and 21 minutes and 247 °C for the 1:0.87 case, Table 4.3. These are shorter than exhibited for the low-temperature cure conditions. After the diallyl component is exhausted in the 'ene' reaction, the maleimide homopolymerization reaction occurs at temperatures above 200 °C.[31]

The end of the reaction at 100 Hz occurs after 100 minutes for the 1:1 case, 36 minutes for the 2:1 mole ratio, and 41 minutes for the 1:0.87 mole ratio condition. Only the 2:1 mole ratio case exhibited a crossover behavior for 11 minutes. The reaction for the 2:1 mole ratio is controlled by translational diffusion of the charged species at the high temperatures.

4.3.3. Low/High Step Cure Condition: BMI/DDS

4.3.3.1. Low-Cure Condition

Table 4.3 also includes the results of BMI:DDS in a 1:1 mole ratio cured at 165 °C to simulate the low-temperature cure condition. The relaxation time and temperature at 100 Hz were 42 minutes at 160 °C. The exotherm occurred at 46 minutes at a temperature of 161 °C. These time parameters are slightly double those observed for BMI:MDA in a 1:1 mole ratio listed in Table 4.1. The $-SO_2$ group in DDS delays the reactivity of the diamine due

to its high electron attracting power. This fact decreases the basicity of the diamine by transferring electrons from NH_2 to the SO_2 group. The chemical reactivity of MDA would be faster than DDS at the cure temperature of 165 °C because the $-CH_2$ group is an electron donor and therefore, MDA would be more reactive than DDS.

4.3.3.2. High-Temperature Cure

Table 4.3 illustrates the processing parameters of BMI:DDS for the high-temperature cure condition. The relaxation time and temperature at 100 Hz are 12 minutes at 195 °C while the exothermic reaction time and temperature are 17 minutes at 202 °C. These are much faster than those observed for BMI:MDA cured at high temperatures, Table 4.1.

In cure monitoring by dielectric analyses, it is hard to use empirical approaches to correlate the chemical changes of molecular structures to the physical processes such as dipoles and ions responding to the alternating electric field. These approaches oversimpifly chemical kinetics and do not take into account chemical reactions such as branching or autocatalytic mechanisms. In our case, dielectric analysis was used to determine the processing variables of bismaleimides.

4.4. Network Characterization

4.4.1. Differential Scanning Calorimetry of BMI/MDA and BMI/DDS

Differential Scanning Calorimetry (DSC) is a valuable instrument, which can be used to determine the range of temperatures in the curing reaction and can be used to follow cure advancement. In using DSC, the heat evolution during polymerization is assumed to be proportional to the extent of reaction.[82] DSC can also determine the curing kinetics of polymerization of a polymer system. BMI appears to be an exception because the melting point of BMI is close to the temperature at which thermal polymerization begins, approximately 155 °C.[83] The melting points of BMI, MDA, and DDS are 155, 89, and 176 °C, respectively.

Figure 4.18 shows a DSC scan for unreacted BMI:MDA powder in a 2:1 mole ratio. Prepolymer blends of powders show two adjacent melting endotherms and a broad polymerization exotherm. The respective endotherms of the two components are slightly shifted to lower temperatures and are broader than the actual melting endotherms of the individual components. With the addition of MDA to BMI, the melting point of the mixture is lower with increasing molar ratios of MDA. The powder melts before curing

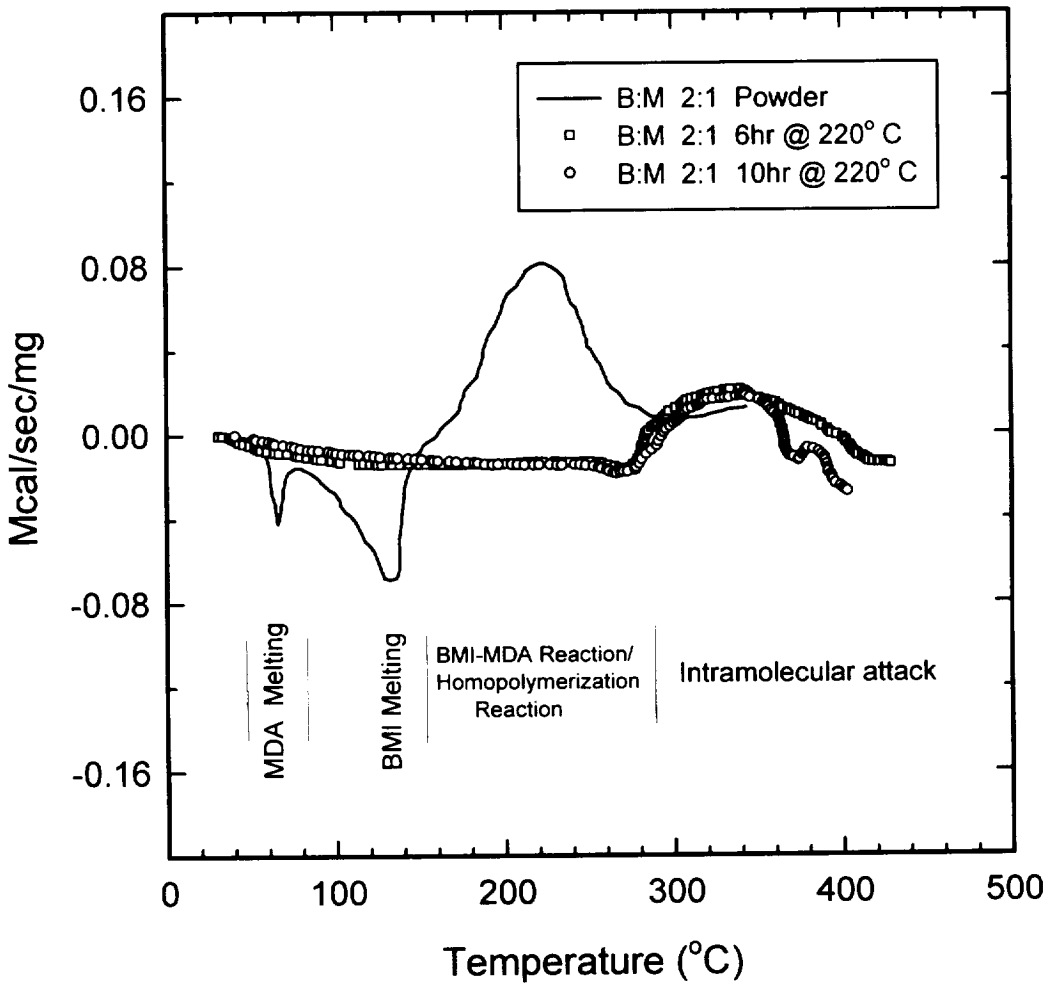

Figure 4.18. DSC scans of unreacted powder and samples cured for 6 and 10 hrs at 220 °C of BMI:MDA in a 2:1 mole ratio.

begins. The first exotherm in the DSC plots is due to the BMI/MDA reaction and the BMI homopolymerization reaction.

A second exotherm is obvious after the main polymerization peak, in Figure 4.18. Barton et al.[83] found, through FTIR studies, that during the second exotherm the concentration of maleimide bonds decreased and alicyclic CH_2 groups increased. Barton determined that a possible reaction was the intramolecular attack of the maleimide groups off of the phenylene ring and forms a bridged ring structure shown below:[83]

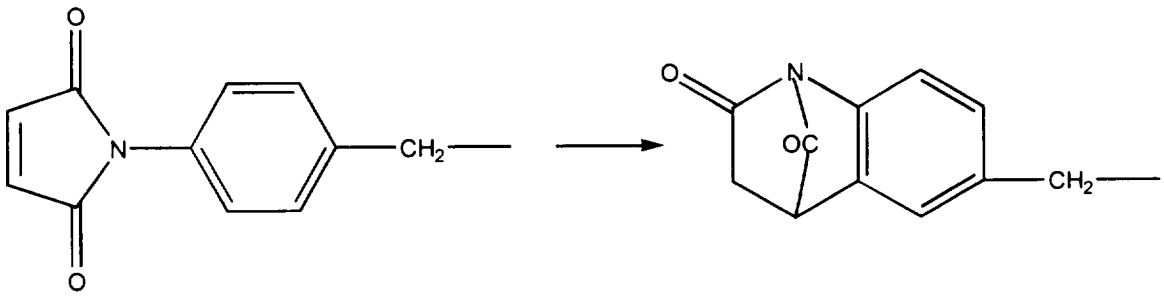

The blended powder was cured for 6 hours and 10 hours at 220 °C and then analyzed with DSC to determine the minimum time needed to completely cure the BMI:MDA system. This was resolved by determining when the polymerization exotherm peak of the DSC scan was minimized. For the high-temperature cure, the minimum time required for curing was 6 hours.

No changes in the exothermic peak were observed from 14 to 18 hours with DSC at 140 °C. Therefore, 16 hours was used as the cure time for the low-temperature cure.

Figure 4.19 illustrates the normalized DSC scans for unreacted powder, and after low-, high-, and low/high-temperature cure conditions for BMI:MDA in a 2:1 mole ratio. For the powder, the melting endotherms are broad and lower than normally observed for each of the components individually. Chain rotation energy is lower in the blended material than for the pure components.[84] The endotherms are followed by a broad exotherm. Here, both chain extension and BMI homopolymerization reactions will occur simultaneously. For the low-temperature cure, there is only one endotherm followed by a large, broad exotherm. Curing starts immediately after the endothermic peak of BMI. The large exothermic peak is due to the homopolymerization reaction of the BMI-endcapped chains.

In Figure 4.19, an endotherm also appears at approximately 165 °C for the low-temperature cure. This is due to the presence of unreacted BMI that remains in the low-temperature cured material since the curing temperature was only 140 °C. Presumably, only chain extension has occurred up to 140 °C. After 140 °C, unreacted BMI will

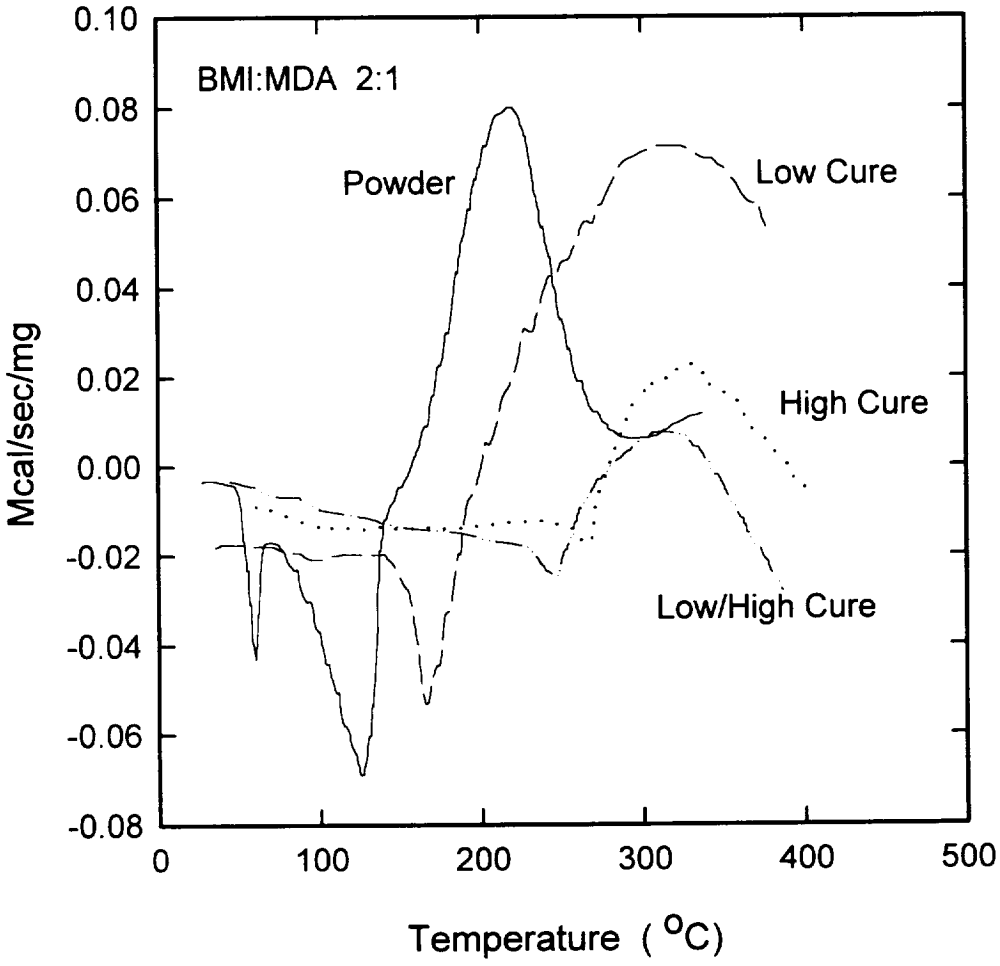

Figure 4.19. Normalized DSC scans of unreacted powder, and samples cured at low-, high-, and low/high-temperature conditions of BMI:MDA in a 2:1 mole ratio.

melt at its normal melting temperature (156-159 °C). At higher temperatures BMI-endcapped chains will begin to homopolymerize, which contribute to the polymerization exotherm.

The high and low/high cure conditions exhibit small endothermic peaks before displaying a polymerization peak or exotherm in the temperature range of 200-300 °C. In the developing network, the loss of mobility of the reacting molecules results in an incomplete reaction. When more thermal energy is added to the system, such as in DSC analysis, the molecular mobility of the reacting molecules increases and further reacts. Thus, the temperature of the polymerization or exothermic peak increases over that of the powder.

The following temperatures were determined from DSC curves and are listed in Table 4.4: T_m, the endothermic temperatures associated with melting, T_{exo}, the temperature corresponding to the exothermic peak, T_1, the temperature of onset of the cure reaction, and T_2, the temperature at the completion of the reaction. As the amount of amine increased, a decrease in T_{exo} was observed. The polymerization of BMI can be initiated at lower

Table 4.4
Critical Temperatures Determined by DSC for BMI:MDA and BMI:DDS Systems.

Sample		T_{endo} (°C)	T_{endo} (°C)	T_1 (°C)	T_{exo} (°C)	T_2 (°C)
BMI:MDA						
2:1	Powder	60	125	140	219	295
	Low	165	--	188	309	*
	Hi	265	--	280	330	*
	Low/Hi	248	--	260	310	*
4:1	Powder	59	141	169	226	275
	Low	--	141	186	257	*
	Hi	--	--	315	*	*
	Low/Hi	--	--	270	*	*
1:1	Powder	51	113	145	209	270
	Low	--	172	270	328	*
	Hi	--	226	273	329	*
	Low/Hi	--	219	274	319	*
BMI:DDS						
1:1	Powder	51	77	125	202	261	362
	Hi	--	--	--	353	367	*
2:1	Powder	50	75	137	206	256	300
	Hi	62	--	--	280	423	*

*Reached machine limits.

temperatures by incorporating a strong nucleophillic diamine.

Figure 4.20 is a composite graph of normalized DSC scans of BMI:MDA in a 4:1 mole ratio. The DSC scan of the low-temperature cured material exhibits a slight exothermic polymerization peak and no others. The low/high- and high-temperature cure conditions exhibit no endotherms for the melting of BMI or MDA and no exotherms below 300 °C. After 300 °C there is evidence of an exothermic peak, which is probably due to the intramolecular attack of maleimide groups attached to the phenylene groups.

For the 1:1 mole ratio of BMI:MDA, more MDA is present, which reveals itself as a sharp endothermic peak at approximately 50 °C, (Figure 4.21). Only the DSC scan of the powder exhibits the presence of the second exotherm at temperatures exceeding 300 °C before degradation begins. For the low-temperature cure condition, an endotherm appears at approximately 175 °C, which is due to the presence of unreacted BMI in the material. The endothermic peaks for the high and the low/high cure conditions are due to the unreacted BMI melting before polymerization begins.

Figures 4.22 and 4.23 are normalized plots of DSC curves for BMI:DDS in a 1:1 and 2:1 mole ratios. Both the

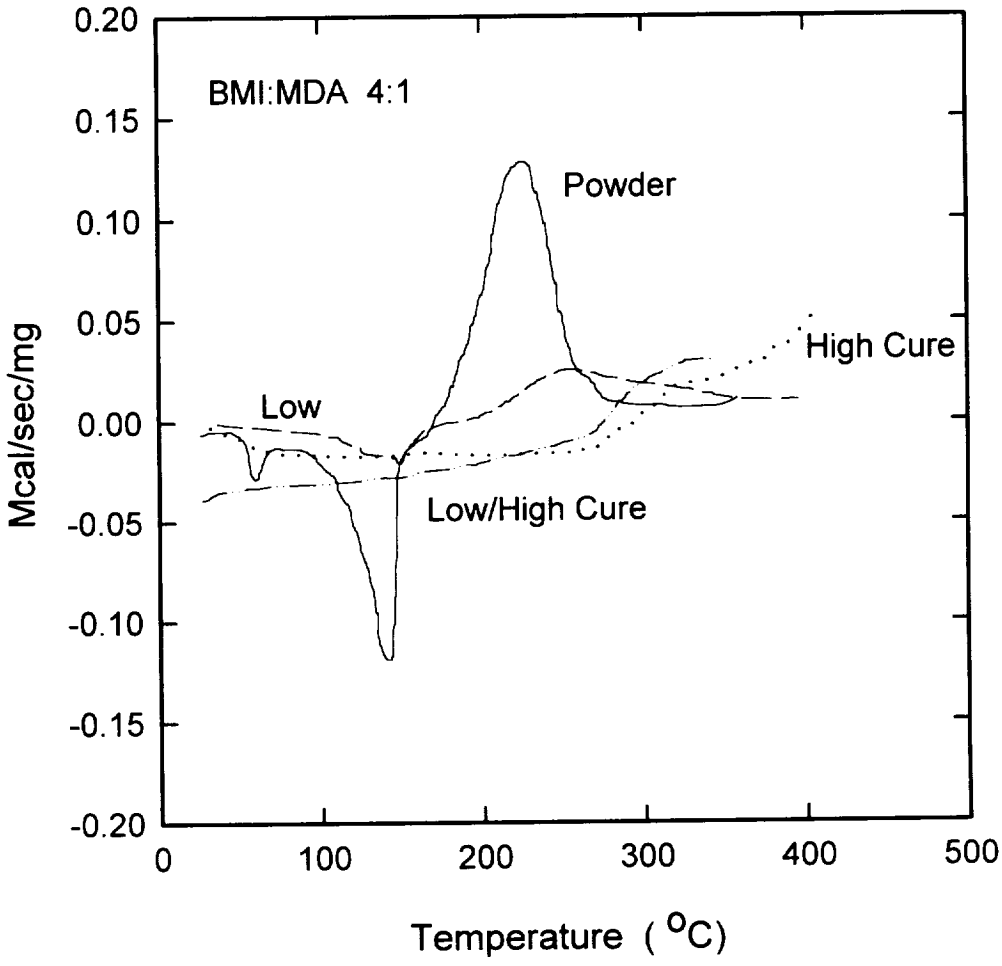

Figure 4.20. Normalized DSC scans for unreacted powder, and samples cured at low-, high-, and low/high-temperature conditions of BMI:MDA in a 4:1 mole ratio.

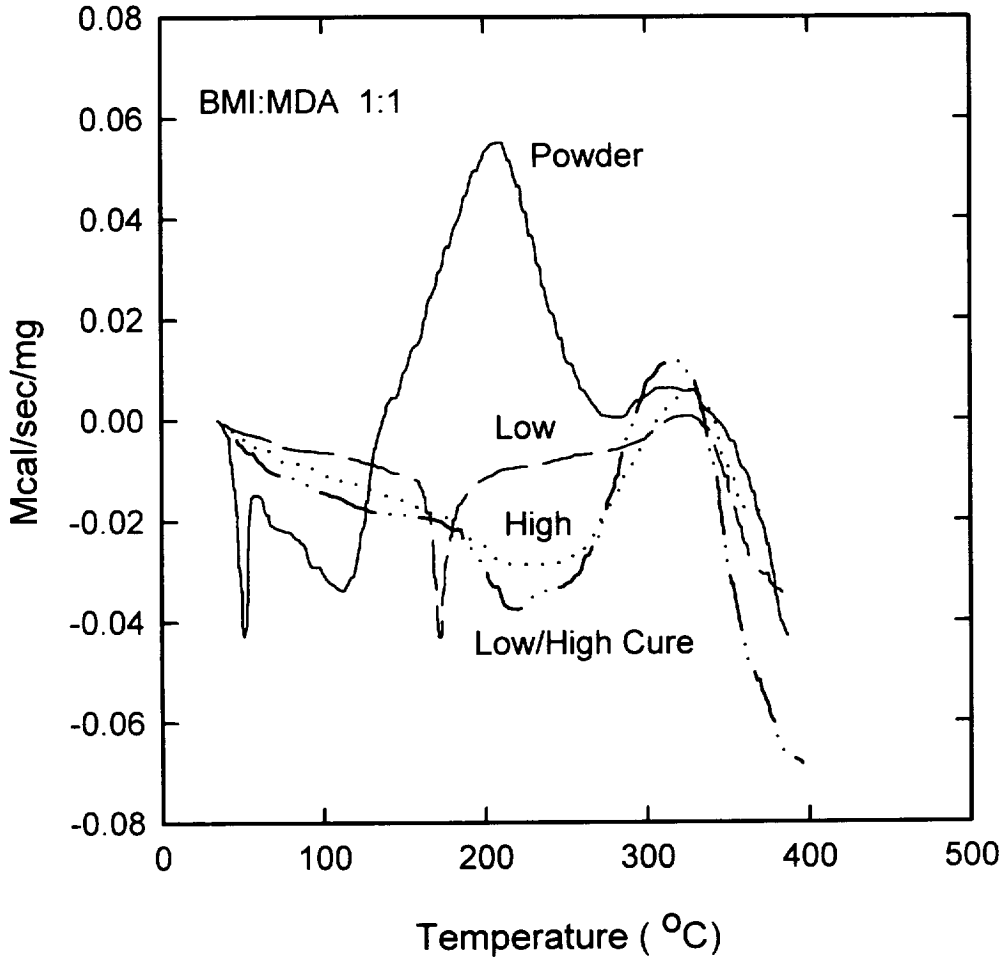

Figure 4.21. Normalized DSC scans for unreacted powder, and samples cured at low, high, and low/high-temperature conditions of BMI:MDA in a 1:1 mole ratio.

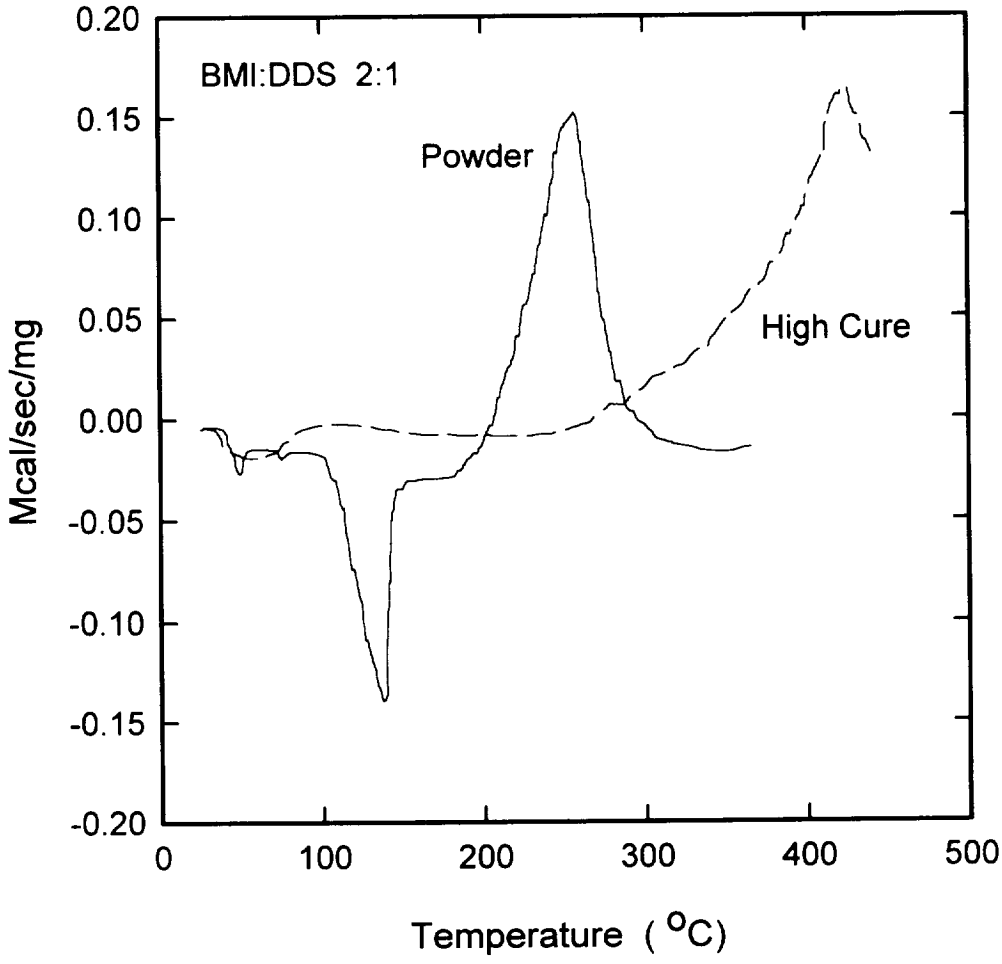

Figure 4.22. Normalized plots of DSC curves for BMI:DDS in a 2:1 mole ratio.

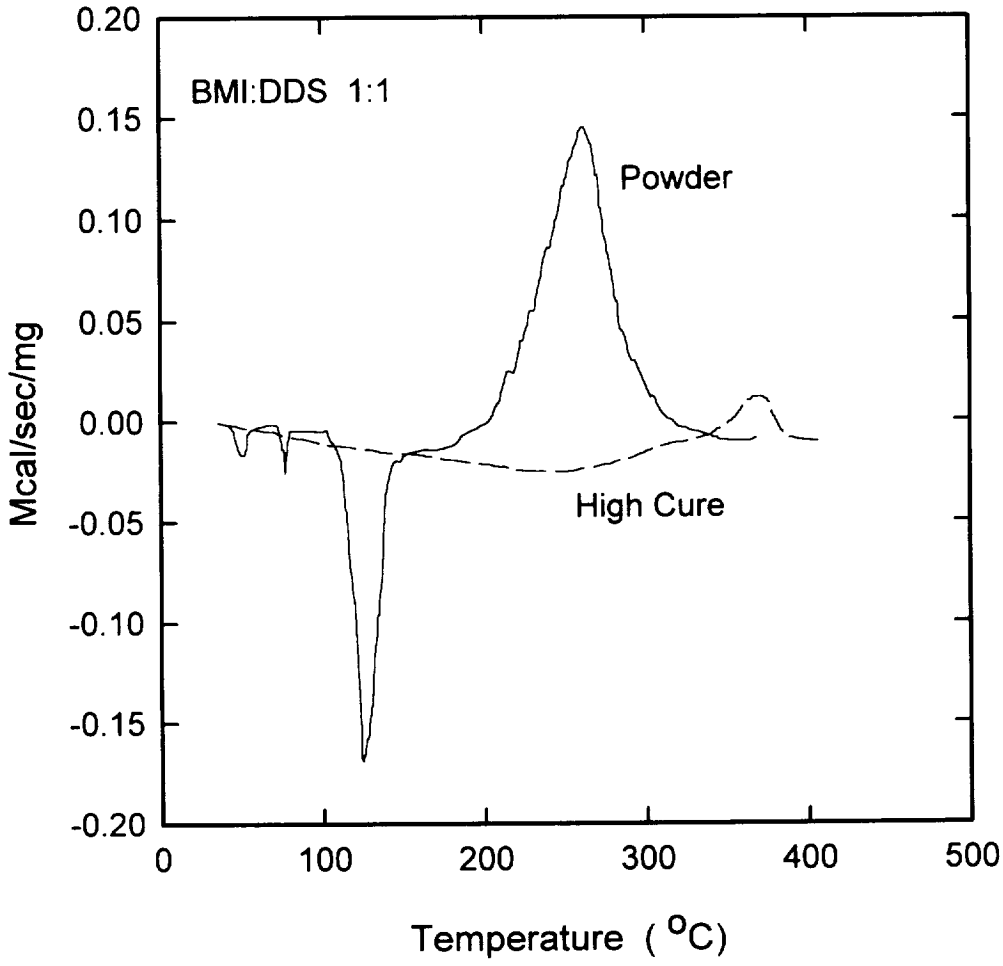

Figure 4.23. Normalized plots of DSC curves for BMI:DDS in a 1:1 mole ratio.

figures exhibit three endotherms for the powders. Table 4.4 lists the results of the DSC curves for the BMI:DDS system. The exothermic peaks for the 2:1 and the 1:1 mole ratios are due to the Michael's addition reaction between BMI and DDS. Strong electron withdrawing groups such as DDS, present in the backbone of a polymer will increase the cure temperature of the polymerization reaction and will reduce the reactivity of the maleimide double bond.[85]

4.4.2. Gel Point Determination

Up to this point in the research, the temperature and time of curing for the various systems and conditions have been determined. The curing process of a thermoset undergoes several macroscopic changes when the material is converted to a glassy state by increasing the crosslink density. Gelation is the formation of a network with branched molecules of very high molecular weight. At gelation, the viscosity of the system increases. Since the DSC does not mark the onset of gelation or vitrification, gel point determination, or gel time, was used to estimate gelation. The gel point was determined according to ASTM D2471.[54]

The gel time is an important processing parameter because it is the point when the resin will no longer flow.

Ideally, all processing must be completed before the gel point is reached. However, gelation does not mean the cure reaction ends. On a microscopic level, gelation corresponds to the formation of an infinite molecular weight network.

Gelation starts at a fixed chemical conversion while vitrification occurs as a result of reduced degrees of freedom. Gelation is solely dependent on chemical reactivities of the functional groups of the resin.

Figure 4.24 is the mole ratio of BMI:MDA versus gel time in seconds per gram for two curing temperatures, 140 and 220 °C. At 140 °C, as the BMI concentration increases, the gel time increased, because there is less chain extension occurring. The time required to form a network, or the gel point, would be long.

As the BMI concentration increased, the time to gel decreased at 220 °C for BMI:MDA and BMI:DDS. From Table 4.4, the exotherms for the 2:1 and 1:1 mole ratios of BMI:DDS are 256 and 261 °C, respectively. At a temperature of 220 °C, the 2:1 mole ratio of BMI:DDS would exhibit a shorter gel time than for the 1:1 mole ratio. The BMI/DDS systems exhibited the longer gel times because the reactivity of DDS is much less than MDA.

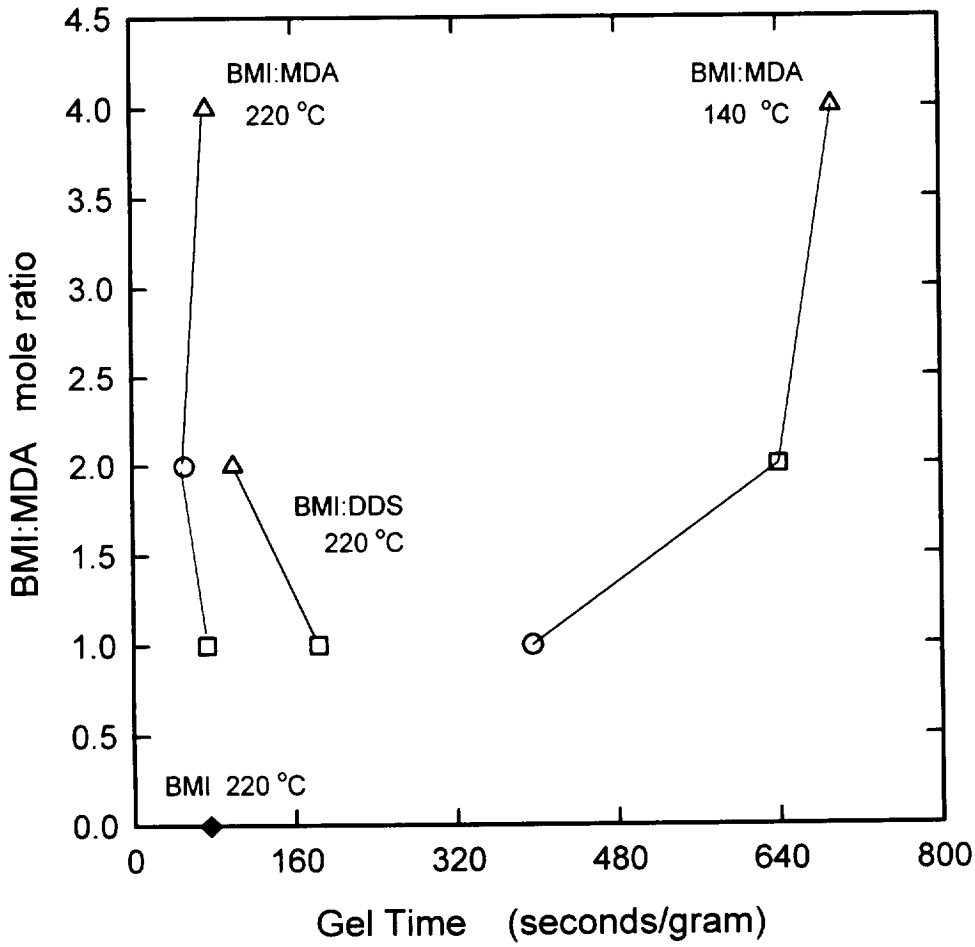

Figure 4.24. Mole ratio of BMI:MDA versus gel time in seconds per grams for cure temperatures of 140 and 220 °C.

At 220 °C, BMI with or without MDA had gel times in the range of 80 seconds/gram. The shortest gel time was observed for the 2:1 mole ratio of BMI:MDA. Presumably, a 2:1 mole ratio of BMI:MDA results in simultaneous homopolymerization and chain extension reactions in an optimum ratio. Consequently, the concentrations of BMI and MDA would be exhausted early at high temperatures.

4.4.3. Gel Permeation Chromatography

Gel Permeation Chromatography (GPC) is a useful tool for determining the approximate molecular weight distributions in polymers. Based on size exclusion, a dilute polymer solution is passed through columns of packed particles with a porous substrate. The solvent is passed through the heated columns at a constant rate. As the dissolved polymer molecules flow past the porous substrate, they become entrapped in the internal pore structure depending on the molecule's size. Larger molecules will only enter a small fraction of internal pores or will be excluded all together. The larger the molecule the less time spent within the columns. A concentration-sensitive detector monitors the difference in refractive index between the pure solvent and the dilute polymer solution as the polymer solution leaves the columns. The set of

columns of different pore sizes is calibrated so that the amount of solute versus retention volume can be converted into a molecular weight distribution. Then based on a standard calibration scale, the number and weight average molecular weights may be determined.

The low cure condition samples of BMI:MDA in a 2:1, 4:1, and 1:1 mole ratio were dissolved in NMP and filtered for GPC analysis. Figure 4.25 is the number and weight average molecular weights verses mole fraction BMI. As the amount of diamine increases, the number and weight average molecular weights increase. With a higher concentration of diamine, during the chain extension reaction, long chains of alternating BMI and MDA are possible. These GPC results have been confirmed by Leung et al.[28] This data also implies that the predominant reaction during the low cure condition is chain extension between the amine and double bond of BMI since the polymer samples dissolved completely.

4.4.4. TGA/FTIR

TGA/FTIR is a technique used in chemical characterization of polymers. During TGA weight loss and its first derivative are monitored versus temperature. The evolved gases are also captured for FTIR spectroscopy analysis. The absorbance of infrared light through the gas

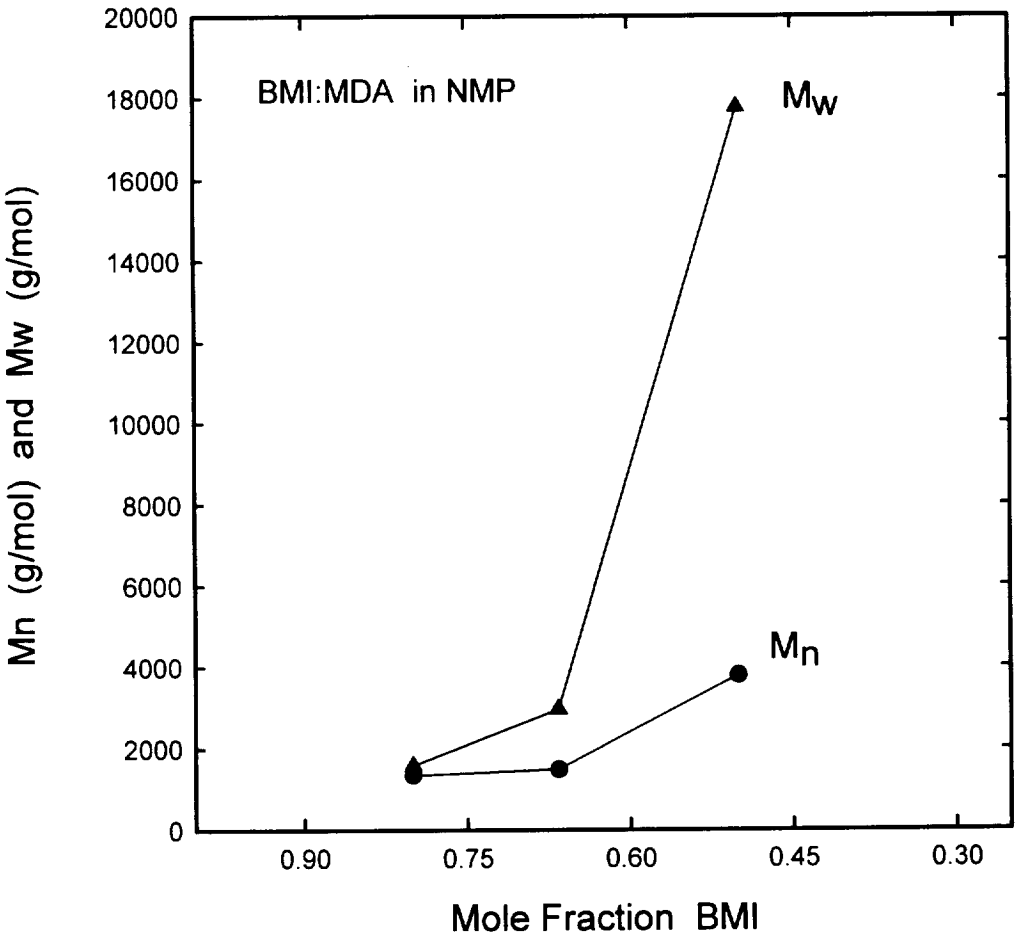

Figure 4.25. Number and weight average molecular weights versus mole fraction BMI for the low cure condition of BMI:MDA in a 2:1, 4:1, and 1:1 mole ratio determined by GPC analysis.

is measured as a function of the wavelength. The absorbance spectrum will demonstrate a "characteristic signature" of the sample.[22] The different peaks in the spectrum are the result of functional groups present in the evolved gas. The areas under these peaks are related to the concentration of the functional groups present. In this study, several "slices of gas" were passed through the FTIR for analysis.

TGA/FTIR was performed on the powder samples of BMI:MDA and BMI:DDS in various mole ratios and for BMI:DABA in 2:1 and 1:1 mole ratios in nitrogen. Initial weight losses of 2-11% were observed in the temperature range of 325-475 °C. These initial weight losses were followed by a major weight loss at T_{max}. The weight remaining and the first derivative of weight loss versus temperature for BMI:MDA in a 4:1 mole ratio is shown in Figure 4.26. Although BMI:MDA's weight loss typically displayed only one weight change rate with respect to temperature, the initial portion of decomposition is quite rapid. According to Ninan et al.[86] the extent of crosslinking is less than the extent of bond rupture when decomposition is rapid. The TGA results for all the samples are listed in Table 4.5. The IDT, or the initial decomposition temperature for the

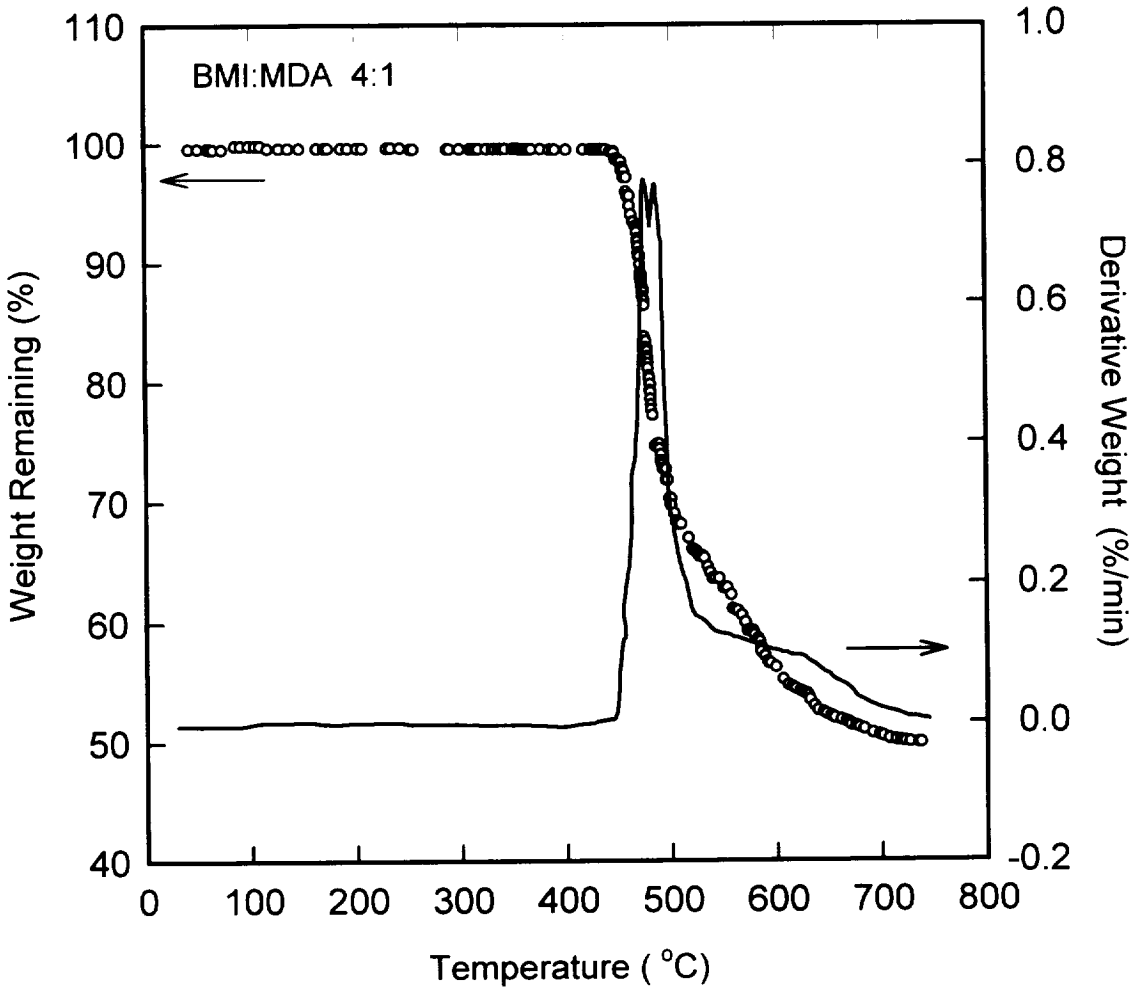

Figure 4.26. Weight percent remaining and the first derivative of weight loss versus temperature for BMI:MDA in a 4:1 mole ratio.

Table 4.5
TGA Properties of the Various BMI-Based Copolymers.

Sample		IDT (°C)	Wt. %	T_{max} (°C)	Wt. %	T_f (°C)	Wt. %	YC %
BMI	Powder	471	97	521	69	638	51	48 @ 700 °C
BMI:MDA 4:1	Powder	464	95	482	79	650	55	51 @ 700 °C
	Lo	438	91	457	77	476	70	55 @ 600 °C
	Hi	436	89	456	75	476	69	55 @ 600 °C
	Lo/Hi	433	92	454	80	475	71	56 @ 600 °C
BMI:MDA 2:1	Powder	389	97	464	78	649	53	51 @ 700 °C
	Lo	404	92	438	78	472	68	53 @ 600 °C
BMI:MDA 1:1	Powder	339	98	451	72	626	49	47 @ 700 °C
	Lo	350	95	415	75	477	59	48 @ 600 °C
	Lo/Hi	358	92	412	77	467	62	49 @ 600 °C

Table 4.5 (cont.)

Sample		IDT (°C)	Wt. %	T_{max} (°C)	Wt. %	T_f (°C)	Wt. %	YC %
BMI:DDS 2:1	Powder	357	97	449	75	659	26	24 @ 700 °C
	Hi	408	91	429	79	450	69	51 @ 600 °C
BMI:DDS 1:1	Powder	325	97	408	70	622	46	43 @ 700 °C
BMI:DABA 2:1	Mixed (unreacted)	403	97	463	71	639	41	38 @ 700 °C
BMI:DABA 1:1	Mixed (unreacted)	409	97	469	62	634	32	30 @ 700 °C
BMI:DABA 1:0.87	Mixed (unreacted)	427	94	457	70	488	40	32 @ 700 °C

powder 4:1 sample was 464 °C while the T_{max}, or the temperature of maximum rate of weight loss is 482 °C. T_f, or the final decomposition temperature was 650 °C for the 4:1 powder sample. The char yield at 700 °C was 51%. For the other cure conditions in a 4:1 mole ratio, the TGA results are virtually identical, Figure 4.27. The other mole ratios of BMI/MDA at various cure conditions display similar results. In Figure 4.28, as the amount of diamine increases for the remaining powder samples, the thermal stability decreases, determined by IDT and T_{max}. With the addition of the -NH- linkage, the thermal stability is lower than for BMI alone. The longer chains result in a decrease in thermal stability.[87]

Small amounts of the evolved gas from the TGA analysis were passed through a Nicolet FTIR for characterization. A typical FTIR trace with IR band identification of the evolved gas for unreacted powder of BMI:MDA in a 4:1 mole ratio determined at 220 °C is presented in Figure 4.29. Evolved gases, due to the degradation process, exhibit peak amounts at T_{max}. The evolved gas is composed of CO_2 (2359 cm^{-1}), CO (2110 cm^{-1}), and H_2O (3750 cm^{-1}) and also contain the following IR assignments of =CH stretching of maleimide

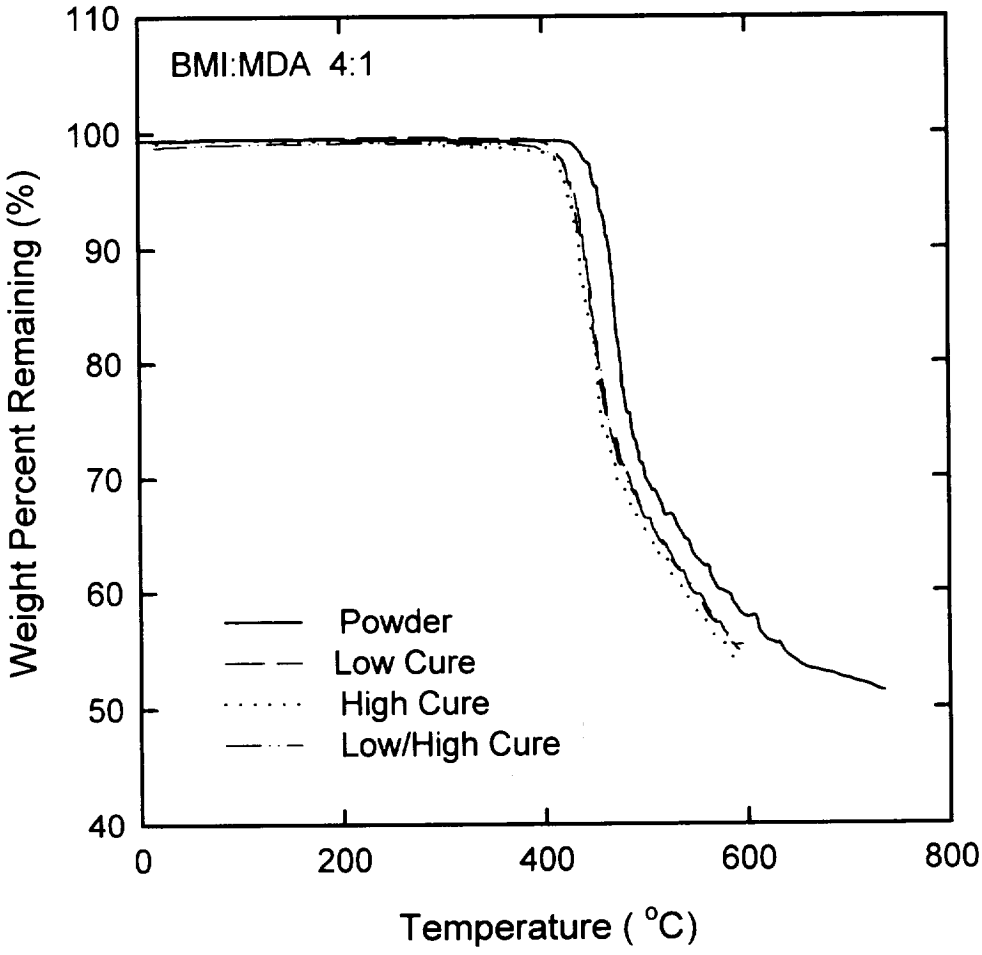

Figure 4.27. Weight percent remaining versus temperature for BMI:MDA in a 4:1 mole ratio after various processing conditions.

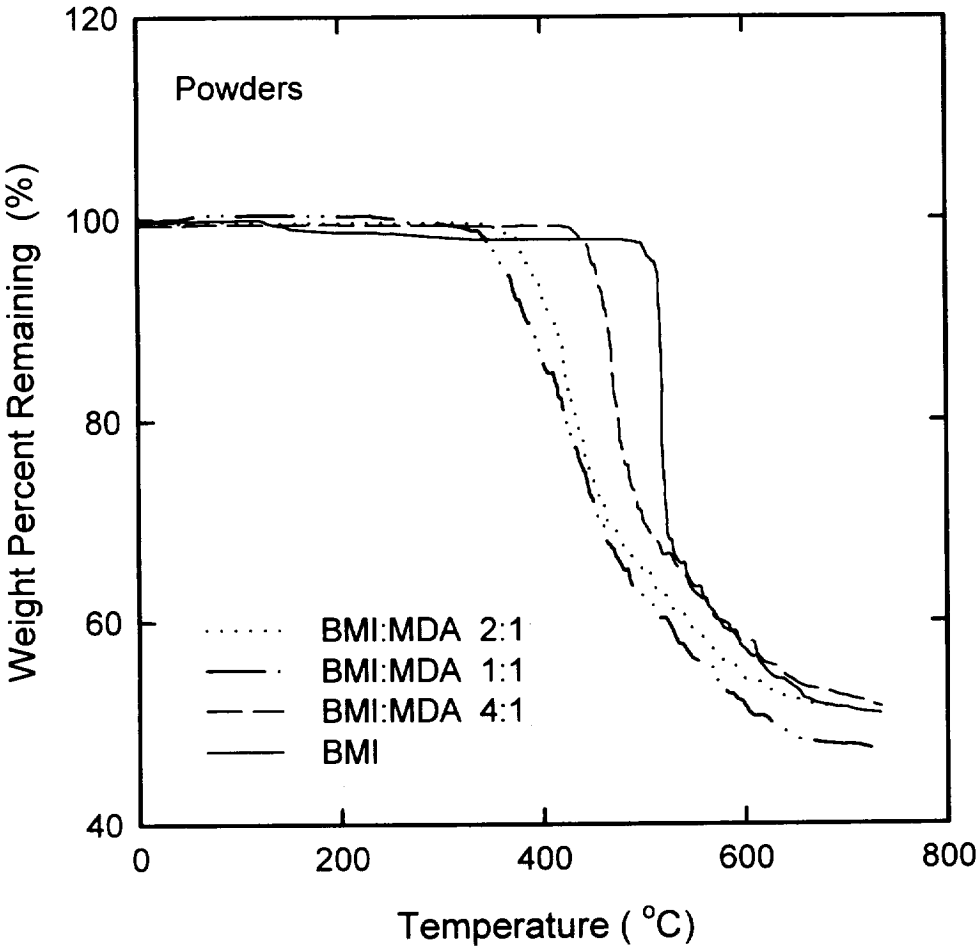

Figure 4.28. Weight percent remaining versus temperature for BMI/MDA unreacted powders in various mole ratios.

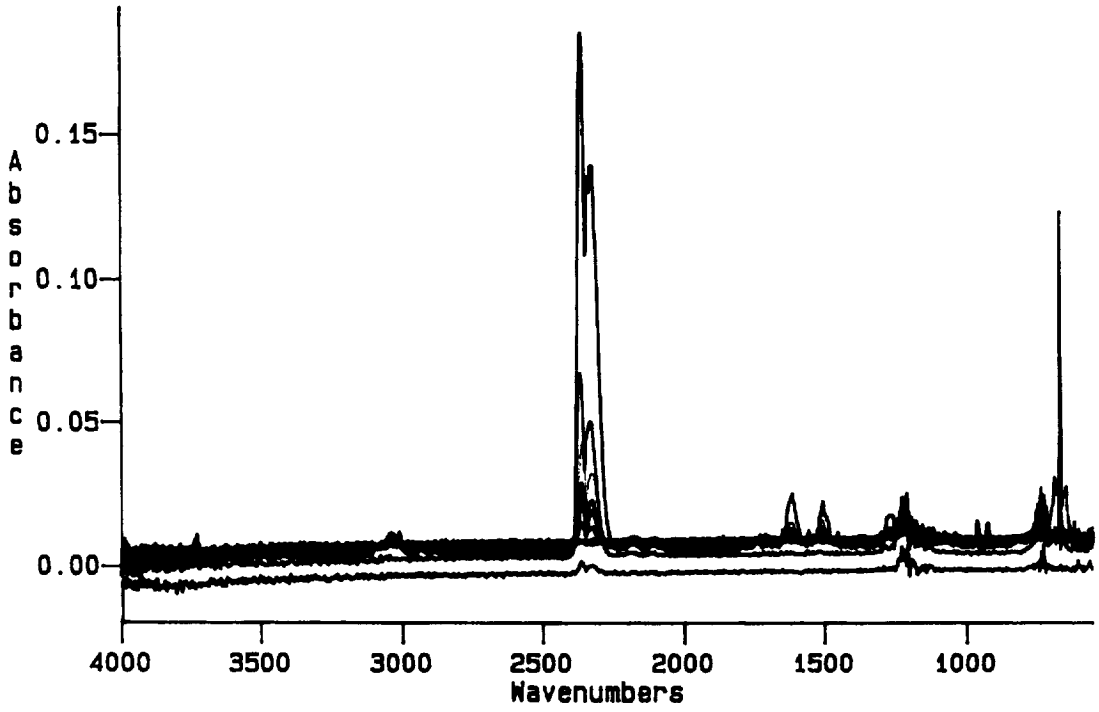

Figure 4.29. Typical FTIR spectrum with IR band identification determined at 220 °C for unreacted powder of BMI:MDA in a 4:1 mole ratio.

(3098 cm^{-1}), aromatic C-C and NH bending (1623 cm^{-1}), aromatic C-C (1514 cm^{-1}) and C-N stretching (1276 cm^{-1}). Table 4.6 lists the evolved gas and IR assignments for the various BMI:MDA and BMI:DDS powders and BMI:DABA samples.

In Figure 4.29, the peak at 1514 cm^{-1} occurs due to aromatic C-C stretching vibration. C-N-C stretching of the maleimide groups causes the peak at 1150 cm^{-1} while the 1173 cm^{-1} peak is the result of C-N-C stretching of the succinimide groups. These two peaks are closely coupled and sometimes hard to distinguish in FTIR spectroscopy. The presence of a peak in the range of 3100-3000 cm^{-1} represents the double bonds in BMI. This suggests that the Michael's addition reaction between the diamine and BMI has not occurred in these uncured powders.[88] The C-N-C groups, produced by the Michael's addition reaction are easier to split during degradation than if BMI appeared alone. BMI does not exhibit the C-N-C stretching of the maleimide groups during degradation. Therefore, the thermal stability of BMI is greater than for BMI:MDA or BMI:DDS copolymers.

4.4.5. Dynamic Mechanical Spectroscopy

A dynamic mechanical spectrometer was used to determine the rheological behavior during linearly rising

Table 4.6
Evolved Gas and IR Assignments for Various BMI:MDA, BMI:DDS, and BMI:DABA Samples.

Wavelength (cm^{-1})								FTIR Assignment
BMI:MDA 4:1	BMI:MDA 1:1	BMI:MDA 2:1	BMI	BMI:DDS 2:1	BMI:DDS 1:1	BMI:DABA 2:1	BMI:DABA 1:1	
3750			3750	3750	3750			H_2O
						3650	3650	OH stretch
3100-3000	3100-3000	3100-3000	3100-3000	3100-3000	3100-3000	3100-3000	3100-3000	=CH (maleimide) + =CH (aromatic)
						2990-2850	2990-2850	CH_3 + CH_2 antisym & sym stretch
2359	2359	2359	2359	2359	2359	2359	2359	CO_2
2110		2110	2110					CO
1623	1623	1623	1623	1623	1623	1623	1623	C-C (aromatic) + NH (bend)
1514	1514	1514	1514	1514	1514	1514	1514	C-C (aromatic)
						1400-1370	1400-1370	CH_3 (deformation)

Table 4.6 (cont.)

Wavelength (cm^{-1})								FTIR Assignment
BMI:MDA 4:1	BMI:MDA 1:1	BMI:MDA 2:1	BMI	BMI:DDS 2:1	BMI:DDS 1:1	BMI:DABA 2:1	BMI:DABA 1:1	
1276	1276	1276	1276	1276	1276	1276	1276	CN (stretch)
1177-1150	1177-1150	1177-1150						CNC (vibrations)
				1140	1140			SO_2 (sym. Stretch)
							1030-950	C-ring breathing
							815	$CH=CH_2$ out-of-plane wag
750	750	750	750	750	750	750	750	=CH (aromatic) out-of-plane bending + NH_2 wagging

temperature conditions. Figure 4.30 is the rheological plot of G', G", and tan δ for the BMI:MDA sample in a 2:1 mole ratio, cured for 6 hours at 220 °C. Normally, the tan δ peak is used to estimate the glass transition temperature, T_g, however, these peaks were often rather broad. Therefore, in this research, the intercept method was used, where T_g is the intersection between lines drawn through the glassy region and the transition region. Even though figures and tables in this dissertation contain the designation "T_g", it is recognized that the glass transition temperature is an apparent measure, not done at near-equilibrium but in a dynamic mechanical test. Broad tan δ peaks may be due to a spread in the crosslink density[89] or due to the presence of unreacted BMI molecules that act like a second phase within the BMI:MDA matrix.

For polyimides, a true plateau is never achieved during dynamic rheological measurements because of further crosslinking as the temperature is increased. However, when an increase in G' occurs after a minimum in the curve at temperatures above T_g, the value at the minimum has often been used to indicate the relative levels of crosslinking. In this dissertation, the apparent minimum before the

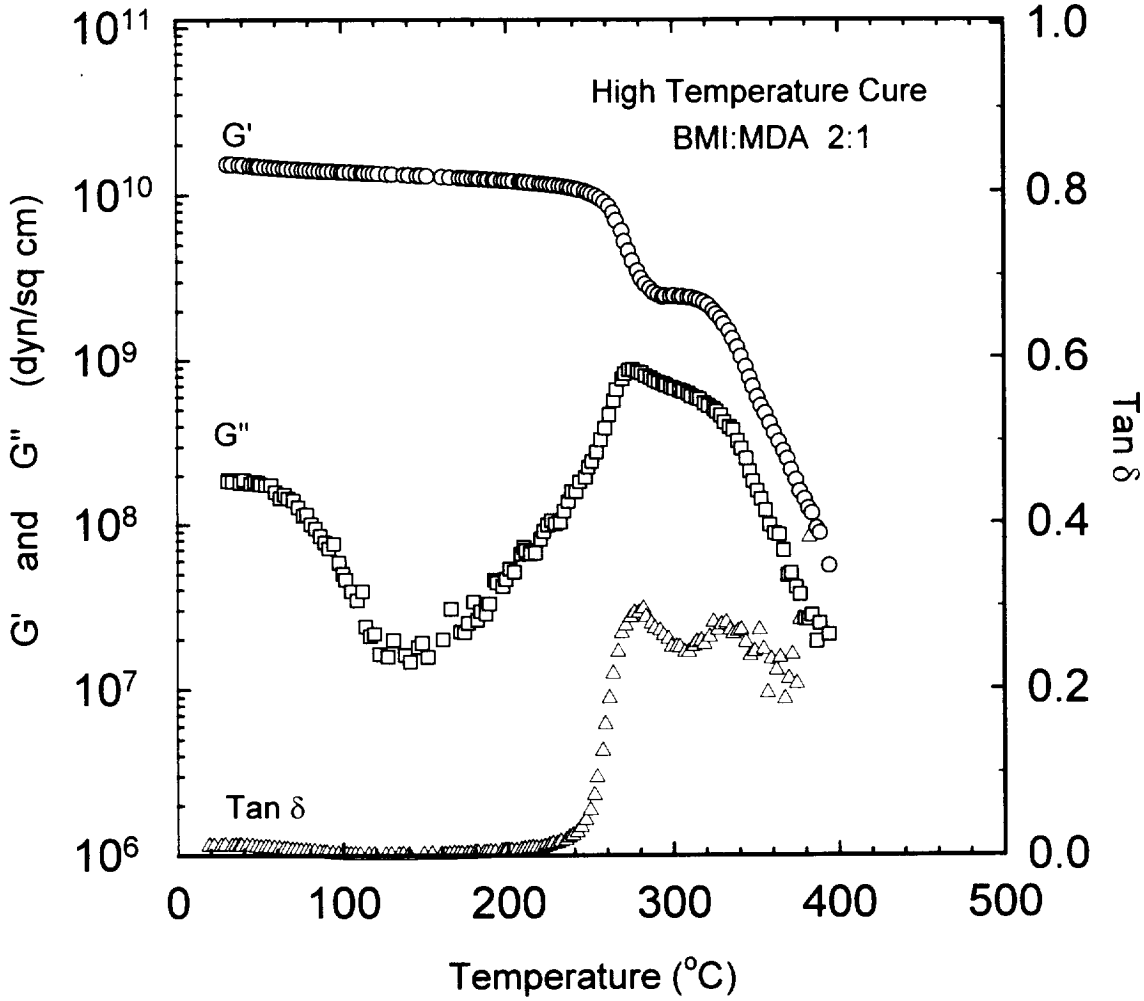

Figure 4.30. Rheological plot of G', G", and tan δ for the BMI:MDA sample in a 2:1 mole ratio, cured for 6 hours at 220 °C. Frequency of test was 1 Hz.

increase in G' will be termed the "rubbery minima" although many authors refer to this value as the rubbery plateau.

4.4.5.1. Rheological Properties of BMI/MDA

Figures 4.31-4.33 are the plots of G', the storage modulus or in-phase modulus, for the various cure cycles (high, low, and low/high) for the three different mole ratios of BMI:MDA. The three different of networks are formed for the 2:1 mole ratio conditions, shown in Figure 4.31. This is evident by three different glass transition temperatures and three different rubbery minima. As the cure proceeds from low to low/high to high the T_g, determined by the intercept method, increases. The rubbery minima increase as the cure proceeds from low to low/high to high, indicating that the molecular weight between crosslinks decreases as the cure proceeds from low to low/high to high cure conditions. With increasing crosslinking, the value of the rubbery minima increases.

The numerical value of a level rubbery minima can be used as an estimate of M_c, the number average molecular weight between crosslinks, based on the theory of rubber elasticity.[57] However, for many reasons, the theory of rubber elasticity is not valid for highly crosslinked

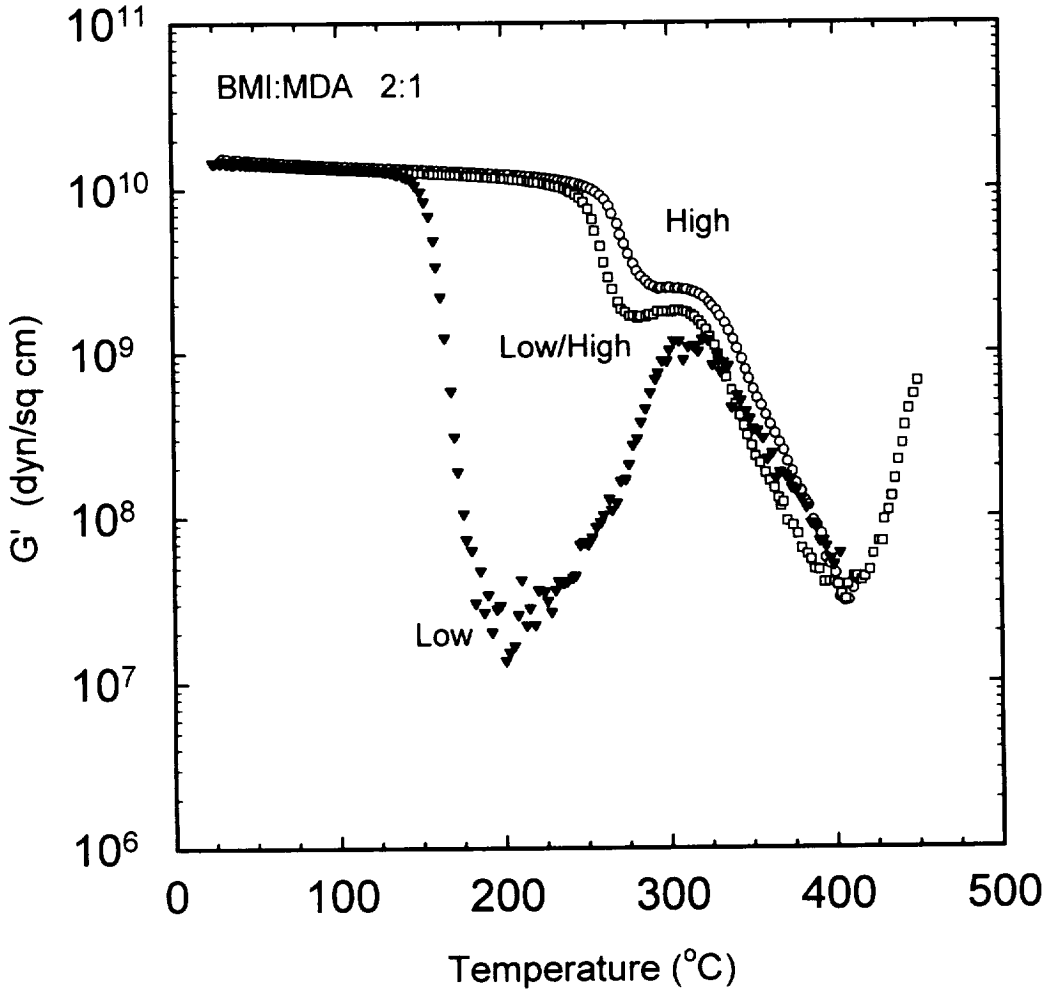

Figure 4.31. Plots of G' for BMI:MDA in a 2:1 mole ratio for the various cure cycles. Frequency of test was 1 Hz.

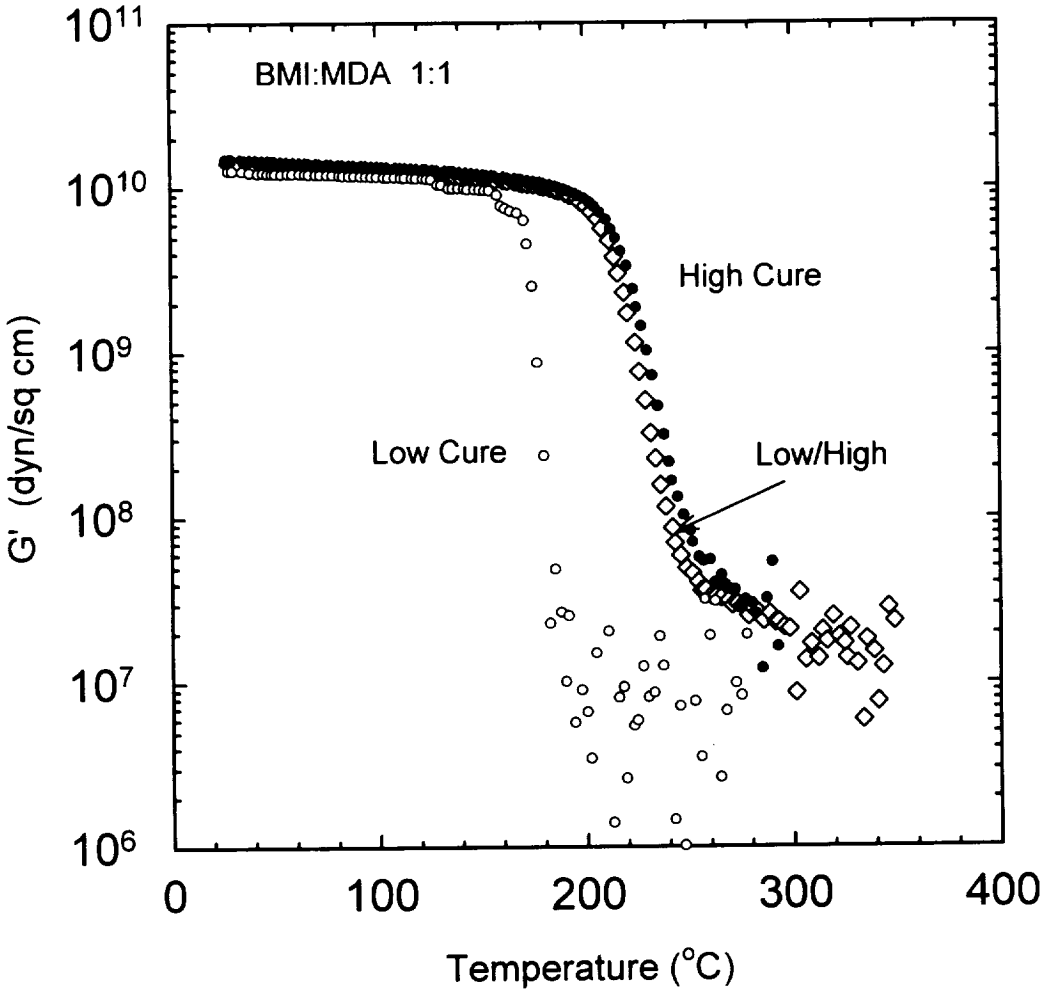

Figure 4.32. Rheological plots of G' for BMI:MDA in a 1:1 mole ratio for the various cure cycles. Frequency of test was 1 Hz.

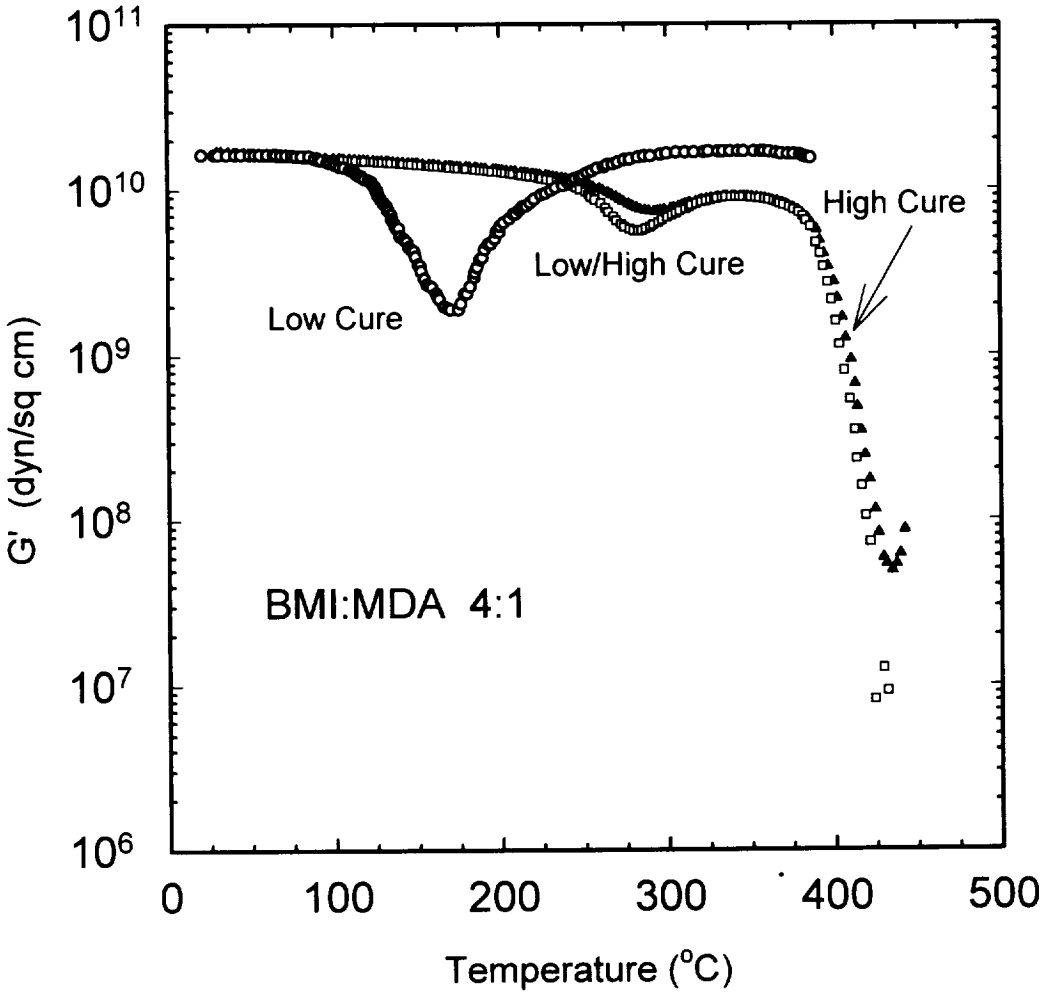

Figure 4.33. Plots of G' for BMI:MDA in a 4:1 mole ratio for the various cure cycles. Frequency of test was 1 Hz.

systems, but has been shown to be useful for an approximation or relative ranking of M_c within a system.[90] Generally the trend between T_g and G_e should be similar. This is expected because as T_g and G_e increase, the crosslink density should increase and M_c should decrease.

The storage moduli increase with temperature, especially for the low-temperature cure, which is indicative of BMI homopolymerization or further reaction during the time frame of the dynamic mechanical testing. As stated earlier, during the dielectric characterization, the curing of a thermoset becomes diffusion controlled at high viscosity or longer cure times since unreacted BMI molecules become trapped within the forming matrix. Regnier et al.[91] reported that at the end of cure, the amount of unreacted maleimide double bonds is approximately 10%. Cure to complete reaction is not possible because the conversion of the liquefied monomers to a highly crosslinked thermoset becomes more restricted as the reaction proceeds. Consequently, the translational movements of the unsaturated imide groups are hindered at high viscosity. During rheological testing, the BMI:MDA chains have the thermal energy to diffuse and with heat, crosslink further. This investigation must account for a

changing network structure as testing procedures involve higher temperatures.

Figure 4.32 is the G' curves for BMI:MDA in a 1:1 mole ratio for the various cure cycles. As the cure proceeds from low to low/high to high, the T_g increases. However, the values of the rubbery minimas are roughly the same, indicating that the molecular weight between crosslinks does not change for the cure condition in the 1:1 mole ratio condition. According to Tungare,[22] in the case of 1:1 BMI:MDA, curing occurs predominately by the amine addition reaction. Most of the BMI is consumed during the low-temperature cure. Therefore, there is less chance for crosslinking during the high cure or second step condition. The low/high and high cure conditions exhibit the same T_g and rubbery minima, possibly indicating that the samples have the similar network topologies.

Figure 4.33 shows the G' curves for BMI:MDA in a 4:1 mole ratio for the various cure conditions. As the cure proceeds from low to low/high to high, the apparent T_g increases. The rubbery minima increase as the cure goes from low to low/high to high. The low cure has the highest number average molecular weight between crosslinks while the high cure condition would exhibit the lowest Mc for the

4:1 mole ratio conditions. Once the amine content is completed, there is excess BMI available for further crosslinking, or homopolymerization. Consequently, after the rubbery minimum, G' increases with further temperature. The unreacted BMI begins to crosslink with the addition of heat, forming new crosslinks. The high cure has a higher rubbery minimum than the low/high cure even though the apparent glass transition temperatures are the same. The high cure of the 4:1 mole ratio BMI:MDA has a qualitatively lower M_c than the low/high cure condition, possibly indicating two different networks with the same T_g.

When comparing the dynamic storage moduli (G') as a function of temperature and BMI content, the rubbery minima increase in the order of G'(1:1), G'(2:1), and G'(4:1). Figure 4.34 indicates that an increase in BMI content increases the relative crosslink density for the high cure condition. The stoichiometric 1:1 mixture of BMI:MDA had the lowest value of rubbery minima for all the mole ratios. For epoxies, when the rubbery minimum is plotted as a function of amine/epoxy ratio with cure schedule as a parameter, the highest modulus would be observed in the stoichiometric mixtures suggesting that the highest crosslink densities are present in those systems.[11]

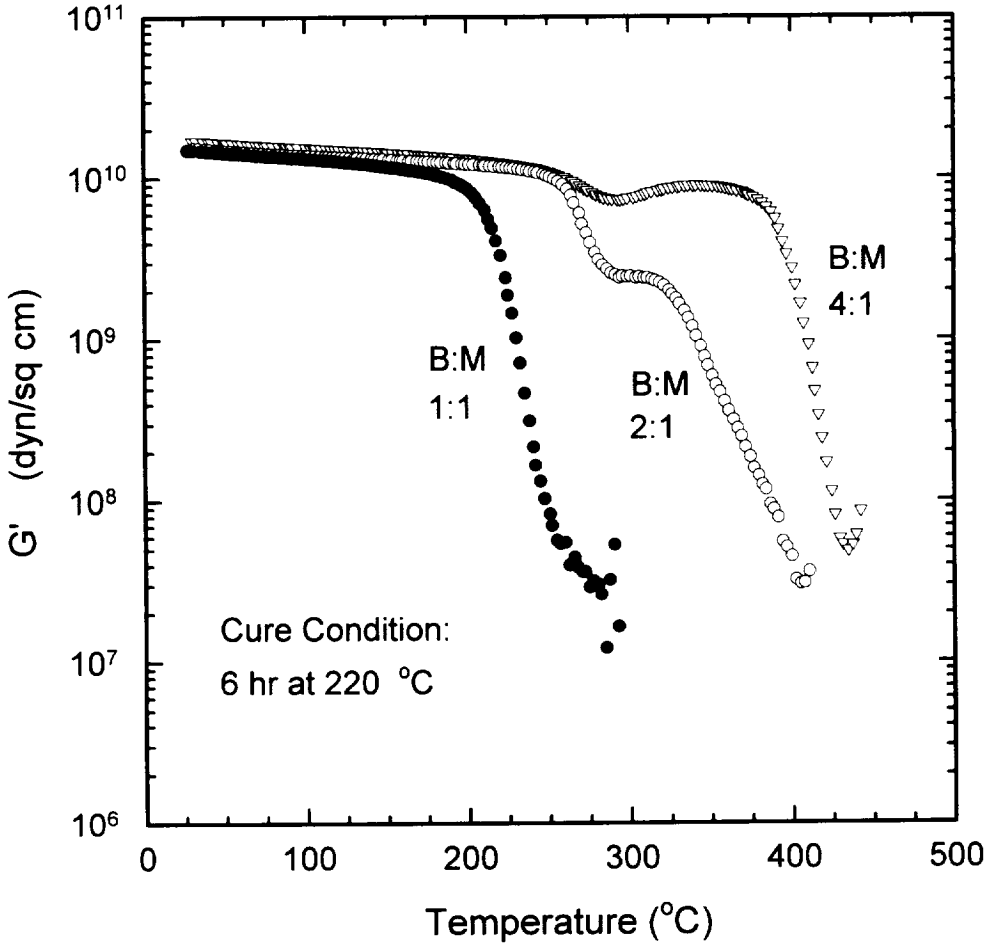

Figure 4.34. Dynamic mechanical plots of G' for the various BMI/MDA mole ratios cured at high temperature. Frequency of test was 1 Hz.

Because there is more BMI content in the 4:1 case, the rise in G' after the rubbery minimum is greater than for the 1:1 or 2:1 conditions due to an extensive homopolymerization reaction.

Many of the physical properties examined have been plotted against mole fraction BMI. In this designation, 0.8 depicts the 4:1 mole ratio of BMI/diamine, 0.667 represents 2:1 mole ratio of BMI/diamine, and 0.5 denotes the 1:1 mole ratio case of BMI/diamine. Figure 4.35 illustrates the effect of mole fraction of BMI on the glass transition temperature of BMI:MDA copolymers for the three different cure conditions. The figure indicates that the higher the isothermal-cure temperature, the higher the glass-transition temperature. During the low-temperature cure, curing occurs by the chain extension reaction, resulting in a network consisting of long chains with a low T_g. In the 1:1 case, lack of sufficient maleimide groups for crosslinking may contribute to a lower T_g for both high and low/high cure conditions.

In any case, the addition of amine increases the T_g for both the low/high and the high cure conditions over BMI alone. The T_g for BMI alone is lower than the cure temperature because the network vitrifies as the glass

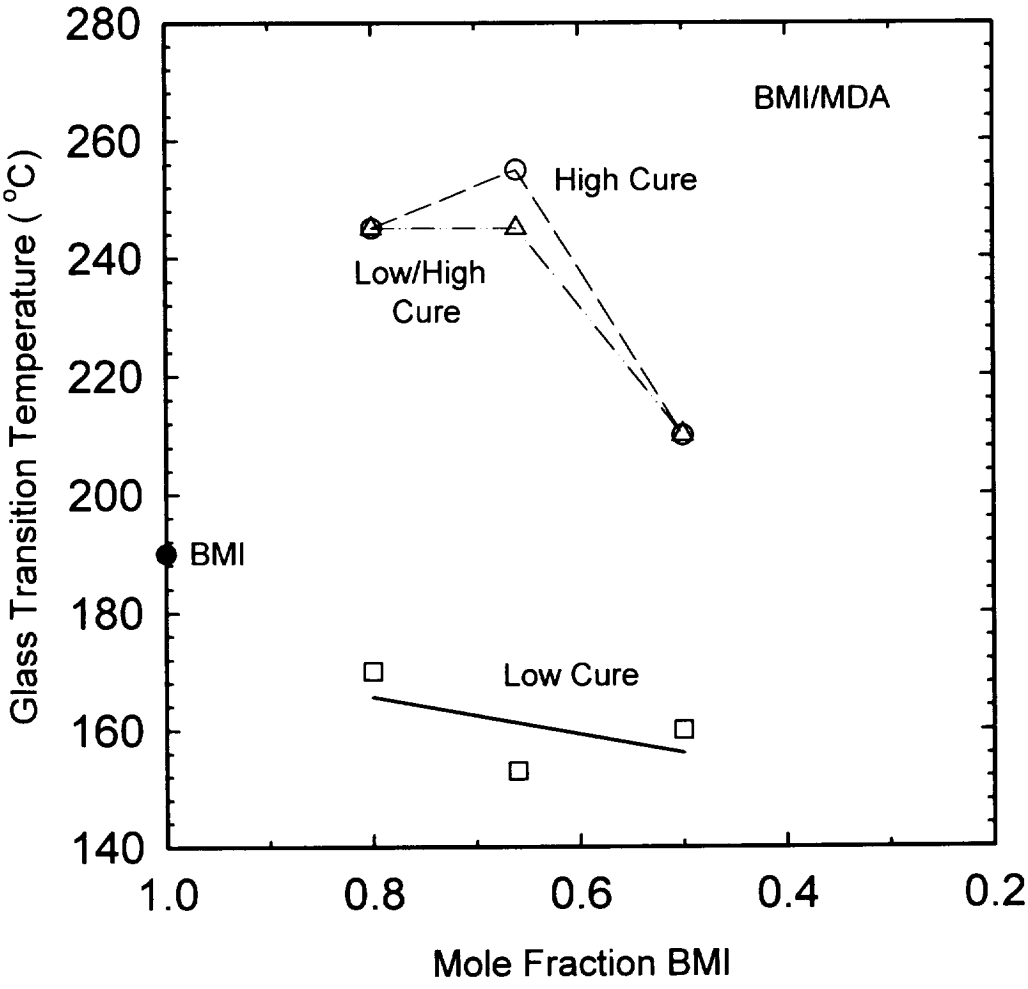

Figure 4.35. The effect of mole fraction BMI on the glass transition temperature of BMI/MDA copolymers for the three different cure conditions.

transition temperature approaches the isothermal cure temperature. During rheological analysis, the addition of heat causes an increase in G'. At higher temperatures, degradation reactions overshadow any increase in G'.

According to Tungare[22] the glass transition data for 2:1, 1:1 and 1:2 BMI:MDA mole ratios under different cure conditions are dependent on the network topology, which in turn, is dependent upon the cure condition. He determined that for the 1:1 condition cured at low-temperatures, the T_g is higher than for 2:1 and 1:2, as a result of network topology. Leung et al.[28] found that in comparing the high cure to the low/high cure condition, the T_g's for the 2:1, 1:1 and 1.5:1 cases were essentially the same. Only in the 2.5:1 case, were the T_g's slightly different. They also found that the T_g's were shifted to higher values as the amount of BMI increased.

For the 4:1 and the 1:1 cases shown in Figure 4.35, the cure conditions did not influence the T_g. Both the high and the low/high conditions produced the same T_g. For the 4:1 case, in both the high and the low/high cure conditions, there is an excess of BMI. BMI homopolymerization will occur at the expense of the chain

addition reaction. Essentially the same network is produced with the 4:1 network, hence the same T_g.

In the 1:1 case, stoichiometry results in a more extensive amine addition reaction than in the 2:1 or 4:1 cases. The 1:1 low-temperature cure condition has a higher T_g than the 2:1 case. This increase in glass transition temperature can be attributed to an increase in molecular weight (linear chain length) of the 1:1 condition where the 1:1 case results in more amine addition than in the 2:1 case. For the 1:1 case, the amine addition reaction is more extensive than in the 2:1 case. This could possibly lead to some chain ends capped with MDA instead of BMI, which would inhibit the homopolymerization reaction. Therefore, for the high and low/high cure conditions, essentially the same network was produced.

The T_g for 1:1 BMI:MDA increases with reaction time until it reaches or slightly exceeds the isothermal cure temperature because the resin vitrifies as the T_g approaches the isothermal cure temperature. The high and the low/high-temperature cure conditions both produce T_g's near the high cure temperature.

The three different cure conditions for the 2:1 BMI:MDA produced three different types of network

topologies, as evident from the different T_g's and rheological curves. The amine addition reaction was predominant during the low-temperature cure reaction. Since there were 2 BMI molecules to every 1 MDA molecule, the chances of endcapping the chains with BMI are favorable. Then, with further cure at high temperature, homopolymerization will occur, resulting in a network with fewer network defects and longer chains. During the high-temperature cure condition, both the amine addition reaction and the BMI homopolymerization reaction may occur simultaneously, resulting in a network with short chains and network defects.

The rheological results indicate that the resin composition, the curing conditions, and the topology of the resulting network have significant effects on the thermal properties of BMI's. In general, a high BMI content leads to a high T_g. The amine addition reaction occurs more readily than BMI homopolymerization and therefore, in the early stages of cure, amine addition occurs until most of the amine is consumed.

4.4.5.2. Rheological Properties of BMI/DABA

Figures 4.36-4.39 are storage modulus curves for BMI:DABA in 1:1, 1:0.87, 2:1 and 1:1.2 mole ratios.

Figure 4.36 is the G' curves for BMI:DABA in a 1:1 mole ratio for the low-, high-, and low/high-temperature cure conditions. The T_g and the rubbery minimum/inflection increase as the cure proceeds from low to low/high to the high cure condition. G' for the low cure condition increases after reaching a minimum. Because of the unreacted BMI within the gelled matrix, additional thermal energy in the form of higher temperatures will result in new crosslinks, causing an increase in G'.

Mijovic and Andjelic[31] determined through FTIR spectroscopy that the principle reaction in the temperature range of 140 to 200 °C was the copolymerization between the maleimide and allyl double bonds or a chain extension 'ene' reaction. This is the only reaction that involves double bonds below 200 °C. The minimum value of G' for the low cure condition occurs at approximately 250 °C. With heat, the unreacted BMI joins to form long chains and additional crosslinks, thereby increasing G'.

For the low/high cure condition, a slight increase in G' is apparent after a minimum is reached. As stated before, below 200 °C, the copolymerization of BMI and DABA occurs in alternating fashion. In addition, at approximately 180 °C, the etherification reaction involving

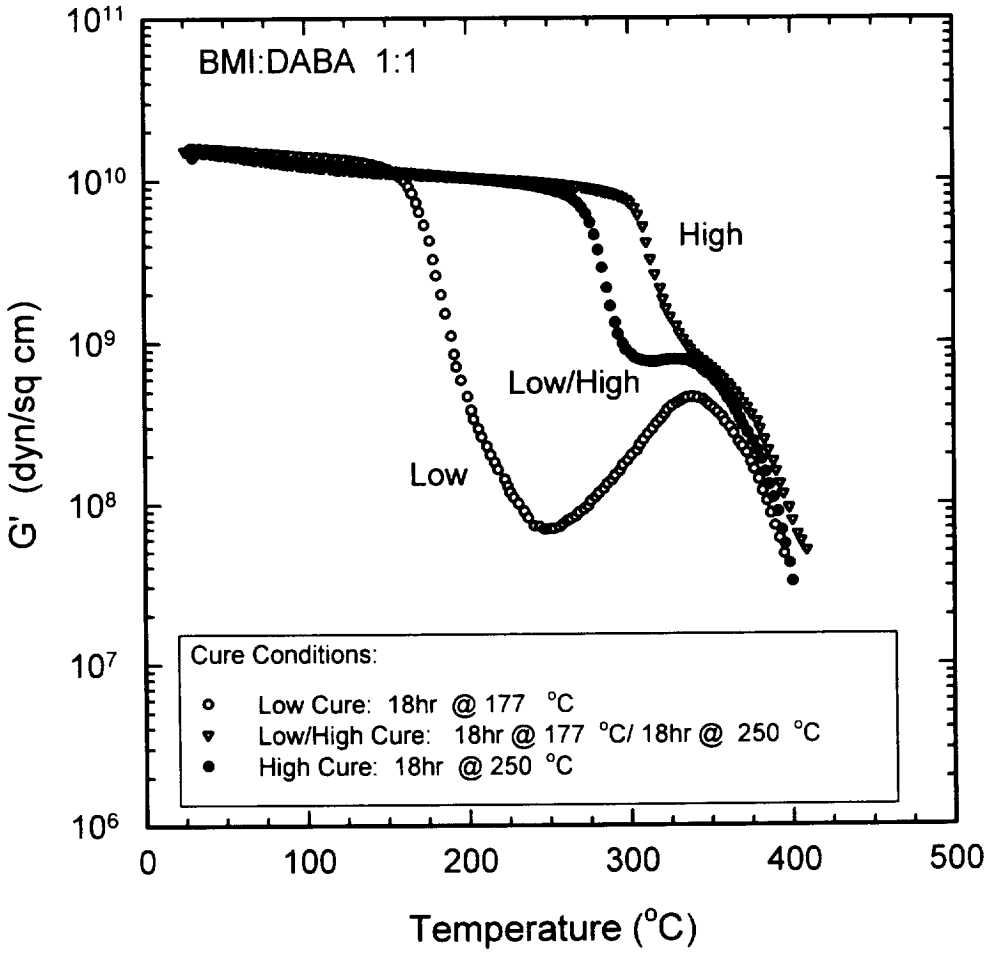

Figure 4.36. G' curves for BMI:DABA in a 1:1 mole ratio for the low-, high-, and low/high-temperature cure conditions. Frequency of test was 1 Hz.

two OH groups occurs, the extent of which determines the crosslink density of the material. Mijovic[31] found that below 200 °C the maleimide and allyl double bonds are almost completely consumed. Above 200 °C, the homopolymerization of BMI occurs. Just above 300 °C, there is a slight increase in G' after the plateau region. This is apparently due to unreacted BMI molecules diffusing through the matrix and forming new crosslinks.

The high cure condition does not display a rubbery minimum or plateau; degradation competes with the rheological process and G' steadily decreases. Mijovic[31] attributed this to addition dehydration and initiation of degradation. The TGA results in Table 4.5 indicate that the maximum weight loss in a nitrogen atmosphere occurs at 469 °C for the BMI:DABA in a 1:1 mole ratio. Dynamic mechanical testing was performed in air. This could account for the difference in degradation temperatures between the TGA and rheological data. Degradation may be detected as a drop in storage modulus at temperatures above 360 °C, which corresponds to onset of visible degradation. During the high-temperature cure, above 200 °C, both the 'ene' reaction and the maleimide homopolymerization will occur simultaneously. However, in the initial stages of

polymerization where there is a high concentration of BMI and when the allyl groups are exhausted, the fast homopolymerization reaction of the maleimide groups is predominant.

Figure 4.37 illustrates the G' curves for the low-, low/high-, and two high-temperature cure conditions for the 1:0.87 mole ratio of BMI:DABA. There are two high-temperature conditions, labeled short time (4 hours) and long time (18 hours). The low-temperature cure condition exhibits the lowest T_g and the lowest value of the rubbery minimum. The low-temperature cure condition also displays an increase in G' after the minimum G', at approximately 240 °C. At temperatures above 240 °C, the homopolymerization reaction of the maleimide bonds occurs, creating new crosslinks. The etherification reactions may also occur at higher temperatures.

The low/high-temperature cure condition and the high-temperature cure condition (long time) both exhibit the same glass transition temperature of 300 °C. At approximately 340 °C, both cure conditions exhibit a rapid decrease in G', due to the initiation of degradation. T_{max} from the TGA data was 457 °C in N_2. The low/high-temperature cure condition experiences a slightly lower

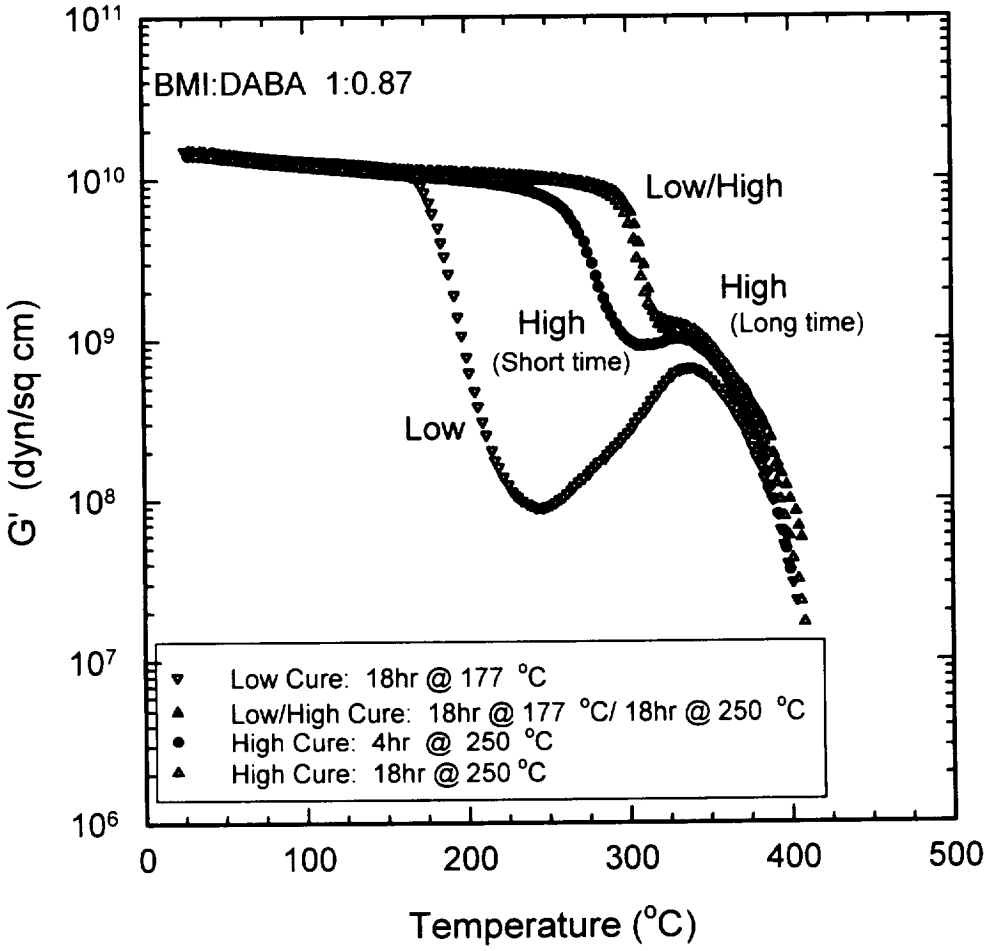

Figure 4.37. Storage modulus curves for BMI:DABA in a 1:0.87 mole ratio for the low-, high-, and the low/high-temperature cure conditions. Frequency of test was 1 Hz.

rubbery minimum value than the high-temperature cure - long time condition. However, the degradation process overshadows the significance of this result.

The glass transition temperature and the value of the rubbery plateau region for the high-temperature cure - short time condition falls between the low- and the low/high-temperature cured material. By increasing the cure time for a given cure condition, the glass transition increases from 270 °C to 300 °C. The longer cure time for the high-temperature cured BMI:DABA in a 1:0.87 mole ratio produced a matrix with a high crosslink density relative to the high-temperature - short time cure condition.

Figure 4.38 contains the G′ curves for the 2:1 mole ratio of BMI:DABA in the various cure conditions. The glass transition temperatures and the rubbery minima increase as the cure proceeds from the low- to high- to low/high-temperature cure conditions. The materials, for each cure condition in the 2:1 mole ratio, are more highly crosslinked compared to the other mole ratios of the corresponding cure conditions as evident by the higher rubbery plateau values. (The value of the rubbery plateau is a relative indicator of crosslink density.) For the low-temperature cure condition, excess BMI remains

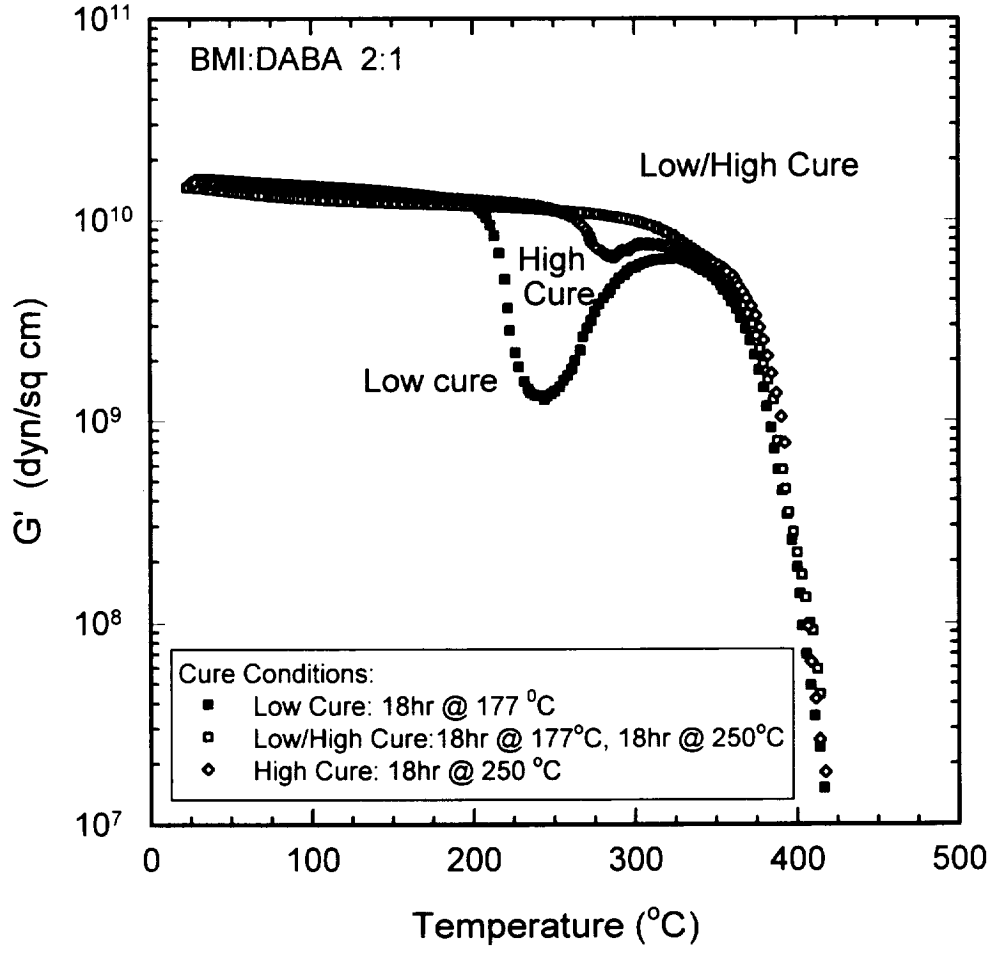

Figure 4.38. Storage modulus curves for BMI:DABA in a 2:1 mole ratio for the low-, high-, and the low/high-temperature cure conditions. Frequency of test was 1 Hz.

unreacted in the material even after the DABA is exhausted during the copolymerization. Therefore, when the test temperature exceeds 250 °C, the unreacted BMI molecules begin to translate and diffuse to produce further crosslinking. Consequently, G' increases with temperature after reaching a minimum.

The high cure condition has a T_g of 280 °C. G' decreases until the minimum at 295 °C. Then G' increases due to the BMI homopolymerization reaction. The low/high-temperature cure condition does not exhibit a rubbery plateau or minimum before degradation begins. The T_g was 300 °C. No increase in G' was observed with temperature after the rubbery plateau.

Figure 4.39 contains the G' curves for the low- and low/high-temperature cure conditions of BMI:DABA in a 1:1.12 mole ratio. As the cure proceeds from low to low/high-temperatures the T_g increases from 160 °C to 278 °C. In the low-temperature cure condition, with DABA in excess, G' still increases with temperature after the minimum at 260 °C.

For the low/high-temperature cure condition, a long rubbery plateau is observed before G' decreases with

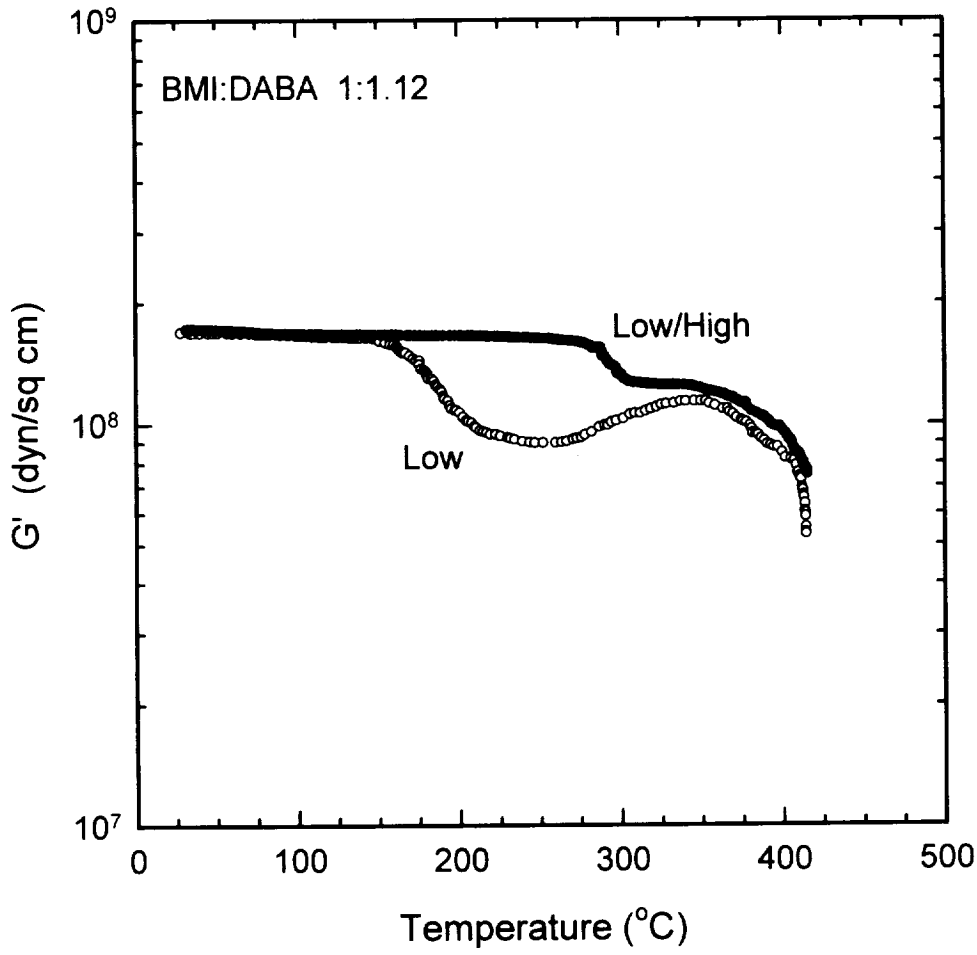

Figure 4.39. G' versus temperature for the low- and low/high-temperature cure conditions of BMI:DABA in a 1:1.12 mole ratio. Frequency of test was 1 Hz.

temperature. The additional curing step increased the T_g, the value of the rubbery plateau, and exhausted the unreacted BMI. No increase in G' was observed with further increase in temperature.

Figure 4.40 shows the effect of mole fraction BMI on the glass transition temperature of BMI/DABA copolymers. For all the cure conditions, as the crosslinking agent increased, the glass transition temperature decreased. Chattha and Dickie[92] have also observed this trend of decreasing T_g with increasing amounts of DABA for a BMI/DABA copolymer with a different thermal history than that performed in this investigation. During the high-temperature cure, BMI homopolymerization initially occurs at a faster rate than the copolymerization of BMI and DABA. The homopolymerization reaction then slows and the copolymerization and etherification reaction rates increase until one of the components is exhausted.[31]

4.4.5.3. Rheological Properties of BMI/DDS

Figure 4.41 contains the storage modulus curves for BMI/DDS in a 2:1 and 1:1 mole ratio. Both samples barely exhibit a rubbery minima region before degradation. TGA results indicate that the T_{max} for the 2:1 mole ratio sample was 429 °C. Because of the very small decrease in G' from

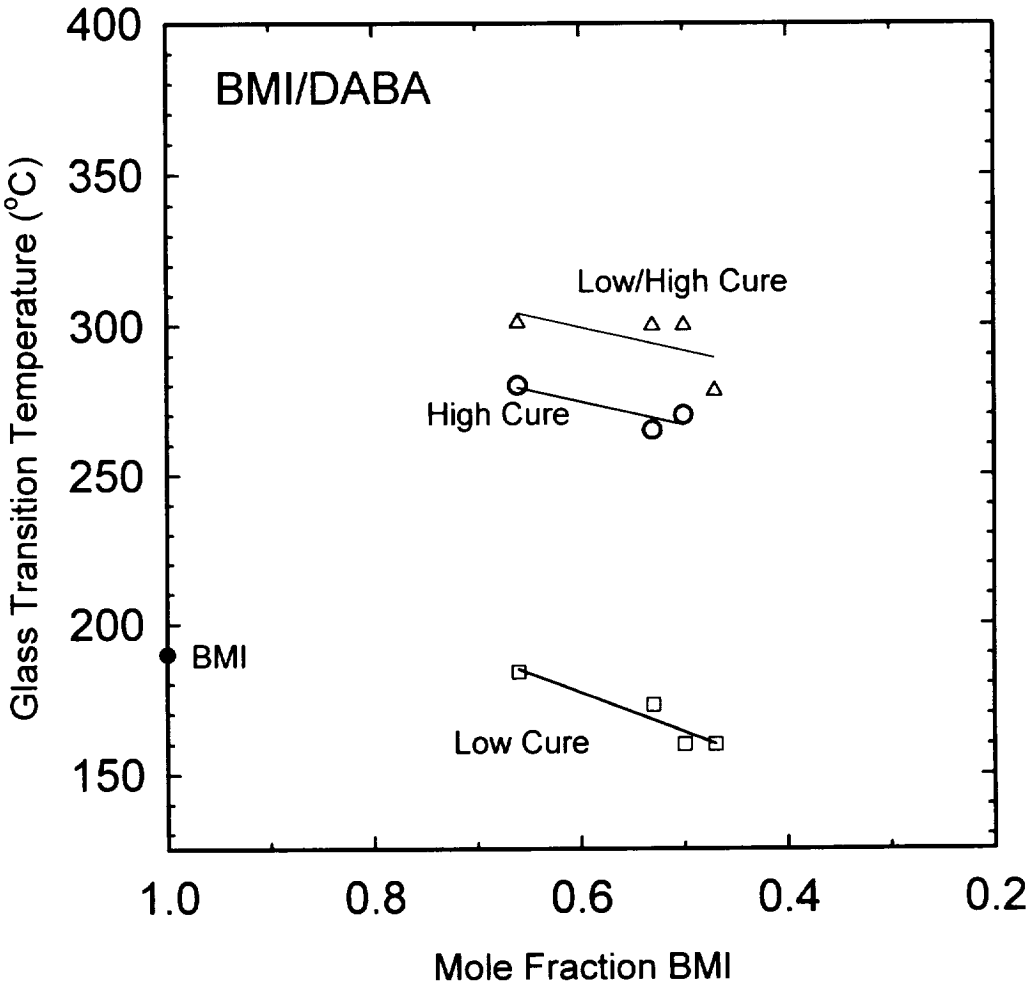

Figure 4.40. The effect of mole fraction BMI on the glass transition temperature of BMI/DABA copolymers.

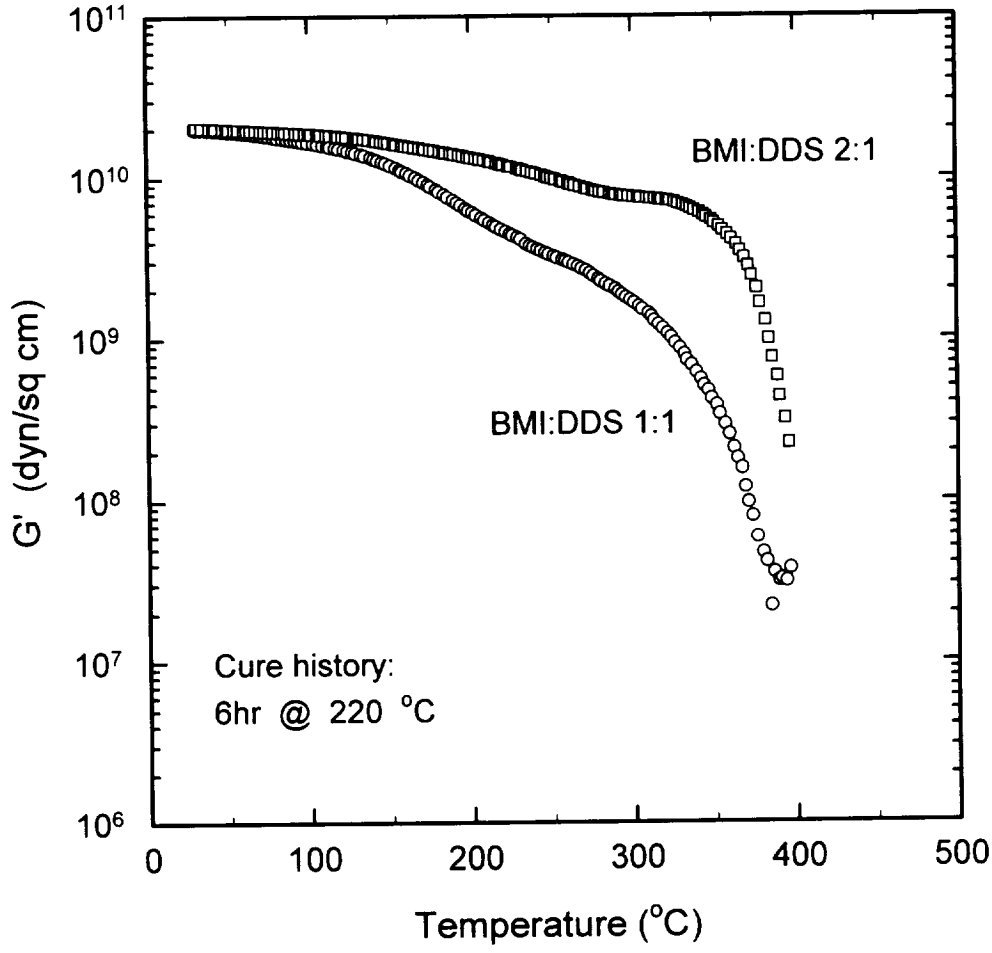

Figure 4.41. Storage modulus curves for BMI/DDS in a 2:1 and 1:1 mole ratio. Frequency of test was 1 Hz.

the glassy region to the rubbery plateau region, the samples exhibited a very high crosslink density and were very brittle.

Figure 4.42 illustrates the effect of mole fraction BMI on the glass transition temperature of the BMI/DDS copolymers. As the amount of DDS increased, the glass transition temperature decreased. The addition of DDS increases the T_g over BMI alone. The DDS system also displayed a higher T_g than the MDA systems. This is because of the high polarity of the $-SO_2$ group compared to the $-CH_2$ group of MDA.

4.4.5.4. Rheological Properties of PMR

Figure 4.43 is the G' versus temperature behavior for cured and postcured PMR. T_g increases from 330 °C to 405 °C with the addition of postcuring. The cured PMR displayed a large transition region before reaching the limits of the test equipment. The postcured PMR exhibited a slight increase in G' with temperature after the minimum at 400 °C.

4.4.6. Density by the Method of Hydrostatic Weighing

Density was measured for all the samples by a simple hydrostatic weighing technique, ASTM D792.[56] Density provides a measure of molecular packing within a network structure. Figure 4.44 exhibits density versus mole

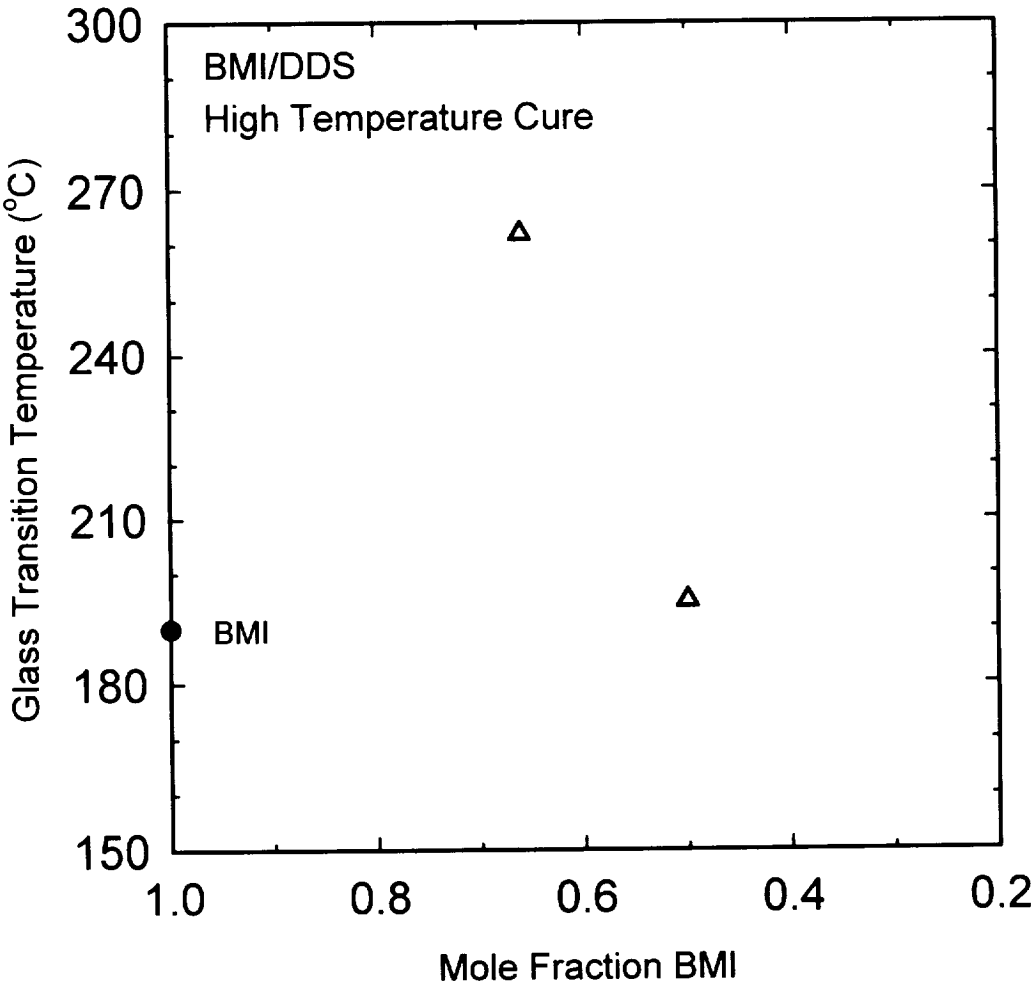

Figure 4.42. The effect of mole fraction BMI on the glass transition temperature of BMI/DDS copolymers.

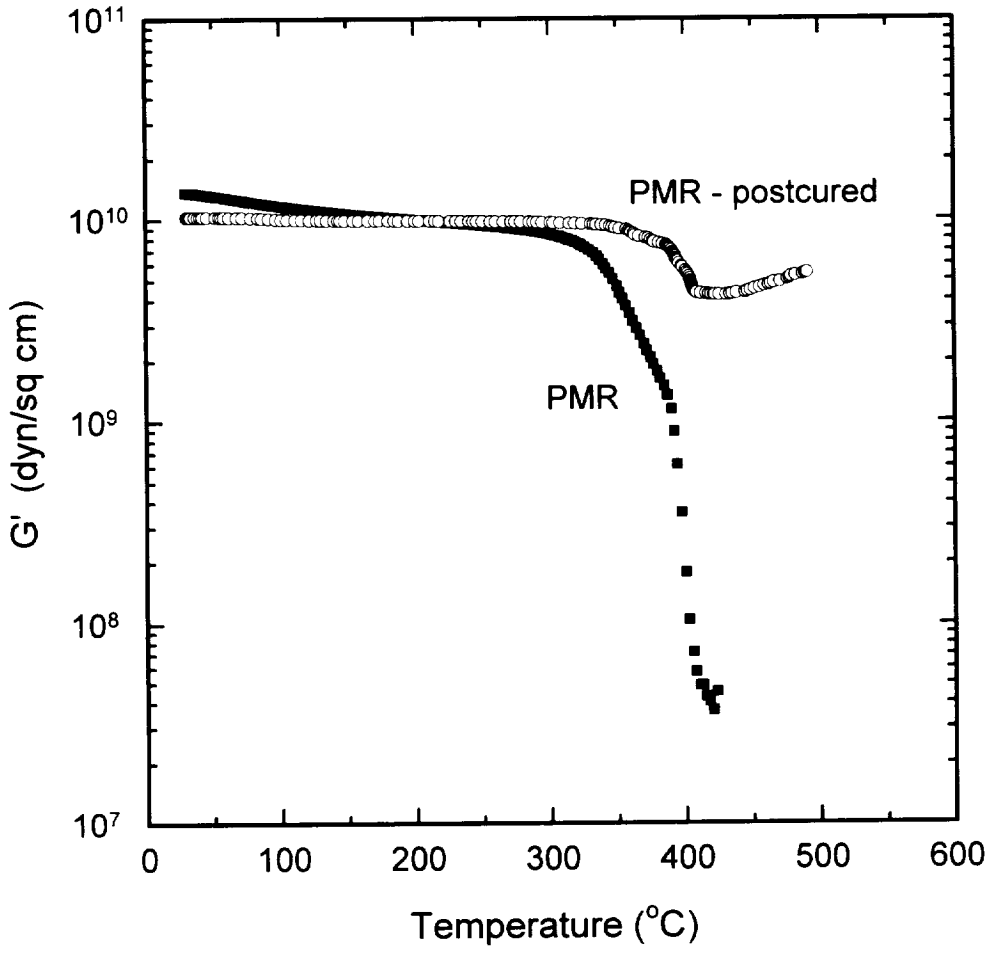

Figure 4.43. G′ versus temperature for cured and postcured PMR. Frequency of test was 1 Hz.

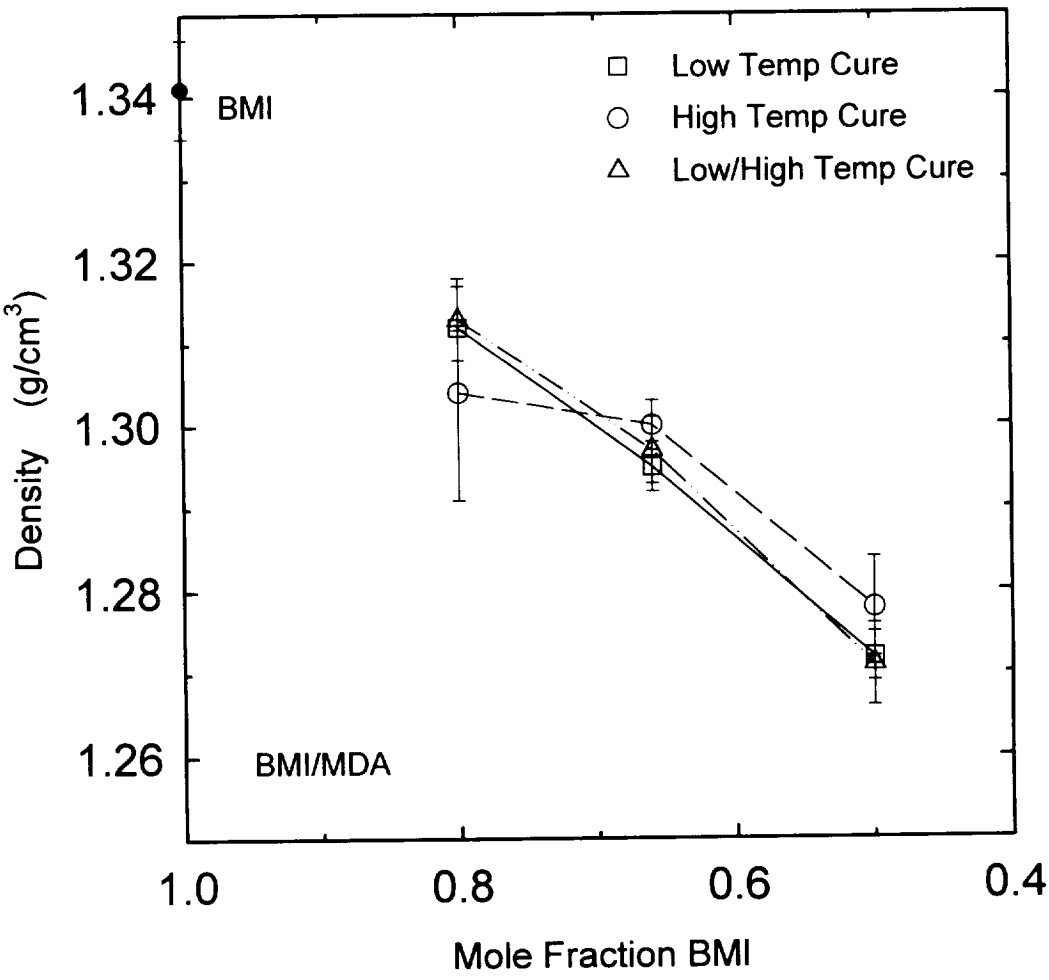

Figure 4.44. Density versus mole fraction BMI for BMI/MDA copolymers.

fraction BMI for BMI/MDA copolymers and pure BMI. BMI has the highest density - 1.34 g/cm^3. Density of the copolymers then decreases as the amount of diamine increases.

Resin density has been correlated with free volume: as the density increases there is a reduction in free volume due to crosslinking. In other words, when fractional free volume is at a high level, intermolecular distances are great and density values are lower. The 1:1 mole ratio cure conditions of BMI/MDA exhibit the lowest density values. This is due to the extensive Michael's addition reaction that occurs during the curing of all 1:1 mole ratio cure conditions, implying that the 1:1 mole ratio materials have the highest free volume compared to the other mole ratios.

Room-temperature density values for BMI/MDA copolymers, irrespective of cure condition, decreased as the concentration of BMI decreased. This implies that the free volume of the samples increased as the amount of diamine increased. There is also an indirect correlation between the free volume and M_c; the longer the molecular chains, the more free volume within the network. The 1:1 mole ratio cases had the lowest density values and therefore, have the highest M_c and free volume. GPC results

confirm that for the low-temperature cure condition, the 1:1 mole ratio case of BMI:MDA had the lowest M_w and M_n. Donnellan and Roylance[6] also confirmed this correlation through dilatometry experiments. They found that the fractional free volume was highest for their 1:1 BMI:MDA materials.

Gupta and Brahatheeswaran[93] investigated crosslinked epoxy networks and found that the samples having the highest crosslink densities had the lowest bulk room-temperature densities. And after postcuring, the densities of all the epoxy samples decreased. This type of behavior was not observed in the present investigation on polyimides. Chemical composition rather than cure history was more important in affecting the density of BMI/MDA. Donnellan and Roylance[6] found similar correlations between chemistry and density to those observed in this investigation.

Figures 4.45-4.47 are plots of density versus mole fraction BMI for the low-, high-, and low/high-temperature cure conditions, respectively, of BMI/MDA, BMI/DDS, and BMI/DABA. In the BMI/MDA and BMI/DABA systems, the room-temperature density decreased as the concentration of BMI decreased for all cure conditions. Furthermore, samples of

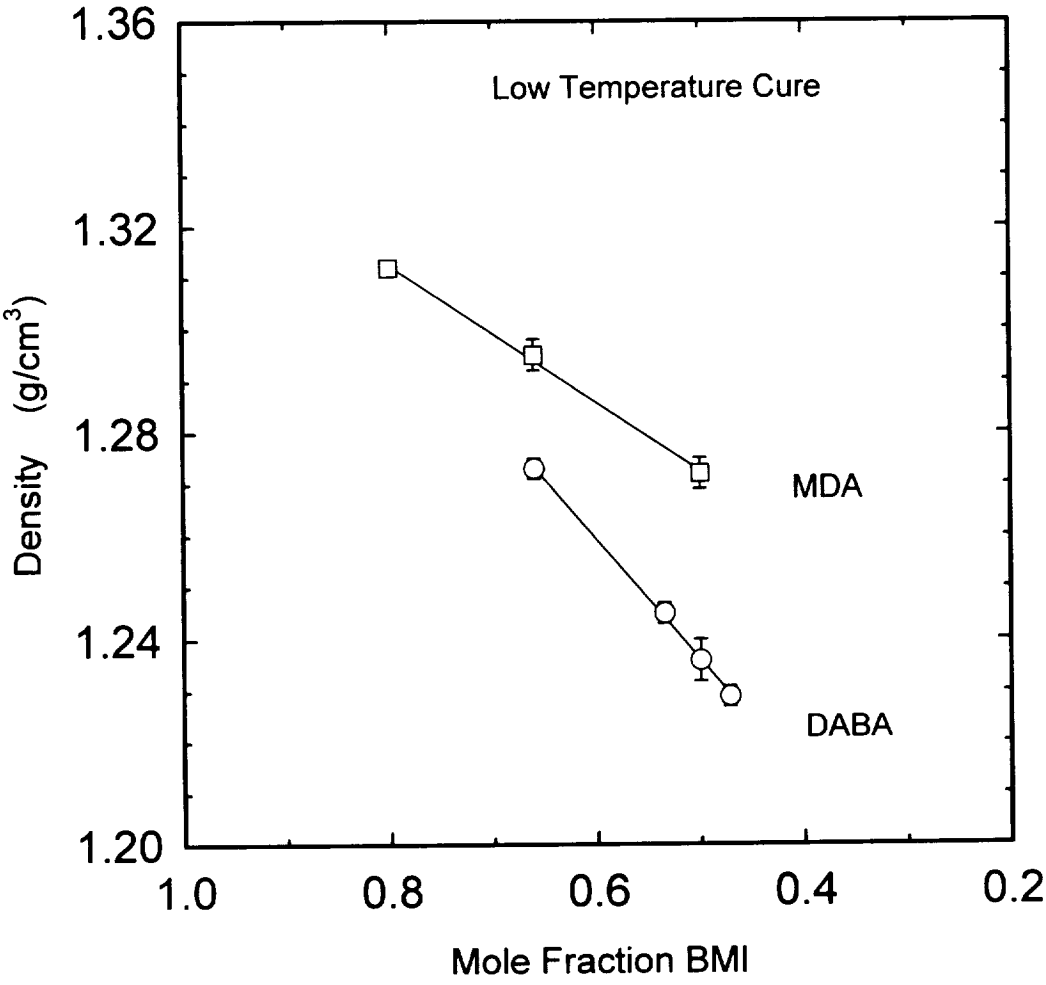

Figure 4.45. Density versus mole fraction BMI for BMI/MDA, and BMI/DABA in the low-temperature cure condition.

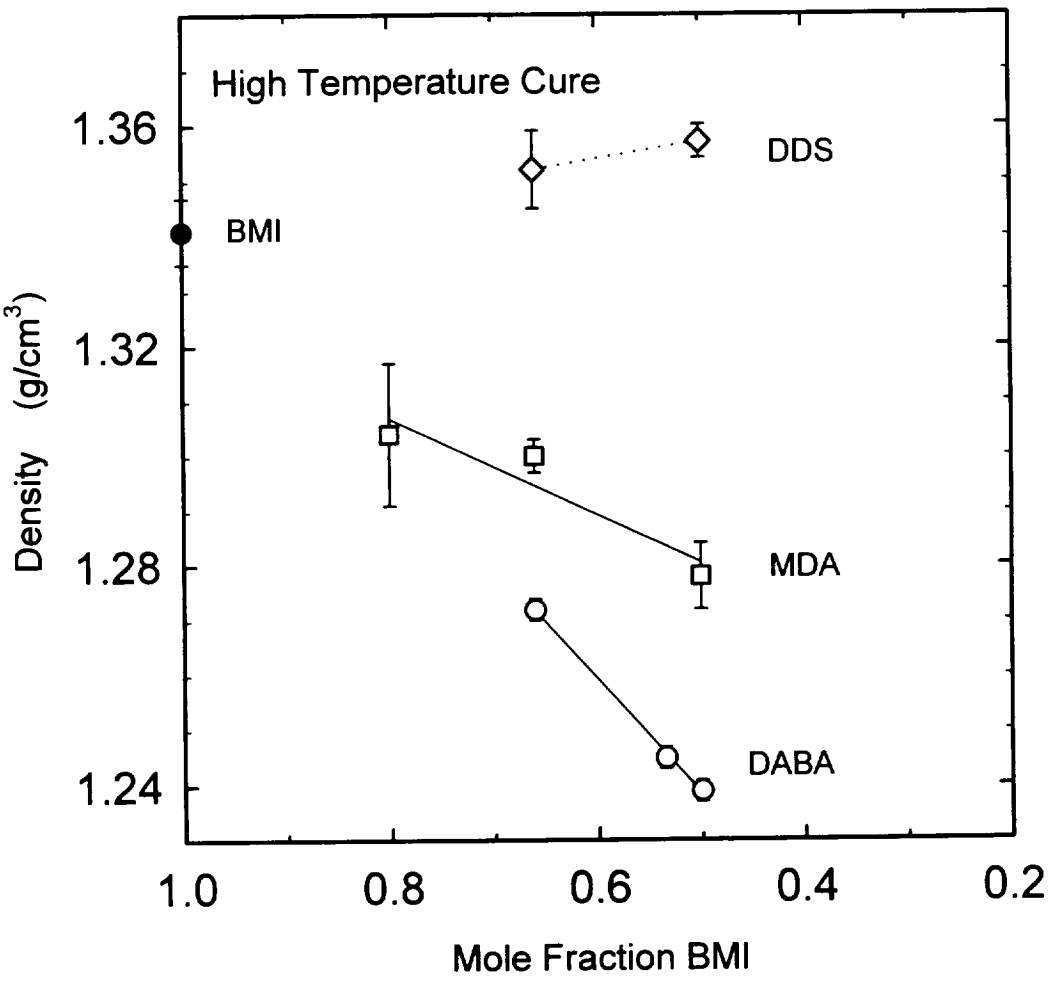

Figure 4.46. Density versus mole fraction BMI for BMI/MDA, BMI/DDS, and BMI/DABA in the high-temperature cure condition.

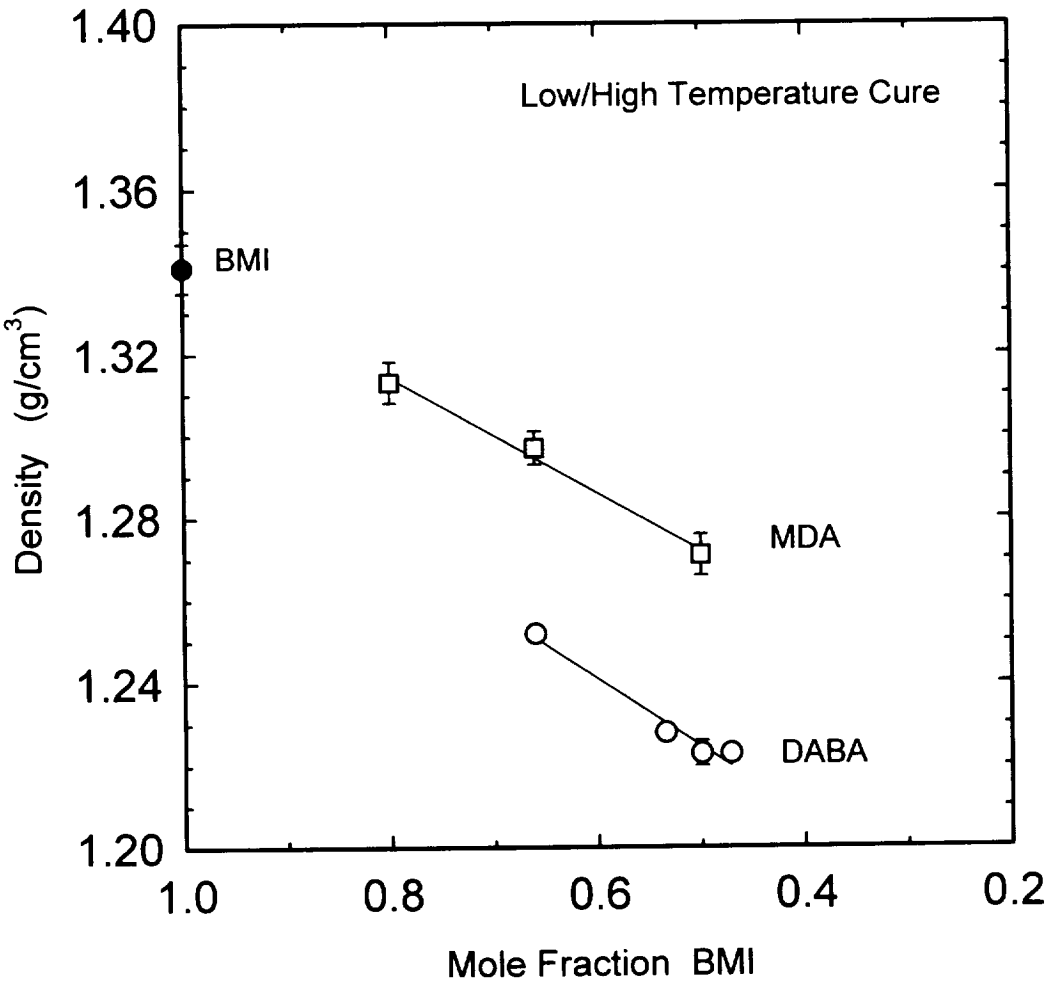

Figure 4.47. Density versus mole fraction BMI for BMI/MDA, and BMI/DABA in the low/high-temperature cure condition.

BMI/DABA had lower densities than the BMI/MDA samples of similar mole ratios. This suggests that the BMI/DABA systems have a higher fractional free volume than the BMI/MDA systems. It is plausible that the bulky structure of DABA prohibits the efficient packing of the BMI/DABA chains, thereby resulting in excess free volume and a lower density for than for BMI/MDA of similar mole ratio.

The room-temperature densities of BMI/DDS samples scarcely increased with increasing amounts of diamine, Figure 4.46. The addition of DDS to BMI increases the room-temperature density over BMI, BMI/MDA, or BMI/DABA. Since the atomic weight of sulfur is higher than carbon, DDS has a higher packing density than MDA or DABA. Consequently, the density of DDS is 1.38 g/cm^3 while the density of MDA is 1.16 g/cm^3. This could account for why the BMI/DDS system has a higher density than the BMI/MDA system.

The room-temperature densities of BMI/DABA samples cured at low-, low/high-, and high-temperature are shown in Figure 4.48. As the amount of DABA increases, the room-temperature density decreases. The low- and high-temperature cure conditions for all mole ratios tested have the same room-temperature densities. With additional heat

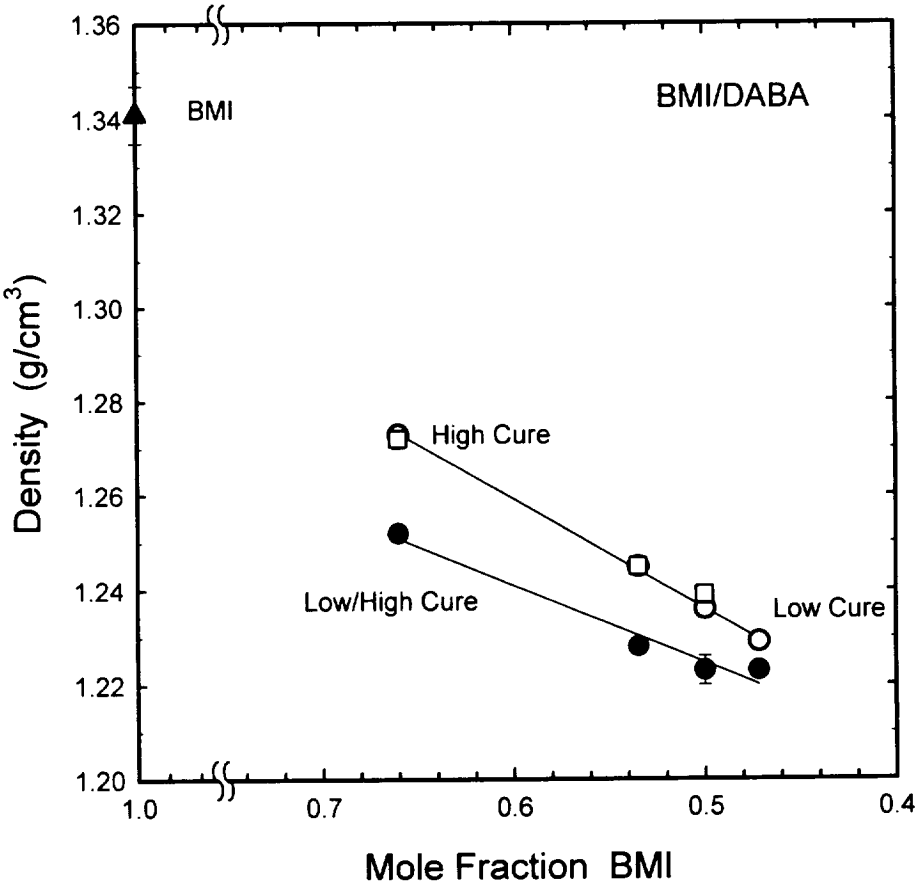

Figure 4.48. Room-temperature densities of BMI/DABA samples cured at low-, low/high-, and high-temperature curing conditions.

treatment, in the form of a step cure from low to high temperature, the density decreases. This suggests two things: 1.) The increased cure temperature leads to higher free volume in the sample and 2.) The same chemical reaction occurs for both the low- and high-temperature cure conditions, namely the chain extension 'ene' reaction. Mijovic[31] recently noted that the DABA and BMI copolymerize in an alternating fashion until the components are exhausted. Even though the temperature of the high cure condition is above the 200 °C "cut-off temperature," the alternating copolymerization reaction has a much higher reaction rate than the BMI homopolymerization reaction. Therefore, both chemical composition and cure history are important in determining the room-temperature density for the BMI/DABA system.

Table 4.7 lists the density values of cured and postcured PMR. Statistically, the density values are the same for the two samples. Postcuring did not affect the room-temperature density or free volume.

Table 4.7
Density Values for PMR.

Sample	Density (g/cm^3)	Stand. Dev.
Cured PMR	1.328	0.002
Postcured PMR	1.326	0.003

4.5. Plane Strain Compression

Yield stress is considered a small strain property, which is influenced by the molecular architecture and free volume or intermolecular packing in a polymer network. Close packing networks result in higher yield stresses.

Yield stresses of the various networks in this investigation were measured by plane strain compression. This particular test is useful in determining the yield properties of polymers because the area under the applied load remains constant and instabilities due to reduction in sample area do not occur. Since there is no geometrical reason for unstable deformation, the yield stress measured in compression is considered the intrinsic yield stress of the material.

However, yield testing of the brittle networks formed in this investigation was not always straightforward. The samples tested in biaxial compression displayed several general types of behavior:

1.) The anticipated behavior was that samples would yield prior to fracture. Approximately one half the samples behaved in this manner. Yielding took the form of a change in the slope of the load-displacement curve which corresponded to permanent set in the sample gage region.

In the majority of the samples, yielding was more subtle, consisting only of a slight change in slope of the load-displacement curve for the sample. For many of these samples fracture also occurred shortly after yielding. Yielding was verified by permanent set in the sample and the consistency of the yield values between similar samples.

2.) Some of the samples were brittle and fracture actually proceeded yielding. Still, a relative yield value was determined. For this type of behavior, fracture usually occurred by fine, almost continuous microcracking, which could be heard as faint clicks during testing. Each individual fracture event was considered very low energy and no load drop was observed. In fact, the plots for these samples showed absolutely no deviation in slope for the load-deflection curve during loading due to individual fracture events. The yield value of the sample was observed when a gentle change in slope was observed in the load-displacement plot. Yielding was then confirmed by a permanent change in thickness of the sample gage. While these values do not represent ideal "yield" values they were very consistent between and within sample plates. Therefore, the values can still be used to determine the

yield strength (and relative chain mobility) of these samples compared to each other and those that displayed normal yield behavior.

3.) Some samples were so brittle that catastrophic failure occurred during elastic loading. These samples actually "exploded" at a given load, resulting in nothing more than a fine pile of powder where the gage sections once existed. In this case, the fracture value for the sample was recorded in place of the yield stress. The fracture values themselves were characteristic of the type of material tested and ranged from 80 to over 250 MPa.

Figure 4.49 is a plot of yield stress versus mole fraction BMI for the BMI/MDA system for the different cure conditions. For the low-temperature cure condition, the various materials fractured and did not yield. These values are reported as "Fracture Stress". As the amount of diamine increased the fracture stress increased. Consequently, no conclusion concerning the effect of diamine on the yield behavior of BMI/MDA copolymers for the low cure condition could be determined.

The yield stress was sensitive to mole fraction BMI for the low/high and high cure condition. As the amount of diamine increased the yield stress decreased. The yield

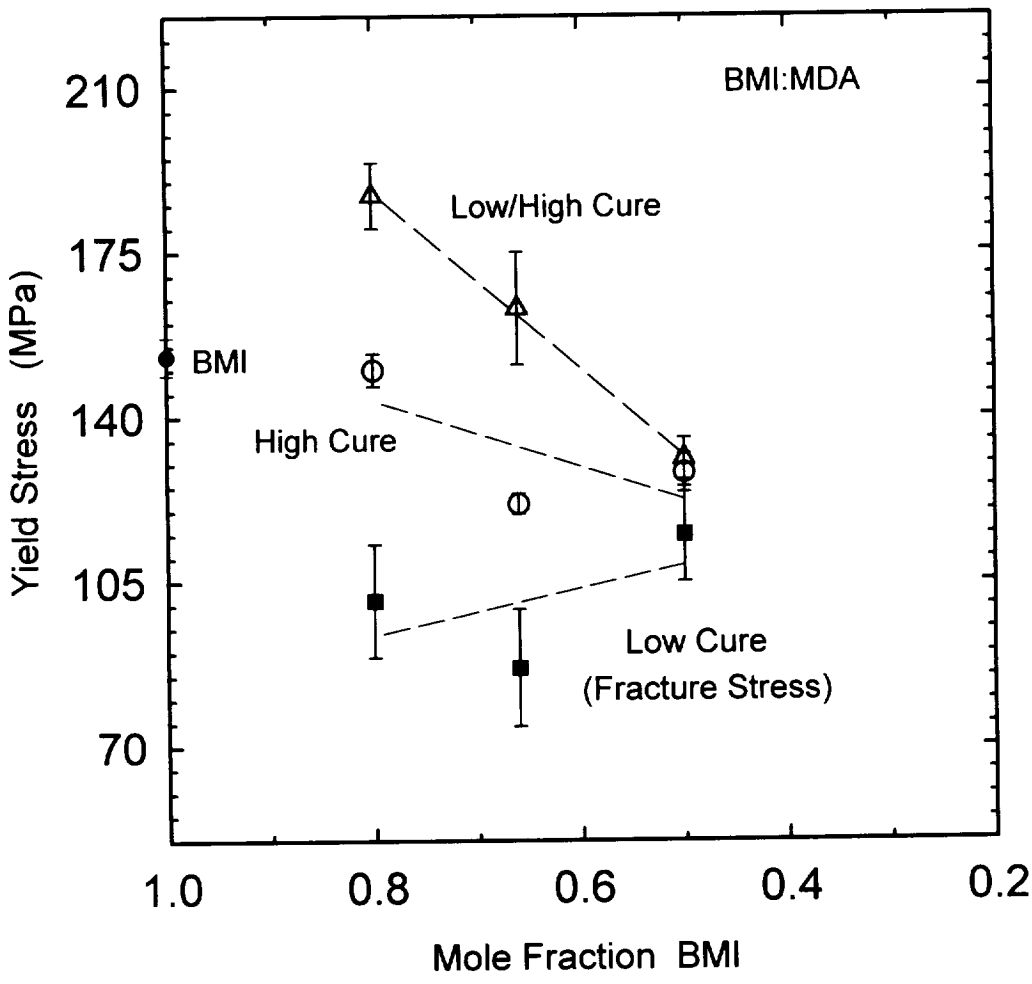

Figure 4.49. Yield stress versus mole fraction BMI for the BMI/MDA system for different cure conditions.

stress decreases as the restriction to molecular deformation decreases or free volume increases. These results are consistent with the epoxy work of Martin[9] and Young.[94] Martin[9] found that the yield stress decreased as the molecular weight between crosslinks increased while Young[94] determined that the yield stress decreased as the amount of hardener (diamine) increased. As stated earlier, BMI/MDA samples in a 1:1 mole ratio, regardless of the cure condition, exhibited the lowest density and therefore, the highest free volume. Hence, the yield stress is lowest for the 1:1 mole ratio cure conditions and M_c is the highest for the 1:1 mole ratio of high and low/high cure conditions.

Figure 4.50 displays the yield stress behavior versus mole fraction BMI for the BMI/DABA system. The low-temperature cure condition exhibited higher yield values than the high-temperature cure condition. For both the low and high cure conditions, the yield stress was essentially independent of the amount of DABA. These trends are different from that observed for the BMI/MDA system and opposite the density measurements, which reflect a decrease in intermolecular packing with increasing diamine.

Typically, the amine-rich epoxies exhibit more mobility due to the large intermolecular separation of the

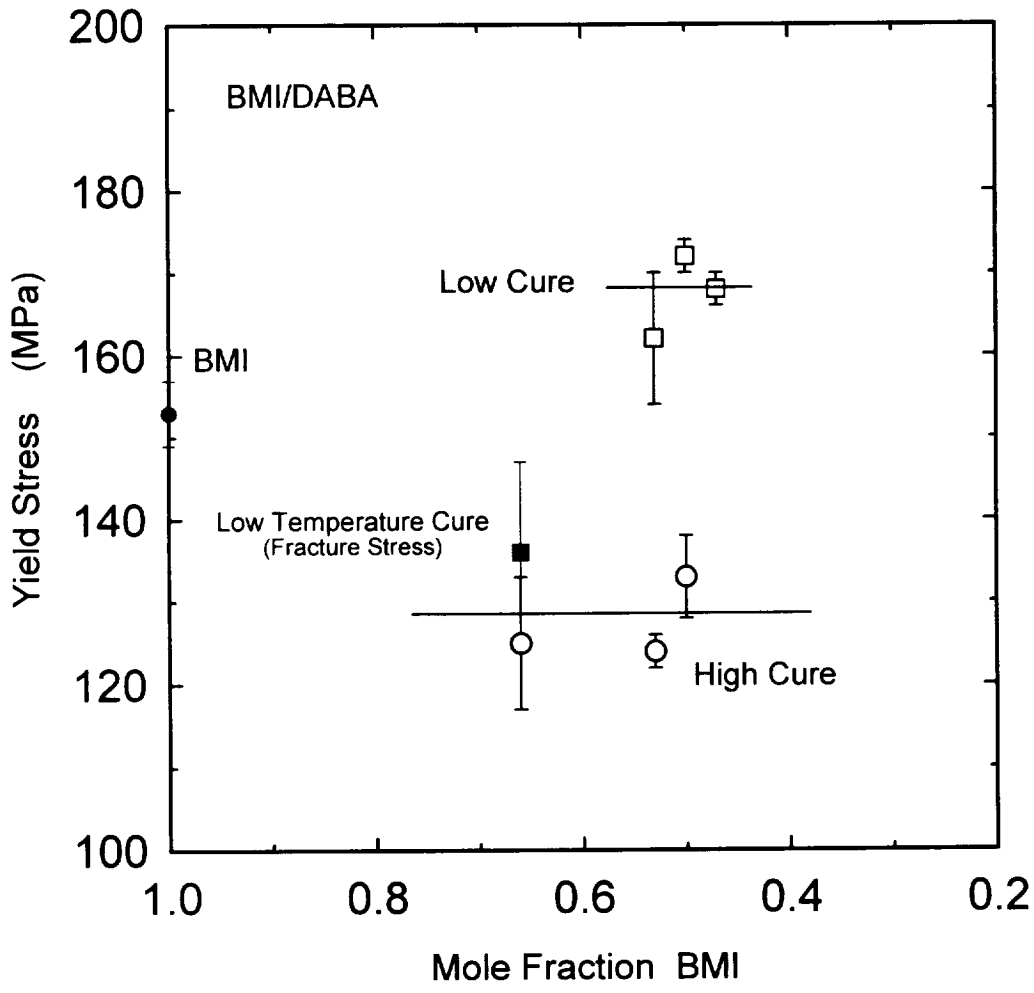

Figure 4.50. Yield stress versus mole fraction BMI for the BMI/DABA system.

chain ends. A low density and low yield stresses are typical for such systems. The resistance to initial deformation arises from intermolecular forces. Once the resistance is overcome, a sample will yield. How the chains pack or how much free volume exists within the sample, plays an important role in yielding of glassy polymers.

As the curing agent increases, the structure would become more linear and the molecular weight between crosslinks would increase. The activation energy required for yielding would decrease. Therefore, a linear polymer, where the chains are held together by secondary forces would have lower yield values than one that was crosslinked with primary forces contributing to the mechanical stability. This behavior was not observed in Figure 4.50. While density is an average property of the total sample, yield stress is more sensitive to intermolecular distances within the sample and involves the cooperative movement of 10 to 20 chain segments. Any processing parameter, which reduces the free volume of the sample enhances the yield stress.

Another plausible explanation for the nearly constant yield stress may be due to an antiplasticization effect,

described by Venditti et al.[95] Anitplasticization is the presence of high concentrations of unreacted low molecular weight material and dangling, unreacted chain ends, which act like defects in the network of a glassy material. The unreacted material and dangling chain ends fill the free volume, reduce the glass transition temperature over that of the glassy material without unreacted material, and increase the yield stress and modulus. The rheological data for the low-temperature cure conditions of DABA exhibit large increases in G′ after the minima were achieved because of uncured species that may have reacted during characterization at temperatures near or above the previous cure temperature. This indicates that unreacted BMI and possibly DABA are present during the time frame of the yield experiments. The unreacted components could sterically hinder chain mobility, reduce free volume, and cause what appears to be a questionable result for yield strength.

Figure 4.51 is a plot of yield stresses versus mole fraction BMI for the high cure conditions of BMI/MDA, BMI/DDS, and BMI/DABA. The figure also includes data for the cured and postcured PMR. The yield stresses of the BMI/MDA and the BMI/DDS systems decrease as the

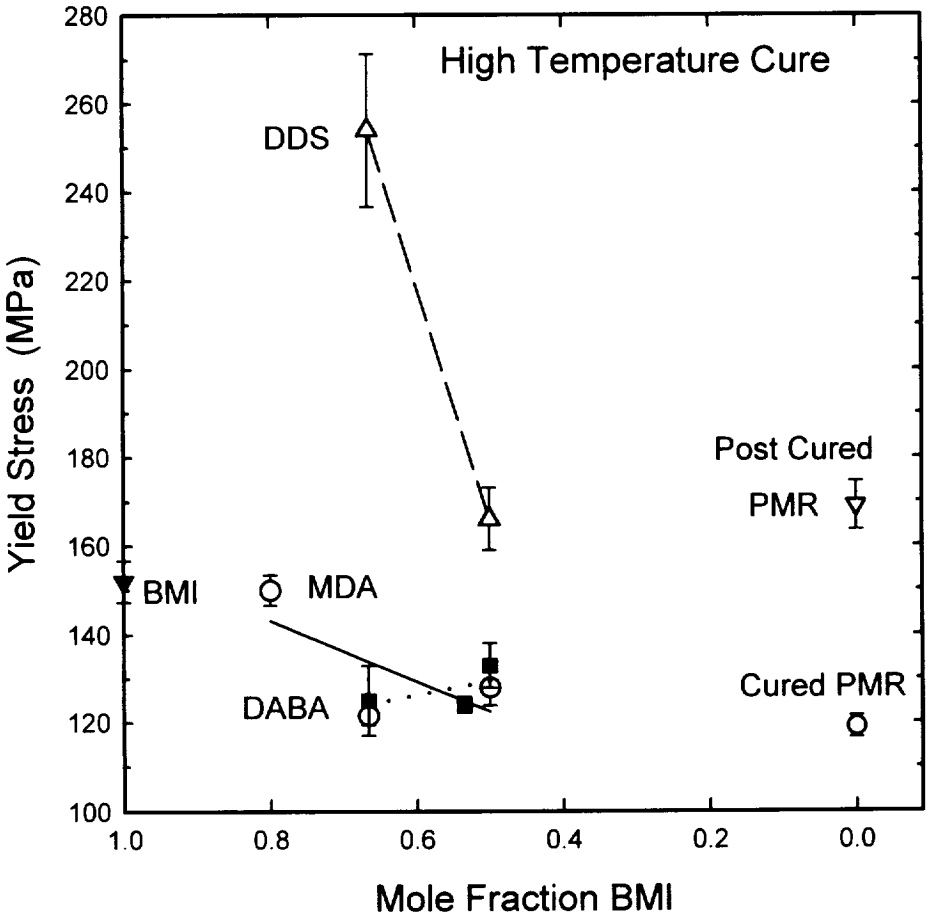

Figure 4.51. Yield stresses versus mole fraction BMI for the high cure conditions of BMI/MDA, BMI/DDS, and BMI/DABA. Data of the cured and postcured PMR are also included.

concentration of BMI decreases. These values also indicate that as the yield stresses decrease, the molecular weight between crosslinks increase. However, the yield stresses of the BMI/DDS system do not follow the trend in density measurements. As the amount of diamine increases, the room temperature densities slightly increase (Figure 4.46), which is due to the enhanced intermolecular packing of DDS. However, the addition of DDS to BMI definitely improves the yield stress or the resistance to deformation over neat BMI. The BMI/DABA yield values are essentially independent of BMI concentration. This, too, is opposite to the trends in density shown in Figure 4.46.

The results indicate that for the copolymer systems studied, using observed trends in density as a first approximation to trends expected in other properties, particularly small strain properties such as yield behavior, is not very appropriate. Yield stress is considered to be controlled by short-range cooperative motions of 10-20 molecular chains and backbone rotations. Since the yield stress of BMI/DABA is independent of BMI concentration, it can be inferred that M_c, a long-range structural parameter, does not influence the short-range motion of chains.[90] However, for BMI/MDA, the yield

stresses do show a strong dependence on the concentration of BMI, and hence, M_c. BMI/MDA chains may be so short that they do affect short range motion and therefore yield strength.

Another instance where yield behavior does not track with density was in the case of the PMR. With the additional heat treatment (post cure) of the PMR, the yield stress increased from 119 MPa to 170 MPa. This was initially surprising since no apparent difference was observed in the density measurements of the two samples. However, postcuring a sample induces a higher crosslink density. The more highly crosslinked a system is, the higher the yield stress since the deformation resistance stresses the whole network, not a few chains or intermolecular forces. A network with a higher crosslink density has a higher glass transition temperature. And the glass transition temperature of postcured PMR increased significantly with the post-cure treatment. This suggests that the crosslink density of the system increased and therefore, the yield stress increased as PMR was postcured.

4.6. Double-Torsion Fracture Energy Measurements

4.6.1. Double-Torsion Fracture Energy

The constant compliance test or double-torsion test is used to determine the plane strain fracture energy of a material. The fracture energy is the energy required to create a unit area of new crack surface. It is also a measure of the ability of the chains at the crack tip to dissipate energy. Figure 4.52 is a plot of fracture energy versus mole fraction BMI for the BMI/MDA system. The low values of the fracture energies for the low cure conditions indicate a very weak structure consisting of short segments and low crosslink density. The addition of chain extender did not improve the fracture energy over BMI alone. The low cure condition failed in a stable, brittle manner and the fracture energy was insensitive to the amount of diamine present. Low fracture energies reflect poor crack resistance in a glassy material.

Both the step cure and the high-temperature cure conditions follow the same dependence, the fracture energies increased as the amount of diamine increased, regardless of the cure histories. In fact the values were statistically indistinguishable. When observed, both the arrest and initiation values of unstable crack growth were

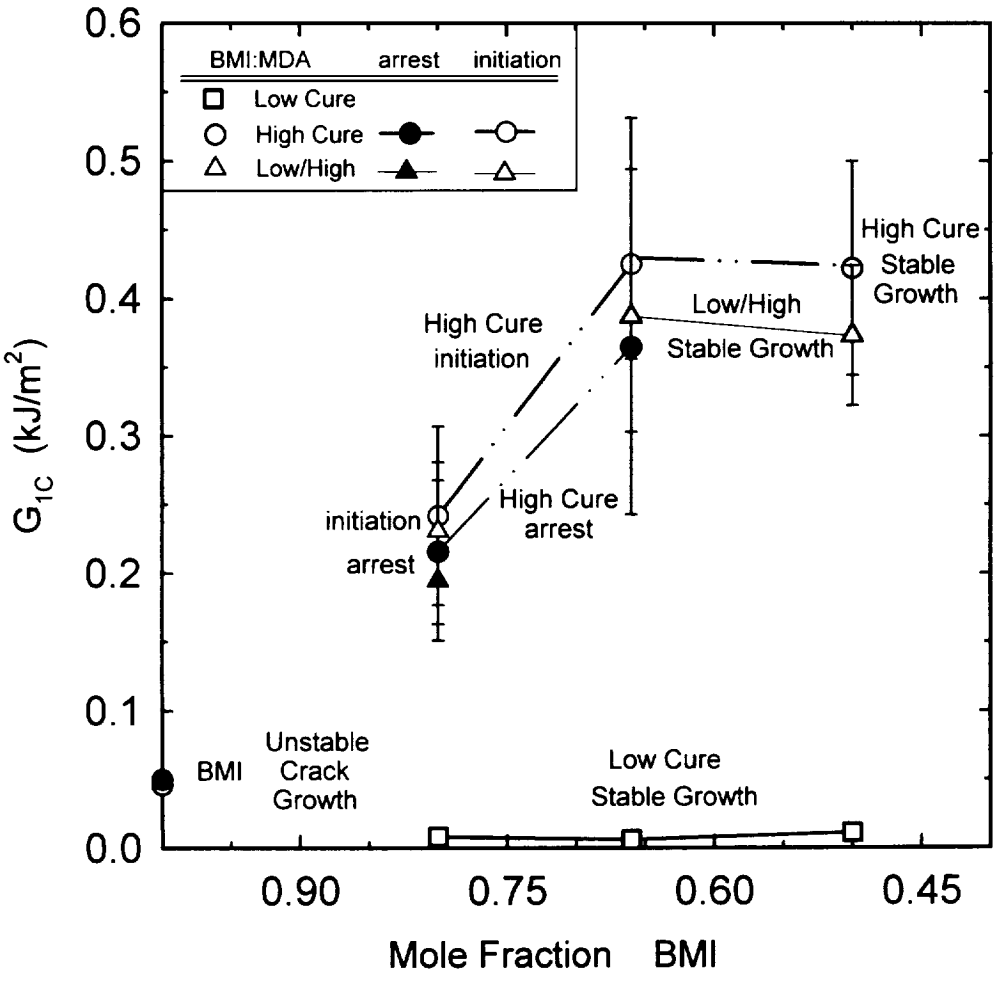

Figure 4.52. Fracture energy, determined by the double-torsion test, versus mole fraction BMI for the BMI/MDA system cured at low-, high-, and low/high-temperature cure conditions.

plotted. They, too, fell within the experimental scatter. For the BMI/MDA system, as the amount of diamine increased, G_{1C} increased due to a more molecularly mobile network. The more diamine present in the system results in higher "flexibility" of the network segments and therefore, higher fracture energies.

These results parallel those of Leung[28] and Enoki et al.[96] The fracture energy increases as the amount of diamine increases. However, Leung[28] reported that the step-cure condition exhibited higher fracture energies than the high-temperature cure condition for all mole ratios due to the lower crosslink densities of the step-cured material. In this study, the high-temperature cure conditions for all mole ratios in Figure 4.52 exhibited higher average fracture energies than the low/high-temperature cure conditions, though in reality the values are statistically indistinguishable. The addition of heat treatment (high or low/high) over the low-temperature cure condition greatly improves the fracture energies or the ability of the chains to dissipate energy at the crack tip.

Stick-slip behavior is the result of yield stress-controlled crack tip blunting and is more prevalent for higher yield strength materials. The yield stress was

observed to decrease as the concentration of BMI decreased. Here, stick-slip behavior occurs for both of the 4:1 mole ratio cases, and for the high-temperature cure condition of the 2:1 mole ratio BMI:MDA. Stick-slip behavior does not occur for the 1:1 mole ratio conditions, which had the lowest yield stresses for each cure condition.

Figure 4.53 illustrates the fracture energies versus mole fraction BMI for the BMI/DABA system. For the high-temperature cure condition, only stable crack growth was observed and the fracture energy increased with increasing amounts of DABA. Despite differences in cure histories, Enoki[96] found the same trends, with 1:1 mole ratio material having the highest fracture energies.

For the low-temperature cure condition, unstable or stick-slip crack growth was observed for all mole ratios of BMI/DABA. The fracture energy of BMI was greatly enhanced with the addition of DABA. The 1:1 mole ratio conditions exhibited the highest fracture energy initiation values and the largest difference between the initiation and arrest values. As stated previously, yield stress-controlled crack tip blunting produces a stick-slip behavior. The yield stress for the low-temperature cure condition was observed to be independent of the amount of DABA, while the

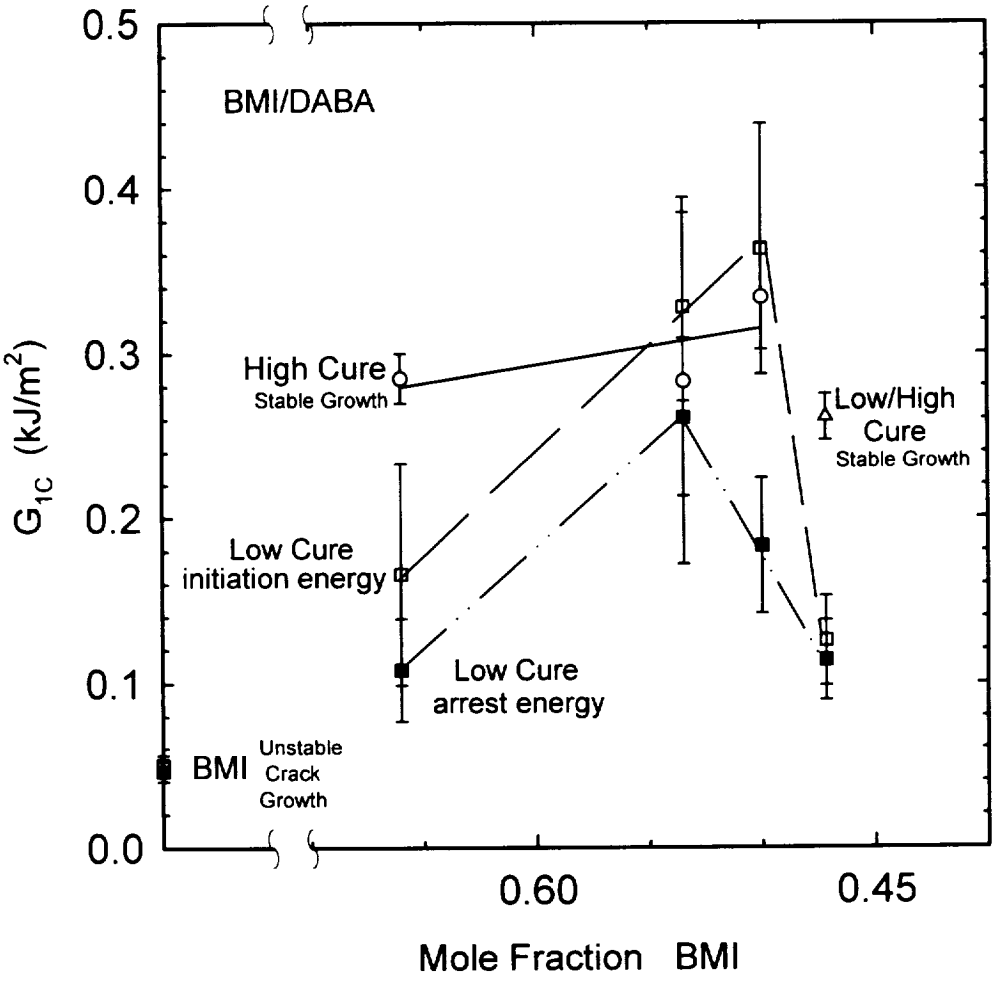

Figure 4.53. Fracture energies versus mole fraction BMI for the BMI/DABA system in the low-, high-, and low/high-temperature cure conditions.

difference in the initiation and arrest values of the fracture energy increased.

Stenzenberger et al.[31] analyzed the fracture energies of BMI as a function of DABA concentration. They found that with up to 40% DABA incorporated in the copolymer, the fracture energy improved. This is roughly 0.535 mole fraction BMI or 1:0.87 mole ratio of BMI/DABA. After 40% DABA, the fracture energy determined by Stenzenberger et al.[31] decreased. However, the cure histories of the samples tested were not revealed. In this research, the peak in fracture energy was observed at the 1:1 mole ratio case, or 0.5 mole fraction BMI, which is close to that observed by Stenzenberger et al.[31] The 1:1 mole ratio material also demonstrated the highest initiation fracture energy for the low-temperature cure condition and highest (stable growth) fracture energy for the high-temperature cure condition. Finally, the step-cure of the 1:1.12 mole ratio BMI:DABA greatly enhanced the fracture energy over that of the low-temperature cure. The low-temperature cure condition displayed a low fracture energy stick-slip unstable crack growth behavior. The inclusion of a two-step cure cycle almost doubles the fracture energy.

Figure 4.54 compares the fracture energies for the high-temperature cure conditions of the BMI:diamine copolymers as a function of mole fraction BMI as well as the PMR material. Neat BMI exhibits the lowest fracture energy with unstable crack growth. The addition of diamine does enhance the fracture energies or the resistance to crack propagation. The fracture energy of thermosets improves as the molecular weight between crosslinks increases. This, however, is usually achieved at the expense of temperature capacity. Fracture energy also depends on the chemical structure and the molecular build of the network and packing density. Sulfone amines have been used to increase or improve toughness. Here, the DDS barely improves the fracture energy over the neat BMI resin. By increasing the molecular weight between crosslinks with the addition of DDS, the fracture energy improved slightly. But failure still occurred in an unstable manner. Finally, no difference in fracture energy can be detected with different mole ratios of BMI/DDS.

By changing the sulfone group of DDS to a methylene group (MDA), the fracture energies greatly improve over that of the BMI/DDS system or neat BMI. Fracture energy is dependent upon chain mobility and flexibility. Since

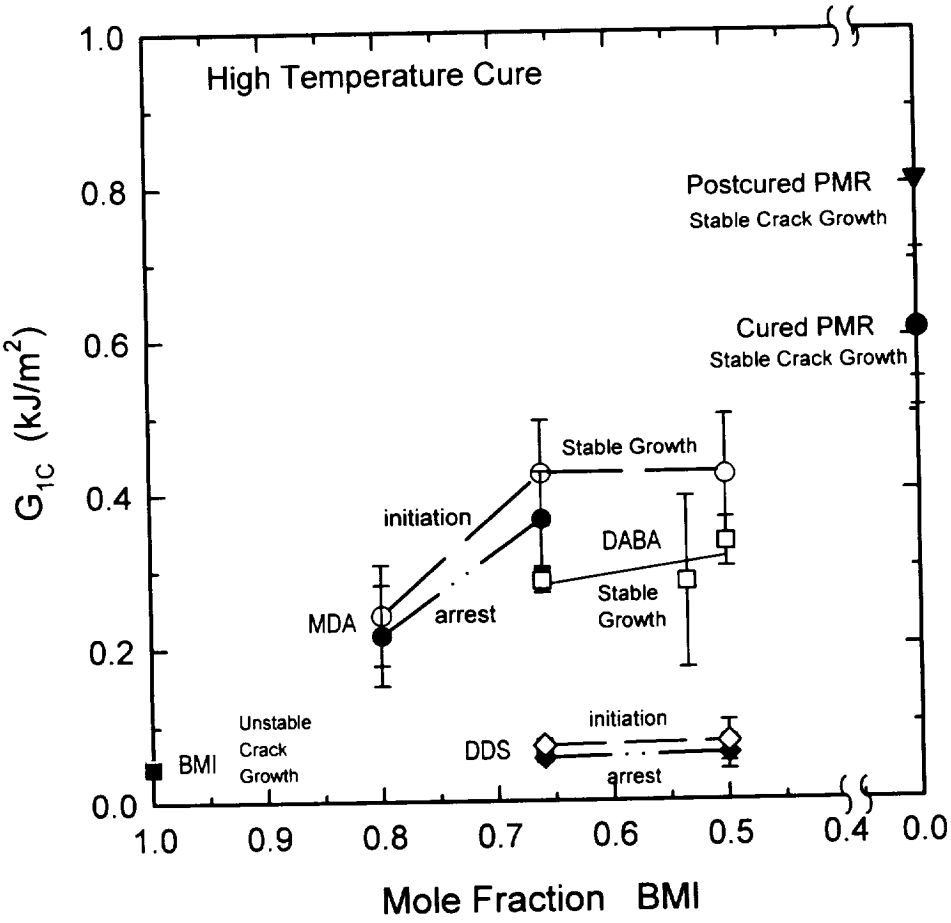

Figure 4.54. Fracture energies for the high-temperature cure conditions of the BMI-based copolymers as a function of mole fraction BMI. Fracture energy values of PMR are included.

BMI/MDA experienced greater fracture toughness than BMI/DDS, and MDA has a lower molecular weight than DDS, it is safe to assume that MDA is more flexible than DDS. The crack propagation behavior was stick-slip for the 4:1 and 2:1 mole ratios of BMI:MDA. For the 1:1 mole ratio cases, whose yield stresses were the lowest, stable crack growth was observed.

The addition of DABA chain extender increased the fracture energy over that of neat BMI and the DDS system. All cases of BMI/DABA failed in a stable manner. As the amount of DABA increased the fracture energy increased. The fracture energy for the BMI/DABA system was not greater than the fracture energies of BMI/MDA. This result is surprising since the molecular weight of DABA is greater than MDA. This suggests that the MDA is more flexible than DABA when incorporated within BMI.

Figure 4.54 also contains the results of fracture energy for the cured and postcured PMR materials. Both the cured and postcured materials experienced stable crack growth. The postcured PMR had a higher fracture energy than the cured material. As the crosslink density increased with postcuring, the fracture energy increased.

Both cured and postcured materials of PMR exhibited higher fracture energies than the other systems tested.

4.6.2. Plastic Zone Size

The radii of the plastic zone in plane strain were determined on the materials previously evaluated using the Irwin Plastic Zone model, the compressive yield strengths, and fracture energies previously determined. Calculations based on models are made because it is extremely difficult to actually witness the plastic zone.[97]

Small plastic zones, whether calculated from a model or observed by experimental techniques, imply that the material is resistant to yielding and more importantly, less resistant to fracture. During loading, after crack arrest, a plastic zone forms at the crack tip. Crack propagation occurs by slow growth through the plastic zone followed by a rapid propagation into the bulk material. Large areas of continuous, densely crosslinked networks can impede plastic deformation. Conversely, the loosest networks have the lowest yield stress and the highest plastic zone sizes. Generally, the larger the plastic zone the more energy required to drive the crack into the bulk material. Therefore, the fracture energy is directly

related to the plastic zone size. The fracture energy is a minimum for the smallest plastic zone sizes.

Stick-slip crack propagation can be explained in terms of crack blunting at the crack tip. Low yield stresses correspond to ductile crack growth while high yield stresses result in an unstable crack growth behavior. Larger crack tip radii form in materials with low yield stresses and therefore, have higher fracture energies. This occurs because, generally as the yield stress decreases, the energy that can be dissipated around the crack tip increases. Therefore, more plastic deformation will occur around the tip of the crack and the crack will become blunted. This leads to an increase in fracture energy of the material.

Figure 4.55 is a plot of the calculated plastic zone size ($2r_p$) versus mole fraction BMI for the BMI/MDA systems. Neat BMI is considered more brittle on a macroscopic scale than most thermosetting polymers.[97] Hence, BMI would be expected to have a very small plastic zone, which is the case here.

For the low cure condition, there is little to no plastic zone calculated. The addition of diamine and increased chain lengths of BMI/MDA by chain extension did

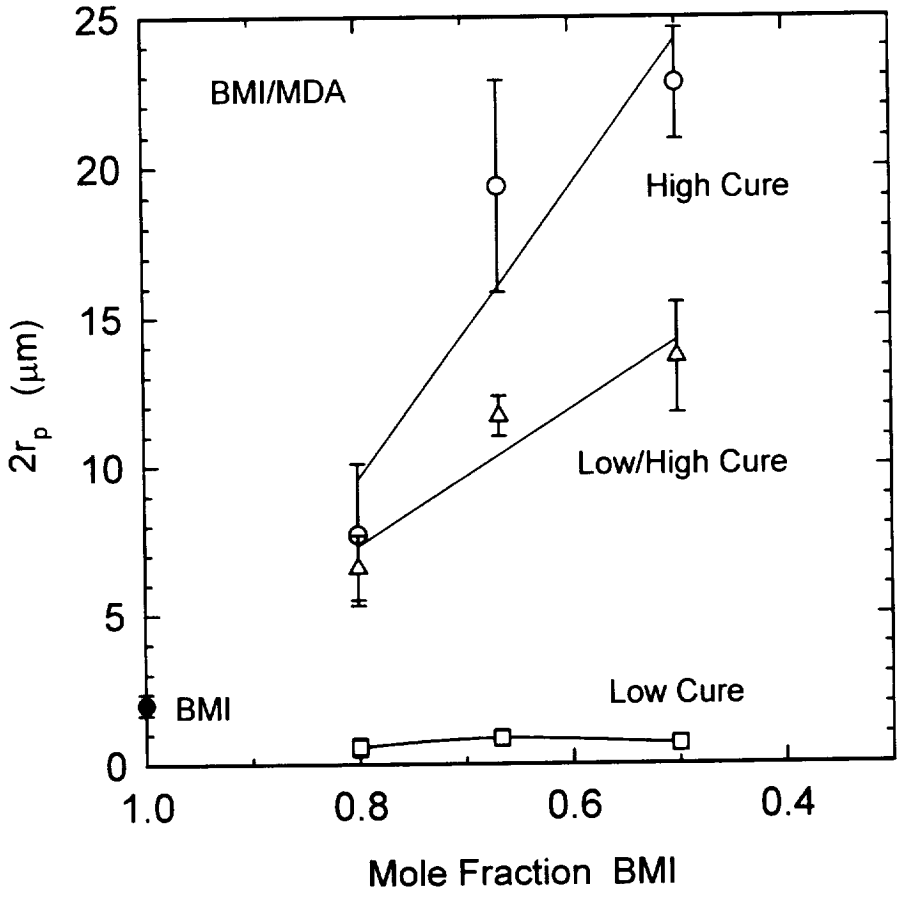

Figure 4.55. Calculated plastic zone size ($2r_p$) versus mole fraction BMI for the low-, high-, and low/high-temperature cure conditions for BMI/MDA.

not influence the calculated plastic zone sizes. The fracture energies for the chain extended BMI/MDA was very low, hence the plastic zone sizes would also be minimal.

The calculated plastic zone sizes for the high-temperature cure condition were larger than the calculated plastic zone sizes for the low/high-temperature condition for the 1:1 and 2:1 mole ratios. In the 4:1 mole ratio case the same network topology was produced as evident from the rheological data and hence, exhibits the same plastic zone size. This would imply that the high cure condition does yield a topology with network defects and short chains. The low/high-temperature cure condition hypothetically should yield a topology with little network defects and longer continuous chains.

Finally, the neat BMI and the 4:1 mole ratio cases experience smaller plastic zone sizes. For both the high- and low/high-temperature cure conditions the 4:1 mole ratio cases had the same calculated plastic zone size. This, along with the rheological data, suggests that the 4:1 mole ratio network topologies are similar. The BMI and the 4:1 mole ratio cases all experience the highest yield values. The higher the yield stress, the more crosslinked the

material and therefore, the smaller the calculated plastic zones sizes.

Figure 4.56 shows the calculated plastic zone size versus mole fraction BMI for the DABA system. According to Williams,[98] the plastic zone is inversely proportional to the yield stress. However, in this system, yield stress was essentially independent of BMI mole fraction. The results for plastic zone size are therefore, influenced more by the fracture energies. Remember, an antiplasticization mechanism is suspected to influence the yield stress, modulus, and therefore the glass transition temperature of the BMI/DABA system. Here, the calculated plastic zone size was shown to increase as the mole fraction of BMI increased for the high-temperature cure condition. The high-temperature cure condition experienced stable crack growth behavior. The low-temperature cure condition has the lower calculated plastic zone size per mole fraction BMI over the high-temperature cure condition.

Figure 4.57 is a comparison of the calculated plastic zone size for the high-temperature cure conditions of BMI/DABA, BMI/DDS, BMI/MDA as a function of BMI and PMR. The neat BMI and the BMI/DDS system have roughly the same calculated plastic zone size. Both materials experienced

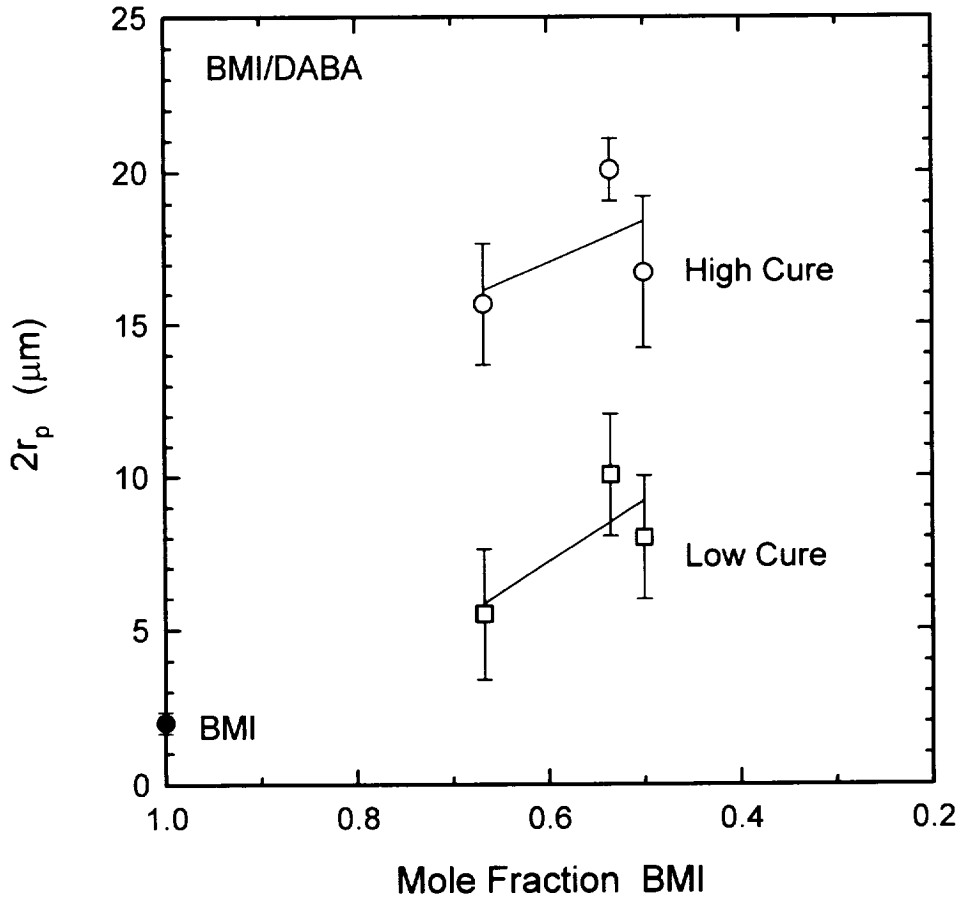

Figure 4.56. Calculated plastic zone size versus mole fraction BMI for the low- and high-temperature cure conditions for the BMI/DABA system.

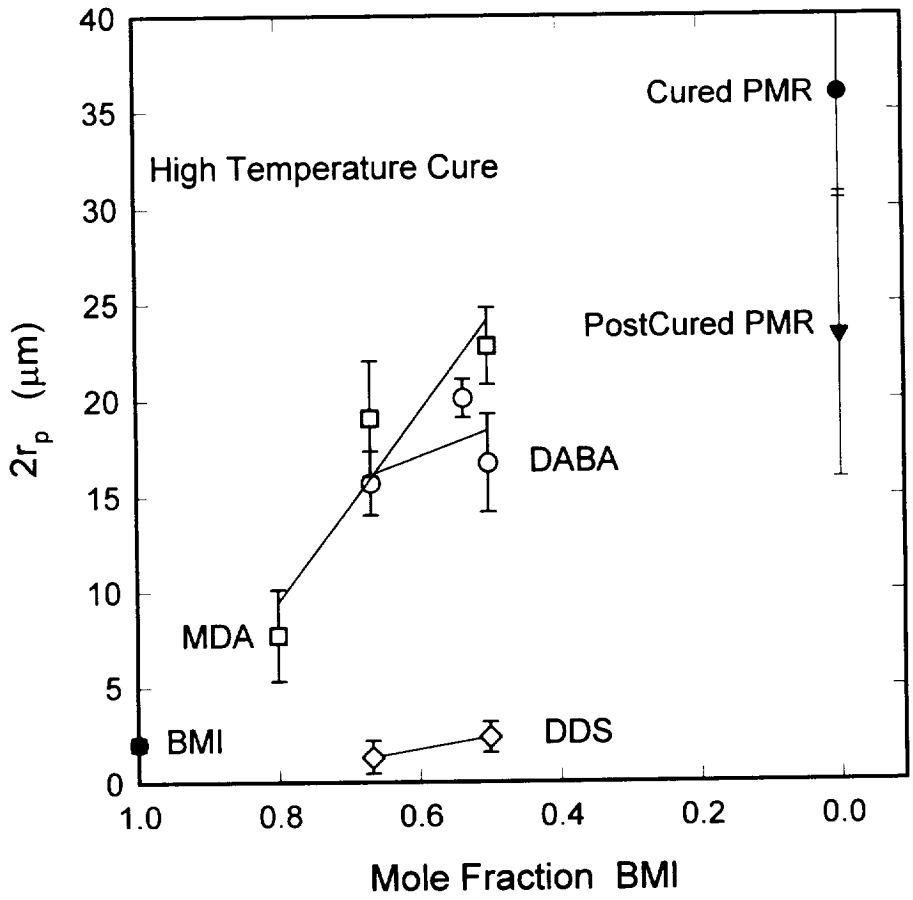

Figure 4.57. Comparison of the calculated plastic zone size for the high-temperature cure conditions of BMI/MDA, BMI/DABA, and BMI/DDS.

the highest yield values and the lowest fracture energies. The DABA system had a higher calculated plastic zone size than the neat BMI or the BMI/DDS. The calculated plastic zone size for the BMI/DABA is essentially independent of DABA concentration. This is the same trend observed for the yield stresses of the DABA system.

As the concentration of MDA increases, the networks become more flexible. For the BMI/MDA system, the fracture energies increase and the yield stresses decrease as the concentration of MDA increases. Therefore, the plastic zone sizes increase as the amount of diamine increases. The primary factor governing the fracture energy is the ability of the resin to yield. Yielding, in turn, allows crack blunting which increases the energy for crack growth.

The cured PMR material had a higher calculated plastic zone size than the postcured PMR. When postcuring, the material's crosslink density increases. The postcured PMR experienced higher yield values, higher fracture energies, and therefore, lower calculated plastic zone sizes.

4.7. Modulus Measurements

4.7.1. Below T_g - Sonic Modulus

In past investigations,[4,15] the flexural modulus in three point bend was used as a measure of the elastic modulus. In this case, a cathetometer is used to measure deflection as a function of load, which can be quite challenging at small strains. Consequently, this method usually underestimates the value of the elastic modulus in bending (Table 4.8).

In this investigation, an alternative method was used to determine elastic modulus - the Impulse Excitation Technique (IET).[99] The IET is used to obtain the dynamic modulus by measuring the resonant frequency of flexural vibrations of a sample after a mechanical impulse or tap has excited it. While the sample is supported at the nodes of resonance with a microphone located beneath it, the sample is tapped once to induce a vibration and the natural resonant frequency is determined. With the samples' geometry and material properties in hand, the Young's modulus or the sonic modulus may be determined. This method is quick, easy, and very reproducible for samples that are isotropic.

To determine if the sonic technique was a viable alternative for determining elastic properties, comparisons were made between the elastic modulus determined in three-point bending using a cathetometer to measure deflection, four-point bending with strain carefully determined with strain gages, and the sonic technique. Table 4.8 shows the results of these comparisons. The sonic moduli and the four-point bend values fell within 3% of each other and within 10% of the literature values.[31] This is much better than the underestimated three-point bend values, which fell 37% below the four-point bend values, where strain was determined by a pair strain gages, or 33% below the literature values.

Table 4.8
Moduli Comparisons for BMI:DABA 1:0.87.

Test Technique	Modulus (GPA)	Comments
3-Point Bend	1.74	J.Jones @ UA
3-Point Bend	2.73	A. Tenteris @ UA
Sonic Modulus	4.50	Grindosonic Method
4-Point Bend	4.36	NASA, Strain Gage
Literature[31]	4.05	Flexural Method

Modulus is a property primarily controlled by short-range structure. At room temperature, free volume or intermolecular packing normally governs the low strain properties of thermosets such as modulus and yield. Close packing of molecules results in high modulus and high yield values.

The sonic modulus versus mole fraction BMI for the various BMI/MDA cure conditions is shown in Figure 4.58. For the low-temperature cure condition, the modulus decreases with decreasing concentration of BMI. For the low-temperature cure condition, mostly chain extension occurs. The higher elastic modulus is most likely the result of steric hindrance by unreacted BMI molecules in the glassy state, which gives the sample higher stiffness or rigidity.[12]

The moduli values for the high- and low/high-temperature cure conditions decreased as the amount of diamine increased. The BMI/MDA chains may be so highly crosslinked that short range motion of molecular chains are affected. All the moduli values mimic the yield strength and density trends.

The sonic moduli of the DABA system versus mole fraction BMI are shown in Figure 4.59. The low-temperature

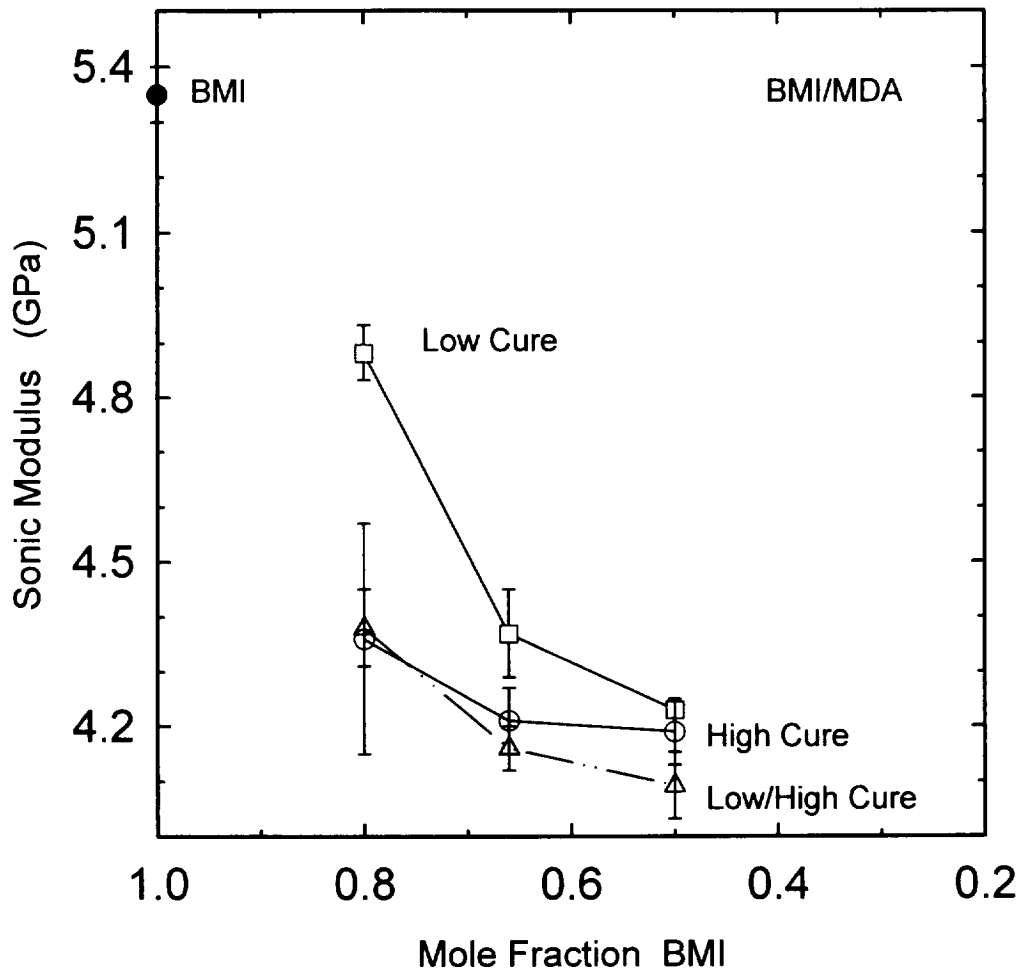

Figure 4.58. Sonic modulus versus mole fraction BMI for the various BMI/MDA cure conditions.

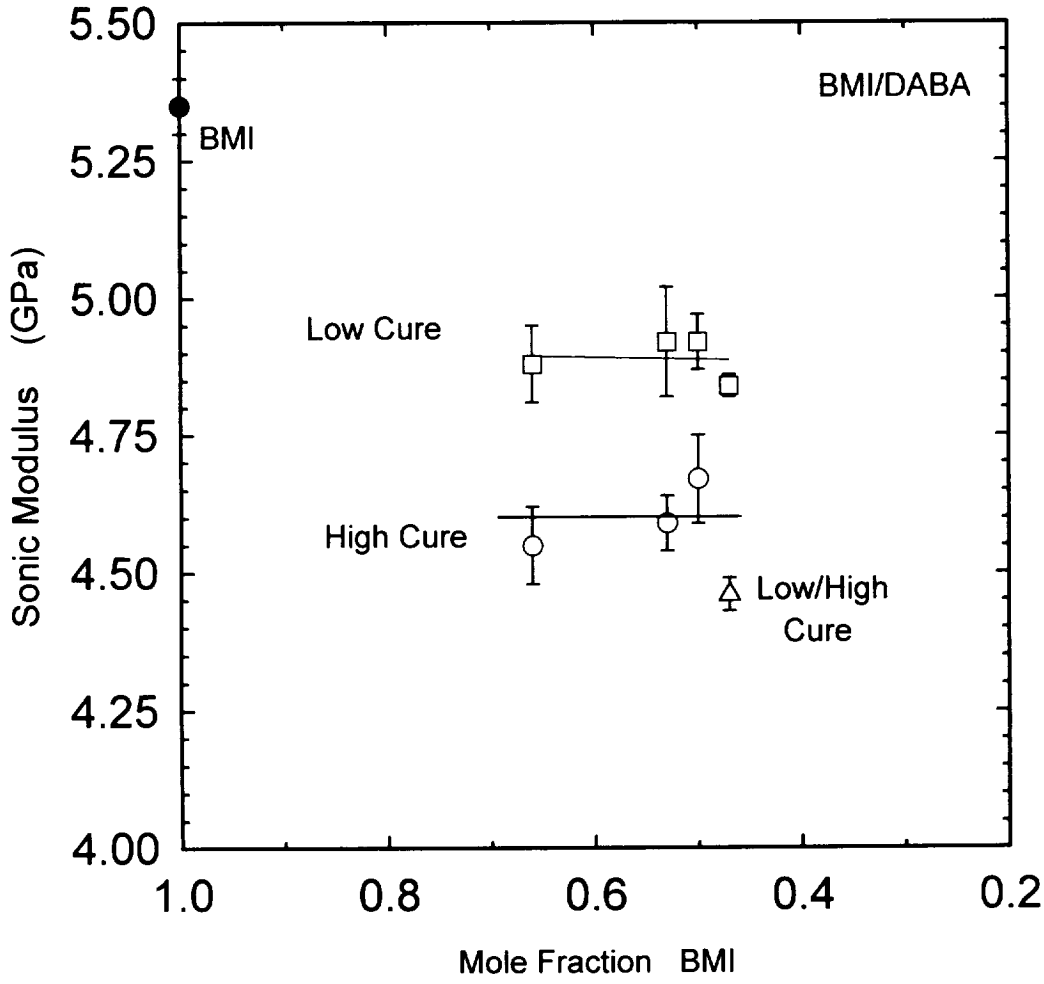

Figure 4.59. Sonic modulus versus mole fraction BMI for the BMI/DABA system.

cure condition exhibited the highest modulus. This may be due to the steric hindrance of unreacted molecules that add to the rigidity of the material. As the amount of DABA increases, the modulus is virtually unaffected. This was the case for both the low- and high-temperature cure conditions. Neither one varied substantially with increasing amounts of DABA. Similarly, Stenzenberger[31] had reported that the flexural modulus did not vary with concentration of DABA. However, the cure histories were not mentioned in his paper. But the values were in the same range as the values reported in Figure 4.59.

As stated previously, the yield stress and glassy modulus are properties that are influenced by the cooperative short-range motion of a few chains. The modulus values for BMI/DABA are independent of the amount of diamine. Assuming that the more reacted BMI in the network, the higher the crosslink density, M_c does not seem to affect the short-range motion of the BMI/DABA chains.

Figure 4.60 is a comparison of the sonic modulus versus mole fraction BMI for the various high-temperature cure systems. The BMI/DDS system exhibited the highest modulus values over the other systems investigated. This tendency followed the density measurements and is probably

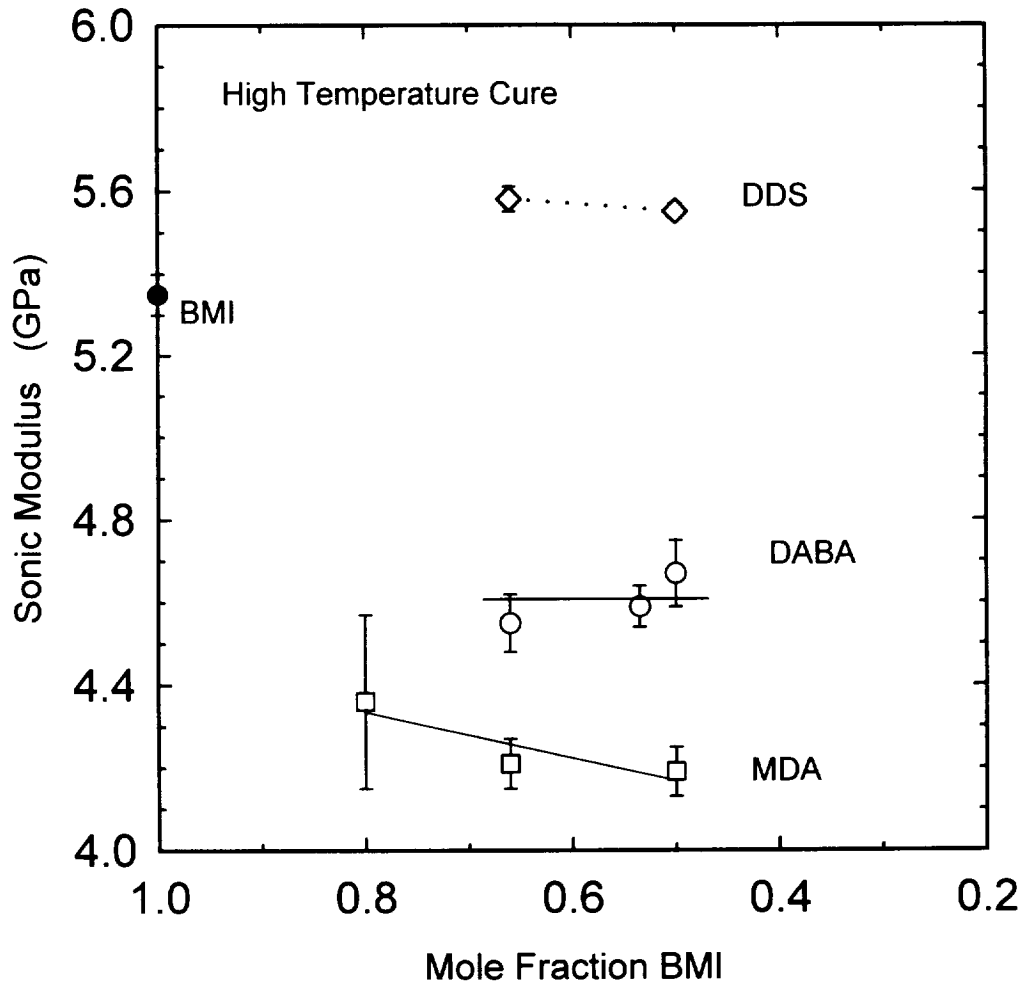

Figure 4.60. Comparison of the sonic modulus versus mole fraction BMI for the various high-temperature cure systems.

due to the close packing ability of the DDS molecule. For at least the BMI/MDA system, the modulus values decrease with increasing additions of MDA. This trend mirrors the yield strength behavior for the BMI/MDA system.

The modulus values of the high-temperature cure condition for BMI/DABA are basically unchanged with DABA concentration. But the values of modulus are higher than the modulus values of BMI/MDA. This is opposite to the density results for which BMI/MDA had the higher density compared to the BMI/DABA system. The modulus values of DABA might be inflated due to unreacted species within the material. In rheological data, the increase in G′ after the minimum is greater for the BMI/DABA materials than for the BMI/MDA system.

The yield values and the modulus values as a function of BMI mole fraction for the BMI/DABA system do not follow the same trends. Deformations at which modulus and yield stresses are measured are different. The results in this investigation might not show the same behavior or trend between the two physical properties. Other factors that need to be considered in explaining modulus should be chain structure and chemical composition. Earlier, it was noted that DDS was less flexible than MDA or DABA. The

inflexibility of the diamine is advantageous for yield strengths and modulus values but is unfavorable for fracture energy. A diamine with a flexible structure, like MDA, contributes to higher fracture energies.

Postcuring PMR actually increases the modulus over that of the cured material, Table 4.9. This follows epoxy work cited by Gupta,[12] where an increase in crosslink density decreases the free volume. As a result, the modulus increases. As PMR is postcured, the crosslink density increases, which tightens the network and produces a high modulus material. Even though modulus trends tend to imitate trends in density, postcuring PMR had no effect on the density values. The density values of the cured and postcured PMR were essentially the same. The different tendencies between the density values and the modulus values may result because density is a total sample - average property while the modulus values focus on resistance to initial deformation by the intermolecular forces.

Table 4.9
Sonic Modulus Values for PMR.

Sample	Sonic Modulus (GPa)	Standard Dev.
Cured PMR	4.46	0.04
Postcured PMR	4.51	0.02

4.7.2. Above T_g - Near Equilibrium Stress-Strain Testing

The temperature at which the transition region intersects the rubbery plateau region, determined from Rheometrics Spectrometer graphs, was used in the determination of M_c. In an Instron, equipped with an environmental chamber set at a temperature 20 to 60 °C above T_g, a sample was loaded to a given deflection while the load relaxed to an equilibrium value. The deflection was increased and the procedure was repeated. The equilibrium load values were plotted against deflection to obtain a near equilibrium stress-strain curve. The slope of the stress-strain curve is proportional to the inverse of M_c.

Measurement of the equilibrium modulus of a network polymer in the rubbery state is a common method for determining the crosslink density, making use of the statistical theory of rubberlike elasticity.[57] In

principle, this method should not be used for densely crosslinked polymers, particularly those polymers with a polar backbone. However, since there seems to be no alternative method to characterize the extent of crosslinking in these materials, several authors,[90] have used the equilibrium rubbery modulus to obtain an apparent Mc, the number average molecular weight between crosslinks in epoxy networks. Surprisingly, the values obtained for a fully reacted, stoichiometric, end-linked epoxies have differed very little from the prepolymer molecular weights. The method used to obtain equilibrium values of modulus employed temperatures at least 40 °C above the crosslinked resin Tg. Stepwise strains were imposed using an Instron tester with a controlled temperature chamber, in which the force required to maintain a constant strain is allowed to relax until an equilibrium value is obtained. The strain level is then increased several times and at each strain level the force is again relaxed to near-equilibrium. The force-deformation values at equilibrium are plotted as a stress-strain curve and the tangent modulus is used to calculate M_c for each network.

This approach is based on rubber elasticity theory even though major assumptions are made in this

investigation. Rubber elasticity theory relates the equilibrium shear modulus, G_e to M_c by the following equation:

$$M_c = \Phi \rho R T/G_e \quad (4.3)$$

where Φ is the front factor, ρ is the density of the sample, R is the gas constant, and T is the test temperature. Constant volume is presumed so that $G_e=E_e/3$. Other assumptions made in this experiment are that Φ is accepted to be unity, Gaussian statistics apply to the network chain configurations, and the internal energy changes on extension are negligible.

A relative ranking or an estimate of the tightness of the network based on this technique is obtained. This procedure is a means to correlate the crosslink density to physical properties even though the network changes with temperature during the time frame of the experiment, based on rheological data.

Figure 4.61 is a representative true stress versus time graph at various strain levels for the high-temperature cure condition of BMI/MDA in a 2:1 mole ratio, tested in nitrogen. The true stress is normalized by a factor of $3\rho RT$ to account for the test temperature; where ρ is the sample's density, R is the gas constant, and T is

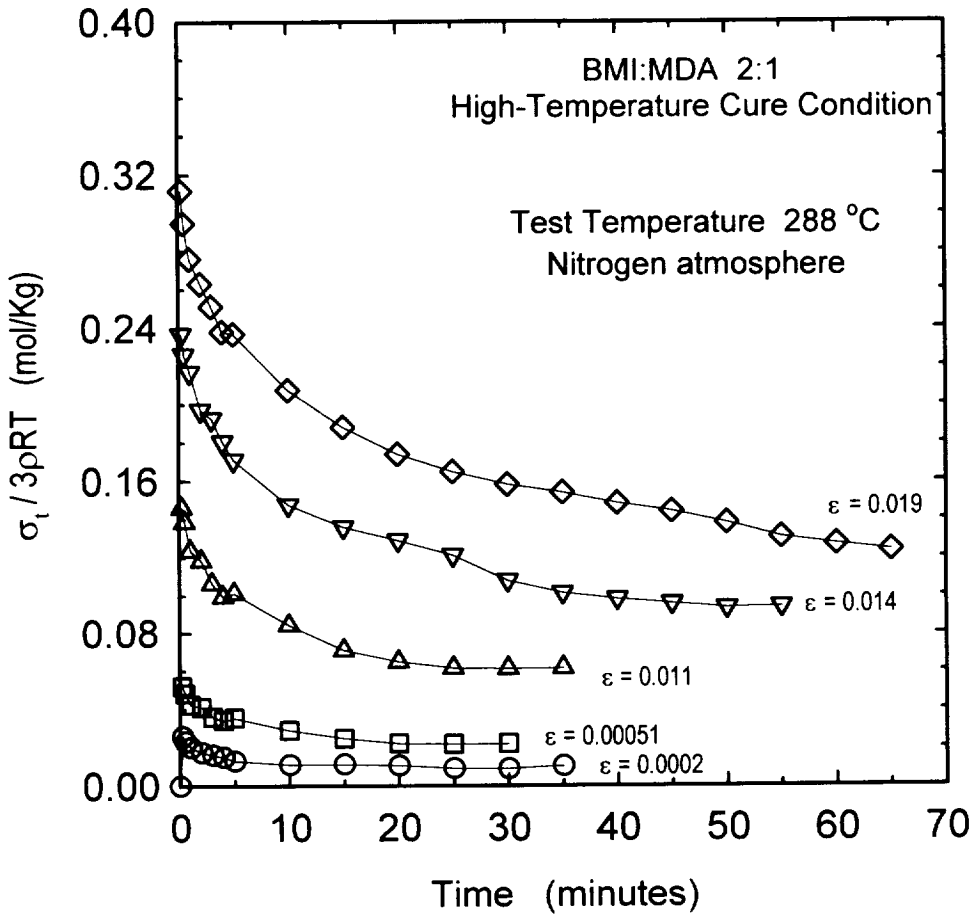

Figure 4.61. Representative true stress versus time graph at various strain levels for the high-temperature cure condition of BMI/MDA in a 2:1 mole ratio, tested in nitrogen.

the temperature of the test. The equilibrium stress values were used to create a near-equilibrium stress-strain curve, shown in Figure 4.62.

Figure 4.62 is a representative true stress versus strain curve for the high-temperature cure condition for BMI/MDA in a 2:1 mole ratio. The true stress is normalized by a factor of $3\rho RT$. The test temperature was 288 °C and the test was performed in a N_2 atmosphere. In extension, stress versus strain is a linear relationship up to a strain of 0.002. Also plotted are the stress-strain measurements in retraction. The retraction data indicate that the near-equilibrium stress-strain behavior was not reversible. This is probably due to further reaction occurring over the time scale of the experiment. In epoxy work,[1] the behavior was reversible up to strains of 10%. The reversibility suggested that the measurements were performed under near-equilibrium conditions and that the networks were stable at high test temperatures.

Even though further reaction at higher test temperatures is suspected in the BMI/MDA system, this approach was used within this investigation to determine a relative ranking of network structures. Comparison to other studies would not necessarily be valid. The near-

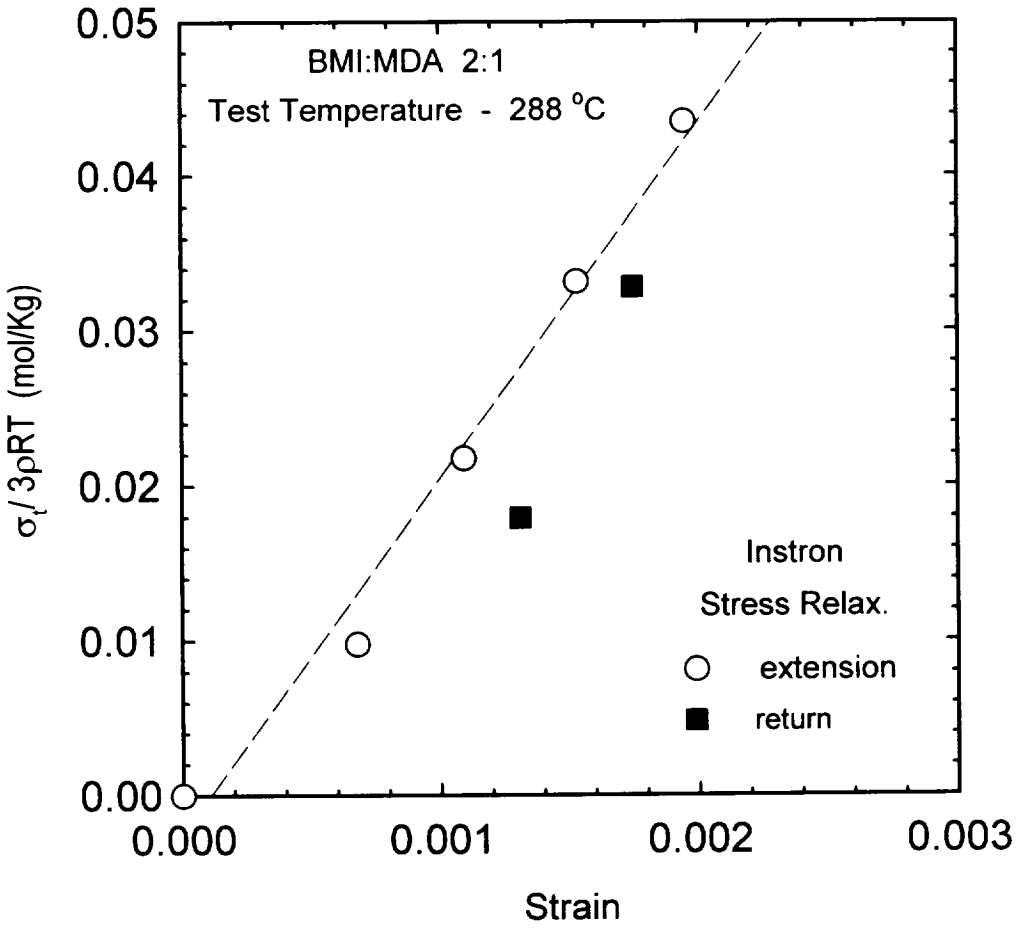

Figure 4.62. A representative true stress versus strain curve for the high-temperature cure condition of BMI/MDA in a 2:1 mole ratio.

equilibrium stress-strain experiments were performed on the high- and low/high-temperature cure conditions of BMI/MDA system only. The BMI, BMI/DDS, and the low-temperature cure condition of BMI/MDA were too brittle to attempt these experiments. The near-equilibrium stress-strain curves were used to determine M_c.

The arrest values of the fracture energies for the BMI/MDA system were plotted against the molecular weight between crosslinks, determined from the near-equilibrium stress-strain curves, Figure 4.63. A ½ -power dependence was observed. This is the same result observed by LeMay[1] for epoxies. M_c is a long-range structural variable, which usually should not influence the short-range molecular properties such as yield strength and modulus.[90] But for BMI/MDA, M_c did influence these properties. M_c determines the plastic zone size, which in turn, influences the fracture energy.[91] This ½ -power dependence, shown in Figure 4.63, implies that the ultimate fracture properties of BMI are proportional to the plastic zone size, which is determined by crosslink density. This is a promising result because it implies that the typical characterization techniques performed on epoxies, as established by LeMay,[1]

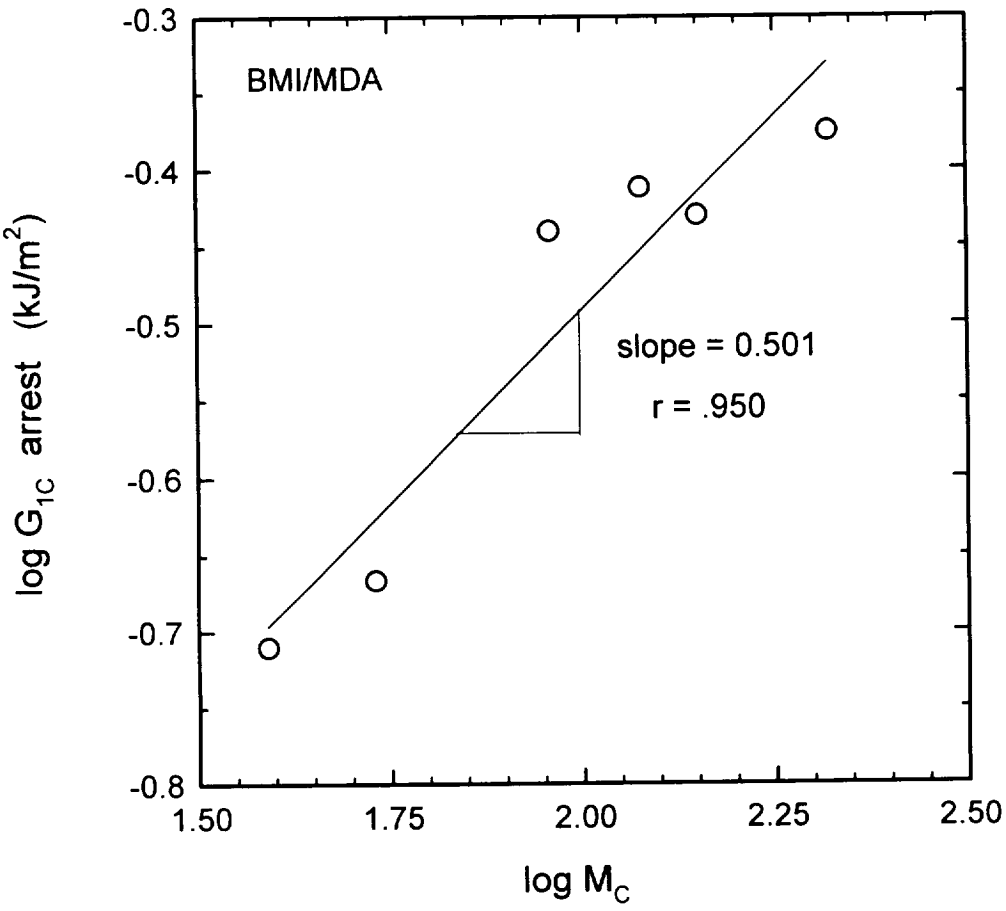

Figure 4.63. Relationship between fracture energy and molecular weight between crosslinks, determined from the near-equilibrium stress-strain curves, for the BMI/MDA system.

can be applied specifically to BMI's and possibly other polyimides.

4.7.3. Intermittent Stress Relaxation

Since the near-equilibrium stress/strain behavior was not reversible, the network is changing during the time frame of the experiment. Consequently, a sample was tested with a Rheometrics Spectrometer to obtain G'. The glass transition temperature was 245 °C, Figure 4.64. When the test temperature reached 288 °C, the sample experienced an isothermal hold for 1 hour to simulate the load-deflection testing at 288 °C. The storage modulus, G' increased during the 1 hour hold. The sample was then cooled to room temperature and retested from room temperature to 400 °C. The glass transition temperature increased from 245 °C to 300 °C. Therefore, it appears that some further reaction is occurring during the load-deflection experiment that was performed at 288 °C.

In crosslinked rubbers, the network can be tested by intermittent and continuous stress relaxation to determine the extent of degradation or continued crosslinking. In the intermittent stress relaxation experiment, the sample is first undeformed. At a given time interval, the sample

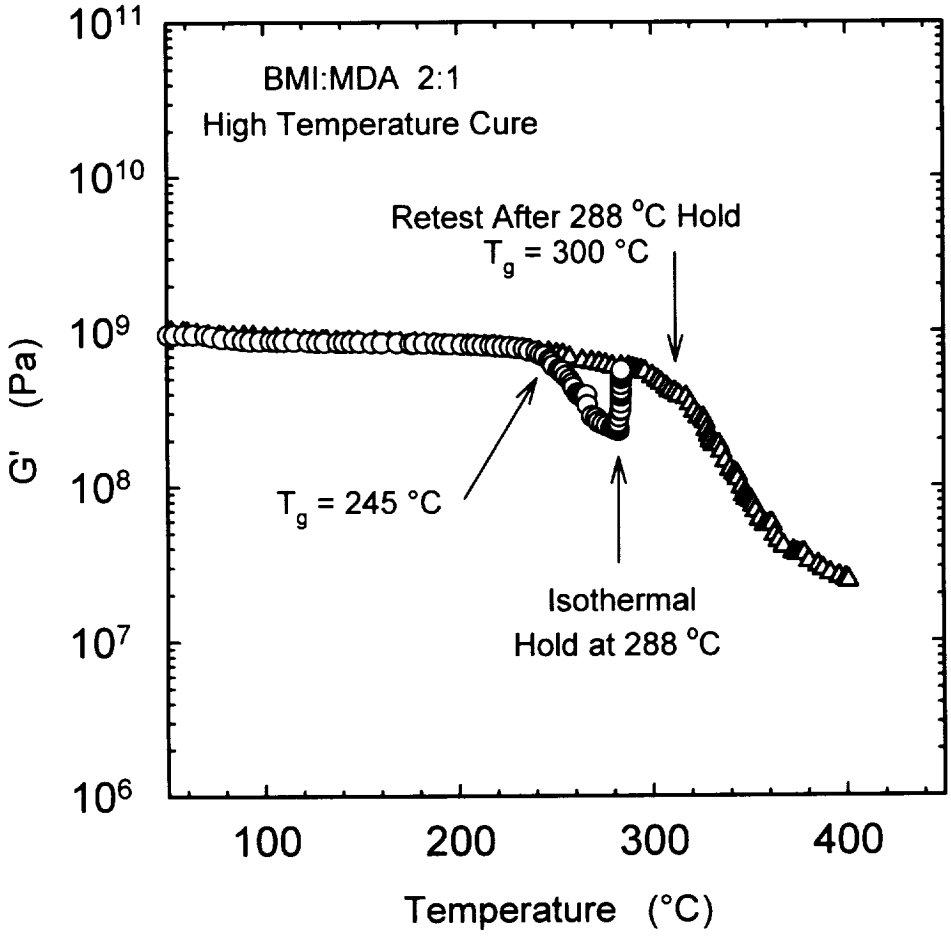

Figure 4.64. Rheological analysis of 2:1 BMI:MDA before and after an isothermal hold at 288 °C. Frequency of test was 1 Hz.

is extended to a predetermined deflection. The peak load value is recorded and the sample is then unloaded during a set time interval. The sample is reloaded to the designated deflection and the peak load value is recorded. This experiment is done at the same test temperature as the continuous stress relaxation procedure. The sample is unloaded from the bottom grip while remaining at the test temperature in order to determine if further reaction will occur within the network.

Figure 4.65 shows three composite graphs of continuous and intermittent stress relaxation showing the possible behaviors that can be observed.[35] The exponentially decaying curve in all three figures is the continuous stress relaxation behavior at one strain level. The intermittent values are indicated as vertical lines. If the peak stress values of the intermittent stress relaxation experiment fall on the continuous stress relaxation curve (part a), the system is undergoing irreversible network degradation. If the peak stress values of the intermittent stress relaxation experiment are greater than the continuous stress relaxation values and constant as in part b, the network is only experiencing

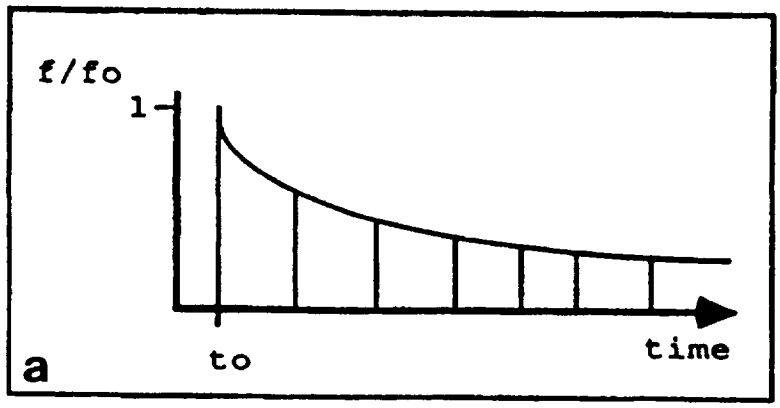

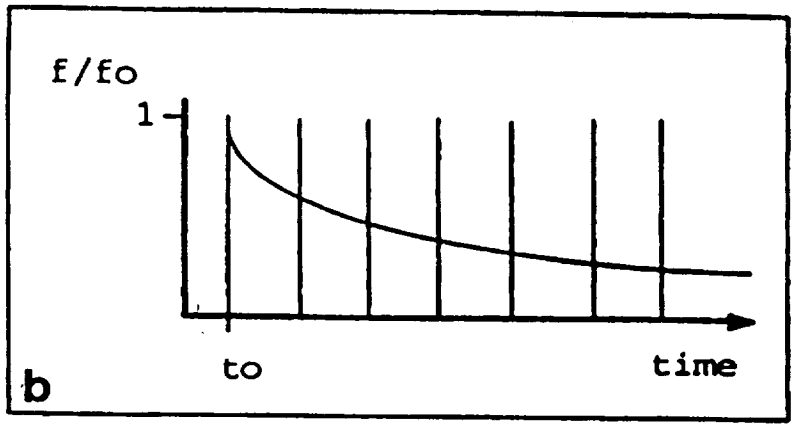

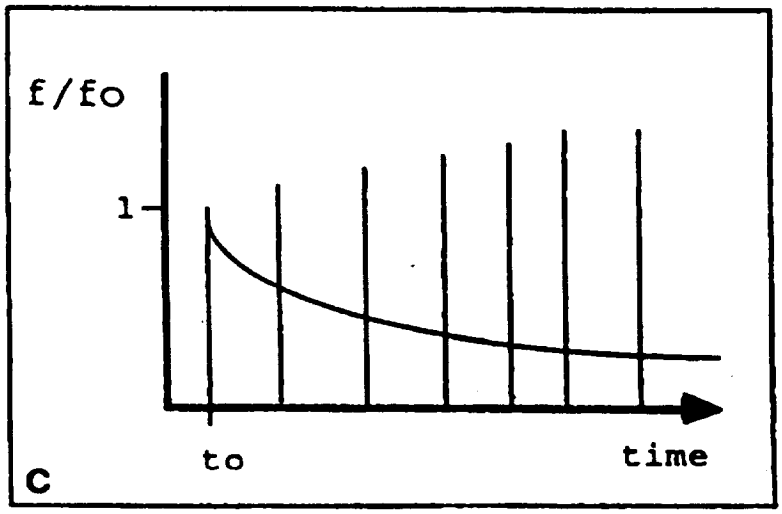

Figure 4.65. Three possible relationships between continuous and intermittent stress relaxation behavior for a polymer network.[35]

rearrangement reactions. If the peak stress values of the intermittent stress relaxation experiment are increasing and greater than the continuous stress relaxation curve, as in part c, then the network is experiencing additional crosslinking reactions which overshadow any degradation reaction that may be occurring simultaneously.

Figure 4.66 is a plot of normalized stress versus strain for the BMI:MDA in a 2:1 mole ratio cured for 6 hrs at 220 °C. The lines indicate the continuous stress relaxation curve for two samples, cured during the high-temperature cure condition. The symbols represent the intermittent normalized stress values for a given time. At strains of e = 0.0173 and 0.0181, the intermittent stress relaxation experiments do reveal an overall increase in stress over time, indicative of additional crosslinking. However, there is considerable scatter in the data over the time frame of the experiment. The material is subjected to very small strains, measured by a cathetometer and bench marks on the sample. Some error is expected with clamping and reclamping of the sample during experimentation at elevated temperatures. But an increasing trend in stress with time is clearly evident.

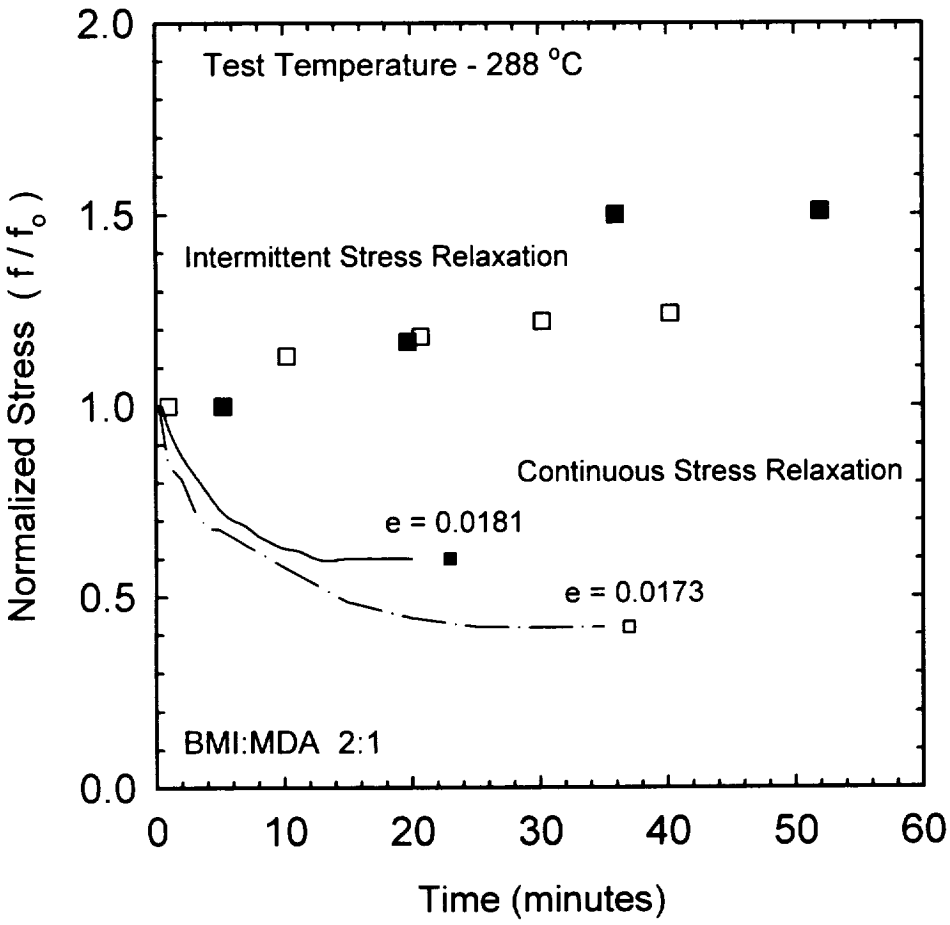

Figure 4.66. Normalized stress versus strain for BMI:MDA in a 2:1 mole ratio cured for 6 hrs at 220 °C. The lines indicate the continuous stress relaxation curve for two samples cured at high temperature and the symbols represent the intermittent normalized stress values for a given time.

This is the first attempt to characterize a thermoset network in this manner. Some refinement of the experimental procedure is certainly necessary. This result, coupled with the rheological data of the isothermal hold and the irreversible true stress-strain behavior, indicates that the material does, in fact, undergo further reactions at temperatures above its T_g, and holds promise that the kinetics of the additional crosslinking reactions might be established.

4.8. Computer Modelling of Thermoset Networks

A computer simulation package developed by Biosym[68] was used to compare the experimentally obtained physical properties of the low-temperature cure condition of BMI/MDA, BMI/DABA, and BMI to the calculated physical properties of the same systems. Computer modelling allows the scientist to experiment with a number of possible polymers with different structures without having to synthesize all possible scenarios. The economic benefits of such an approach in terms of time and money are obvious. However, with the current technology, computer modelling is best suited for predicting trends rather than generating

absolute (accurate) numbers for physical, mechanical, and thermal properties.

The specific model used in this investigation was Synthia, based on connectivity indices as opposed to group contributions and a database.[46] The connectivity indices method of modelling defines atomic indices that describe the bonding and the electronic environment of each non-hydrogen atom. Therefore, it can be used to estimate properties for any amorphous atactic homopolymer or random copolymer based on nine elements: C, H, O, N, Si, S, Br, Cl, and F. Chain stiffness, thermophysical properties, mechanical properties, electrical and optical properties, and transport properties are the different types of behaviors that can be modeled with Synthia.

No dependence on molecular weight is used in the calculations. All simulations are based on a typically high molecular weight polymer. The low-temperature cure conditions employed in this investigation were compared because the model, in its present state, cannot handle crosslinks between chains or cyclic structures. The main assumption for the low-temperature cure condition of the BMI/MDA and the BMI/DABA systems is that no crosslinks occur during the chain extension reaction. The model also

cannot take into account unreacted species. Therefore, only the low-temperature cure condition of the MDA and the DABA systems were modeled. The calculated properties of the DDS system were not included here since only the high-temperature cure condition was implemented for that particular system. The results would be meaningless if included here.

Another objective of the modelling was to substitute three other diamines for MDA and compare the calculated physical properties to the BMI/MDA system. The diamines were; 4,4' diaminobiphenyl (DBP), p-phenylene diamine (PPD), and p-xylylene diamine (PXD).

In this investigation, the reliability of the computer model and simulation was examined. It was also hoped that comparison of the modeled results with experiment would lead to further insight into the structure of the systems studied. Finally, the ability to use computer modeling to predict the behavior to unknown and unfamiliar systems was tested.

Figure 4.67 illustrates the glass transition temperature as a function of mole fraction BMI for the BMI/MDA system. Also included is the result of the low-temperature cure model of glass transition temperature

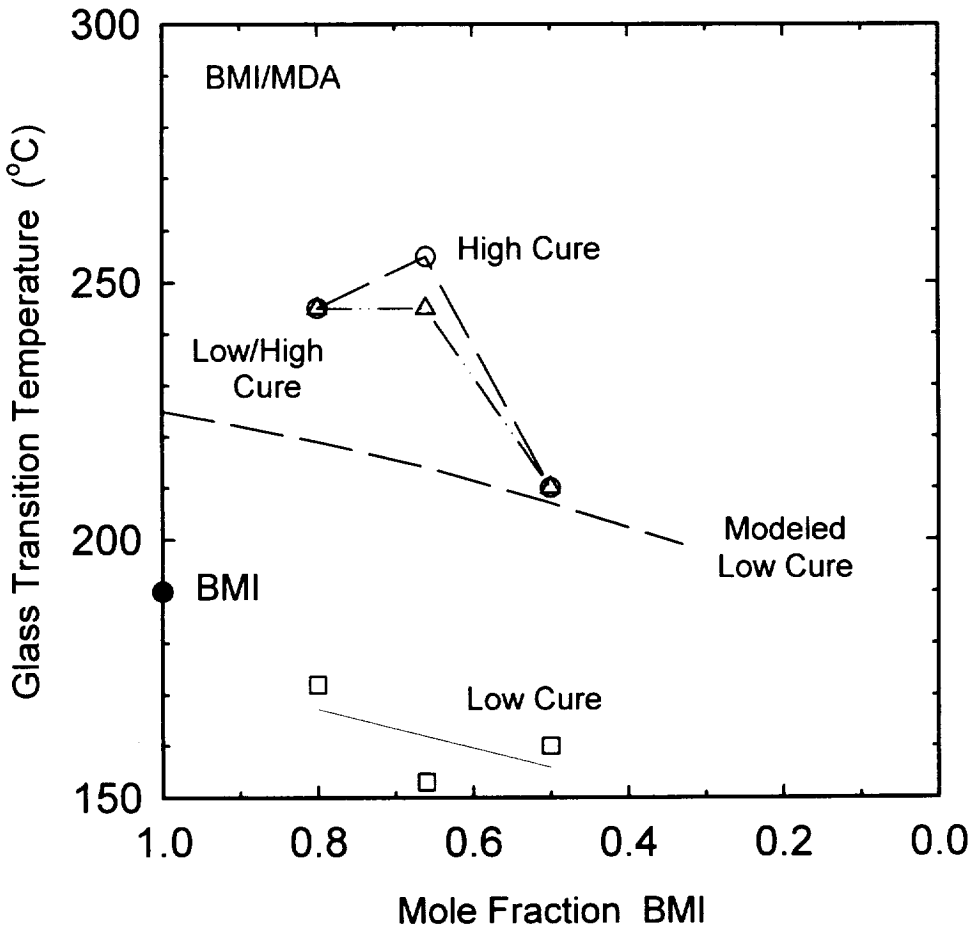

Figure 4.67. Comparison of the measured and modeled glass transition temperature as a function of mole fraction BMI for the BMI/MDA system.

versus mole fraction BMI. The computer simulation overestimated the actual T_g of the low-temperature condition but the model does follow the general trend in experimental data. As the amount of diamine decreases, the glass transition temperature increases.

Figure 4.68 displays the T_g versus mole fraction BMI for the BMI/DABA low-temperature cure condition. The model for the low-temperature cure condition underestimates the glass transition temperature but the trend is the same. The T_g increases as the amount of BMI increases. One possible reason for underestimating the T_g is that the model does not take into account crosslinking or etherification. Some crosslinking or etherification of the DABA could be occurring even at curing temperatures of 177 °C.

Figure 4.69 is the glass transition temperature versus mole fraction BMI for the three different diamines, MDA, and the experimental data previously shown. As stated before, the simulation underestimated the MDA properties. DBP exhibited the highest calculated T_g while PXD had the lowest T_g of the systems analyzed. It would expected that the addition of phenyl rings in the backbone chain increases the stiffness and therefore, the T_g of the DBP system.

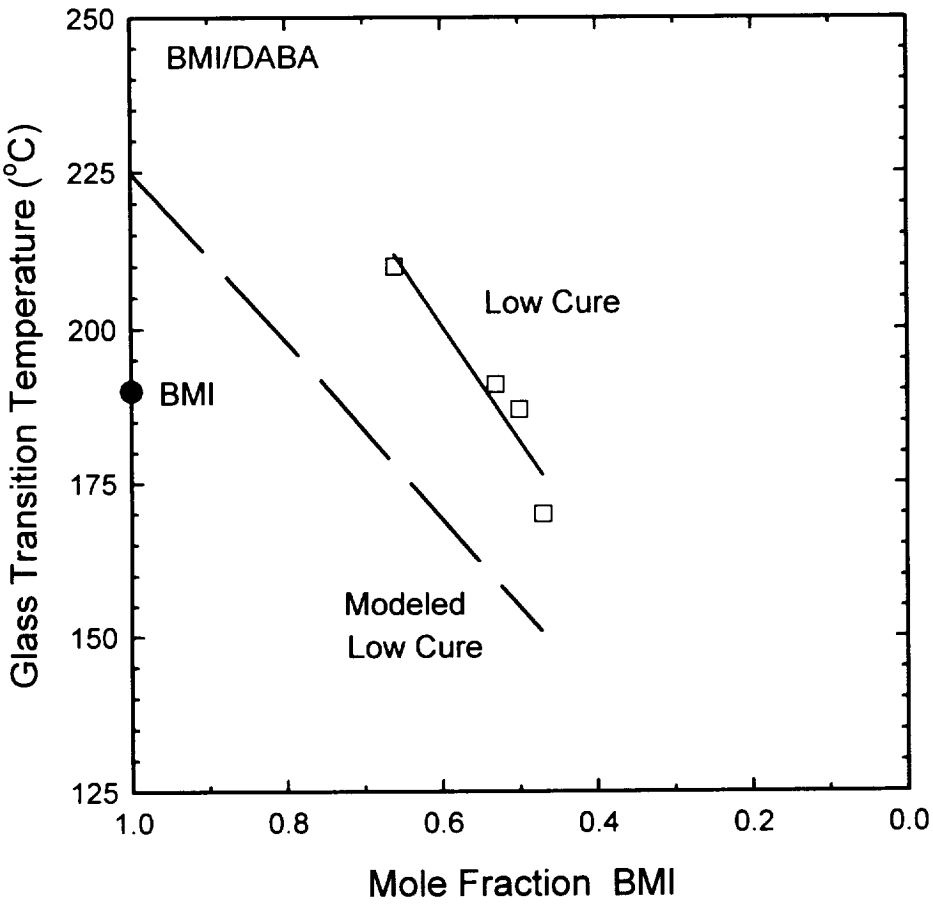

Figure 4.68. Comparison of the measured and modeled glass transition temperature versus mole fraction BMI for the BMI/DABA low-temperature cure condition.

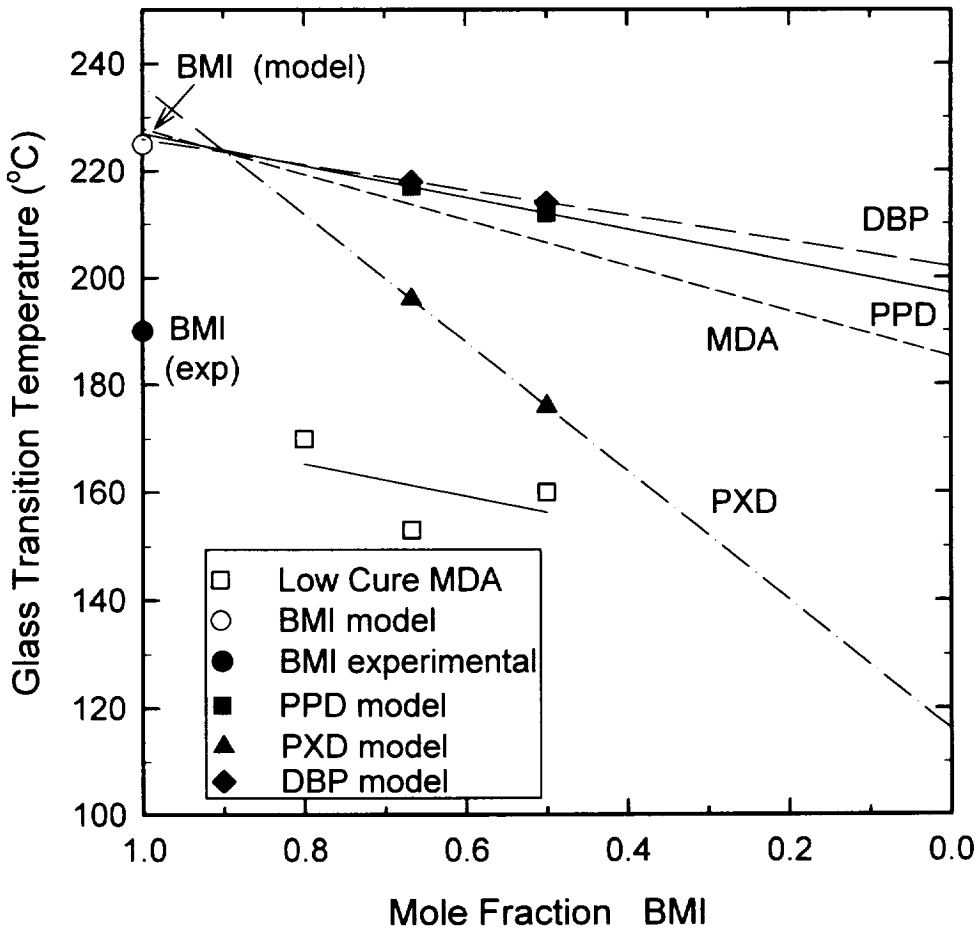

Figure 4.69. Glass transition temperature versus mole fraction BMI for the experimental data previously shown for BMI/MDA, and modeled data for three other diamines: DBP, PPD, and PXD.

Figure 4.70 shows the experimental values of density of BMI/MDA and the calculated density values versus mole fraction BMI. The modeled behavior determines the affect of diamine on density perfectly. Chemical composition rather than cure history controls the experimental or calculated density measurements for the BMI/MDA system.

Figure 4.71 is the BMI/DABA counterpart of Figure 4.70. The computer simulation underestimates the density values of the low-temperature cured material investigated in this study. This result implies that the low-cure condition for BMI/DABA resulted in some crosslinking of the material. The effect on density of having no crosslinks and only long, linear chains is that the calculated density measurements are lower than the experimental values.

Figure 4.72 shows the density values versus mole fraction BMI for the three diamines and the experimental values of MDA. PPD had the highest calculated density values. Obviously, the $-NH_2$ groups and the phenyl ring can pack efficiently to produce higher density values. Adding another phenyl group decreases the calculated density for a given BMI mole fraction from the density values of PPD. Finally, adding $-CH_2$ groups lowers the calculated density

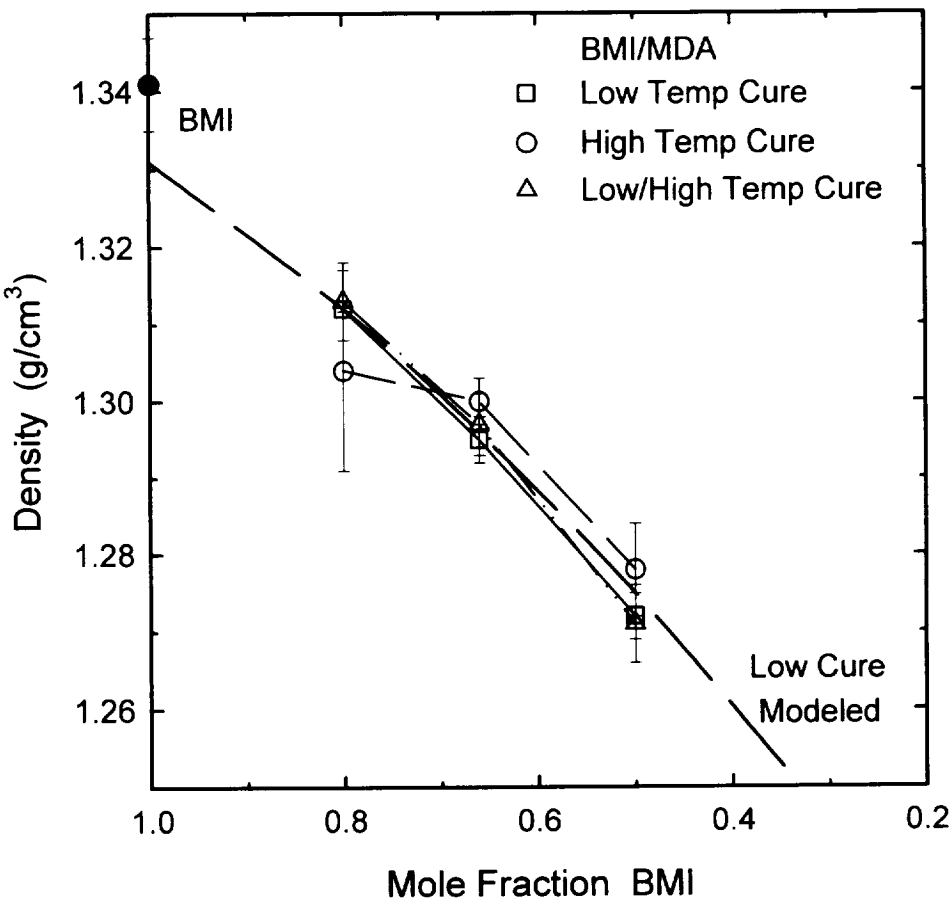

Figure 4.70. Experimentally determined and modeled density values as a function of BMI mole fraction for the BMI/MDA system.

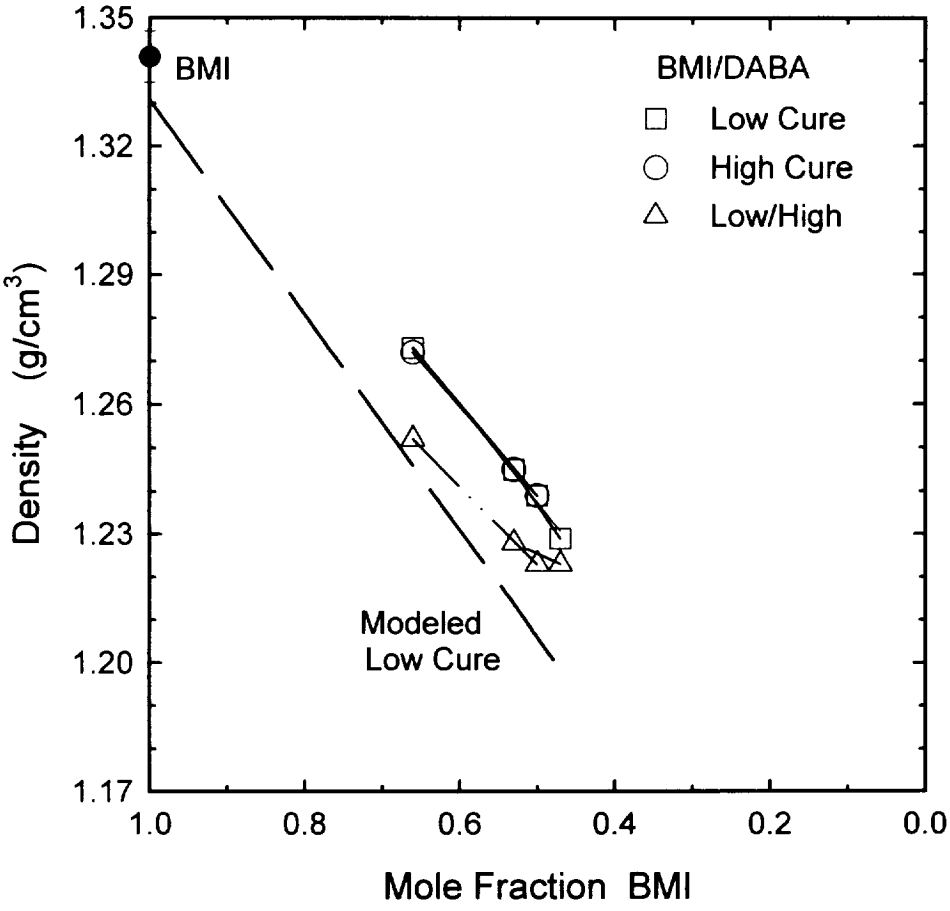

Figure 4.71. Experimentally determined and modeled density values as a function of BMI mole fraction for the BMI/DABA system.

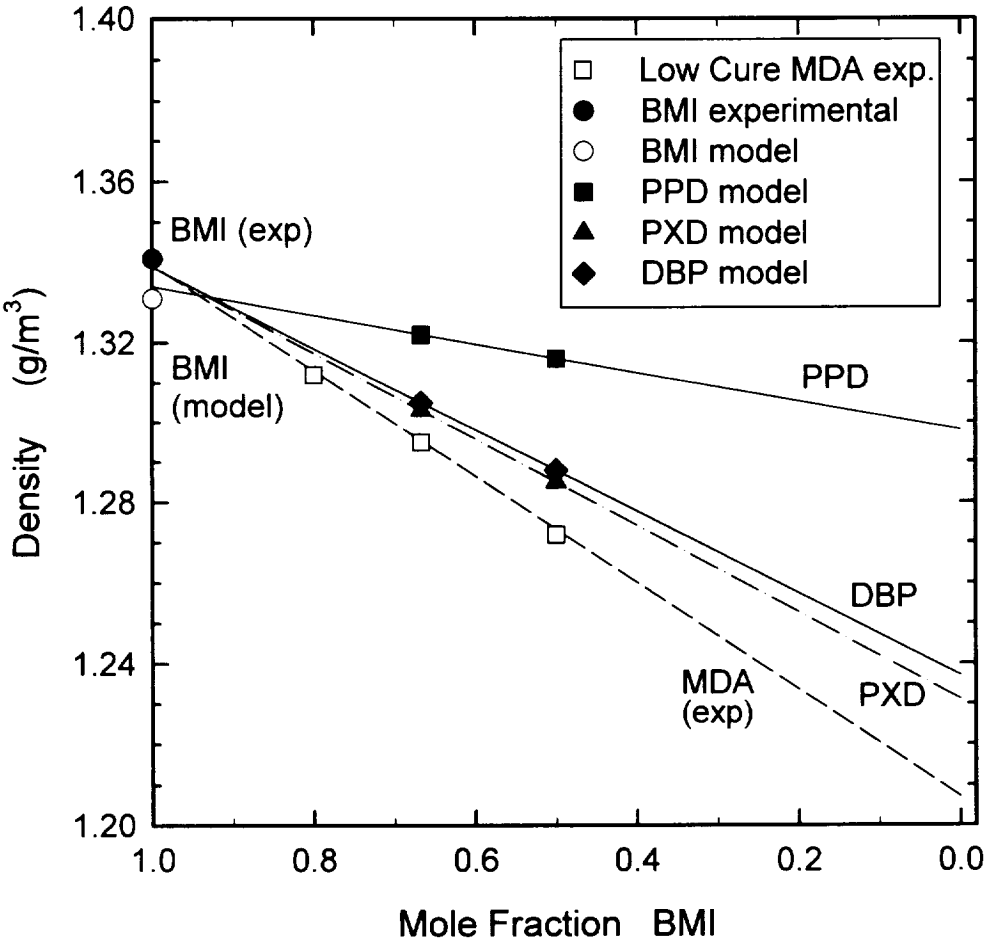

Figure 4.72. Density versus mole fraction BMI for the modeled behavior of three BMI/diamine systems and the experimental values for BMI/MDA.

values as observed in PXD and MDA. The methylene groups do not allow close packing of the molecular chains.

Figure 4.73 is a plot of modulus versus mole fraction BMI for the BMI/MDA system and the modeled low-temperature cure condition. The experimental modulus values are much higher than the calculated values. This could be due to unreacted species within the material which sterically hinder molecular mobility. The computer simulation does not account for unreacted species and crosslinks. However, the model does predict that the modulus will increase with increasing amounts of BMI.

Figure 4.74 is a plot of the experimental data for modulus versus mole fraction BMI for the BMI/DABA system and the calculated modulus values from the computer simulation for the low-temperature cure condition. The low-temperature cure condition of BMI/DABA experiences much higher modulus values than the modeled modulus values. This, too, is probably due to unreacted species and crosslinks present within the material. The model can not account for these types of imperfections, which can have significant effects on certain properties such as modulus.

Finally, Figure 4.75 summarizes the calculated modulus results versus mole fraction BMI for various BMI/diamine

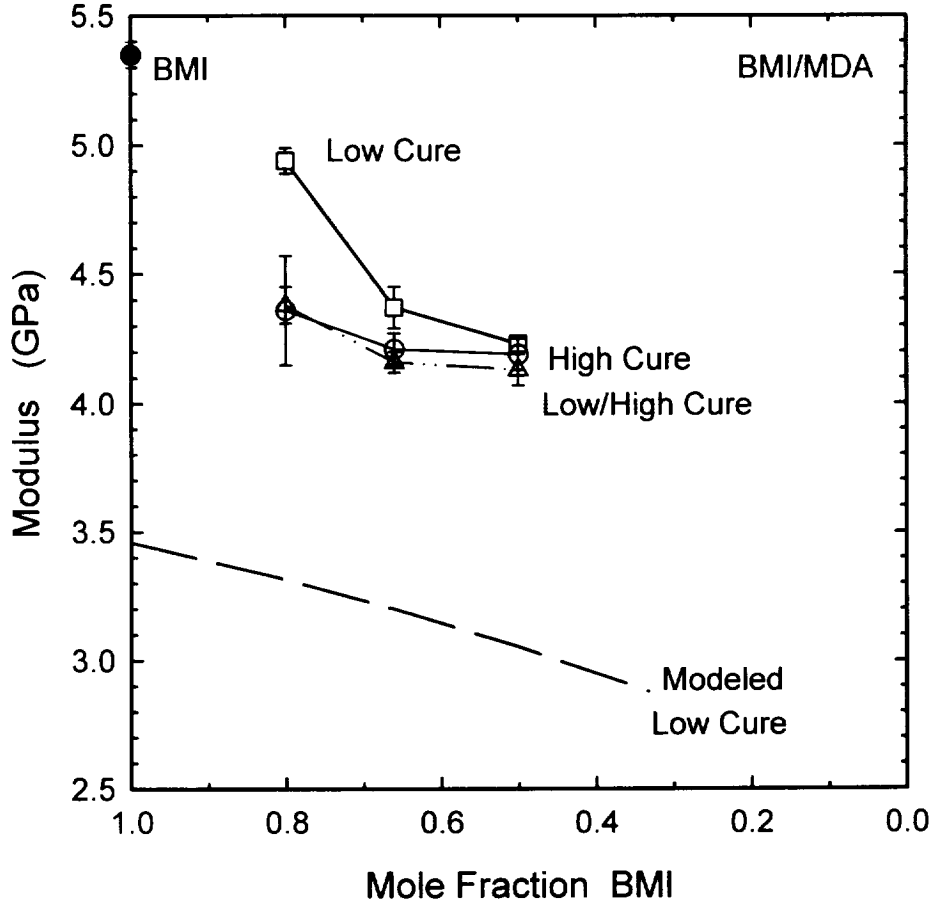

Figure 4.73. Modulus versus mole fraction BMI for the BMI/MDA system and the modeled low-temperature cure results.

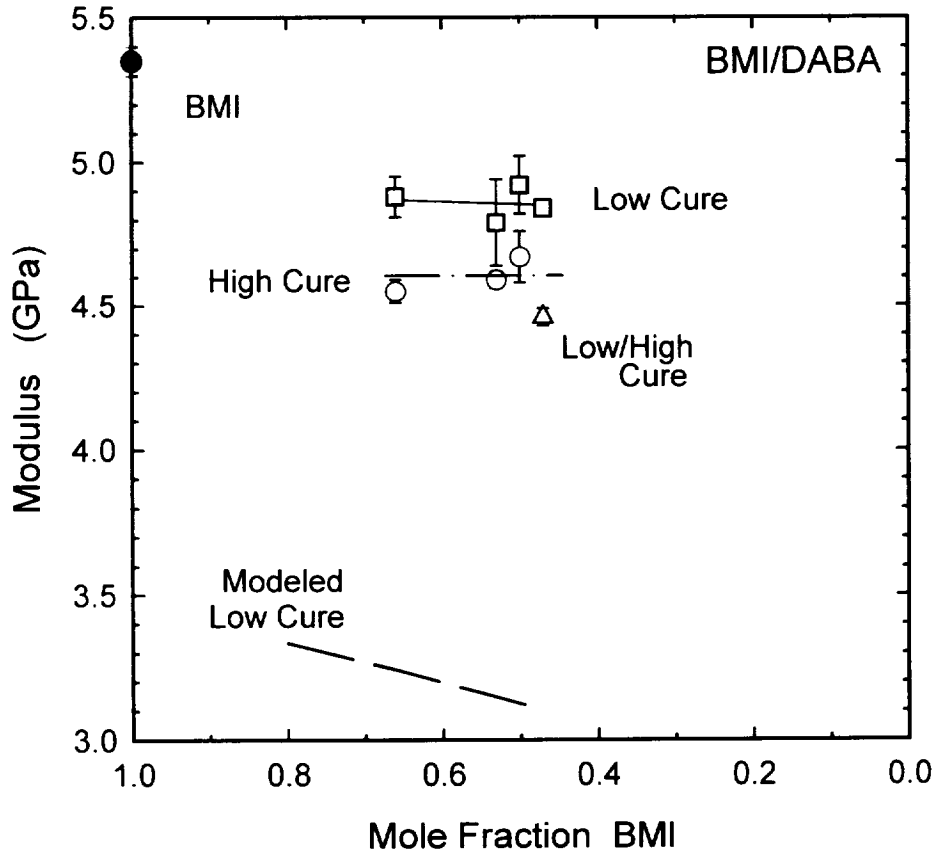

Figure 4.74. Modulus versus mole fraction BMI for the BMI/DABA system and the calculated modulus values from the computer simulation for the low-temperature cure condition.

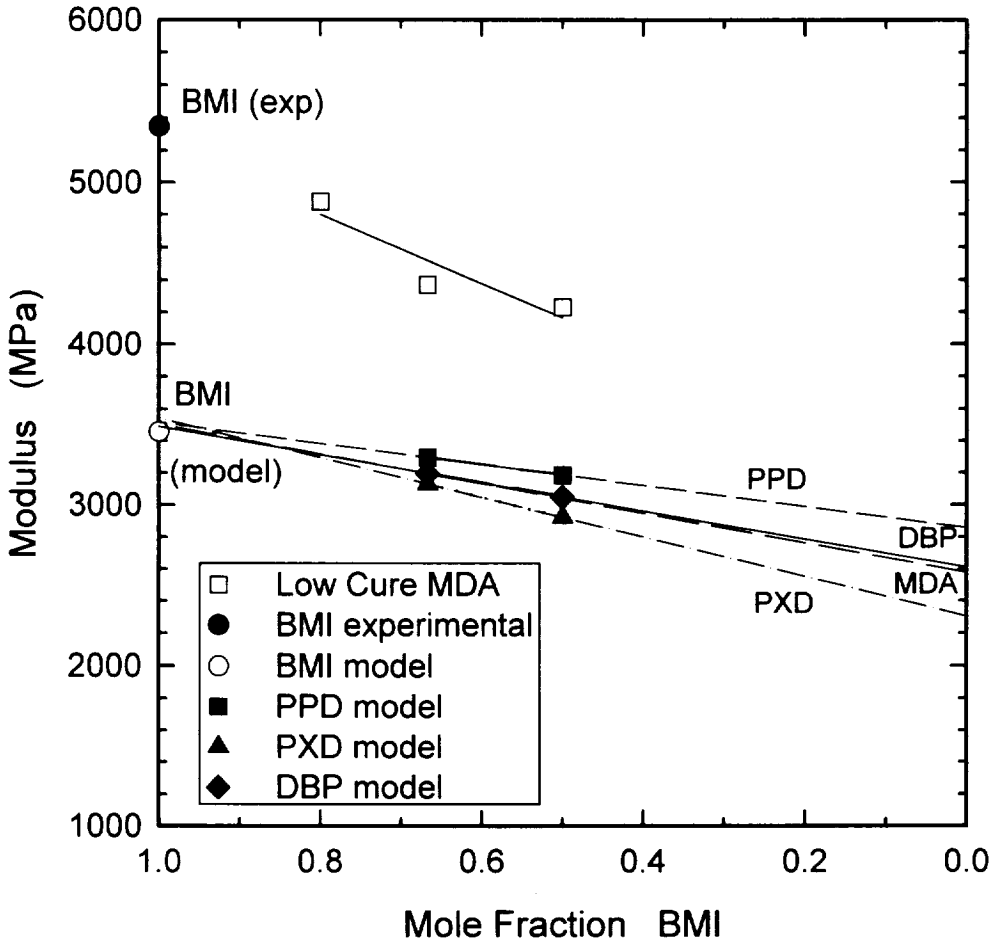

Figure 4.75. Calculated modulus results versus mole fraction BMI for various BMI/diamine systems compared to the experimental values for BMI/MDA.

systems. The modulus reflects short-range structure. At room temperature, free volume or intermolecular packing normally governs the low strain properties of thermosets such as modulus and yield. Close packing of molecules results in high modulus values. PPD was calculated to have the highest modulus per given mole fraction. This result coupled with the density data indicates that PPD has the closest packing of molecules compared to the other diamines modeled. DBP, with two phenyl rings also followed the same trend as the calculated density values.

As demonstrated above, computer simulation can be a useful tool when used in conjunction with experimental results. Modeling serves as a benchmark or a starting point in designing experimental matrices for research or for verifying trends in the data. The modeled results when compared to the experimental data pointed towards the following conclusions: 1) For the BMI/MDA system the modeled values tended to underestimate the experimental values, except in the case of density. This implies that the low-temperature cured material examined in this study may contain some crosslinks and unreacted material. The fact that density was insensitive to cure condition and was accurately modeled for BMI/MDA implies that, in the case of

density, chemistry is a more important factor than structure. 2) Likewise, the modeled results tended to seriously underestimate the experimentally determined properties for the low-temperature cured BMI/DABA for the same reason: the presence of crosslinks and unreacted material. 3) Finally, BMI/PPD was calculated to have higher density and modulus values and a relatively high glass transition temperature for the low-temperature cure condition relative to the other systems experimentally or analytically investigated in this study. Consequently, this may be an interesting system to add to future studies of various BMI/diamine systems.

CHAPTER V

SUMMARY AND RECCOMMENDATIONS

5.1. Summary of Results

1. The powder-melt method of processing was a successful alternative to solvent processing and proved to be an acceptable method for producing BMI/diamine copolymers. The process involves the melting of the lower melting point constituent, mixing in the second powder component, allowing the mix to cool, and then grinding the mixture into a fine powder, which is finally used in the molding process. Intimate mixing was shown to occur for BMI and MDA.

2. FTIR analysis indicates the presence of a peak in the range of 3100-3000 cm^{-1} which represents the double bond of BMI, and infers that the Michael's addition reaction has not occurred between the two components in the as-ground powders. Therefore, the powders prepared for the molding process have not reacted and the double bond is available for crosslinking during curing.

3. Dielectric analysis of cure monitoring is a complementary tool in network characterization. This characterization process is not useful by itself but is used in conjunction with other rheological techniques. In this investigation, dielectric analysis was used to determine the processing variables of bismaleimides. Temperature ranges for curing BMI/MDA were resolved. At low temperatures, a plot of log conductivity versus 1/T yielded a single relaxation time for low frequencies. At higher frequencies, there is a distribution of relaxation times. From the Cole-Cole plot, a single relaxation time occurs for BMI/DABA, cured at low temperatures. The exothermic parameters of BMI/DDS were double that of the BMI/MDA system. This is due to the increased chemical reactivity of MDA.

4. Curing times were determined from DSC analysis and used in conjunction with dielectric analysis results. With the addition of MDA to BMI, the melting points of the mixtures lowered with increasing molar ratios of MDA. The presence of DDS with BMI increased the curing temperature over that of BMI/MDA.

5. GPC results indicate that the predominant reaction during low temperature cure is chain extension between the amine and the double bond of BMI. The polymer samples dissolved in NMP.

6. Only a single weight loss event was observed with respect to temperature during TGA analysis of all samples. This indicates that a single decomposition reaction occurs in these thermoset systems. As the amount of diamine increased for the powder samples, the thermal stability decreased, determined by IDT and T_{max}.

7. Rheological results indicate that the resin composition, curing conditions, and topologies of the resulting network have a significant effect on thermal properties of BMI's. A high BMI content leads to a high T_g. The cure histories do not affect T_g except for the low-temperature cure condition and for the BMI:MDA in a 2:1 mole ratio. The low-temperature cure condition favors chain extension that reduces T_g for a given mole fraction BMI. Low-temperature cure of BMI:MDA 1:1 has a higher T_g than BMI:MDA 2:1 because extensive amine addition occurs in the former material. For the 4:1 and 1:2 cases of BMI:MDA, cure histories did not affect T_g. The storage modulus, G', increased after G_e due to continued reaction of unreacted species within the network. T_g decreases with increasing amounts of DABA and DDS. Postcuring PMR increased the T_g from 330 to 405 ° C.

8. Chemical composition rather than cure history controls room-temperature density. Density measurements decrease with decreasing amounts of BMI for the BMI/MDA and

BMI/DABA systems. Low-temperature and high-temperature cure conditions for all mole ratios of DABA have the same room-temperature density values. The step-cure condition of the BMI/DABA system produced lower density values for a given mole ratio. Additions of DDS to BMI increased the room-temperature density over that of BMI, BMI/MDA, or BMI/DABA because DDS apparently has a higher packing density than MDA or DABA. The density values of cured and postcured PMR's were statistically the same.

9. Sonic techniques are a viable alternative to three-point bend measurements for determining modulus. For the low-temperature cure condition of BMI/MDA, the modulus decreases with decreasing concentration of BMI. The low-temperature cure condition for a given mole fraction BMI had the highest modulus compared to the low/high- or high-temperature cure condition. This may be due to the steric hindrance of unreacted BMI molecules in the glassy state.

10. The sonic modulus values of BMI/DABA for both the low- and high-temperature cure conditions did not vary substantially with mole fraction BMI. The low temperature cure condition of BMI/DABA displayed the highest modulus values over that of the high-temperature cure condition. The BMI/DDS system exhibited the highest modulus values over the other systems investigated. The postcured PMR samples

had a higher modulus (4.51 GPa) compared to cured PMR (4.46 GPa).

11. The low-temperature cured samples all fractured in compression tests instead of yielding for BMI/MDA. As the amount of diamine increased, the fracture stress increased. The addition of MDA to BMI did not enhance the yield strength for the low-temperature cure condition. The yield stress for the high-temperature and the low/high-temperature cure conditions were sensitive to the concentration of BMI. As the amount of diamine increased, the yield stress decreased.

12. The yield stresses for the low- and high-temperature cure conditions of the BMI/DABA system were insensitive to mole fraction BMI, possibly due to an antiplasticization effect, where unreacted species act like defects and increase the yield stress. The yield stress for BMI/DDS decreased as the concentration of BMI decreased. Postcuring PMR increased the yield strength from 119 to 170 MPa due to an increase in crosslink density.

13. The low-temperature cured samples, which favors chain extension in the BMI/MDA system, fractured in a stable, brittle manner and had the lowest fracture energies. Fracture energy was insensitive to the amount of diamine present for the low-temperature cure condition. Crosslinking, which occurs in both the high- and low/high-

temperature cure histories of BMI/MDA increases the fracture energy for a given BMI mole fraction. Fracture energies increased as the amount of diamine increased. Stick-slip behavior did not occur for the low-temperature cure condition of BMI/MDA, for the low/high-temperature cure condition of BMI/MDA in a 2:1 mole ratio, or any cure condition of BMI/MDA in a 1:1 mole ratio.

14. For the BMI/DABA system, stable crack growth was observed and fracture energies increased with increasing amounts of DABA. For the low-temperature cure condition, stick-slip behavior was observed for all ratios of BMI/DABA. The 1:1 mole ratio conditions exhibited the highest fracture initiation values. The step-cure of BMI:DABA 1:1.12 greatly enhanced the fracture energy over that of the low-temperature cure condition.

15. Neat BMI exhibits the lowest fracture energy with unstable crack growth. The addition of DDS to BMI barely improves the fracture energy. Failure occurred in an unstable manner. Both the cured and postcured PMR materials experienced stable crack growth. The postcured PMR material had a higher fracture energy than the cured material. As the crosslink density increased with postcuring, the fracture energy increased.

16. For the low-temperature cure condition of BMI/MDA, the plastic zone size could not be calculated. Calculated

plastic zone sizes for the high-temperature cure conditions were greater than the plastic zones calculated for the low/high-temperature cure conditions. For the BMI/DABA system, the calculated plastic zone sizes increased as the concentration of BMI increased for the high-temperature cure condition. The low-temperature cure condition had lower calculated plastic zone sizes than the high-temperature cure condition of BMI/DABA. Neat BMI and BMI/DDS had roughly the same calculated plastic zone size. Cured PMR had higher calculated plastic zone sizes than the postcured PMR. The higher the crosslink density, the smaller the calculated plastic zone size.

17. Results indicate that a log-log plot of the fracture energy arrest values versus the molecular weight between crosslinks exhibit a ½ -power dependence, indicating that the fracture energy dependence for bismaleimides is similar to that found for epoxies.

18. Preliminary results of intermittent stress relaxation tests on BMI:MDA in a 2:1 mole ratio indicate that crosslinking is occurring in the relaxed state.

19. Computer simulation is a useful tool to be employed in conjunction with experimental results. Modeling of the low temperature cure conditions of BMI/MDA and BMI/DABA predicted the correct trends of physical properties versus mole fraction BMI. However, there was some

discrepancy in the absolute values of the modeled versus experimentally determined properties. This was probably due to some crosslinking and/or the presence of unreacted species in the low-temperature cured material studied in this investigation. For the low temperature cure condition, BMI/PPD (para-phenylene diamine) was calculated to have higher density and modulus values and a relatively higher T_g compared to BMI/MDA.

20. The experimental procedures used to study epoxies can be applied to systems such as bismaleimides.

5.2. Suggestions for Future Work

1. Further work should be done on the intermittent stress relaxation of thermosets. In particular, it should be demonstrated that intermittent stress relaxation can be applied effectively to understand the continued reactions occurring at high temperatures in thermosets like epoxies or polyimides.

2. Testing the physical properties of bismaleimides at elevated temperatures or after long-term exposure to elevated temperature should be further investigated. It is known that bismaleimides as high-temperature materials undergo changes to their network structures with increasing temperature.

3. Physical aging of polymers, in general, has been studied extensively. Investigating the physical aging of bismaleimides should be considered, especially if the presence of unreacted species can affect the free volume of the system.

REFERENCES

1. LeMay, J. D.: Ph.D. Dissertation, The University of Akron, (1985).

2. Swetlin, B. J.: Ph.D. Dissertation, The University of Akron, (1984).

3. Mudrich, S. F.: Ph.D. Dissertation, The University of Akron, (1991).

4. Ajbani, M.: Ph.D. Dissertation, The University of Akron, (1995).

5. Donnellan, T. M.; and Roylance, D.: *Poly. Eng. Sci.*, 32, 409, (1992).

6. Donnellan, T. M.; and Roylance, D.: *Poly. Eng. Sci.*, 32, 415, (1992).

7. Day, D.: "Dielectric Properties of Polymeric Materials," Eumetric System III Microdielectrometer Manual, Micromet Instruments , Inc., Cambridge, (1991).

8. Pater, R. H.: SAMPE J., 30, 29, (1994).

9. Vakil, U. M.; and Martin, G. C.: J. Mater. Sci., 28, 4442, (1993).

10. Phillips, D. C.; Scott, J. M.; and Jones, M.: J. Mater. Sci., 13, 311, (1978).

11. Meyers, F.; Sanz, G.; Eceiza, A.; Mondragon, I.; and Mijovic, J.: Polymer, 36, 1407, (1995).

12. Gupta, V. B.; Drzal, L. T.; Lee, C. Y.-C.; and Rich, M. J.: Poly. Eng. Sci., 25, 812, (1995).

13. Kim, S. L.; Skibo, M. D.; Manson, J. A.; Hertzberg, R. W.; and Janiszewski, J.: Poly. Eng. Sci., 18, 1093, (1978).

14. Chang, T. D.; Carr, S. H.; and Brittain, J. O.: Poly. Eng. Sci., 22, 1213, (1982).

15. Geisler, B.: Ph.D. Dissertation, The University of Akron, (1993).

16. Pater, R. H.; Whitley, K.; Morgan, C.; and Chang, A.: Polym Comp., 12, 126, (1991).

17. Varma, I. K.; Sangita; and Ralli, D. K.: Polym. News, 12, 294, (1987).

18. Stenzenberger, H. D.: Adv. Polym. Sci., 117, 165, (1994).

19. Varma, I. K.; Gupta, S. P.; and Varma, D. S.: Die Angew. Makromol. Chem., 153, 15, (1987).

20. Tungare, A. V.; and Martin, G. C.: J. Appl. Polym. Sci., 46, 1125, (1992).

21. Stenzenberger, H. D.: J. Appl. Poly. Sci. App. Poly. Symp., 22, 77, (1977).

22. Tungare, A. V.: Ph.D. Dissertation, Syracuse University, (1990).

23. Tungare, A. V.; and Martin, G. C.: Polym. Eng. Sci., 33, 614, (1993).

24. Barton, J. M.; Hamerton, I.; Rose, J. B.; and Warner, D.: Polymer, 32, 2482, (1991).

25. Manson, J. A.; Kim, S. L.; and Sperling, L. H.: AFML-TR-76-124, Air Force Materials Laboratory, Wright Patterson AFB, Ohio, (1976).

26. Leung, C. L.; Liao, T. T.; and Dynes, P. J.: 28th National SAMPE Symposium, 818, (1983).

27. Barton, J. M.; Hamerton, I.; Rose, J. B.; and Warner, D.: High Perform. Polym., 6, 21, (1994).

28. Leung, C. L.; Liao, T. T.; and Tung, C. M.: Proc. ACS Div. Poly. Mater. Sci. Eng., 52, 134, (1985).

29. Tung, C. M.; Leung, C. L.; and Liao, T. T.: Proc ACS Div. Mater. Sci. Eng., 52, 139, (1985).

30. Morgan, R. J.; Jurek, R.; Larive, D. E.; English, E. J.; Tung, C.; and Donnellan, T.: 22nd Intern. SAMPE Techn. Conf., 145, (1990).

31. Mijovic, J.; and Andjelic, S.: Macromol., 29, 239, (1996).

32. Stenzenberger, H. D.; Konig, P.; Herzog, M.; and Romer, W.: Proceed. 19th Intern. SAMPE Tech. Conf., vol. 19, 372, (1987).

33. Chaudhari, M.; Galvin, T.; and King, J.: SAMPE J., 21, 17, (1985).

34. Tobolsky, A. V.; Takahashi, Y.; and Naganuma, S.: Polym. J., 3, 60, (1972).

35. Bjork, F.; Dickman, O.; Stenberg, B.: Rubb. Chem. Techn., 62, 387, (1989).

36. Sheppard, N. F.; Day, D. R.; Lee, H. L.; and Senturia, S. D.: Sens. Actuat., 2, 263, (1982).

37. Kranbuehl, D. E.: J. Non-Cryst. Solids, 131, 930, (1991).

38. Kranbuehl, D. E.: in Developments in Reinforced Plastics - 5, G. Pritchard, Ed., Elsevier Applied Science Publishers: New York, p. 181, (1986).

39. Senturia, S. D.; Sheppard, N. F.; Lee, H. L.; and Day, D. R.: Adhes., 15, 69, (1982).

40. Jang, B. Z.; and Shih, W. K.: Mater. Manuf. Process., 5, 301, (1990).

41. Greenfield, E. W.: "Introduction to Dielectric Theory and Measurements", Washington State University, (1970).

42. Elias, H. G.: in Macromolecules Structure Properties, Volume 1, Plenum Press: New York, p. 480 (1984).

43. Senturia, S. D.; and Sheppard, N. F.: Adv. Polym. Sci., 80, 3, (1986).

44. Day, D. R.: Polym. Eng. Sci., 26, 362, (1986).

45. Gotro, J.; and Yandrasits, M.: Polym. Eng. Sci., 29, 278, (1989).

46. Polymer Users Guide Version 6, Biosym Technologies, San Diego, CA, (1993).

47. Stenzenberger, H.: in Structural Adhesives Developments in Resins and Primers, A. J. Kinloch, Ed., Elsevier Applied Science Publishers, New York, p. 77, (1987).

48. Morgan, R. J.; Jurek, R. J.; Yen, A.; and Donnellan, T.: Polymer, 34, 835, (1993).

49. Snyder, C.: Personal Communication, Ciba-Geigy, Hawthorne, NY, (1993).

50. Serafini, T. T.; Delvigs, P.; and Alston, W. B.: Proceed. 27th Nat. SAMPE Symp., vol. 27, 320, (1982)

51. Roberts, G.; and Lauver, R. W.: J. Appl. Poly. Sci., 33, 2893, (1987).

52. Mittleman, M. L.; Johnson, D.; and Wilkie, C. A: Trends in Poly. Sci., 2, 391, (1994).

53. Bargain, A. C.; and Grojean, P.: British Patent No. 1,190,718, 6 May, 1970.

54. ASTM D2471-88. Standard Test Method for Gel Time and Peak Exothermic Temperature of Reacting Thermosetting Resins, (1988).

55. Roberts, G.: Personal Communication, NASA Lewis Research Center, Cleveland, OH, April, (1993).

56. ASTM 792-86. Standard Test Methods for Density and Specific Gravity of Plastics by Displacement, (1991).

57. Treoloar, L. R. G.: The Physics of Rubber Elasticity, 3rd. Ed., Oxford Univ. Press, Oxford, (1975).

58. Sawyer, L. C; and Grubb, D. T.: Polymer Microscopy, Chapman and Hall, New York, (1987).

59. Williams, J. G.; and Ford, H.: J. Mech. Eng. Sci., 6, 405, (1964).

60. Outwater, J. O.; and Gerry, D. J.: J. Adhes., 1, 290, (1969).

61. Kies, J. A.; and Clark, B. J., in Fracture 1969, P. L. Pratt, Ed., London: Chapman and Hall Ltd., 483, (1969).

62. Yamini, S.; and Young, R. J.: Polymer, 18, 1075,.(1977).

63. Evans, A. G.; Russell, L. R.; and Richerson, D., W.: Metall. Trans. A., 6A, 707, (1975).

64. Kinloch, A. J.; and Williams, J. G.: J. Mater. Sci., 15, 987, (1980).

65. Knott, J. F.: Mater. Sci. Eng., 7, 1, (1971).

66. Wronski, A. S.: J. Mater. Sci., 12, 28, (1977).

67. Grindosonic Manual, Lemmens-Elecktroniks, Belgium.

68. Biosym Technologies, Biosym/MSI Workshop, "Polymer Modeling and Property Prediction 1995", (1994).

69. Knight, G. J.: in Developments in Reinforced Plastics - 1 - Resin Matrix Aspects, Edited by G. Pritchard, Applied Science Publishers Ltd.: London, p. 145, (1980).

70. Donnellan, T.: Personal Communication, (1993).

71. Kuhn, W. E.; Friedman, I. L.; Summers, W.; and Szegvari, A.: in Metals Handbook, Ninth Ed., Vol. 7, American Society For Metals: Metals Park, p. 56 (1984).

72. Kranbuehl, D. E.: in International Encyclopedia of Composites, Volume. 1, Edited by S. Lee, VCH: New York, p. 534, (1990).

73. Wang, M.; Johari, G. P.; and Szabo, J. P.: Polymer, 33, 4747, (1992).

74. Sheppard, N. F.; Coln, M. C. W.; and Senturia, S. D.: Proc. 29th National SAMPE Symposium and Exhibition, 1243, (1984).

75. Olyphant, M.: Proc 6th IEEE Electrical Insulation Conf., 12 (1965).

76. Mangion, M. B. M.; and Johari, G. P.: J. Poly. Sci.: Part B: Poly. Phys., 28, 1621, (1990).

77. Delides, G. C.; Hayward, D.; Pethrick, R. A.; and Vatalis, A. S.: J. Appl. Poly. Sci., 47, 2037, (1993).

78. Uemura, S. J.: J. Poly. Sci. Poly. Phys. Edn., 12, 1177, (1974).

79. Starkweather, H. W.; and Avakian, P.: J. Poly. Sci.: Part B: Poly. Phys., 30, 637, (1992).

80. Finzel, M. C.; Hawley, M. C.; and Jow, J.: Poly. Eng. Sci., 31, 1240, (1991).

81. Kranbuehl, D. E.: "Dielectric Monitoring of Polymerization and Cure", in press, (1995).

82. Kenny, J. M.; Trivisano, A.; and Nicolais, L.: in Advances in Chemistry Series, vol. 227, Edited by Clara D. Craver and Theodore Provder, American Chemical Society, Washington, DC, p. 539, (1990).

83. Barton, J. M.; Hamerton, I.; Rose, J. B.; and Warner, D.: in Polyimides and other High-Temperature Polymers, edited by M. J .M. Abadie and B. Sillion, Elsevier Science Publishers, Amsterdam, p. 283, (1991).

84. Watson, E. S.; O'Neill, M. J.; Justin, J.; and Brenner, N.: Anal. Chem., 36, 1233, (1964).

85. Varma, I. K.; Sangita; and Varma, D. S.: J. Poly. Sci.: Poly. Chem. Edn., 22, 1419, (1984).

86. Ninan, K. N.; Krishnan, K.; and Mathew, J.: J. Appl. Poly. Sci., 32, 6033, (1986).

87. Nanjan, M. J.; and Sivaraj, K.: J. Poly. Sci.: Part A: Poly. Chem., 27, 375, (1984).

88. Patel, H. S.; and Shah, V. J.: Int. J. Polymeric. Mater., 26, 79, (1994).

89. Arridge, R. G. C.; and Speake, J. H.: Polymer, 13, 443, (1972).

90. LeMay, J. D.; and Kelley, F. N.: Adv. Polym. Sci., 78, 115, (1986).

91. Regnier, N.; and Mortaigne, B.: Polym. Adv. Techn., 5, 513, (1994).

92. Chattha, M. S.; and Dickie, R. A.: J. Appl. Poly. Sci., 40, 411, (1990).

93. Gupta, V. P.; and Brahatheeswaran, C.: Polymer, 32, 1875, (1991).

94. Yamini, S.; and Young, R. J.: J. Mater. Sci., 15, 1814, (1980).

95. Venditti, R. A.; Gillham, J. K.; Jean, Y. C.; and Lou, Y.: J. Appl. Polym. Sci., 56, 1207, (1995).

96. Enoki, T.; Takeda, T.; and Ishii, K.: J. Thermosetting Plast., 14, 131, (1993).

97. Pritchard, G.; and Swan, M.: Poly. Int., 36, 1, (1995).

98. Williams, J. G.: Fracture Mechanics of Polymers, Ellis Horwood Publishing LTD., Chichester, England, (1984).

99. Heritage, K.; Frisby, C.; and Wolfenden, A.: Rev. Sci. Instrum., 59, 773, (1988).